

The molecular regulation of neural stem cell lineage progression in the postnatal subventricular zone by Galectin-3

A thesis submitted to the Department of Physiology, Anatomy and Genetics, in fulfillment of the requirements for the degree of *Doctor of Philosophy*

By: Osama Ahmad Odeh Al Dalahmah

St. Anne's College, University of Oxford, United Kingdom
Trinity term, 2015

Abstract

Neurogenesis continues postnatally in two major neural stem cell (NSC) niches: The subventricular zone (SVZ) and dentate gurus of the hippocampus. SVZ NSCs self-renew and produce transit amplifying progenitor cells that, in turn, divide and give rise to neuroblasts. These neuroblasts migrate to the olfactory bulbs, via the rostral migratory stream (RMS), where they terminally differentiate into mature neurons. The postnatal SVZ (pSVZ) is more gliogenic than its adult counterpart (aSVZ), contributing to robust postnatal astrocytogenesis and oligodendrogenesis in the surrounding brain parenchyma. Studies examining Galectin-3 (Gal-3) in the aSVZ showed it has functions in regulating neuroblast migration, microglial activation, oligodendrocytic differentiation, and angiogenesis. However, the role of Gal-3 in pSVZ lineage progression is unknown. This thesis aims to unravel the roles of Gal-3 in regulating pSVZ lineage progression, fate choices, and NSC activation. In doing so, the thesis tackles the molecular pathways possibly involved in mediating the effects of Gal-3.

I found through co-immunoprecipitation that Gal-3 was bound to β-catenin and both proteins were co-expressed in the aSVZ. In addition, expression of Gal-3 and Wnt/β-catenin signalling were downregulated as SVZ cells progressed through the lineage and became migratory. I hypothesised that Gal-3 may regulate lineage progression through regulation of Wnt/β-catenin signalling. To explore this hypothesis, Gal-3 overexpression, knockdown or control plasmids were co-electroporated with a Wnt/β-catenin reporter into the SVZ of postnatal day two mice. I found lineage progression was not altered by Gal-3 overexpression. Surprisingly, contrary to evidence described in the cancer literature, Gal-3 overexpression reduced Wnt/β-catenin signalling. This was accompanied by an acute reduction in proliferation. Also, more cells expressed p27/Kip1 in the SVZ, and more cells migrated into the RMS, suggesting increased cell cycle exit. However, NSC proliferation and clonal neurosphere forming capacity were not altered by Gal-3 overexpression, indicating that NSC activation was not influenced by Gal-3. While olfactory neuronogenesis was not altered by Gal-3 overexpression, striatal astrocytogenesis was increased while oligodendrogenesis was dampened. Further experiments revealed phosphorylation of Smad proteins 1/5/8 was increased in vivo and in vitro after Gal-3 overexpression. These findings indicate that Gal-3 positively regulated BMP signalling in the SVZ, possibly contributing to Gal-3's pro-gliogenic effects.

Taken together, this thesis supports a model whereby a subpopulation of Gal-3-responsive pSVZ cells reacted to Gal-3 overexpression by acutely exiting the cell cycle, and possibly through the same mechanisms, switched from oligodendrocytic to astrocytic fate. These cellular responses might have been brought about, at least partially, by acute suppression of Wnt/β-catenin and activation of BMP signalling. These novel findings emphasise the regulatory actions of Gal-3 on pSVZ lineage progression through Wnt/β-catenin and BMP signalling.

Acknowledgements

My experience in Oxford has been rewarding and challenging in many aspects. I am in debt to my family who shared with me both happiness and hardship. Without their love and generous support, my work in Oxford could not have been possible. I will carry in my heart all the selfless sacrifices my Mother and Father had to make in order for my brothers, sisters, and I to receive the best education possible. My Mother's kind warm words and my Father's sincere encouragement helped me weather all of the storms. I will always remember the continuous support from my family and Uncle Ghazi, who made sure I still enjoyed strong Jordanian coffee and ceylon tea with sage. I thank my family for all they did for me, and dedicate this work to them.

My supervisor Dr. Francis Szele has been a great mentor and a true friend. I am thankful for all the generous support and trust he provided me with over the course of my DPhil. His deep scientific insight and creativity enriched my quest for knowledge. Francis has always welcomed well-founded scientific debate and encouraged ambitious experiments, and that helped shape my scientific thinking. I take to heart his kind concern for my wellbeing, personal development, and career, which shows his warm and considerate character. I look forward to coming to future Szele lab retreats with Francis and his wife Jane, who have always made me feel like part of their family.

I thank all the past and present Szele lab members who helped me in editing this thesis. In particular, I thank Dr. Istvan Adorjan, Dr. James Hillis, Mr. Martin Ducker, and Dr. Roderick Walker for their comments and edits on the thesis. I also thank Dr. Tracy Lane, Mr. Bin Sun, Dr. Julie Davies, and Dr. Christopher Young for their valued feedback and input into my work. I am

grateful for the help I received from Dr. Anne Mullen, Dr. Helen Christian and Dr. Roger Patient, without whom my DPhil would not have been possible. Dr. Patrick Nolan's guidance in my transfer of status examination and Dr. Eric O'Neill's insight in my confirmation of status examination were invaluable in shaping my thesis. Dr. Jo Begbie, Dr. Richard Wade-Martin, and their lab members; especially Dr. Hugo Fernandes and Dr. Steven Fleenor who provided me with much appreciated technical support and generous access to their facilities. I also thank Dr.Shankar Srinivas and his lab for help with microscopy, as well as Dr. Zoltan Molnar and his lab, who have been generous in their guidance and friendship. This work could not have been possible without the support from the staff of the Oxford Biomedical Services and the Department of Physiology, Anatomy, and Genetics.

My past supervisors and mentors: Dr. Said Ismail, Dr. Amin Al-Ahmad, and Dr. Dan Hoch have been a great source of inspiration and support. Without them, I would not have been in Oxford.

Finally, I would like to thank all my friends who enriched my life over the past 4 years. I am grateful to Cedric Leyrat, Yichen Li, Shan Huang, Kurosaki Ichigo, Alex Giannakoulas, Sufian Al Mousa, Saad Al Wreikat, Anas Abu Humaidan and many others I hold dearly in my heart. I especially thank Chelsea Robles for all her love, support and companionship. Without her, my life would not be the same.

July 2015, Oxford

Authorship Statement

I conceptualised the research questions in this thesis and conceived the experimental plans therein with generous input from my supervisor Dr. Francis Szele.

For characterization of the impact of Galentin-3 overexpression on subventricular zone lineage progression, Mr. James Nicholson assisted in immunohistochemistry, imaging, quantification, and in vitro neurosphere culture under my supervision as part of his Master degree thesis.

For analysis of the impact of Galectin-3 on BMP signalling, Mrs. Mayara Mundim – a visiting PhD student- conducted the western blot analysis and band intensity measurement.

I double-checked and verified all quantifications and measurements in this thesis performed by Mr. James Nicholson and Mrs. Mayara Mundim. I performed all other experimental procedures, quantifications, and analysis in this thesis. Valued input from my colleagues in the Szele lab and the scientific community in University of Oxford helped me in the overall study design.

Copyright © 2015 by Osama Al-Dalahmah

All rights reserved.

Table of Contents

Abstract 2

Acknowledgements 3

Authorship Statement 5

Table of Contents 6

List of Figures 11

List of Tables 12

Abbreviations 13

1 Introduction 17

1.1 Stem cells and the stem cell niche 17
1.1.1 Stem cells: definitions 17
1.1.2 Studying stem cell behaviour: Practical considerations 18
1.2 Neural development: a brief look 22
1.3 The postnatal SVZ: a unique NSC niche 25
1.3.1 Development of the postnatal SVZ 25
1.3.2 The neurogenic lineage and niche: a closer look 26
1.4 The heterogeneous output of the postnatal SVZ 32
1.5 The regulation of pSVZ niche physiology 35
1.5.1 Soluble factors 36
1.5.2 Cell-bound signals 38
1.5.3 Morphogens 41
1.5.4 Crosstalk between pathways 46
1.6 Galectin-3: a potential regulator of pSVZ signalling 47
1.6.1 Galectins in the subventricular zone 47
1.6.2 Gal-3: a closer look 47

1.6.3 Galectin-3 in the SVZ 51
1.7 Research Questions 52

2 Materials and Methods 58

2.1 Animals *58*
2.2 In vivo brain electroporation *58*
2.3 Thymidine analogue injection *59*
2.4 RNA extraction, DNA analysis and Cloning *59*
2.4.1 RNA extraction and cDNA synthesis 59
2.4.2 PCR and Gel electrophoresis 60
2.4.3 DNA and RNA concentration and purity 60
2.4.4 Plasmids 62
2.4.5 Ligation of DNA sequences 64
2.4.6 Transformation of chemically competent bacteria and DNA extraction 65
2.5 Protein isolation, Western blotting, and Immunoprecipitation *66*
2.5.1 Protein extraction 66
2.5.2 Protein quantification 66
2.5.3 Western blotting 67
2.5.4 Co-Immunoprecipitation 68
2.6 Cell culture, Transfection, Nucleofection and Flowcytometry *70*
2.6.1 HEK293T culture 70
2.6.2 Transfection 70
2.6.3 SVZ dissection and Neurosphere culture 71
2.6.4 Nucleofection 72
2.6.5 Clonal density/self renewal assay 72
2.6.6 Flowcytometry 73
2.6.7 BMP4 luciferase assay 74
2.7 Histology and Fluorescent Immunohistochemistry *75*
2.7.1 Perfusion and tissue preparation 75
2.7.2 Microtome sectioning 76
2.7.3 Standard Fluorescent Immunohistochemistry 76
2.7.4 Bromodeoxyuridine and p27Kip1 immunohistochemistry 77
2.7.5 Ethenyldeoxyuridine detection 78

2.8 Microscopy and Imaging *79*
2.8.1 Microscopy 79
2.8.2 p27Kip1 Digital Thresholding 80
2.8.3 Mean fluorescent intensity quantification of Gal-3 levels 80
2.9 Statistical Analysis *82*

3 Galectin-3 regulated Wnt/β-catenin signalling and proliferation in the postnatal SVZ 84

3.1 Introduction *84*
3.2 Results *87*
3.2.1 Galectin-3 and β-catenin were co-expressed in the SVZ niche 87
3.2.2 Galectin-3 was complexed with β-catenin in the aSVZ 91
3.2.3 In vivo brain electroporation as means to manipulate Gal-3 levels and report Wnt/β-catenin in the postnatal SVZ 94
3.2.4 Wnt signalling and Galectin-3 expression were downregulated with SVZ lineage progression 98
3.2.5 Galectin-3 regulated Wnt signalling in the plSVZ in vivo 100
3.2.6 Galectin-3 regulated Wnt/β-catenin signalling in NSCs in vitro 102
3.2.7 Overexpression of Galectin-3 reduced proliferation and increased cell cycle exit in the plSVZ 106
3.2.8 Gal-3 did not increase cell death in the lSVZ 113
3.3 Discussion *115*
3.3.1 Gal-3 and β-catenin are co-expressed in the adult lSVZ 115
3.3.2 Gal-3 expression and Wnt/β-catenin signalling were downregulated with postnatal lSVZ lineage progression 117
3.3.3 Gal-3 negatively regulated Wnt/β-catenin signalling in the plSVZ 119
3.3.4 Gal-3 upregulation reduced proliferation of plSVZ cells and induced cell cycle exit. 123
3.3.5 Downregulation of Wnt/β-catenin signalling might account for the reduction in proliferation after Gal-3 upregulation. 127
3.4 Conclusion *130*

4 Upregulation of Galectin-3 did not alter stem cell behaviour in the postnatal SVZ 132

4.1 Introduction 132
4.2 Results 135
4.2.1 SVZ NSC proliferation is not affected by Gal-3 gain-of-function 135
4.2.2 Sox2 expression was not changed by Galectin-3 upregulation 141
4.2.3 Galectin-3 overexpression did not alter NSC morphology 141
4.2.4 SVZ transit amplifying progenitors were unaffected by Galectin-3 gain-of-function 144
4.2.5 Galectin-3 Overexpression did not change neuroblast production 147
4.2.6 Clonal neurosphere assay showed preserved NSC function after Gal-3 upregulation 149
4.2.7 Other SVZ cells were not overtly affected by Gal-3 overexpression 151
4.3 Discussion 154
4.3.1 Galectin-3 overexpression did not chronically change proliferation, NSC activity, or lineage progression in the plSVZ 154
4.3.2 Retained neurogenic potential in the plSVZ 157
4.3.3 The postnatal SVZ niche is gliogenic 159
4.3.4 The fleeting oligodendrogenesis in the postnatal lateral SVZ 161
4.3.5 SVZ microglia were not affected by Galectin-3 163
4.4 Conclusion 164

5 Galectin-3 regulated fate choices in the postnatal SVZ 166

5.1 Introduction 166
5.2 Results 169
5.2.1 Olfactory neuronogenesis was not altered by Galectin-3 overexpression 169
5.2.2 The plSVZ rarely gave rise to striatal neurons 173
5.2.3 Striatal gliogenesis from the plSVZ was increased by Gal-3 gain-of-function 175
5.2.1 Gal-3 increased striatal astrocytic maturity 177
5.2.2 Gal-3 overexpression reduced the oligodendrocytic output from the plSVZ 179
5.2.3 Galectin-3 gain-of-function increased BMP signalling in vivo 181
5.2.4 Galectin-3 upregulation increased BMP signalling in vitro 183
5.2.5 Gal-3 regulated phosphorylation of Smads 1/5/8 186
5.3 Discussion 189
5.3.1 Gal-3 gain-of-function did not influence olfactory neuronogenesis and maturation 189
5.3.2 Pallidal neuronogenesis is limited postnatally 194
5.3.3 Striatal gliogenesis from the plSVZ 194
5.3.4 Upregulation of Gal-3 was accompanied by increased striatal astrocytic fate and maturity on the expense of oligodendrogenesis 198
5.3.5 BMP signalling was regulated by Gal-3 203
5.4 Conclusion 209

6 General Discussion 211

6.1 Galectin-3 regulates postnatal lSVZ lineage progression: Towards a molecular model 212
6.1.1 The link between the molecular and cellular effects of Gal-3 upregulation 214
6.1.2 A potential Gal-3-responsive subpopulation in the plSVZ 216
6.1.3 A possible molecular basis for the temporally diversified plSVZ responses to Gal-3 upregulation 217
6.1.4 A molecular model to explain Gal-3's cellular effects on the plSVZ 219
6.2 Limitations 223
6.3 Future directions 227

7 Appendices 231

7.1 Additional work not included in thesis 231
7.1.1 C1orf103 project 231
7.1.2 Investigating the role of Galectin-3 in neurogenesis after stroke in mice 231
7.1.3 Characterization of nuclear β-catenin Gal-3 knockout mice 231
7.1.4 Evaluating the effects of the cancer-related IDH1 R132H on the brain 232
7.2 Appendix: Solutions and recipes 233
7.3 Appendicular figures 236
7.4 References 239

List of Figures

Figure 1.1 Development of the subventricular zone 24
Figure 1.2 The adult SVZ niche 27
Figure 1.3 Heterogeneity of the postnatal SVZ 34
Figure 1.4 Canonical Wnt/β-catenin signalling 44
Figure 1.5 Structure and oligomerisation of Gal-3 48
Figure 1.6 Summary of Thesis Hypotheses and Aims 56
Figure 3.1 Gal-3 and β-catenin co-expression in the aSVZ lineage 89
Figure 3.2 Gal-3 and β-catenin co-expression patterns in the aSVZ 90
Figure 3.3 Gal-3 was bound to β-catenin in the SVZ 93
Figure 3.4 Gal-3 construct validation 97
Figure 3.5 Gal-3 and Wnt/β-catenin signalling were downregulated with plSVZ lineage progression 99
Figure 3.6 Gal-3 regulated Wnt/β-catenin signalling in vivo 101
Figure 3.7 Gal-3 regulated Wnt/β-catenin signalling in vitro 104
Figure 3.8 Wnt/β-catenin signalling was downregulated with increased survival in vitro 105
Figure 3.9 Gal-3 OE reduced plSVZ proliferation 107
Figure 3.10 More Gal-3 overexpressing neuroblasts reached the RMS 110
Figure 3.11 Proliferation dynamics after Gal-3 OE 112
Figure 3.12 Acute cell non-autonomous anti-apoptotic effects of Gal-3 114
Figure 4.1 Chronic Gal-3 upregulation did not alter NSC activation or SVZ cell proliferation 17 DPE 138
Figure 4.2 Gal-3 overexpression did not alter NSC activation or SVZ cell proliferation 7 DPE 139
Figure 4.3 Proliferation and cell cycle re-entry were not altered by Gal-3 overexpression 7 DPE. 140
Figure 4.4 Sox2 expression is not influenced by Gal-3 overexpression 142

Figure 4.5 Gal-3 upregulation did not change the proportion of cells with radial morphology....143
Figure 4.6 Gal-3 OE did not change Mash1 or Olig2 expression....146
Figure 4.7 Neuroblast production was unimpeded by Gal-3 upregulation....148
Figure 4.8 Gal-3 overexpression did not influence stemness or self-renewal in vitro....150
Figure 4.9 Developmental CD45 expression was not influenced by Gal-3 upregulation....152
Figure 4.10 Ependymal S100β expression did not vary after Gal-3 overexpression....153
Figure 5.1 Gal-3 did not alter olfactory neuronogenesis 7 DPE....171
Figure 5.2 Olfactory neuronal differentiation was not affected by Gal-3 OE 17 DPE....172
Figure 5.3 limited Pallidal neuronogenesis from the plSVZ....174
Figure 5.4 Gal-3 upregulation increased striatal gliogenesis from the plSVZ....176
Figure 5.5 Gal-3 overexpression increased astrocytic differentiation and fate-choice....178
Figure 5.6 Gal-3 overexpression reduced striatal oligodendrocytic fate-choice from the plSVZ....180
Figure 5.7 Gal-3 overexpression increased Smad1/5/8 phosphorylation in vivo....182
Figure 5.8 In vitro Gal-3 upregulation increased BMP signalling....185
Figure 5.9 Gal-3 regulated Smad phosphorylation....188
Figure 6.1 Summary of Gal-3's role in regulating plSVZ neurogenesis....213
Figure 6.2 A model to explain Gal-3's effects on the plSVZ....220

List of Tables

Table 1.1 Selected signalling pathways regulated by and binding partners of Galectin-3....50
Table 2-1. Primers used for PCR, cloning, and sequencing....61
Table 2-2. Short-hairpin sequences....64

Abbreviations

a-a	amino acids
AJ	adherens junctions
ANOVA	analysis of variance
aSVZ	adult SVZ
BMP	bone morphogenetic protein
BrdU	5-bromo-2'-deoxyuridine
CNTF	ciliary neurotrophic factor
CRD	Carbohydrate recognition domain
CSF	cerebrospinal fluid
DAPI	4',6-diamidino-2-phenylindole
Dcx	doublecortin
DG	dentate gyrus
dGFP	destabilised green fluorescent protein
Dkk	Dickkopf
dlSVZ	dorsolateral SVZ
DPE	days post electroporation
dSVZ	dorsal SVZ
E2	embryonic day 2
ECM	extracellular matrix
EdU	5-ethynyl-2'-deoxyuridine
EGF	epidermal growth factor
eSVZ	embryonic SVZ
FACS	Fluorescent activated-cell sorting
FAK	focal adhesion kinase
FGF	fibroblast growth factor
FGFR	fibroblast growth factor receptor
FSC	forward scatter
Fz	frizzled
Gal	Galectin
Gal-3	Galectin-3
Gal-3 OE	Galectin-3 overexpression

GF	growth factors
GFAP	glial fibrillary acidic protein
GRP	glial restricted progenitors
Gr-N	granule neuron
GSK-3β	glycogen synthase kinase 3β
hipk1	homeodomain-interacting protein kinase 1
HRP	horseradish peroxidase
I°	primary
IB	immunoblotting
IGF	insulin-like growth factor
II°	secondary
IP	immunoprecipitation
JAK/STAT	Janus-kinase/signal transducer and activator of transcription
LGE	lateral ganglionic eminence
LIF	leukaemia inhibitory factor
LRP5/6	low-density lipoprotein-receptor-related protein
lSVZ	lateral (striatal) SVZ
LV	lateral ventricle
MAPK	mitogen-activated protein kinase
MFI	mean fluorescence intensity
MGE	medial ganglionic eminence
NCAM	neural cell adhesion molecule
NEC	neuroepithelial cell
NS	neurosphere
NSC	neural stem cell
NTD	N-terminal domain
p-β-catenin	phosphorylated β-catenin
P2	postnatal day 2
PB	phosphate buffer
PBS	phosphate buffered saline
PCR	polymerase chain reaction
PDGF	Platelet derived growth factor
PGC	periglomerular cell
PI3K	phosphatidylinositol-3 kinase

plSVZ	postnatal lateral SVZ
pSVZ	postnatal SVZ
Ptc	patched
qPCR	quantitative PCR
RGC	radial glial cell
RMS	rostral migratory stream
SC	stem cell
SDS-PAGE	sodium dodecyl sulfate polyacrylamide gel electrophoresis
sFrp	secreted frizzled-related protein
shGal-3	Galectin-3 knockdown shRNA
Shh	sonic hedgehog
shNT	non-targeting shRNA
Smo	smoothened
SSC	side scatter
SVZ	subventricular zone
TAP	transit amplifying progenitor
TBST	0.1M Tris buffered saline with 0.5% Tween-20
Tcf/Lef	T-cell factor/ lymphoid enhancer-binding factor
TGFα	transforming growth factor α
TLB	Triton-X-100 lysis buffer
TMEV	Theiler's Murine Encephalomyelitis Virus
vSVZ	ventral SVZ
Wnt	wingless

Chapter 1

1 Introduction 17

1.1 Stem cells and the stem cell niche *17*

1.2 Neural development: a brief look *22*

1.3 The postnatal SVZ: a unique NSC niche *25*

1.4 The heterogeneous output of the postnatal SVZ *32*

1.5 The regulation of pSVZ niche physiology *35*

1.6 Galectin-3: a potential regulator of pSVZ signalling *47*

1.7 Research Questions *52*

1 Introduction

1.1 Stem cells and the stem cell niche

1.1.1 Stem cells: definitions

Stem cells (SCs) exist in numerous mammalian tissues throughout development and some persist into adulthood. Stemness is a set of behavioural features SCs exhibit, and that can only be tested functionally. Interrogating stemness attributes often requires manipulating the cells themselves, or artificially changing their niche conditions, which can conceivably alter the SCs behaviour (Potten and Loeffler, 1990). Studying stem cell behaviour is therefore challenging and requires functional, morphological, and immunohistochemical examination both in vivo and in vitro. It is useful to first define SCs and their features before delving into studying their molecular regulation. SCs are relatively undifferentiated clonogenic cells that possess the following capabilities: (1) Proliferation, (2) self-renewal or self-maintenance, (3) regeneration of their home tissue after injury, and (4) production of a differentiated progeny of multiple lineages (Fuchs and Segre, 2000; Potten and Loeffler, 1990; Weissman, 2000).

Clonogenicity is the ability of a single cell to produce a large number of its progeny i.e. a clone. Proliferation is the process of cell division and can be symmetric or asymmetric. Symmetric cell division gives rise to identical daughter cells, which can be SCs (expanding symmetric division) or differentiated cells (symmetric terminal division). Asymmetric division (self-maintaining) produces one SC and one progenitor or differentiated cell (Nowakowski RS, 2002; Potten and Loeffler, 1990). Asymmetric cell division maintains the baseline SC population, whereas symmetric division is triggered

when additional SCs are needed; for example, after injury in order to regenerate the affected tissue (Lajtha, 1979b; Potten and Loeffler, 1990).

Differentiation is a qualitative state that characterises a cell wherein addition of specific gene products contributes to functional competence. Gradual accumulation of differentiation events can lead to a measureable quantitative maturation (Lajtha, 1979a; Potten and Loeffler, 1990). Differentiation can often be identified by immunolabelling for a specific differentiation marker or functional examination of functions specific to differentiated tissues; such as contractility in muscle cells and firing action potentials in neurons. Undifferentiated cells in contrast lack the expression of specialised gene products and do not perform tissue-specific functions (Lajtha, 1979b; Potten and Loeffler, 1990). Finally, the potency of SCs is their ability to produce progeny of multiple lineages, and this can vary across different developmental settings; from totipotent early embryonic SCs (ESCs) able to give rise to any cell in the organism, to tripotent adult neural SC (aNSC) capable of producing neurons, astrocytes, and oligodendrocytes (Kriegstein and Alvarez-Buylla, 2009; Potten and Loeffler, 1990; Weissman, 2000).

1.1.2 Studying stem cell behaviour: Practical considerations

A cell is defined as a SC once it has been empirically proven to possess the four defining stem cell characteristics. However, in practice, it may not be possible to sufficiently prove each feature (Potten and Loeffler, 1990). For example, to show a SCs ability to regenerate/repopulate a tissue, ablation of resident tissue cells either chemically or by irradiation is required, which is

artificial and may not always be experimentally feasible. In addition, a SC at any point might not display all stemness attributes; for example, a quiescent stem cell will not proliferate, but will retain the ability to do so (Yabut and Pleasure, 2014). Furthermore, proving certain stemness features like self-renewal and regeneration may require manipulating the cells in question, possibly altering their behaviour (Pastrana et al., 2011; Potten and Loeffler, 1990). Fortunately, identifying proliferation and differentiation can be sensitively achieved by morphological analysis and immunohistochemical labelling of mitotic and differentiation markers, respectively (Codega et al., 2014; Doetsch, 2003a; Pastrana et al., 2011). Therefore, studying stemness involves a combination of marker expression, functional, and morphological studies.

A transit population of progenitors exists between SCs and their differentiated progeny. These transit progenitors serve to amplify SC output, possibly protecting SCs from unnecessary genetic risks from repeated mitosis (Potten and Loeffler, 1990). Transit amplifying progenitor cells (TAPs) in the subventricular zone (SVZ) express markers of relatively more differentiated cells, like Dlx2 and Mash1, but retain the ability to proliferate (Ihrie and Alvarez-Buylla, 2011). In general, TAPs have limited self-renewal or self-maintenance potential at baseline (Potten and Loeffler, 1990), but can behave like SCs under special circumstances (Doetsch et al., 2002a). Contrasted with SCs, the hallmarks of TAPs are their high proliferative potential, limited self-maintenance, imminent differentiation, and restricted potency (Fuchs and Segre, 2000; Lajtha, 1979b; Potten and Loeffler, 1990). Although SCs can be heterogeneous in their marker expression or cell cycle dynamics, they are still

distinct from TAPs in those regards (Giachino et al., 2013; Ponti et al., 2013; Weissman, 2000). For example, activated NSCs re-enter the cell cycle more frequently than quiescent SCs, which stay in G_0 until recruited to proliferate (Codega et al., 2014). Moreover, long-term hematopoietic SCs (HSCs) persist throughout the life of the organism, whereas short-term HSC rapidly cycle approximately eight times before they cease self-renewal (Weissman, 2000). Interestingly, quiescence and activation are dynamic NSC states; it is possible for a NSC to switch from quiescent to active states and vice versa (Codega et al., 2014). Finally, SCs have a longer G_1 and a shorter S phase compared to TAPs. Thus, when examining SC proliferation, the heterogeneity of the proliferative cell population must be taken into account to allow valid data interpretation.

SCs usually occupy specialised niches that influence their activity. Niches are defined microenvironments composed of SCs, their progeny, support cells, extracellular matrix (ECM), blood vessels, soluble factors from the circulation or other sources, and in the case of NSC, nerve fibres (Fuchs and Segre, 2000; Ihrie and Alvarez-Buylla, 2011; Riquelme et al., 2008; Shen et al., 2008). Examples of SC niches include the bone marrow for HSC, hair follicle for bulge cells, intestinal crypts for intestinal SC, and the SVZ and subgranular zone of the dentate gyrus (DG) for NSCs (Fuchs and Segre, 2000). Importantly, niche components, both cellular and non-cellular, influence SC behaviour (Aguirre et al., 2010; Mercier and Douet, 2014; Song et al., 2012). To interrogate SC behaviour, investigating SCs in the context of their niche is required, and entails examining and possibly tracing the SC lineage (Spradling et al., 2001). The dynamic nature of SC marker expression,

lack of specific SC markers, and the heterogeneity of SCs and their niches can make identification of SCs in vivo based on marker expression alone more challenging (Mamber et al., 2013; Pastrana et al., 2011). Notably, examining the cellular niche components (see below) can facilitate SC identification based on their location or morphology (Aguirre et al., 2010; Ihrie and Alvarez-Buylla, 2011; Mirzadeh et al., 2008). A caveat in studying SCs is that the defining SCs attributes like self-maintenance and multipotency can be more easily appreciated on a population scale. This can be especially true when SCs do not display all their defining features within the time-constraints of the study, making data interpretation more complicated (Taverna et al., 2014). In fact, recent evidence from the SVZ NSC niche indicates that stemness is maintained at population level, and individual NSCs are depleted once activated, which requires the niche to activate additional quiescent NSCs later on to maintain the niche's neurogenic output (Calzolari et al., 2015). In sum, SC features can be better appreciated and studied in the context of their niche and progeny.

This thesis is limited to investigating NSCs, which will be considered in the context of the SVZ niche only, wherein different states of NSC activation coexist in a specialised niche with lineage-restricted TAPs and more differentiated progeny (Potten and Loeffler, 1990; Riquelme et al., 2008). The population size is coupled to physiological demands by controlling the rate of growth, migration, differentiation, and death. If more differentiated cells are required NSCs can re-enter the cell cycle and their progeny subsequently progresses through the lineage to provide the required cells. The population's growth rate; the proportion of new cells per unit time, is determined by the

length of the cell cycle, the proportion of the population in the cell cycle (growth fraction), and the balance between cell cycle re-entry and exit. Importantly, one can assume the population to be normally distributed across the different cell cycle phases (Nowakowski RS, 2002; Ponti et al., 2013). Taking these concepts into consideration, interrogating the population's proliferative dynamics supplemented with appropriate marker labelling can highlight both NSC and TAP features; making this a suitable platform to examine the molecular regulation of NSC behaviour.

Establishing lineage relationships between NSCs and their progeny on single-cell basis is difficult when interrogating NSCs at population-level. To that end, live imaging of labelled cells (Ortega et al., 2011), sparse labelling of NSCs and progeny (Calzolari et al., 2015; Fuentealba et al., 2015), or unique labelling with DNA tagging (Fuentealba et al., 2015) can be employed. In this thesis, I examined NSCs at population-level and their progeny in the SVZ niche using a combination of marker expression, morphological, and functional studies.

1.2 Neural development: a brief look

The postnatal and adult SVZ niches are on a continuum of neural development, thus, it is useful to briefly consider neural development. In the embryo, early neuroepithelial cells (NECs) lining the neural tube and then radial glial cells (RGCs) act as founding SC for almost all neurons and glial cells in the forebrain. RGCs are polarised such that they contact the developing ventricles (neural tube cavity) apically, and extend a long process to the pial surface basally. Like other glial cells in the astrocyte lineage,

murine RGCs contain glycogen granules, contact vasculature, and express astroglial markers such as glutamate transporters, brain lipid-binding protein (BLBP), and Tenascin-C, Nestin, Vimentin, and RC1 and RC2 epitopes (Mori et al. 2005). In mouse, the neurogenic process starts around embryonic day E9-10 with neuroepithelial cells transforming into RGC, which reside in the ventricular zone (VZ). The pallial VZ gives rise to the neocortex, whereas the subpallial VZ produces the basal ganglia. RGCs switch later in development from symmetric cell division, favoured previously by NEC, to asymmetric neurogenic divisions (Kriegstein and Alvarez-Buylla, 2009; Noctor et al., 2008). The subpallial embryonic SVZ (eSVZ) appears between E10.5-13.5 as distinct aggregations of progenitors appear beneath the VZ in regions identified as medial, lateral, and caudal ganglionic eminences (MGE, LGE, and CGE, respectively)(Brazel et al., 2003b). eSVZ progenitors are different from RGCs in that they predominantly divide symmetrically, and do not vary their nuclear position in respect to the ventricular surface in different cell cycle phases: an RGC-specific phenomenon called interkinetic nuclear migration. In addition, the eSVZ is believed to contribute interneurons and projection neurons as opposed to VZ-derived cortical projection neurons (Brazel et al., 2003b; Kriegstein and Alvarez-Buylla, 2009). Neurogenesis in the VZ and eSVZ continues to add neurons in an inside-out manner, with deeper cortical layers being born earlier than superficial layers -with the exception of cortical layer I, and gradually ceases before birth (Kriegstein and Alvarez-Buylla, 2009; Levers et al., 2001). Towards the end of embryogenesis, glial cells constitute the main output of the VZ and SVZ, with more astrocytes being produced than oligodendrocytes. In the first postnatal week, roughly equal

numbers of astrocytes and oligodendrocytes are produced, however, the balance later shifts in favour of oligodendrocytic production, which persists into adulthood (Lyck et al., 2007; Parnavelas, 1999). Notably, VZ NSCs persist postnatally and give rise to bona fide undifferentiated NSCs capable of self-maintenance, proliferation, multi-lineage differentiation, as well as niche regeneration after injury. These NSCs mainly reside postnatally in the SVZ of the lateral ventricles (LV) (Alvarez-Buylla and Lim, 2004; Doetsch, 2003b; Fuentealba et al., 2015; Merkle et al., 2004). Therefore, the embryonic NSC niche first gives rise to neurons then glial cells, and maintains NSCs postnatally (Figure 1.1).

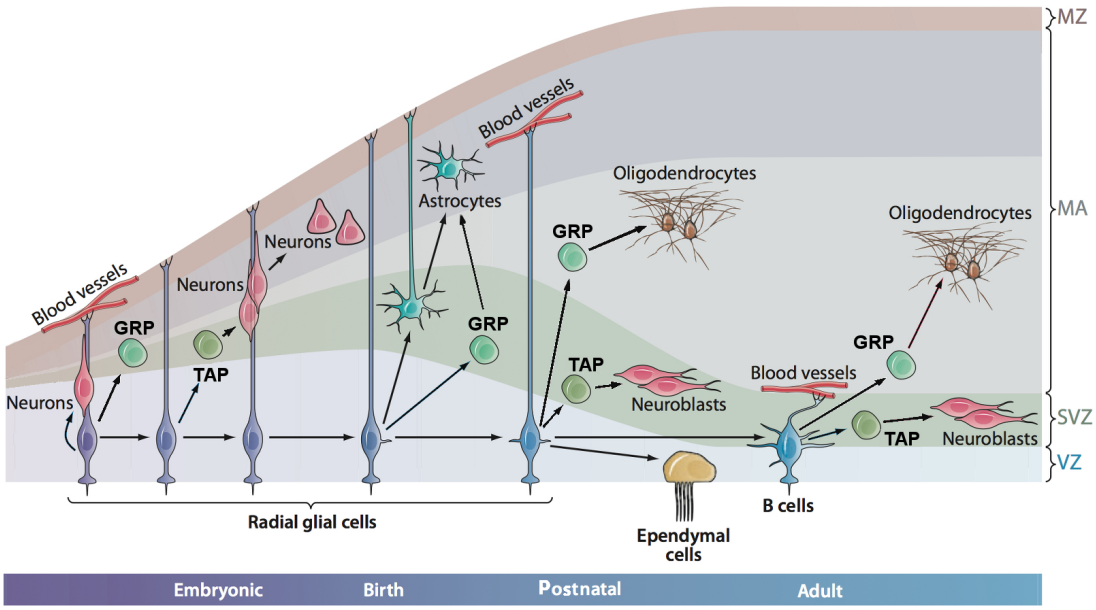


Figure 1.1 Development of the subventricular zone

Cartoon depiction showing the development of the subventricular zone (SVZ) niche in the ventricular wall, from late embryonic to adult life. Radial glial cells (RGCs) are the neural stem cells (NSCs) during embryonic and early postnatal periods in the ventricular zone (VZ) and the SVZ, respectively. Embryonic output of the VZ/SVZ is predominantly neural, with young migratory neurons (called neuroblasts) migrating radially along RGC processes into the mantle area (MA). An intermediate phase of amplification occurs at the level of transit amplifying progenitors (TAPs). Later on in the postnatal SVZ (pSVZ), neuroblasts migrate tangentially to the olfactory bulb. This continues in adulthood through specialised glial tubes that unsheathe the migratory neuroblasts. Astrocytes develop from late embryonic and early postnatal VZ and SVZ RGC by direct RGC transformation or through glial restricted progenitors (GRP). Later on in pSVZ and adulthood, GRP contribute to astrocyte and oligodendrocyte production. Ependymal cells are born around birth and mature during the first postnatal week. RGCs give rise to the adult NSC (Type-B cells). Modified from (Kriegstein and Alvarez-Buylla, 2009). MA: mantle area, MZ: marginal zone.

Postnatal neurogenesis continues into adulthood in two major neurogenic niches, the larger postnatal SVZ (pSVZ) and the smaller DG in the hippocampus (Kriegstein and Alvarez-Buylla, 2009). This thesis will be limited to exploring postnatal regulation of neurogenesis in the pSVZ and not the DG.

1.3 The postnatal SVZ: a unique NSC niche

1.3.1 Development of the postnatal SVZ

After birth, the receding VZ and underlying eSVZ give rise to progenitors and NSC of the postnatal and adult SVZ. RGCs gradually give rise to glial cells and NSCs over the first 2-3 weeks of postnatal life (Fuentealba et al., 2015; Kriegstein and Alvarez-Buylla, 2009; Merkle et al., 2004; Peretto et al., 2005; Tramontin et al., 2003). The pSVZ enlarges in the first postnatal week only to shrink in thickness during the third and fourth postnatal weeks, at which stage it becomes difficult to distinguish it from the adult SVZ (aSVZ) (Peretto et al., 2005; Tramontin et al., 2003). This postnatal period is characterised by robust gliogenesis that slows down after the second postnatal week (Levison and Goldman, 1993). Thus, it can be concluded that the pSVZ lasts from birth until the end of the third postnatal week. At that stage, all RGCs have already transformed into ependymal cells and astrocytes, a subset of which are the bona fide NSCs that persist into adulthood.

Until recently it was unclear whether eSVZ and pSVZ NSCs share lineage relationships, and whether both neuronal and glial progeny were clonally related. Early reports indicated that oligodendrocytes do not share a lineage with astrocytes (Luskin and McDermott, 1994; Luskin et al., 1993), whereas other reports documented the opposite (Levison and Goldman,

1993, 1997). Similarly, a shared clonal lineage between neurons and oligodendrocytes was documented by some groups (Menn et al., 2006), but not by others (Ortega et al., 2013). Recently, an elegant study by the Alvarez-Buylla group demonstrated using DNA barcoding of labelled embryonic RGCs that pSVZ NSCs originate from RGCs born before E15, after which they diverge from other embryonic RGCs and remain quiescent until activated postnatally. Significantly, pSVZ NSCs gave rise to clonally related olfactory neurons, astrocytes, and oligodendrocytes, as well as neurons in different parts of the forebrain (Fuentealba et al., 2015). Therefore, it is now evident that NSCs in the postnatal and adult SVZ are multipotent in vivo and are derived from early embryonic NSCs.

1.3.2 The neurogenic lineage and niche: a closer look

The pSVZ niche is transient and gradually changes into a mature aSVZ niche. Also, almost all studies characterising niche components focused on the aSVZ (Ihrie and Alvarez-Buylla, 2008, 2011; Lim and Alvarez-Buylla, 2014). Thus, it will be useful to describe the fully developed aSVZ then emphasise the key differences between the aSVZ and pSVZ niches. Similar to other SCs niches, the aSVZ has both cellular and non-cellular components (Figure 1.2). The cellular components of the niche include ependymal cells, astrocytes, progenitors, endothelial, and microglial cells (Ihrie and Alvarez-Buylla, 2011). Multi-ciliated (E1 cells) and bi-ciliated (E2) ependymal cells line the ventricular lumen and regulate cerebrospinal fluid (CSF) flow and NSC behaviour (Lim et al., 2000; Mirzadeh et al., 2008). aSVZ astrocytes express GFAP and are called Type-B cells, a subset of which are the bona fide NSCs of the niche

(Doetsch, 2003a; Doetsch F et al., 1999). NSCs are termed Type-B1 cells and are bipolar in morphology with an apical process carrying a primary cilium protruding between ependymal cells and a basal process contacting a blood vessel away from the ventricular lumen (Mirzadeh et al., 2008).

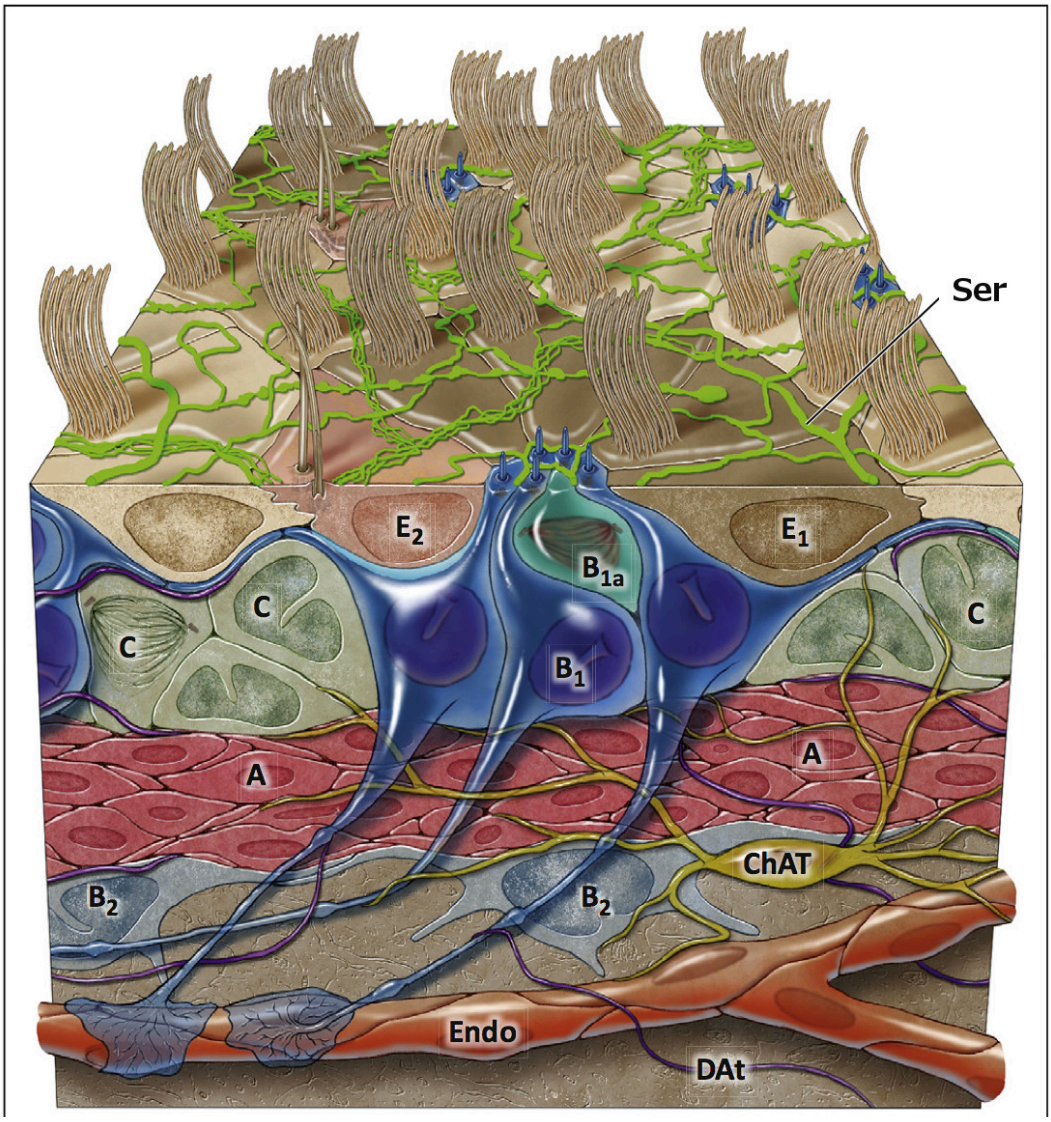


Figure 1.2 The adult SVZ niche

Cartoon showing the adult SVZ niche. NSCs are bipolar astrocytes and are called Type-B1 cells (dark blue). Once activated (B1a; light blue) they give rise to rapidly proliferating TAPs called type-C cells (green) which, after 3-4 rounds of mitosis, produce migratory neuroblasts called type-A cells (pink). Neuroblasts are shielded from the striatum by niche astrocytes (B2 cells: navy blue). B1 cells contact the ventricle with an apical process that bears a primary cilium. This process intervenes between multi-ciliated and bi-ciliated ependymal cells (E1 and E2 cells; brown). E cells surround central apical processes of B1 cells in a pinwheel structure. The basal process of B1 cells contacts endothelial cells lining leaky SVZ blood vessels (Red). On the ventricular surface there is a rich network of serotonergic axons (Ser; bright green). Choline acetyltransferase (ChAT)-positive neurons on the SVZ boundary innervate the SVZ (olive brown) [51]. Dopaminergic terminals (DAt; purple) innervate SVZ cells as well. Modified from (Lim and Alvarez-Buylla, 2014).

Niche astrocytes (Type-B2 cells) are multipolar GFAP+ cells that separate the niche from the neighbouring striatum, but are thought to be non-neurogenic (Doetsch et al., 1997). Type-B1 astrocytes are heterogeneous in marker expression and proliferative potential; activated NSCs (Type-B1a) express epidermal growth factor receptor (EGFR) and are highly proliferative, whereas quiescent Type-B1 cells lack EGFR expression and are typically in the G_0-phase of the cell cycle. Activated Type-B1 cells give rise to rapidly proliferative Mash1+ TAPs (Type-C cells) which amplify the progeny by re-entering the cell cycle 3-4 times (Ponti et al., 2013). Once exhausted, TAP progeny differentiates into doublecortin+ (Dcx) neuroblasts (Type-A cells), which migrate through the rostral migratory stream (RMS) to the olfactory bulb (OB) where they differentiate into periglomerular cells (PGCs) and granule neurons (Gr-N). NSCs and TAPs express Sox2, but expression is downregulated in neuroblasts (Pevny and Nicolis, 2010). Notably, TAPs can be either neurogenic, or gliogenic, but not both (Ortega et al., 2013). TAPs giving rise to glia are called glial restricted progenitors (GRP) here. GRPs can give rise to astrocytes (Sohn et al., 2015) and/or oligodendrocytes that migrate radially into the neighbouring parenchyma (Menn et al., 2006). Recently, it was shown that once quiescent NSCs are activated, they undergo several rounds of TAP production before being completely exhausted and depleted, making way for new quiescent NSCs to be activated afterwards (Calzolari et al., 2015). Thus, neurogenic lineage progression from NSCs to neurons passes through rounds of amplification in TAPs, and migration of differentiated progeny to their final destinations.

The neuronal progeny of the pSVZ integrates into the layers and circuitry of the OB. For example; Gr-Ns establish synaptic contacts with dendrites of mitral and tufted cells: the output cells of the OB. These inputs are required for olfactory discrimination and long-term olfactory memory (Butti et al., 2014). After injury, rodent newborn SVZ neuroblasts migrate into injured sites and contribute to neural replacement (Arvidsson et al., 2002) as well as neuro-protection by secretion of trophic factors (Butti et al., 2014). Astrocytes perform numerous functions in the nervous system, which include: maintenance of the blood-brain barrier, regulation of blood flow, synapse formation and maintenance, nutrient supply, waste product removal, secretion of trophic factors, and response to injury (Wang and Bordey, 2008). Mature oligodendrocytes myelinate nerve axons and maintain neural conductivity, while immature oligodendrocytes and oligodendrocytic precursors serve as reserves for cell turnover, renewal, and response to injury (Bradl and Lassmann, 2010).

Other cellular niche components do not share embryonic origins with previously described SVZ cells. For starters, microglia are derived from early embryonic myeloid precursors and mediate immune functions like immune surveillance. Additionally, they regulate proliferation and differentiation of NSCs and their progeny (Sato, 2015). Moreover, SVZ blood vessels are mesenchymal in origin and the endothelial cells that line them communicate with SVZ cells including NSCs and TAPs regulating quiescence and proliferation. Importantly, compared to other non-neurogenic brain regions, SVZ blood vessels are leaky and lack an intact blood brain barrier (Ottone et al., 2014; Tavazoie et al., 2008). Input from neurons outside the niche can

regulate NSC behaviour. For example, the dopaminergic, cholinergic, GABAergic, and serotonergic innervation of aSVZ cells regulates SVZ cell proliferation (Figure 1.2)(Ihrie and Alvarez-Buylla, 2011; Lim and Alvarez-Buylla, 2014). In sum, diverse niche cells expose the neurogenic lineage to humoral, immune, and neural signals that regulate key aspects of NSC function.

Non-cellular niche components include an extracellular matrix (ECM) that is continuous with the vascular basement membrane and contains Collagen IV, heparan and chondroitin sulphate proteoglycans, Tenascin-C, and laminins (Gattazzo et al., 2014). Other non-cellular components include soluble factors from the CSF, blood, and resident cells. These include growth factors (GF), cytokines, neurotransmitters, and enzymes. ECM Proteoglycans can bind and regulate the availability of GFs and cytokines such as EGF, FGF and BMP (Douet et al., 2012; Ihrie and Alvarez-Buylla, 2011; Mercier and Douet, 2014). Thus, the aSVZ niche resides in a rich ECM that regulates the availability and impact of several soluble factors.

Several unique features distinguish the pSVZ from its adult counterpart (Figure 1.3). It is well established that the pSVZ and aSVZ continue to produce olfactory neurons after birth (Lois and Alvarez-Buylla, 1994; Luskin, 1993). However, the pSVZ is significantly thicker than the aSVZ, measuring up to 300μm compared to <100μm in adulthood (Figure 1.3B) (Fiorelli et al., 2015). In parallel, the pSVZ has a higher neurogenic potential than the aSVZ. In fact, more than 75% of olfactory neurons originate in the pSVZ (Bayer, 1983). In addition, limited cortical and striatal neurogenesis can be observed in the pSVZ (Bandeira et al., 2009; Levison and Goldman, 1993).

Furthermore, the pSVZ is highly gliogenic and is characterised by robust astrocytogenic and oligodendrogenic potentials (Marshall et al., 2003). Interestingly, the pSVZ harbours eSVZ progenitors from the MGE and LGE, which are thought to be mostly gliogenic GRPs (Brazel et al., 2003a). Similar to the aSVZ, GRPs migrate radially at roughly the same rostro-caudal level of their parent NSCs into the surrounding parenchyma (Goldman, 2003). Additionally, a subset of RGCs in the pSVZ transforms gradually into ependymal cells during the first four postnatal days, and the ependyma gradually matures later on in the first postnatal week caudo-rostrally, ventro-dorsally and medio-laterally (Spassky et al., 2005). This suggests that CSF flow, Noggin expression, and other ependymal functions are different between regions in the pSVZ, and between pSVZ and aSVZ niches. This carries implications on the establishment of chemo-repellent and chemo-attractant gradients observed in adults, and responsiveness of NSCs to different morphogens. Significantly, unlike the aSVZ, the NSC component of the pSVZ includes RGCs, adult-like (Type-B1) NSCs, and cells in transition. Because of this heterogeneity, NSCs of the pSVZ will be referred to as RGCs in early postnatal life, and as NSCs from P9 onwards. Additionally, glial tubes that unsheathe migratory neuroblasts do not fully form until roughly the last week of the first postnatal month, and chain migration occurs only in the third postnatal week (Peretto et al., 2005). Hence, the pSVZ is a unique NSC niche that gradually transitions from eSVZ-like to an aSVZ-like structure during the first postnatal 3 weeks or so. Despite these highlighted differences, pSVZ lineage progression is fundamentally the same as in aSVZ, hence the previous description of the aSVZ lineage will suffice.

In this thesis, I used both the adult and postnatal SVZ niches to address my research questions. In chapter 3, I used marker expression to characterize the expression of Galectin-3 (Section 1.5) and β-catenin in the aSVZ lineage. After confirming co-expression of these proteins, functional interrogation of NSC function with respect to Gal-3 expression was conducted in the pSVZ. Experiments presented in the chapters 4 and 5 were limited to the pSVZ.

1.4 The heterogeneous output of the postnatal SVZ

Neuronogenesis and gliogenesis in the pSVZ provide neurons and glia, respectively, but its precise cellular output varies in time and space. Clear examples of pSVZ temporal regulation can be appreciated when examining subtypes of OB neurons produced over time. For instance, tyrosine hydroxylase (TH)+ PGC and Parvalbumin+ external plexiform layer neuron production peaks during embryogenesis and the first postnatal week but declines afterwards. In contrast, calbindin and calretinin positive Gr-Ns are continuously generated throughout adulthood (Sequerra, 2014). Similarly, superficial Gr-N are produced more robustly during the first few postnatal weeks, but the aSVZ predominantly generates deep Gr-Ns (Sequerra, 2014). Temporal heterogeneity can also be appreciated when examining the glial progeny of the pSVZ. For example, pSVZ astrocytic production peaks around birth and decreases over the first two postnatal weeks (Parnavelas, 1999). In contrast, little oligodendrogenesis occurs around birth, but output peaks in the third and fourth postnatal weeks and is sustained into adulthood (Lyck et al., 2007). More specifically, when the dorsolateral pSVZ (pdlSVZ) of P2-3 rats

was labelled both astrocytes and oligodendrocytes were observed 4 weeks later; however, labelling of P14 pdlSVZ resulted in oligodendrocytes only. Additionally, early pdlSVZ derived oligodendrocytes populate the white and grey matters but later born cells only inhabit the white matter (Levison et al., 1993; Levison and Goldman, 1993). Thus, pSVZ gliogenic output varies with developmental age.

Regional variation in glial output also exists in the pSVZ such that each pSVZ region retains its embryonic positional identity (Figure 1.3A). This positional identity is paralleled with a molecular identity encoded by specific expression of transcription factor (TF) combination. For instance, RGC in the dorsal pSVZ (pdSVZ) express the TF Emx1 and give rise to neocortical and striatal astrocytes. Conversely, RGCs in the pdlSVZ and ventral pSVZ (vpSVZ) expressing Dbx1 and Nkx2.1 give rise to superficial dorsal and ventral striatal astrocytes, respectively (Tsai et al., 2012). Importantly, postnatal astrocytes were born along the trajectories of their parent RGCs. This is similar to the preserved positional and molecular identity of postnatal olfactory neurons. To elaborate, postnatal NSCs retain the molecular signature of their parent RGC during development (Young et al., 2007). For example, ventral NSCs give rise to deep Gr-N and calbindin+ PGCs, while NSCs in the dSVZ give rise to superficial Gr-N and TH+ PGC. Septal (medial) and anteriorly located NSCs produce Calretinin+ Gr-N and PGC. New olfactory neuronal types were recently identified and are derived from specific locations in the SVZ corresponding to expression distinct TF combinations (Merkle et al., 2013). Strikingly, superficial Gr-N cells and TH+ PGCs were clonally related to NSCs that produced cortical pyramidal neurons, while deep

Gr-N and Calretinin+ PGC were clonally related to NSCs that gave rise to striatal and septal neurons, respectively. Significantly, this pervasive regional/positional identity characterising NSCs was traced back to the position of embryonic parent RGCs (Fuentealba et al., 2015). Therefore, the pSVZ niche is heterogeneous with regards to its neurogenic and gliogenic output and this heterogeneity is temporally and regionally specified according to the embryonic transcriptional blueprint.

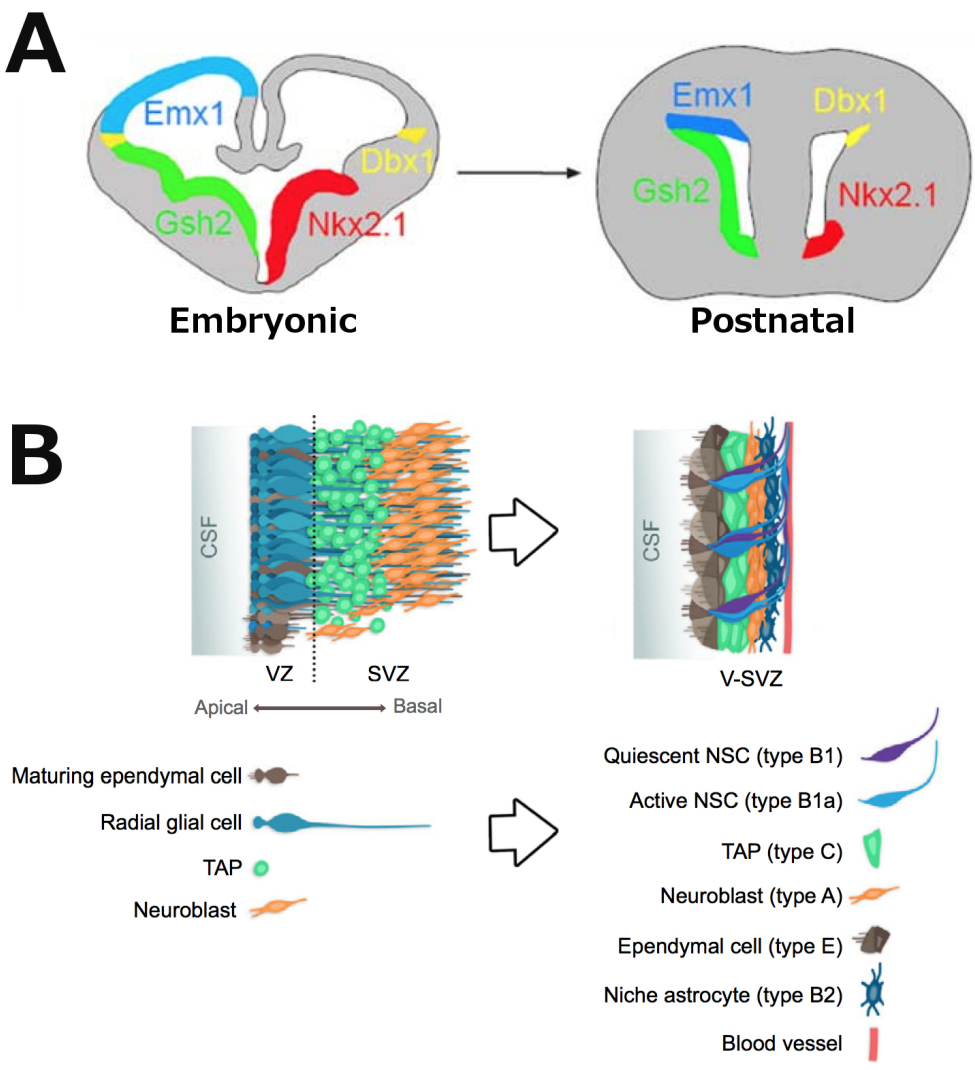


Figure 1.3 Heterogeneity of the postnatal SVZ

(**A**) Embryonic regional specialisation encoded by expression of the specific transcription factor combination is carried over into postnatal and adult SVZ niches. Modified from (Young et al., 2007). (**B**) The postnatal SVZ (Left) differs in structural origination from the adult SVZ (Right). Modified from (Fiorelli et al., 2015).

1.5 The regulation of pSVZ niche physiology

Diverse cellular and non-cellular constituents of the pSVZ niche provide a wide range of signals that can influence the behaviour of SVZ cells. Long-range signals can be produced in distant sites and are transported through the circulation (endocrine). Alternatively, signals can originate in neighbouring sites and diffuse locally (paracrine). On the other hand, local signals can influence the cell from which they were produced (autocrine). Other niche signals may be expressed on the surface of cells and are mediated upon cell-cell contact. Here, niche signals are divided into soluble, cell-bound, and morphogenetic signals. Simply put, niche signals are transduced across the cell membranes of SVZ cells to modify the activation levels of nuclear transcriptional programmes or cause epigenetic changes resulting in cell behavioural changes. These changes can be translated into a change in cell cycle status, differentiation properties, viability, or secretory activity. Significantly, these signals vary along the SVZ rostro-caudal and dorso-ventral axes, and the response of regionally heterogeneous cells across SVZ regions may well vary as well (Fiorelli et al., 2015). For example, dSVZ cells are not responsive to sonic hedgehog (Shh) compared to vSVZ (Ihrie et al., 2011), but are more responsive to wingless (Wnt) signalling than the lSVZ (Azim et al., 2014a). Additionally, NSC response to a signal depends upon the degree of stimulation (concentration) and the presence or absence of additional signals (context-dependent responses). For example, bone morphogenetic protein (BMP) signalling induces NSC quiescence in vitro in the presence of FGF2, but promotes terminal astrocytic differentiation in its

absence (Martynoga et al., 2013). I will next give a brief overview of the major SVZ niche signals and their transduction pathways.

1.5.1 Soluble factors

Soluble factors can influence cellular behaviour over short or long distances and include growth factors (GF), neurotrophic factors, cytokines, nutrients and many more. Here, I will discuss growth and neurotrophic factors. GFs and their receptors are extensively expressed in the SVZ. In general, GF receptors have intracellular tyrosine kinase activity that mediates signalling through mitogen-activated protein kinase (MAPK) and phosphoinisitide-3-kinase (PI3K) pathways.

Insulin-like growth factors 1 and 2 (IGF-I and IGF-II) have distinct roles on SVZ cells. IGF-I promotes differentiation while both of IGFI and IGF-II stimulate proliferation of SVZ cells. Furthermore, IGF-II has been shown to induce NSC self-renewal (Yuan et al., 2014; Ziegler et al., 2014; Ziegler et al., 2012). The MEK/ERK (MAPK pathway) and PI3K/pAkt pathways were demonstrated to be responsible for proliferative and pro-differentiation effects of IGF-I, respectively (Yuan et al., 2014).

Fibroblast growth factors (FGFs) are a family of 23 protein GFs, with FGF-2 being the most studied in the SVZ. FGF-2 is primarily produced by astrocytes, and binds to SVZ-expressed FGF receptors (FGFR1, FGFR2, and FGFR3). Upon binding, FGFRs dimerise and cross-phosphorylate specific tyrosine residues, which allow docking proteins to bind and activate PI3K/pAkt and Ras/Raf/MAPK pathways (Galvez-Contreras et al., 2012). FGF-2 signalling in the SVZ is mitogenic to embryonic and postnatal SVZ NSC and

TAP populations (Frinchi et al., 2008; Galvez-Contreras et al., 2012; Mudo et al., 2009). In vitro, FGF-2 is used to maintain NSCs in culture (Pastrana et al., 2011). Moreover, FGF-2 signalling has roles in increasing oligodendrogenesis through inhibition of glycogen synthase kinase 3β (GSK-3β) and upregulating Cyclin-D1 (Azim et al., 2014b; Frinchi et al., 2008).

Epidermal GF (EGF) is commonly used along with FGF-2 to maintain NSCs in vitro (Pastrana et al., 2011). It binds to the EGF receptor (EGFR) and promotes downstream signalling through PI3K, MAPK, and JAK/STAT pathways (Citri and Yarden, 2006). In vivo infusion of EGF increased SVZ cell proliferation and induced subependymal hyperplastic nodules. EGF was also shown to revert TAPs to activated NSC phenotype with increased self-renewal and multipotency (Doetsch et al., 2002a). Overexpression of EGFR in a subset of TAPs expanded the neural progenitor population and reduced the proliferation and self-renewal of NSCs through inhibition of notch signalling (Aguirre et al., 2010). Besides, it increased astrocytic differentiation into the striatum and OB (Kuhn et al., 1997) as well as oligodendrocytic differentiation of newborn SVZ cells into neighbouring white matter and parenchyma (Gonzalez-Perez et al., 2009). Related to EGF, TGFα is expressed by SVZ astrocytes and promotes progenitor proliferation redundantly with EGF (Ihrie and Alvarez-Buylla, 2011; Mudo et al., 2009). Platelet derived GF (PDGF) and vascular-secreted pigment epithelium-derived factor have also been demonstrated to promote NSC proliferation and self-renewal (Mamber et al., 2013; Ramirez-Castillejo et al., 2006). PDGF infusion into the LV induces hyperplastic nodules, as seen with EGF (Jackson et al., 2006).

Vascular endothelial GF (VEGF) signals through receptor tyrosine kinases (RTK) Flk-1 and Flt-1. VEGF is a mitogen for progenitors and is important for neurogenesis and angiogenesis (Faigle and Song, 2013). Intra-ventricular infusion results in increased SVZ cell proliferation (Schanzer et al., 2004), and activation of dormant neurogenic programmes in ependymal cells across the neuraxis (Luo et al., 2015).

Neurotrophic factors like neurotrophin 3 (NT-3), neurotrophin 4/5 (NT-4/5), brain derived neurotrophic factor (BDNF), and neural growth factor (NGF) are less well studied in the SVZ. However, studies on hippocampal neurogenesis found pro-proliferation and pro-differentiation effects for BDNF and NT-3. In contrast, SVZ neurogenesis was not stimulated by BDNF (Faigle and Song, 2013). However, vasculature-derived BDNF has been shown to regulate neuroblast migration, while NT-3 from the same source maintained NSC quiescence and inhibited their proliferation (Ottone and Parrinello, 2015). Ciliary neurotrophic factor (CNTF) is expressed by astrocytes and promotes both NSC self-renewal (Mudo et al., 2009) and astrocytic differentiation (Kanski et al., 2014).

1.5.2 Cell-bound signals

In contrast to the soluble factors described above, specific signals are bound on the surface of cells, and are transduced when ligands on one cell stimulate receptors on another cell. This requires cells to establish transient or long-term contacts. Interestingly, ECM and adhesion molecules are highly enriched in quiescent stem cells (Codega et al., 2014; Martynoga et al., 2013). Below are some of the major signals transduced upon adhesion and cell-cell contact.

1.5.2.1 Notch

Canonical Notch signalling involves binding of Notch receptors to membrane-bound Notch ligands (Delta and Jagged) on the surface of neighbouring cells. This is followed by cleavage of notch intracellular domain (NICD), which binds to CSL (RBP_{jk}) in the nucleus, and mediates transcription of downstream notch targets, such as TFs Hes and Hey, which inhibit neuronal differentiation programmes mediated by TFs Mash1 and Neurogenins (Imayoshi et al., 2013). Notch signalling has been shown to maintain NSC identity and proliferation in the SVZ, a state antagonised cell non-autonomously by EGFR signalling in neighbouring progenitors (Aguirre et al., 2010). Since both quiescent and activated NSCs actively signal through Notch, the signalling pathway has been proposed to regulate NSC activation (Basak et al., 2012; Giachino et al., 2013; Giachino and Taylor, 2014). Recently, SVZ blood vessel-derived Jagged-1 was shown to promote quiescence and NSC maintenance through activating canonical notch signalling on NSCs (Ottone et al., 2014).

1.5.2.2 Ephrins and Eph receptors

Eph receptors are tyrosine kinases that autophosphorylate in response to diverse Ephrin ligands expressed by neighbouring cells. Several signalling pathways are downstream of Eph-Ephrin signalling; these include MAPK, PI3K/pAkt, Src, and focal adhesion kinase (FAK) (Pasquale, 2008). In the SVZ, endothelial cells express Ephrin-B2 that activates Eph signalling on NSCs and subsequently suppresses MAPK activity and cyclin-D1 expression, thereby preventing NSC proliferation (Ottone et al., 2014).

1.5.2.3 Cell adhesion molecules: Integrins and Cadherins

Integrins are trans-membrane proteins that are heterodimers of α and β chains. They mediate adhesion to ECM components such as collagens, laminins, and fibronectin as well as some cell-surface molecules like vascular cell adhesion molecule (VCAM-1) (Chen et al., 2013), which is involved in NSC maintenance and quiescence (Kokovay et al., 2012). Adhesive signals can be transmitted through several pathways including PI3K, MAPK, and FAK (Chen et al., 2013). Examples of integrin-regulated SVZ functions are numerous; for instance, α6β1 integrin heterodimers facilitate neuroblast migration (Emsley and Hagg, 2003), NSC/TAP proliferation (Jacques et al., 1998; Sakaguchi et al., 2010) and survival (Leone et al., 2005). In addition, proliferating SVZ progenitors use α6β1 integrins to bind the vascular endothelium basal lamina (Ottone and Parrinello, 2015). Importantly, NSC self-maintenance through Notch signalling has been linked to integrin functions (Chen et al., 2013). Moreover, β1 integrin and linked kinases regulate astrocytic differentiation and fate choice in vitro (Pan et al., 2014).

Cadherins also participate in cell-cell adhesion through adherens junctions (AJ), which are formed extracellularly by homotypic E-cadherin contacts, and are linked to the actin cytoskeleton intracellularly through E-cadherin binding to α and β-catenins (Maher et al., 2009). Cadherin-mediated adhesion sequesters free cytoplasmic β-catenin that would otherwise be available for Wnt/β-catenin signalling, thereby controlling proliferation and differentiation of embryonic NSC/TAPs (Noles and Chenn, 2007). Interestingly, adult NSCs form AJ's with ependymal cells, and E-cadherin-dependent adhesion was shown to promote NSC self-maintenance

(Karpowicz et al., 2009). Moreover, inhibiting VCAM-1 function disrupts aSVZ niche architecture and leads to NSC depletion (Kokovay et al., 2012). Taken together, adhesive signals in the niche maintain NSC identity and preserve niche architecture.

1.5.3 Morphogens

Morphogens are molecules secreted from distinct sources to diffuse across a tissue forming a concentration gradient. Cells at various distances from the morphogenetic source are exposed to different concentrations of morphogens and respond distinctly by activating specific transcriptional programmes (Wartlick et al., 2009). Of note, GFs and adhesion related-molecules can serve as morphogens, and they include Wnts, Wnt antagonists such as secreted Frizzled-related proteins (sFrp), Cerebrus and Dickkopf (Dkk), BMPs, BMP antagonists like Noggin, Chordin and Folliastatin, Shh, retinoic acid, IGFs, and FGFs. During development, morphogens participate in neural induction, antero-posterior and dorso-ventral patterning of the nervous system (Pera et al., 2014). Morphogen gradients created during development can still be observed postnatally; for instance, Shh signalling is active in the ventral SVZ while Wnt signalling is more active dorsally. Postnatally, morphogens assume diverse functions; from mitogenic actions as seen with FGFs, IGFs, Shh, and Wnts, to fate determination as observed with Shh, Wnts, and BMP (Faigle and Song, 2013; Sequerra, 2014). Next, I will introduce three morphogenetic signalling pathways active in the pSVZ; Shh, Wnt/β-catenin, and BMP. More focus will be geared towards the last two pathways due to their relevance in following chapters.

1.5.3.1 Shh

Shh is mainly produced by neurons in the basal forebrain and brainstem, and could be transported anterogradely to distant sites. Shh protein is present in the CSF, DG, and neuropil around the vSVZ. Shh receptors Smoothened (Smo) and Patched (Ptc) are expressed in the vSVZ, however, Smo expression extends dorsally. Smo receptor is freed from tonic inhibition once Shh binds Ptc, resulting in the activation of Gli TFs (Alvarez-Buylla and Ihrie, 2014). Shh signalling is required for NSC maintenance, positional identity, and TAP proliferation (Alvarez-Buylla and Ihrie, 2014). Interestingly, NSCs primary cilium senses CSF Shh and Wnts, thereby mediating signalling through these pathways (Ihrie and Alvarez-Buylla, 2011). Ablation of primary cilia in NSCs results in similar phenotypes as seen in Shh or Smo loss; namely reduced NSC self-renewal and proliferation (Alvarez-Buylla and Ihrie, 2014; Tong et al., 2014). In the pSVZ, ventrally derived Calbindin+ Gr-N and PGCs are regulated by Shh signalling (Ihrie et al., 2011). Recently, Shh was shown to primarily function in the ventral SVZ and regulate neuroblast migration (Faigle and Song, 2013). In summary, Shh is important for NSC maintenance, proliferation, positional identity, and neuroblast migration.

1.5.3.2 Wnt

Numerous temporally and regionally varied Wnt proteins are expressed in the postnatal brain. Wnt glycoproteins Wnt1, Wnt5a, Wnt7a, and Wnt7b, and Frizzled receptor (Fz) proteins Fz3, Fz4, Fz7, Fz8, and Fz9 are expressed in the SVZ/RMS (Shimogori et al., 2004). Callosal oligodendrocytic precursors near the SVZ were proposed to be the main source of Wnt ligands in the

postnatal brain (Ortega et al., 2013). Interestingly, despite being secreted, Wnt ligands primarily mediate their action over short distances (autocrine and paracrine), especially at cell-cell contacts (Clevers and Nusse, 2012). Thus, Wnt is not a classical morphogen. In fact, all Wnts harbour a covalent lipid modification vital for secretion and receptor binding (Clevers et al., 2014). Hence, Wnt signals are well poised to function in stem cell niches, where short-range and adhesive signals are vital for maintenance of niche SCs (see above).

In canonical Wnt/β-catenin signalling (Figure 1.4), Wnt ligands bind and activate Fz proteins and co-receptors low-density lipoprotein receptor-related protein 5/6 (LRP5/6). The signal activates intracellular Dishevelled (Dvl) protein by phosphorylation, which subsequently inactivates GSK-3β, disinhibiting β-catenin. In addition, phosphorylated LRP5/6 binds Axin and sequesters it from the destruction complex, thereby reversing the inhibition on β-catenin. Cytoplasmic β-catenin accumulates and translocates into the nucleus, where it displaces the inhibitory TF Groucho from the T-cell factor/ Lymphoid enhancer-binding factor (Tcf/Lef) TF complex, thereby transactivating Wnt-driven transcriptional programmes like Axin2. In the absence of Wnt signalling, cytoplasmic β-catenin that is not complexed in the AJ's is quickly bound in the β-catenin destruction complex, which includes scaffolding proteins Axin, adenomatosis polyposis coli (APC), β-TrCP, Casein Kinase I (CK I), and GSK-3β. The latter kinases consequently phosphorylate β-catenin and prime it for ubiquitinylation and subsequent proteasomal degradation (Clevers and Nusse, 2012).

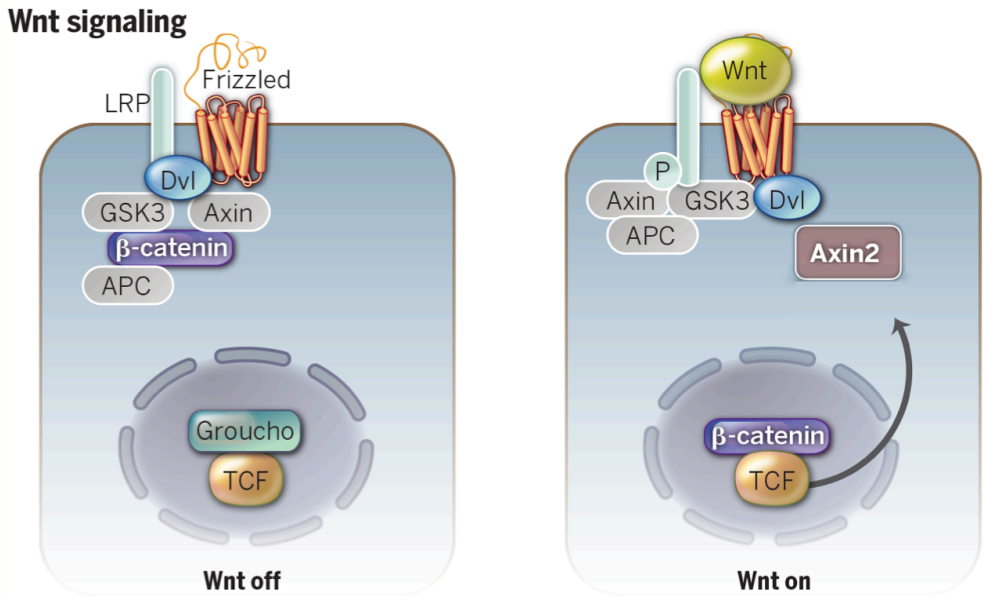


Figure 1.4 Canonical Wnt/β-catenin signalling

Canonical Wnt/β-catenin signalling is activated upon ligand binding to surface receptors, which free β-catenin from repression by the destruction complex containing GSK3β, APC, and Axin. Modified from (Clevers et al., 2014).

Canonical Wnt/β-catenin signalling has many function in the SVZ including: NSC maintenance (Qu et al., 2010), symmetric division of NSCs (Piccin and Morshead, 2011) and TAPs (Adachi et al., 2007), oligodendrocytic fate, glutamatergic olfactory neuronal subtype (Azim et al., 2014a), in vivo neuronal differentiation in the adult but not postnatal or embryonic SVZ (Marinaro et al., 2012), and in vitro proliferation and neuronal differentiation of NSCs/TAPs (Yu et al., 2006). Inhibitors of Wnt/β-catenin signalling, including Dkk1 and sFrp2, antagonise proliferative and NSC maintenance effects (Adachi et al., 2007; Piccin and Morshead, 2011). Of note, Wnt/β-catenin signalling was shown to be more active in the dSVZ compared with the lSVZ, both in adult and postnatal settings (Azim et al., 2014a; Azim et al., 2014b; Ortega et al., 2013). However, the plSVZ still retains long-lived Wnt responsive NSCs (Bowman et al., 2013). Because little is known about Wnt/β-catenin signalling in the plSVZ,

this thesis will focus on canonical Wnt/β-catenin signalling in that less-well studied region.

Non-canonical Wnt signalling through the planar cell polarity pathway involves Fz, Dvl, and APC, but not LRP5/6 or β-catenin. Briefly, this pathway controls asymmetric division such that the Wnt-source-proximal cells retains SC identity and the Wnt-source-distal daughter cell differentiates (Clevers et al., 2014). Because I focus on the interaction between Galectin-3 and β-catenin, canonical Wnt/β-catenin signalling is more relevant to my research questions, and non-canonical Wnt signalling falls out of the scope of this thesis.

1.5.3.3 BMP

BMP proteins are part of the transforming GF-β (TGF-β) superfamily of extracellular signalling molecules (Mehler et al., 1997). Postnatally, BMP 2, 4, 6, and 7, receptor serine threonine kinases BMPRIa, BMPRIb, and BMPRII, and BMP inhibitor Noggin are all expressed in the SVZ niche (Colak et al., 2008; Lim et al., 2000). Endothelial cells, astrocytes, NSCs, and TAPs express BMPs 2 and 4 in the adult SVZ (Hegarty et al., 2013; Lim et al., 2000). Conversely, ependymal cells express Noggin and LRP2, both of which are BMP antagonists (Lim et al., 2000; Sun et al., 2011). Upon binding to ligands, constitutively active BMPRII transphosphorylates BMPRI, which then recruits and phosphorylates receptor-regulated Smad proteins (R-Smads; Smad1, 5, and 8). R-Smads then hetero-dimerise with common-mediator Smad (Co-Smad; Smad4) and travel to the nucleus to mediate downstream transcriptional activation or repression (Hegarty et al., 2013).

In the aSVZ, baseline BMP signalling is required for allowing neurogenesis (Colak et al., 2008), but increased BMP levels suppress it. More specifically, increased BMP signalling reduces proliferation, induces cell cycle exit, and increases survival (Coskun et al., 2001; Gajera et al., 2010; Lim et al., 2000; Mercier and Douet, 2014). Moreover, BMP signalling regulates fate choices of SVZ progeny; for it promotes astrocytic fate choice and maturation (Bonaguidi et al., 2005; Ciceroni et al., 2010; Gomes et al., 2003) and suppresses oligodendrogenesis (Colak et al., 2008; Grinspan et al., 2000; Hegarty et al., 2013). In contrast, Noggin antagonises BMP's actions on proliferation and fate choices (Colak et al., 2008; Lim et al., 2000; Morell et al., 2014). Combined, a balance between BMP signalling and its antagonists regulates the SVZ niche proliferation and differentiation dynamics.

1.5.4 Crosstalk between pathways

Crosstalk between signalling pathways in the SVZ has been documented. For example, in vivo FGF2 infusion in the LV of postnatal mice pups inhibited GSK-3β and potentiated Wnt/β-catenin signalling in the pdSVZ, while EGF and BMP4 had the opposite effect (Azim et al., 2014b). In other contexts FGF2 and EGF activate PI3K/pAkt to inhibit GSK-3β (Galvez-Contreras et al., 2012). Similarly, BMP and Wnt/β-catenin signalling were reported to work together in promoting dorsal spinal cord neurogenesis (Hegarty et al., 2013). Furthermore, FGF2 suppresses BMP signalling effects on terminal astrocytic differentiation in vitro (Martynoga et al., 2013; Sun et al., 2011). It is thus apparent that considerable crosstalk between signalling pathways occurs and fine-tunes cellular responses to different combinations of extracellular signals,

and this can be widely variable depending on the context.

1.6 Galectin-3: a potential regulator of pSVZ signalling

1.6.1 Galectins in the subventricular zone

Galectins (Gal) are a family of 15 β-galactoside binding proteins that share a conserved carbohydrate recognition domain (CRD). There are three galectin subtypes: 1) proto-galectins (Gal-1, 2, 5, 7, 10, 11, 13, 14, and 15) harbour a single CRD, 2) chimeric galectins feature a single CRD and an N-terminal domain (NTD), and 3) tandem-repeat galectins (Gal-4, 6, 8, 9 and 12) carry two or more CRDs linked by a small peptide domain (Dumic et al., 2006). Gal-3 (29-35kDa) is the only known member of the chimera subtype, and its unique NTD allows it to form oligomers (Massa et al., 1993). Branched N-glycans on cell surface and ECM glycoproteins are the major ligands galectins bind to via their CRD domains (Boscher et al., 2011).

At the protein level, Gal-1 and Gal-3 are both expressed in the SVZ (Comte et al., 2011; Sakaguchi et al., 2006). Gals -1, -8, and -9 are expressed at lower levels compared with Gal-3 as detected by quantitative polymerase chain reaction (qPCR) (Al-Dalahmah, O. and Hillis, J. unpublished data). This thesis focuses on Gal-3 and not other members of the galectin family.

1.6.2 Gal-3: a closer look

Gal-3 shares its 130 amino acids (a-a) CRD in the C-terminus with other Galectins; however, Gal-3's C-terminus also houses an anti-apoptotic Asn-Trp-Gly-Arg (NWGR) domain homologous to that in Bcl-2 protein (Akahani et al., 1997; Dumic et al., 2006). Conversely, Gal-3 is unique in its NTD that

consists of 110-130 a-a, depending on the species (Ochieng et al., 1994). The first 12 amino acids in the NTD contain two serine residues the phosphorylation of which regulates the nuclear to cytoplasmic export of Gal-3 and its carbohydrate-binding affinity (Haudek et al., 2010). Moreover, it contains repeats of α-collagen-like sequence (Pro-Gly-Ala) that are amenable to digestion by matrix metalloproteases (Ochieng et al., 1998a). Finally, Gal-3 uses its NTD for oligomer formation and to participate in carbohydrate-independent protein-to-protein interactions (Haudek et al., 2010). The structure of Gal-3 is illustrated in Figure 1.5.

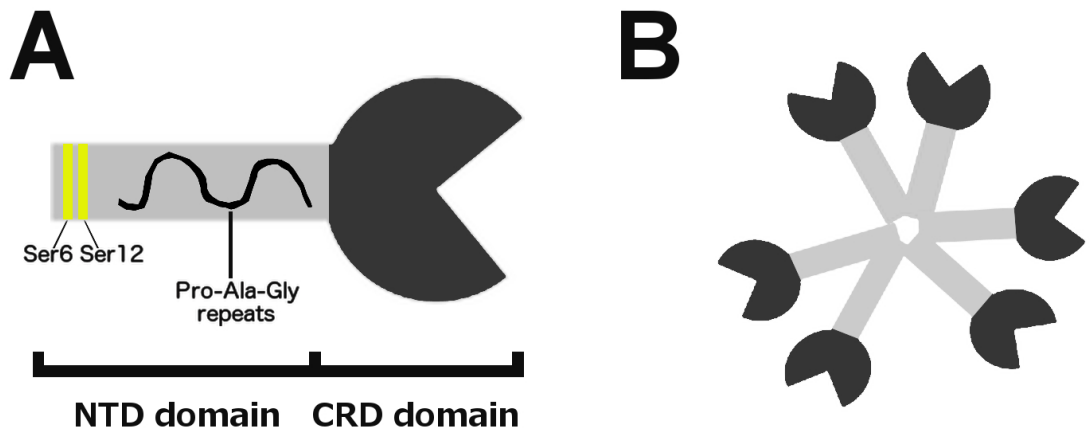


Figure 1.5 Structure and oligomerisation of Gal-3

(A) Major elements in Galectin-3 protein structure. (**B**) Oligomerisation of Gal-3. NTD: N-terminal domain, CRD: carbohydrate recognition domain.

Gal-3 distributes in both the intracellular and extracellular compartments despite lacking a classical secretion signal (Hughes, 1999). By binding cell-surface receptors, it forms a glycan-glycoprotein lattice that compartmentalises the cell membrane and regulates surface receptor membrane residency time and hence, signalling (Garner and Baum, 2008).

This was demonstrated for receptors like EGFR (Partridge et al., 2004), VEGFR2 (Markowska et al., 2011), and integrins (Ochieng et al., 1998b). Conceivably, Gal-3 mediates cell-cell adhesion by cross-linking glycoproteins on neighbouring cells (Henderson and Sethi, 2009) and also binds several ECM proteins like Collagen IV, Fibronectin, laminins, Hensin, and tenascins (Dumic et al., 2006).

Gal-3 has numerous binding partners due to the prevalence of glycosylation in most proteins. Thus, numerous functions in multiple tissues and cell lines have been attributed to Gal-3. By acting on cell surface receptors, Gal-3 regulates a multitude of signalling pathways. This thesis aims mainly to investigate the function of intracellular Gal-3. Table 1.1 shows a selection of Gal-3's binding partners and the signalling pathways it influences.

Intracellularly, Gal-3 localises to the cytoplasm and/or nucleus, and its functions include the regulation of apoptosis, signalling pathways, vesicular trafficking, and membrane-protein targeting (Dumic et al., 2006; Garner and Baum, 2008). In the nucleus, Gal-3 participates in pre-mRNA splicing and trans-activation of TFs like cyclic AMP response element binding protein (CREB), Sp1, and Nkx2.1 (Dumic et al., 2006). These TFs are involved in multiple signalling pathways, and Nkx2.1 is specifically involved in Shh signalling. Furthermore, Gal-3 binds β-catenin and Tcf-4 in breast cancer cell line, thereby regulating Wnt/β-catenin signalling (Shimura et al., 2004). Additionally, Gal-3 can inhibit apoptosis by binding Synexin to inhibit Cytochrome-C efflux from the mitochondria (Nangia-Makker et al., 2007). It also regulates EGFR trafficking by cooperating with Alix scaffolding protein in keratinocytes (Liu et al., 2012). Finally, Gal-3 prolongs EGF-induced K-Ras

activation in HEK293T cells, leading to augmenting and inhibiting PI3K and MAPK signalling, respectively (Elad-Sfadia et al., 2004).

Table 1.1 Selected signalling pathways regulated by and binding partners of Galectin-3

Binding partner (function)	Tissue/cell line	Signalling pathway	Reference
Integrin α1β1 (Adhesion)	Human breast cancer and fibrosarcoma	N/D	(Ochieng et al., 1998b)
NCAM, L1, MAG (Adhesion)	Mouse brain purified protein	N/D	Z(Rainer Probstmeier, 1995)
N-cadherin (AJ stabilization)	Mammary carcinoma cell line	N/D	(Boscher et al., 2012)
Integrin αvβ3 (Angiogenesis)	Human umbilical vein endothelial cells	FAK	(Markowska et al., 2010)
Integrin α3β1 (Formation of lamellipodia)	Corneal epithelial cells	FAK	(Saravanan et al., 2009)
NG2 (N/D)	Human glioblastoma cell lines	N/D	(Wen et al., 2006)
IGFR-I (Pro-Inflamamatory)	Mouse brain	JAK/STAT	(Lalancette-Hebert et al., 2012)
VEGFR2 (Angiogenesis)	Human umbilical vein endothelial cells	Membrane receptor retention	(Markowska et al., 2011)
Notch1 (Inhibition of differentiation)	HEK293 cells	Notch/NICD	(Nakajima et al., 2014)
N/D (Migration, angiogenesis)	BV2 microglial cell line	ILK, MAPK PI3K/pAkt,	(Wesley et al., 2013)
N/D (Pro-inflammatory)	Primary rat/mouse cortical microglia and astrocytes	JAK/STAT	(Jeon et al., 2010)
TGFβRII, EGFR (Decreasing Receptor recycling)	Melanoma, colorectal, breast, and other cancer cell lines	Smad2/3, MAPK	(Partridge et al., 2004)
Rb, CDK4, Cyclin D1 (Inhibition of Senescence)	Mouse embryonic fibroblasts, Human skin fibroblasts	Rb, CDK4-Cyclin-D1, Skp2-p27Kip1	(Kim et al., 2014)

Abbreviations: N/D: not determined. AJ: Adherens junction. ILK: Integrin linked kinase. JAK/STAT: Janus kinase/ Signal Transducer and Activator of Transcription. MAG: Myelin-associated glycoprotein. Rb: Retinoblastoma protein. CDK4: Cyclin-dependent Kinase 4. Skp2: S-phase Kinase-associated protein 2.

1.6.3 Galectin-3 in the SVZ

In the uninjured brain, SVZ ependymal cells, TAPs, and astrocytes- including a subset of NSCs, express Gal-3. Neuroblasts, on the other hand, do not. In Gal-3 null mice, neuroblast migration to the OB's is decreased, SVZ astrocytes exhibit more tortuous thicker processes, and ependymal cells display short sparse cilia. Overall proliferation in the SVZ was not altered by Gal-3 loss; however, classical long-term BrdU retention studies to examine long-term BrdU retaining SVZ NSCs were not conducted (Comte et al., 2011). After stroke, the Gal-3 nulls did not exhibit altered SVZ cell proliferation, apoptosis, or olfactory neurogenesis; however, they showed a decreased angiogenic response in the ischemic striatum, with concomitant absence of VEGF up-regulation (Young et al., 2014). Others groups demonstrated that Gal-3 was required for microglial activation and proliferation after stroke (Lalancette-Hebert et al., 2012). Moreover, in vitro oligodendrocytic fate choice and maturation were reduced in Gal-3 null SVZ NSCs (Pasquini et al., 2011). Additionally, Gal-3 loss caused defective microglial activation after demyelination, which was accompanied by disrupted oligodendrocytic differentiation and remyelination (Hoyos et al., 2014). Additionally, antibody-neutralization of Gal-3 function in the SVZ hampered stoke-induced neurogenesis, SVZ and endothelial cell proliferation, and angiogenesis (Yan et al., 2009).

1.7 Research Questions

Increasing evidence has shown that Gal-3 has context-dependent functions in different SVZ cells; regulating proliferation, fate choice, differentiation, migration, and angiogenesis. In doing so, Gal-3 was shown to influence multiple signalling pathways and to also mediate opposing roles depending on the system it was studied in and its subcellular and tissue localization. For example, extracellular and intracellular Gal-3 promoted and inhibited apoptosis, respectively (Nangia-Makker et al., 2007). Furthermore, Gal-3 was shown to activate, inhibit, or have no influence on MAPK signalling in different systems (Elad-Sfadia et al., 2004; Lalancette-Hebert et al., 2012; Wesley et al., 2013). Therefore, Gal-3 is a versatile regulator of various signalling pathways and cellular functions.

The function of Gal-3 in the pSVZ has not been investigated before. In fact, compared to the aSVZ, there are very few studies that focused on the pSVZ niche and lineage. Thus, this thesis aims to investigate the role of Gal-3 in the molecular regulation of pSVZ lineage progression and answer the following questions. Given the specific absence of Gal-3 from all neuroblasts, does Gal-3 expression need to be downregulated to allow lineage progression? Moreover, considering the lack of detailed analysis into the proliferative actions of Gal-3, does it impact upon NSCs activation or proliferation? Also, given that Gal-3 may regulate oligodendrocytic fate in vitro (Pasquini et al., 2011), does it influence fate choices in vivo in the pSVZ? The aforementioned research questions will be addressed in detail in chapters 3, 4, and 5, respectively. In chapters 3 and 5, I will explore the molecular underpinnings of Gal-3's actions in the pSVZ. More specifically, given the

importance of Wnt and BMP signalling in the SVZ, does Gal-3 functionally interact with these pathways?

Importantly, Gal-3 is a prognostic factor for and has functions in many cancers. It has been shown to positively regulate Wnt/β-catenin in multiple cancer cell lines. For example Gal-3 binds the β-catenin/Tcf complex in the cytoplasm and nucleus in colorectal carcinoma cell lines promoting transcription of cyclin-D_1 and c-Myc (Shimura et al., 2004). Gal-3 also positively modulates β-catenin activity through inactivation of GSK-3β via the PI3K/Akt pathway, which phosphorylates and inactivates GSK-3β (Song et al., 2009). Furthermore, Gal-3 knockdown increases degradation of β-catenin in pancreatic carcinoma (Kobayashi et al., 2011) and oral tongue squamous cell carcinoma (Zhang et al., 2013) cell lines. Consistently, Gal-3 overexpression stabilises β-catenin and promotes Wnt/β-catenin signalling in oral tongue squamous cell carcinoma (Wang et al., 2013). Gal-3 was additionally shown to bind Axin, which mediates GSK-3β-induced phosphorylation of both Gal-3 itself and β-catenin, priming the latter for ubiquitinylation and proteasomal degradation (Shimura et al., 2005). However, whether Gal-3 positively or even negatively regulates β-catenin in the pSVZ is unknown. I will explore this in chapter 3, with the aim of adding to what is currently known about the Gal-3-β-catenin interaction.

How individual signalling pathways are coordinated is a major hurdle in developmental biology. One potential mechanism is via proteins that regulate them in common. As I will describe in chapter 5, Gal-3 overexpression resulted in an astrocytogenic phenotype strongly suggestive of BMP signalling activity. Although Gal-3 had not been described previously to regulate BMP

signalling, I hypothesised that it did so in the pSVZ and indeed showed that this was true. I therefore have uncovered a novel function for Gal-3 as well as a mechanism that links and potentially coordinates two major signalling pathways in the pSVZ.

Most studies investigating Gal-3's function in the SVZ employed Gal-3 knockout animals. These constitutive knockout models are lead to Gal-3 loss-of-function throughout embryogenesis and postnatal life (Colnot et al., 1998). The Szele group has characterized the SVZ of Gal-3 null mice and found only a handful of deficits despite the numerous binding partners of Gal-3 (Comte et al., 2011). Additionally, in a preliminary work, I found no differences in SVZ lineage marker and β-catenin expression in Gal-3 nulls compared to controls. Given the redundancy of some of the functions mediated by some Galectins and their shared binding partners; e.g. Gal-3 and Gal-1 (Boscher et al., 2011), compensatory upregulation of other Galectins may mask the effects of Gal-3 loss-of-function in the knockout mice. Therefore, in this thesis, I used acute knockdown studies using Gal-3-specific shRNA plasmids that rapidly deplete Gal-3 protein levels. This is important because it minimizes the chances of compensatory mechanism confounding the effects of Gal-3 loss-of-function, allowing more confident analysis of Gal-3 specific functions in the SVZ.

When this work commenced, the research lines tackling Gal-3's functions in the Szele group focused on the use of Gal-3 knockout animals in disease states. For example, one study addressed the effects of Gal-3 loss on the SVZ response to stroke, and whether Gal-3 nulls exhibited increased susceptibility to parenchymal damage (Young et al., 2014). Another project examined whether Gal-3 loss altered the response of the SVZ to the

aspiration model of traumatic brain injury (Mundim, M. and Szele, F. unpublished). In addition, Gal-3 loss-of-function was studied in the context of inflammatory demyelination after infection with Theiler's Murine Encephalomyelitis Virus (TMEV) (James et al., 2015). A common feature between these disease models is that Gal-3 was upregulated in the SVZ following the different types of injury. In addition, other groups showed that Gal-3 was similarly upregulated after neonatal hypoxia-ischemia (Doverhag et al., 2010) as well as closed skull injury model (Venkatesan et al., 2010) of traumatic brain injury. The abovementioned disease models are characterised by a robust inflammatory response that accompanies Gal-3 upregulation. Therefore it is difficult to distinguish whether the effects of Gal-3 were related to inflammation, direct influences on the SVZ niche, or a combination of both. To disentangle SVZ-specific from inflammation-related Gal-3 functions, I used Gal-3 gain-of-function studies to increase Gal-3 levels without inducing an inflammatory response. More specifically, I employed Gal-3 overexpression in the pSVZ to unravel its role in the regulation of SVZ lineage progression, proliferation, and fate-choices. I also utilised Gal-3 loss-of-function in parallel with Gal-3 overexpression to examine how it influenced Wnt/β-catenin signalling both in vivo and in vitro. Finally, I attempted to provide a molecular model to explain Gal-3's functions in the pSVZ. These combined approaches, presented in this thesis provide novel insights into the roles of Gal-3 in the molecular regulation of pSVZ neurogenesis. Figure 1.6 summarises the hypotheses and aims of this thesis, and shows a schematic of the brain areas studied.

Hypotheses:

1. The downregulation of Gal-3 may be necessary to allow lineage progression.

2. Gal-3 regulates Wnt/β-catenin signalling in the SVZ

Aims:

1. Determine whether Gal-3 downregulation was necessary to allow lineage progression and neuroblast migration.
2. Examine whether and how Gal-3 gain-of-function influences NSCs activation, proliferation, or fate choices in vivo in the pSVZ.
3. Explore the molecular underpinnings of Gal-3's action on the postnatal SVZ in relation to Wnt/β-catenin and BMP signalling.

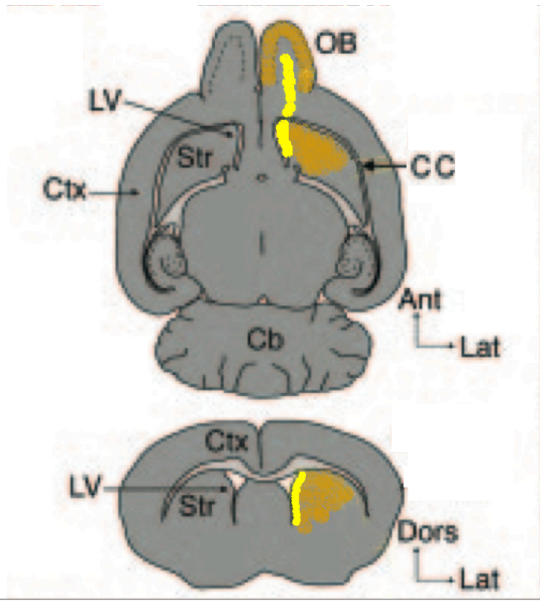


Figure 1.6 Summary of Thesis Hypotheses and Aims

The box on the left lists the main hypotheses examined in this thesis, and recounts the aims to be achieved from this study. The schematic on the right indicates the main brain structures studied in this thesis. The upper panel is a horizontal section through the brain, while the lower panel is a coronal section. The area marked in Yellow represents the SVZ-RMS niche. The lower right panel specifies that the lateral (striatal) SVZ as the main area of interest. The areas marked in Orange include the striatum and olfactory bulbs as additional structures studied in this thesis.
Abbreviations: Dors: Dorsal, Lat: Lateral, Ant: Anterior, Ctx: Cortex, Cb: Cerebellum, LV: Lateral Ventricle, CC: Corpus Callosum, OB: Olfactory Bulb.
Modified from (Merkle et al., 2004)

Chapter 2

Materials and Methods

2.1 Animals *58*

2.2 In vivo brain electroporation *58*

2.3 Thymidine analogue injection *59*

2.4 RNA extraction, DNA analysis and Cloning *59*

2.5 Protein isolation, Western blotting, and Immunoprecipitation *66*

2.6 Cell culture, Transfection, Nucleofection and Flowcytometry *70*

2.7 Histology and Fluorescent Immunohistochemistry *75*

2.8 Microscopy and Imaging *79*

2.9 Statistical Analysis *82*

2 Materials and Methods

2.1 Animals

All animal studies were conducted according to the Animals (Scientific Procedures) Act of 1986 (UK) and were covered under UK project licenses and my personal license. Mice were housed in individually ventilated cages on 12-hour light/dark cycles, with free access to food and water. Galectin-3 knockout (Gal-3 KO) mice were a gift from Francoise Poirier (Colnot et al., 1998) and were maintained on 129Sva background. Wildtype (WT) 129Sva were used as controls. C57BL/6 were used for in vivo electroporation, and ICR (CD1®) or C57BL/6 for *in vitro* neurosphere culture, nucleofection, and western blotting. For protein co-Immunoprecipitation 129sv, ICR (CD1®), or C57BL/6 mice were used. Both ICR (CD1®) and C57BL/6 mice were purchased from Harlan UK (Oxon, United Kingdom).

2.2 In vivo brain electroporation

The electroporation procedure was conducted in postnatal day 2 (P2) C57BL/6 mice as described in (Boutin et al., 2008; Fernandez et al., 2011; Platel et al., 2010). Plasmid solutions for electroporation were prepared at 2µg endotoxin free DNA/µl per plasmid in 0.1% fast green in Endotoxin-free water. Electroporation pipettes were made using Steolting 5/1, 1brl, GF glass pipettes pulled on a micropuller. 5µl per plasmid solution were pipetted into electroporation pipettes in preparation for the procedure. The electroporation procedure took less than 5 minutes per pup from anaesthesia to recovery stage. First, pups were anaesthetised by hypothermia (ice-immersion) for 2

minutes. Next, the scalp was cleaned with 70% ethanol and 1-2µl of Plasmid(s) solution was injected into the right lateral ventricle. The point of injection was 1mm posterior to the imaginary line extending from the right eye to the Lambda suture. Electroporation followed and entailed administering five 100V pulses each lasting 50-milliseconds (ms) with 850ms interval in between using CUY650-P5 tweezers (Sonidel) coated with electroconductive gel connected to a BTX ECM830 square wave electroporator. Finally, the pups were allowed to recover in a heated chamber set to 36°C for 15-20 minutes before being taken back to their mother. Animals were perfused 3 days post electroporation (DPE) at P5 (cohort 1); or 7DPE at P9 (cohort 2), or 17 DPE (cohort3). The success rate of the procedure was approximately 70% and the survival rate of test animals was >95%.

2.3 Thymidine analogue injection

5-Bromo-2′-deoxyuridine (BrdU; Sigma Aldrich) and 5-ethynyl-2′-deoxyuridine (EdU; Life Technologies) were dissolved in sterile normal Saline at 10 mg/ml. A single intraperitoneal (i.p.) injection of BrdU (50mg/kg) was given 2 DPE. This was followed by an i.p. dose of EdU (50mg/kg, i.p.) 24 hours later (3DPE), 2 hours before sacrifice.

2.4 RNA extraction, DNA analysis and Cloning

2.4.1 RNA extraction and cDNA synthesis

RNA was extracted from SVZ tissue or cell pellets using RNeasy Minikit (Qiagen) according to the manufacturer instructions. First, tissue or cells were lysed in an appropriate volume of RLT buffer (Qiagen) supplemented with 1% β-Mercaptoethanol (βME). Next, RNA was bound to a silica-based spin-

column, washed, and eluted in nuclease free water. RNA concentration and purity was determined using Nanodrop 1000 (ThermoScientific). 1µg of RNA was used to synthesise cDNA using High-Capacity RNA-to-cDNA kit (Life Technologies) in a 20µl reaction incubated at 37°C for 1 hour in a thermal cycler. cDNA was then stored at -20°C.

2.4.2 PCR and Gel electrophoresis

All polymerase chain reactions (PCR) were performed using Phusion® High-Fidelity DNA (New England Biolabs). The 50µl-reaction mix contained 1 unit of the polymerase, 1X Phusion Buffer, 0.5µM forward and reverse primers, 200µM dNTP's, 3% dimethyl sulfoxide (DMSO), and 250ng of the template. When plasmid DNA was template, 100ng was used. The PCR mix was incubated in thermal cycler according to this protocol: denaturation at 97° C for 3 min, then 34 cycles with denaturation at 97° C for 15 seconds, annealing at 55-72° C for 30 seconds, and elongation at 72° C for 1 min, followed by final elongation at 72° C for 5 minutes. The optimal annealing temperature for primers was determined using a temperature gradient PCR (55-72°C). PCR products were electrophoresed in a 1-1.5% Agarose gel (+5 µg ethidium bromide/100 mL Agarose) at 100-150V in TAE buffer and visualised on a UVP transilluminator (Bio-Rad). Gal-3 cDNA (NM_010705) was PCR-amplified from SVZ-derived cDNA and sequenced (SourceBioscience) to confirm construct fidelity. All single nucleotide polymorphisms (SNP's) found were synonymous. Primers sequences are detailed in Table 2.1.

2.4.3 DNA and RNA concentration and purity

DNA and RNA concentration and purity were determined by light absorption ratios at wavelengths 260/280 and 260/230 using a Nanodrop1000 (ThermoScientific). 260/230 values > 1.5 and 260/280 values >1.8 for DNA and >2.0 for RNA were considered good purity.

Table 2-1. Primers used for PCR, cloning, and sequencing

Primer name	Sequence	Function/comments
Gal-3 F	ATGGCAGACAGCTTTTCGCTTAACGATGCC	Forward and reverse primers to amplify Gal-3 cDNA
Gal-3 R	TTAGATCATGGCGTGGTTAGCGCTGGTGAG	
Actin_F	GCGGCGGCGCCCTATAAAAC	Internal control primers; bind to Actin transcript, to assess the success of PCR from cDNA
Actin_R	GACCCCGTCACCGGAGTCCA	
CAG_F	GCAACGTGCTGGTTATTGTG	Sequencing pCAGIG and derived plasmids
IRES_R	CTTATTCCAAGCGGCTTCGG	
Gal-3_e3_F	TACCCAGGGGCTGCTTATC	Bind to exon3 in Gal-3 cDNA, to check for success of Gal-3 cloning by sequencing
Gal-3_e3_R	GATAGCCTCCAGGAGCACTG	
5' aaaa-spacer_EcoRI_koz_Gal3F	aaaagaattcGCCACCATGGCAGACAGCTTTTCG	Forward primer to clone Gal-3 into pCAGIG; contains a spacer to allow efficient restriction, an EcoRI restriction site (both shown in lowercase), and a Kozak sequence to enhance translation
3' Spacer_NotI_Gal3R	tacgtagcggccgcTTAGATCATGGCG	Reverse primer to clone Gal-3 into pCAGIG, contains a spacer and a NotI restriction site (in lowercase)
SP6plus4_rev	CAACGATTTAGGTGACACTATAG	Sequencing pSilencer plasmids to assess success of cloning of short-hairpins
pSilen_F	AGCTTGTCTGTAAGCGGATG	

2.4.4 Plasmids

pCAGIG was a gift from Connie Cepko (Addgene plasmid # 11159)(Matsuda and Cepko, 2004). pCAG-Cre-IRES2-GFP (Addgene plasmid # 26646) (Woodhead et al., 2006) and pTOP-dGFP-CAG-mCherry (Mutch et al., 2009) were gifts from Anjen Chenn. pGL3-BRE Luciferase was a gift from Martine Roussel & Peter ten Dijke (Addgene plasmid # 45126)(Korchynskyi and ten Dijke, 2002), thence referred to as BRE-Luciferase. pGL4.75 [hRluc/CMV] plasmid (GenBank: AY738231, Promega) was a gift from Ian Tomlinson, thence referred to as Renilla Luciferase. p*Silencer* 2.0-U6 (Ambion CAT #AM7209) containing a non-targeting sequence (shNT) was a gift from Jo Begbie. pCS-TdTomato-m2A was a gift for Shankar Srinivas. All plasmid DNA sequences, including ones in the sections below, were verified by sequencing.

2.4.4.1 pCAG-Gal-3-IRES-GFP plasmid

The Gal-3 sequence was re-amplified using primers containing EcoRI and NotI restriction sites to allow sub-cloning into the pCAGIG vector. Both the amplified Gal-3 sequence and pCAGIG plasmid were digested using EcoRI-HF ® and NotI-HF ® restriction enzymes at 37°C for 1 hour in CutSmart® buffer (NEB) in a thermal cycler. An inactivation step at 65°C for 20 minutes followed. The relevant products were then electrophoresed in a 1% agarose gel and the bands gel-extracted (Qiagen Gel extraction kit). The DNA was then PCR-purified to increase DNA quality (Qiagen PCR purification kit) and ligated using the Sticky end ligation method.

2.4.4.2 pCAG-Gal-3 plasmid

pCAG-Gal-3-IRES-GFP was digested using NotI-HF ® and BsrGI restriction enzymes at 37°C for 1 hour in CutSmart® buffer (NEB) in a thermal cycler. The products were electrophoresed on a 1% Agarose gel and the band corresponding to the pCAG-Gal-3 segment, approximately 5.6kb, was gel extracted then PCR-purified to increase DNA purity. The purified DNA was then ligated using the blunt end Ligation method to produce the final pCAG-Gal-3 plasmid.

2.4.4.3 shGal-3 plasmids

Four Gal-3 short-hairpin sequences were used to produce four shGal-3 plasmids according to the supplier's instructions. 4 Gal-3 short-hairpin sense and antisense sequences (Henderson et al., 2006)(Table 2.2) were manufactured by Sigma. They were then reconstituted in nuclease-free water at 1µg/µl then 2µl of each strand were diluted in 46µl of annealing buffer (10mM Tris, 20mM NaCl, pH 8.0). Next, sense-antisense pairs were annealed by incubating the mixture at 90°C for 3 minutes followed by cooling at 37°C for 1 hour in a thermal cycler. The pSilencer 2.0-U6 (Ambion®) vector was enzymatically digested using BamHI-HF® and HindIII-HF® in Cut Smart® buffer (NEB) at 37°C for one hour followed by inactivation at 65°C for 20 minutes. The digested plasmid was electrophoresed, gel extracted, PCR-purified, and then ligated to the annealed hairpins at molar ratio of 100:1 (insert : vector). The molar ratios were calculated using NEB Bio Calculator (http://nebiocalculator.neb.com/).

Table 2-2. Short-hairpin sequences

Sequence name	Sequence	Comments
shGal3_v1-sense	GATCCGATGTTGCCTTCCACTTTA**T TCAAGAGA**TAAAGTGGAAGGCAA CATCTTTTTTGGAAA	Sequences for 4 short-hairpins specific to murine Gal-3 transcripts. Sense and antisense traces are shown, V1 and V3 bind to Gal-3 mRNA variant 1,2, and 3, whereas V2 and V4 bind to all mRNA variants. V1 can also silence human Gal-3. BamHI and HindIII restriction sites flank the 5' and 3' ends of the sense and antisense hairpins, respectively. The **TTCAAGAGA** in the sense strand, and the **AAGTTCTCT** in the antisense strands, represent loop-sequences. The TTTTTT and AAAAAA sequences in the sense and antisense strands, respectively, represent the termination signal for the RNA Polymerase III enzyme.
shGal3_v1-antisense	GCTACAACGGAAGGTGAAAT**AAG TTCTCT**ATTTCACCTTCCGTTGTAG AAAAAACCTTTTCGA	
shGal3_v2-sense	GATCCGCAGACAGCTTTTCGCTTA **TTCAAGAGA**TAAGCGAAAAGCTG TCTGCTTTTTTGGAAA	
shGal3_v2-antisense	GCGTCTGTCGAAAAGCGAAT**AAGT TCTCT**ATTCGCTTTTCGACAGACG AAAAAACCTTTTCGA	
shGal3_v3-sense	GATCCGGTCAACGATGCTCACCTA **TTCAAGAGA**TAGGTGAGCATCGTT GACCTTTTTTGGAAA	
shGal3_v3-antisense	GCCAGTTGCTACGAGTGGAT**AAGT TCTCT**ATCCACTCGTAGCAACTGG AAAAAACCTTTTCGA	
shGal3_v4-sense	GATCCGGACAGGCTCCTCCTAGTG **TTCAAGAGA**CACTAGGAGGAGCC TGTCCTTTTTTGGAAA	
shGal3_v4-antisense	GCCTGTCCGAGGAGGATCAC**AAGT TCTCT**GTGATCCTCCTCGGACAGG AAAAAACCTTTTCGA	

2.4.5 Ligation of DNA sequences

For blunt end ligation, the NEB Quick Blunting Kit (E1201) was used according to the manufacturer's instructions. Briefly, 1µg of purified DNA was added to a solution containing 1µl Blunt Enzyme mix (contains T4 DNA Polymerase and T4 Polynucleotide Kinase), 2.5µl dNTP mix (1 mM), and 2.5µl 10X Blunting buffer, and up to 25µl of nuclease free water. The solution was incubated at room temperature for 15 minutes and inactivated in a

thermal cycler set to 70°C for 10 minutes. Ligation of the now-blunt DNA ends was performed using the same method for sticky end ligation. For sticky end ligation, purified DNA products were Ligated using T4 DNA Ligase (NEB) in a 20µl solution containing 1X T4 Ligase Buffer (contains 1mM ATP) and endonuclease-free water. An insert : vector ratio of 3:1 was used based on molecular weight with total DNA not exceeding 100ng. The mixture was incubated at room temperature overnight before transformation.

2.4.6 Transformation of chemically competent bacteria and DNA extraction

DH5α chemically competent E.Coli (Invitrogen, stored at -80°C) were thawed slowly on ice, this was followed by addition of 2µl of the ligation reaction and gentle stirring in 1.5ml Eppendorf tubes. The cells were then incubated on ice for 30 minutes and heat-shocked (42°C) in a water bath for 20 seconds. Next, they were incubated again on ice for 2 minutes and then cultured in Lysogeny broth (LB) at 37°C for 1 hour in a rotating incubator at 220rpm. 200µl of the culture was seeded onto LB agar plates containing 100µg/ml Ampicillin at 37°C for 8-12 hours. After successful transformation, single colonies were picked, seeded into starter cultures (3ml's of LB broth + 100µg/ml Ampicillin), and cultured as above for 6-8 hours before DNA was extracted (Qiagen MiniPrep) and sent for sequencing with appropriate primers (see Table 2.1). In parallel, the picked colonies were seeded onto another LB agar + Ampicillin plate, to allow for reseeding the colonies with the correct sequence into starter cultures for 6 hours then expansion cultures (250ml's LB broth + Ampicillin) for 18 hours. DNA from those cultures was extracted using Qiagen Endo-Free MaxiPrep Kit.

2.5 Protein isolation, Western blotting, and Immunoprecipitation

2.5.1 Protein extraction

Dissected SVZ tissue from 4-6 mice was pooled and lysed in Triton-X-100 lysis buffer (TLB; 1% Triton-X-100, 150mM NaCl, 50mM Tris HCl pH 8.0, Roche Complete protease inhibitor cocktail) by trituration. For membrane and soluble protein extraction, ProteoExtract™ Native Membrane Protein Extraction Kit (Calbiochem 444810) was used according to the manufacturer's protocol. Briefly, dissected SVZ tissue from four brains was washed twice with ice-cold wash buffer then mechanically dissociated using a Dounce homogeniser (Sigma) in the Buffer I + protease inhibitors. Following a 10 minute incubation on a rotator at 4°C, the soluble protein fraction was isolated after spinning the homogenate at 16,000g at 4°C and taking the supernatant. The pellet was then resuspended using Buffer II + protease inhibitor, incubated and spun as described. The supernatant containing the membrane protein fraction was transferred to a fresh ice-cold 1.5ml Eppendorf tube and stored at -80°C.

2.5.2 Protein quantification

Protein concentration was calculated using a modified Lowry colorimetric assay (Bio-Rad DC Protein Assay 500-0116; Bio-Rad) according to the manufacturer's instructions. The Lowry assay is based on measuring the colorimetric change brought about by the reduction of Cu^{2+} into Cu^{+} in an alkali solution, which is dependent on amino acid residue concentration, and the subsequent reduction product of Folin reagent. Five dilutions of bovine serum albumin (BSA) protein standard and sample proteins in TLB were

loaded on 96-well plates (Costar) in triplicates. 20µl of Reagent A (Alkaline Copper Tartrate) and 200µl of Reagent B (Folin reagent) were added to each well containing 5µl of sample dilutions. Light absorbance at 750nm was read in a microplate absorbance reader (Synergy HT, Biotek). Three absorbance readings for each sample were averaged and the concentration calculated against the BSA standard curve on Gen5 software®.

2.5.3 Western blotting

Protein samples were first mixed with 2X Laemmli buffer (Bio-Rad) containing 5% βME, then denatured by boiling at 97°C for 3-5 minutes and loaded in 8-10% Sodium Dodecyl Sulfate Polyacrylamide (SDS-PAGE) gels (see appendix 7.2). Proteins were electrophoresed at 200V for 45-50 minutes in 1X running buffer (see Appendix 7.2) until the blue line from the loading dye front reached the end of the gel. The gel was then carefully removed and washed with 1X transfer buffer (see appendix 7.2) on a shaking rotator for 5 minutes. In the meanwhile, the Polyvinylidene Fluoride (PVDF) membrane (Bio-Rad) was activated in methanol for 30 seconds and allowed to equilibrate in 1X transfer buffer. A wet transfer sandwich was prepared with the membrane positioned on the anode (+) side and the gel on cathode (-) side. The sandwich was inserted into the transfer box (Criterion Blotter, Bio Rad) containing an ice block and a magnetic stirrer, and filled with cold 1X transfer buffer containing 15% methanol. Proteins were transferred from the gel to the membrane at 120V for 70 minutes at 4°C. Complete transfer of the visible molecular weight standards (Promokine) from the gel onto the membrane denoted successful protein transfer. The membrane was rinsed in water to remove any gel debris, incubated in 100% methanol for 30 seconds, allowed

to dry for one minute, returned to Methanol for 30 seconds, and finally washed in 0.1M Tris buffered saline with 0.5% Tween-20 (TBST). Membranes were dried to improve protein retention for repeated immunoblotting of the membrane.

Immunoblotting (IB) was performed by first blocking the membranes in 5% non-fat milk (NFM) in TBST for one hour at room temperature. Membranes were next incubated in primary antibody diluted in blocking buffer at 4°C overnight. 3 x 10 minute washes with TBST preceded and followed a one-hour incubation with horseradish peroxidase (HRP)-labelled secondary antibodies diluted in 1% NFM in TBST. The signal from membranes was recorded on BioRad UVP transilluminator after 1-5 minutes development in Immobilon HRP substrate for Enhanced Chemiluminescence (EMD Millipore). Antibodies used for IB are listed in Table 2.4. Membranes were next stripped from antibodies by incubation in stripping buffer (see appendix 7.2). The membranes were then dried and kept at room temperature for further use.

2.5.4 Co-Immunoprecipitation

Immunoprecipitation (IP) was performed using μMACS™ protein A/G microBead magnetic separation (Miltenyi Biotec 130-071-001) according to the manufacturer's manual. Briefly, 200-300μg of protein, 1μg of monoclonal antibody or 2μg of rat IgG control, and 50μl of protein G microbeads (Miltenyi Biotec) were mixed by vortexing and incubated for 30 minutes on ice. The magnetically labelled protein solution was passed through a MACS μcolumn placed in a magnetic field. The column was washed with 4 x 200μl of TLB, 1X200μl low salt buffer (20mM Tris HCl, pH 7.5), followed by an elution step

with 1X SDS gel loading buffer at 95°C (see Appendix 7.2). Samples were then electrophoresed on an SDS-PAGE gel for IB. Antibodies used for IP are listed below in Table 2.3.

Table 2-3 Antibodies used for Immunoblotting (IB) and Immunoprecipitation (IP)

Antigen	Host	Dilution/ amount	Supplier Catalogue #	Use
β-catenin	Rabbit	1:1000	Sigma-Aldrich C2206	IB
β-catenin	Rabbit	1µg	Cell Signalling H9562	IP
Galectin-3	Rabbit	1:100	Santa Cruz SC-20157	IB
Galectin-3	Rat monoclonal	1µg	Santa Cruz SC-23938	IP
FGFR1	Rabbit	1:100/1µg	Santa Cruz SC-121	IB/IP
Laminin	Rabbit	1:1000	Sigma #L9393	IB
NCAM	Rabbit	1:200	Santa Cruz SC-10735	IB
PSA-NCAM	Rat monoclonal	1:100/1µg	BD Pharmingen 556325	IP/IB
pβ-catenin Ser33/37/Thr41	Rabbit	1:1000/1µg	Cell Signalling #9561	IP/IB
pβ-catenin Thr41/Ser45	Rabbit	1:1000/1µg	Cell Signalling #9565	IP/IB
pβ-catenin Ser552	Rabbit	1:1000/1µg	Cell Signalling #5651	IP/IB
pβ-catenin Ser675	Rabbit	1:1000/1µg	Cell Signalling #4176	IP/IB
p-Smad 1/5/9	Rabbit monoclonal	1:500	Cell Signalling# 13820	IB
p-Smad 1/5	Rabbit monoclonal	1:500	Cell Signalling# 9516	IB
Total Smad 1/5	Rabbit monoclonal	1:500	Cell Signalling# 6944	IB
Smad 4	Rabbit monoclonal	1:500	Cell Signalling# 9515	IB
β-Actin	Rabbit	1:1000	Abcam# Ab8227	IB
β-Actin	Rabbit	1:1000	Cell Signalling# 4967	IB

Abbreviation: p-: phospho. PSA-:polysialylated

2.6 Cell culture, transfection, nucleofection and flowcytometry

2.6.1 HEK293T culture

HEK293T cells were cultured as adherent cultures in tissue culture treated T75 flasks or 6-well plates (BD Falcon) in growth media (DMEM + 10% Fetal Bovine Serum + 100I.U/ml Penicillin G and 100mg/ml Streptomycin). Cells were passaged twice weekly by first, removing the media in the flask, washing the cells with sterile PBS, incubating them with 0.05% Trypsin/EDTA (Sigma), inactivating the trypsin, washing the cells by adding growth media, and centrifugation before reseeding.

2.6.2 Transfection

HEK293T cells were seeded into 6-well plates at density of 4 X 10^5 cells/well in 2ml of growth media without antibiotics 24 hours before transfection. The following day, cells achieved 70% confluence, suitable for transfection. Lipofectamine 2000® (Life Technologies) was used for transfection according to the supplier's instructions. Briefly, 9µl of Lipofectamine reagent was added to 150µl of Opti-MEM® (Life Technologies) medium per well to be transfected. Next, 2µg per plasmid/well were diluted in 150µl of Opti-MEM/well. The aforementioned solutions were then mixed together and incubated for 5 minutes at room temperature. Next, 250µl of the combined mixture was added to each well and the media changed the following day. Cells were used 48-72 hours after transfection.

2.6.3 SVZ dissection and Neurosphere culture

P4 mouse pups were used for SVZ dissection. First, pups were submerged in ice for 2-3 minutes to induce hypothermia. Decapitation, brain extraction, and washing in Hank's Balanced Salt solution (HBSS) followed. Next, the brains were sectioned into 500µm slices on a McIlwain tissue chopper. The lateral wall of the lateral ventricle was then microdissected under a Leica MZ12 dissecting microscope. The tissue was cut into small pieces using fine iris scissors, and then dissociated by incubation with Accutase® (Sigma) for 10 minutes at 37°C in a water bath, followed by trituration using a p1000 pipette. The Accutase reaction was stopped by the addition of Neurobasal A+ medium (NB-A+; Neurobasal-A medium (Gibco 10888-022) + B-27 supplement (1%; Gibco 17504-044) + GlutaMax (1X; Gibco 35050-038) + Penicillin/Streptomycin 1X; Gibco 15070). The cell suspension was centrifuged after being passed through a 40nm cell strainer (BD Falcon) to enrich single cells and remove large tissue clumps. The cell pellet was resuspended in NB-A+ medium, and then cells underwent 2 additional washes in NB-A+. Cells were counted in a haemocytometer and/or Scepter™ 2.0 (Millipore), and cell viability was quantified using Trypan blue (Flukar) exclusion method. After the final wash, SVZ cells were diluted to 1 x 10^5 cells/ml in growth medium (NB-A+ GF: NB-A+ supplemented with 20ng/ml EGF (Sigma E9644) and 20ng/ml bFGF (R&D Systems 233-FB)). 2mls/well were seeded into non-tissue-culture-treated 6 wells plates (BD Falcon) and culture plates were stored at 37°C with 5% CO2 in a humidifying incubator. Cultured neurospheres were passaged every 4-6 days by dissociation

(Accutase/trituration), washing, counting and replating in new 6 well plates at 1 x 10^5 cells/ml.

2.6.4 Nucleofection

NSC/TAP cells from tertiary neurospheres were nucleofected using an Amaxa™ Biosystems Nucleofector 1 machine as instructed by the Amaxa™ Mouse Neural Stem Cell Nucleofector™ Kit. Briefly, 1-4 x10^6 single cells were resuspended in the nucleofection solution containing 5µg DNA/plasmid in kit-provided mouse NSC nucleofection solution + supplement (100µl final volume). The cell suspensions were then transferred to electroporation cuvettes and electroporated using programme A-033. Cells were then rescued by adding 0.5ml of pH pre-equilibrated NBA+GF medium, diluted, and plated for subsequent culture conditions. The following conditions were used for flowcytometry analysis and clonal density cultures: control (shNT + pTOP-dGFP-CAG-mCh), shGal-3 (shGal-3 v1 + pTOP-dGFP-CAG-mCh), and Gal-3 OE (pCAG-Gal-3 + pTOP-dGFP-CAG-mCh). For flowcytometry, control conditions included pCAGIG (GFP only) and pCS-TdTomato-m2a (mCherry only) and un-nucleofected cells. For Luciferase assays, cells were nucleofected with shNT, ShGal-3 v1, or pCAG-Gal-3 along with 1µg of BRE luciferase and Renilla luciferase (20:1 ratio).

2.6.5 Clonal density/self renewal assay

In each nucleofection experiment, cells were seeded in two 96-well plates (Costar®) at clonal density (10cells/µl), 200µl per well, 20 wells/condition, and cultured in NB-A+GF medium. After seven days one plate was imaged to assess neurosphere forming capacity and size then disposed of. During the

imaging of the first plate, cells from the second plate were passaged and reseeded at clonal density in NB-A+GF medium (200µl/well) in a fresh 96-well plate. Seven days later the second plate was imaged to assess for self-renewal.

2.6.6 Flowcytometry

2.6.6.1 Preparation of cells for FACS

After culture for 24 hours, nucleofected cells were dissociated by Accutase and trituration. The absence of cell clusters was verified under the microscope. Enzymatic dissociation was stopped by the addition NB-A+ medium. The cells were then pelleted by centrifugation at 1400rpm for seven minutes at 4°C. Next, two washes in ice cold PBS followed before fixation in 2% paraformaldehyde (PFA) for 15 minutes at room temperature. PFA was inactivated by adding equivalent volume of 0.1M Glycine in PBS and cells were then washed once in ice-cold PBS. A final wash in PBS + 1% BSA preceded the suspension of cells in the wash solution and stoarage on ice for FACS analysis.

2.6.6.2 Live/Dead Assay

For labelling dead cells, Live/Dead® Fixable Violet Dead Cell Stain Kit (Life Technologies # L34957) was used. A fluorescent dye can permeate the membranes of dead cells and react with intracellular amines, enabling detection. The procedure was performed as instructed by supplier's manual. After dissociation, cells were counted using a Scepter™ 2.0 (Millipore) and 1 X 10^6 cells were resuspended in 1ml PBS. 1µl of the dissolved dye was mixed with the cell suspension and incubated at room temperature on a rotating

shaker for 30 minutes. Next, the cells were fixed and prepared for flowcytometry as described in section 2.6.6.1.

2.6.6.3 FACS analysis

Flowcytometric Analysis was performed using a CyAn™ ADP Analyzer (Beckman Coulter). Fluorophores were detected with a 405nm laser and 450/50 emission filter for the Live/Dead Violet stain, and a 488nm blue laser and 530/40 and 575/25 emission filters for GFP and mCherry, respectively. I used compensation factors of 18% and 1.3% for GFP to mCherry and mCherry to GFP, respectively. Control cells nucleofected with pCAGIG and pCS-TdTomato-m2a were used as Single-Fluorescence controls for GFP and mCherry, respectively. These controls were used to calculate compensation factors. Un-nucleofected control cells were used to set laser voltages and determine background levels. Cell debris and dead cells were gated out using forward scatter (FSC), sideward scatter (SSC) and Live/Dead Cell stain. Single cells were gated on by FSC-H/Pulse width (Appendicular Figure A2). Data acquisition and analysis was done on Summit® software.

2.6.7 BMP4 luciferase assay

Cells from tertiary neurospheres were nucleofected with a 20:1 mixture of BRE-luciferase to Renilla-luciferase in conjunction with control, Gal-3 knockdown, and Gal-3 overexpression plasmids (as previously described). Nucleofected cells were cultured in NB-A+GF medium in 6-well plates, one plate/condition, for 24 hours. Next plain NB-A+GF, NB-A+GF +LiCl, or NB-A+GF +BMP4 media was added to give final concentrations of 5mM LiCl and 5ng/ml BMP4, and cells were cultured for a further 24 hours. Cells were then

lysed for protein extraction using Passive Lysis buffer (Promega®). From each 6-well plate, two wells were pooled to give a total of three technical replicates per experimental condition. Firefly and Renilla luciferase activities were measured sequentially with the Dual-Luciferase® Reporter Assay System (Promega E1910) according to the manufacturer's protocol. Luminescence was measured on a Dynex luminometer equipped with 2 injectors to allow high-throughput analysis. First, Luciferase Assay Reagent II ® (LARII) and Stop & Glo® (SGR) Reagents were prepared as instructed by the manual. The Dynex luminometer injectors were then, primed with the aforementioned reagents. Next, 20µl of protein per technical replicate was pipetted into a 96-well polystyrene microplate (Greiner Bio-One) kept on ice. The plate was loaded into the microplate reader, 100µl/well LARII was added, luminescence measured for Firefly Luciferase for 10 seconds, then 100µl/well SGR was added, and the Renilla luminescence was measured for 10 seconds. Adding SGR quenched Firefly luciferase activity and provided a substrate for Renilla Luciferase. Un-nucleofected control cells were used to determine background luminescence levels. Average luminescence values for each well were recorded after subtracting the background and results were expressed as ratios of firefly-luciferase activity to Renilla-luciferase activity.

2.7 Histology and Fluorescent Immunohistochemistry

2.7.1 Perfusion and tissue preparation

At sacrifice, animals were first overdosed with i.p. Pentobarbital. Next, thoracotomy followed to flush the blood out by transcardial perfusion with cold normal saline after nicking the right atrium. Fixation followed with perfusion of

cold 4% PFA before brains were carefully dissected out of the skull, post-fixed overnight in 4% PFA at 4°C, cryoprotected in 30% sucrose in 0.1M phosphate buffer (PB) until they sank in the 15-ml Falcon® tubes, then finally frozen (-80°C).

2.7.2 Microtome sectioning

Frozen brains were section on a sliding microtome (SM2000R, Leica). 30µm-thick serial coronal sections were obtained from the olfactory bulbs till the rostral hippocampus. The section were put in 48-well plates (Costar®) containing cryoprotectanct (see Appendix 7.2) and stored at -20°C.

2.7.3 Standard Fluorescent Immunohistochemistry

Free-floating fluorescent immunohistochemistry (Frfl-IHC) was performed over two days at room temperature. Up to six free-floating brain sections were placed in porous well inserts (CLS3477, Sigma-Aldrich) in 12-well-plates (2-3ml of solution/well) to facilitate transfer of sections between wells. Sections were first washed thrice with 0.1M phosphate buffered saline (PBS) for 10 minutes/wash, followed by a 15-minute incubation in 50mM glycine in PBS on a rotating shaker. A second set of 3 x 10-minute PBS washes followed. A blocking step in PBS+ (PBS + 10% Donkey serum (Sigma) + 0.1% Triton-X-100) for one hour at room temperature preceded incubation with primary antibodies diluted in PBS+ at 4°C overnight (Table 2.4). For double and triple labelling, primary antibodies were co-incubated except for experiments that involved GFP and mCherry labelling, whereby sections were first incubated at room temperature for 3 hours in primary antibody solution for GFP and/or

mCherry, then washed with PBS 3 x 10 minutes, before a second incubation in a primary antibody solution containing 1-2 antibodies overnight at 4°C.

On the next day, 3 x 10 minutes PBS washes preceded and followed incubation with species-appropriate fluorophore-conjugated secondary antibodies (1:500 in PBS+, 1 hour at room temperature in the dark). This was followed by a 15-minute treatment with 4',6-diamidino-2-phenylindole (DAPI, 10µg/mL, Sigma) at a 1:1000 dilution in PBS. Next, 3 x 10 minutes washes with 0.1M Phosphate buffer (PB) followed. Sections were mounted on Superfrost Plus™ slides, air-dried for 1 hour, and cover-slipped with Fluorsave mounting media (Calbiochem). Slides were then dried overnight at room temperature and stored at 4°C in darkness.

Secondary antibodies conjugated to Alexa Fluor 488, 568, 594, and 647 (Invitrogen, Sigma, and Jackson Laboratories) raised against the host species of the primary antibodies were used as appropriate. Negative controls lacking primary but including secondary antibodies were carried out for all experiments. For GFP and mCherry labelling, sections from animals that were not electroporated were used as controls. In double and triple label experiments where species cross-reactivity was possible, i.e. rat and mouse primary antibodies, cross-labelling was ruled out by applying each primary antibody with non-corresponding secondary antibody combinations, which showed no signal.

2.7.4 Bromodeoxyuridine and p27Kip1 immunohistochemistry

For BrdU and p27Kip1 detection, after the first PBS washes, an antigen retrieval step was performed to facilitate access of the antibodies to their

epitopes. This involved incubation in 2N Hydrochloric Acid (HCl) at 37°C. 3 x 10 minutes PBS washes followed. The rest of the protocol was as in 2.7.3.

2.7.5 Ethenyldeoxyuridine detection

For EdU detection, Click-iT® EdU detection kit (Invitrogen) was used. The protocol was adapted for frfl-IHC and 2ml/well was used. The EdU detection cocktail was prepared fresh when the sections were in the PBS wash step after the secondary antibody incubation. Per well, the cocktail consisted of 1.8ml of 1X-Click-iT® reaction buffer, 80µl $CuSO_4$, 5 µl Alexa Fluor 594 Azide, and 200µl of reaction buffer additive. The sections were incubated for 30 minutes in the cocktail, and washed 3 x 10 minutes in 0.1M PB before mounting on slides.

Table 2-4 Primary Antibodies used in Immunohistochemistry

Antigen	Host	Dilution	Supplier
β-catenin	Rabbit	1:500	Sigma #C2206
Dcx	Goat	1:100	Santa Cruz #SC 8066
Galectin-3	Rat monoclonal	1:100	Santa Cruz #SC 23938
GFAP	Rat monoclonal	1:400	Invitrogen #13-0300
GFAP	Goat	1:100	Santa Cruz #SC-6171
GFAP	Chicken	1:5000	Abcam #Ab4674
GFAP	Rabbit	1:200	Sigma #G9269
Mash1	Mouse	1:100	BD #556604
Vimentin IgM	Mouse	1:100	DSHB #3CB2
phospho-Smad 1/5/8	Rabbit	1:500	Cell Signalling #9561
Mcherry	Rabbit	1:750	Abcam #Ab167453
GFP	Chicken	1:500	Aves-labs # GFP 10-10
S100b	Rabbit	1:200	Dako #GA504
Cleaved caspase-3	Rabbit	1:500	Cell Signalling #9661
BrdU	Rat	1:600	Novus Biologicals #NB500-169
Iba-1	Goat	1:500	Abcam #ab5076
CD-45	Rat	1:400	Millipore #CBL1326
Olig2	Rabbit	1:1000	Millipore #AB9610
NeuN	Mouse	1:400	Millipore #MAB377
PHi-3	Mouse	1:2000	Millipore #05-806

Antigen	Host	Dilution	Supplier
Sox2	Rabbit	1:500	Millipore #5603
Ki67	Rabbit	1:500	Abcam #Ab16667
p27Kip1	Mouse	1:500	BD #G173-524

2.8 Microscopy and Imaging

2.8.1 Microscopy

For Fluorescent-IHC, images were taken using confocal microscopy (Zeiss LSM 710 laser scanning microscope). Four excitation lasers; 405, 488, 561, and 633 nm were used to excite DAPI, Alexa Fluor 488, 567 / 594, and 647 fluorophores, respectively. Emission spectra were set to rule out bleed through on Zeiss Zen™ software. For IHC performed on Gal-3 nulls and controls, at least 6 confocal single optical plane images were taken from at least 6 sections to allow quantification. For GFAP IHC, z-stacks were taken as described below. For IHC performed on cohorts 1, 2, and 3 (3, 7, and 17 DPE, respectively), at least three brain sections were used to take 3 representative z-stacks of 15 optical slices (z interval= 1.0µm) using a 40x oil immersion objective lens (Plan-NeoFluar 40X/1.3 Oil DIC). Additionally, for imaging striatal cells from cohort 3 (P19, 17DPE), a 20x objective lens (Zeiss Plan-Neofluar 20X/0.50) was used and z-stacks of 12 optical slices (z interval=1.3µm) were acquired. Channels were acquired sequentially to minimise bleed through. For quantification of neurosphere size and number, 10 entire wells/condition from Costar® 96-well plates were fully imaged (8 images- full well coverage) using a 4X objective on a Life technologies EVOS FL Auto Fluorescent microscope. For imaging nucleofected cells before

Flowcytometry, a 20X objective was used on Leica DMIRB microscope with a digital camera (Hamamatsu C4742-95).

In cohorts 1, 2, and 3 Images were acquired from the plSVZ (Striatal wall), where electroporated cells were most abundant, avoiding the dorsolateral (DL) corner, which contains neuroblasts migrating from more caudal planes. All images shown represent single optical planes, unless stated otherwise, with orthogonal views also displayed in the same figure. All images were acquired using the same acquisition parameters for animals in the same experiment. Images were analysed in LSM Image Browser 4.2 (Zeiss), Volocity 6.3 (Improvision), and FIGI (NIH ImageJ, NIH, USA) software packages. Figures were compiled in Gimp 2.0.

2.8.2 p27Kip1 Digital Thresholding

Consistent with previous reports (Li et al., 2009) p27kip1 was ubiquitously expressed in the SVZ; however, since cells could be separated into two populations (High/low levels of p27Kip1), a manual thresholding approach was used. All images were acquired using the same acquisition parameters and the p27Kip1 signal histogram threshold set in FIGI software to show high p27Kip1 cells only, which corresponded to the top 2.5% of the histogram.

2.8.3 Mean fluorescent intensity quantification of Gal-3 levels

Measurement of Gal-3 mean fluorescent intensity (MFI) was conducted as follows: Using Volocity 6.3 image analysis package (Improvision), 3D objects representing cells were identified in 15µm z-stack using the algorithm detailed below (The steps and thresholds for this algorithm were determined empirically):

1. Drag “Find objects” function into work space (set filter at > 80µm3 for volume): Call population “>80 objects”
2. Filter clustered objects by adding a new filter on the “>80 objects” population; set the filter at > 590 µm3 for volume: Call population “Objects >590”
3. Subtract population “Objects>590” from “objects>80” using the “Subtract” function; call population “objects>80<590”.
4. Use “Objects>80<590” to separate touching objects: drag the function “Separate touching objects” into workspace, then pick “Objects>80<590” population and set object size filter at 80 µm3: call population “Separated >80<590 objects”.
5. Consolidate smaller objects from “Separated >80<590 objects” by setting a “filter population” function at =<100µm3 for volume. Then use “Open function with 6 iterations (in the same operation). Next, filter the population for objects >80µm3 for volume. This consolidates smaller objects and allows the algorithm to detect new consolidated objects. Call population “Consolidated 80-100 objects”.
6. Combine smaller consolidated objects from step 5 (Consolidated 80-100 objects) with (Separated >80<590 objects) using the “Combine” function. Call the population “separated and consolidated objects>80<590”.
7. Repeat steps 4-6 on population “>590” to detect objects.
8. In the analysis panel, record the MFI values for DAPI, Gal-3, and mCherry channels and copy them into MS Excel.

9. Filter objects based on DAPI to exclude residual cell processes; exclude DAPI MFI < 35 units.
10. For the remaining objects, normalise Gal-3 and compare statistically compare experimental groups.

2.9 Statistical Analysis

All quantifications were done blinded to experimental conditions. At least 3 images were quantified per animal and considered technical replicates. The mean of technical replicates was used as one biological replicate. The data was presented as mean ± standard error of the mean (SEM). Differences between two groups were assessed using Student's t-test when normality could be checked using Shapiro-Wilkin test ($n \geq 5$) or Mann-Whitney nonparametric test ($n=3$ or 4). For differences between three or more groups, Kruskal-Wallis test or analysis of variance (ANOVA) with Tukey or Sidak's post-hoc tests was employed as appropriate. Groups were considered significantly different when at least a 95% confidence level ($P < 0.05$) was obtained. Analyses and graphical representations were performed in Microsoft Excel 2011 and GraphPad Prism 6 (GraphPad, La Jolla, CA, USA) software packages.

Chapter 3

Galectin-3 regulates Wnt/β-catenin signalling and proliferation in the postnatal SVZ

3.1 Introduction *84*

3.2 Results *87*

3.3 Discussion *115*

3.4 Conclusion *130*

3 Galectin-3 regulated Wnt/β-catenin signalling and proliferation in the postnatal SVZ

3.1 Introduction

The stem cell field is in great need for a specific marker to label the bona fide NSCs in order to facilitate purification and subsequent use for further study or even therapeutic purposes. There was hope for finding that marker when the Götz group identified Gal-3 as one of the most differentially expressed genes in adult NSCs (Beckervordersandforth et al., 2010). However, like other cell markers, Gal-3 is also expressed in cells other than NSCs, and the search is still ongoing. Significantly, the Szele group has described Gal-3 expression pattern in the aSVZ and found it was most highly expressed in ependymal cells, but also expressed in a subset of NSCs and TAPs (Comte et al., 2011). This was not surprising given the myriad functions Gal-3 can undertake, in addition to the multiple intracellular and extracellular compartments Gal-3 can be distributed in (Dumic et al., 2006). One example highlighting the spatially diverse functions Gal-3 exert comes from its role in regulating cell death; where extracellular Gal-3 promoted and intracellular Gal-3 inhibited apoptosis (Nangia-Makker et al., 2007). Another example underscores the temporally varied inflammatory functions of Gal-3, where it promotes neutrophil activation during acute inflammation, and is required for alternative macrophage activation in chronic inflammation and fibrosis (Henderson and Sethi, 2009). In the SVZ, Gal-3 was required for microglial activation after stroke (Lalancette-Hebert et al., 2012) and demyelination (Hoyos et al., 2014). Studies from the Szele group revealed novel functions for Gal-3 in regulating neuroblast migration and post-stroke angiogenesis (Comte et al., 2011;

Young et al., 2014). These studies showed Gal-3 loss did not alter aSVZ neurogenesis at baseline or after injury. However, little is known about whether Gal-3 regulates lineage progression in the pSVZ.

In a prelude to this work, I sought to identify Gal-3's binding partners in the SVZ. I discovered that it was bound to Laminin, FGFR1, and β-catenin but not to EGFR, VEGFR2, or NCAM (n=2-3 trials per interaction, data not shown). β-catenin is known for its pivotal role in Wnt signalling and cell adhesion. In the SVZ, it can promote proliferation, differentiation, and/or survival (Zhang et al., 2011), processes central to neurogenic lineage progression. Thus, studying the interaction between Gal-3 and β-catenin allowed me to interrogate Gal-3's potential roles in SVZ lineage progression. I therefore focused on characterising the co-expression patterns and subcellular localisation of Gal-3 and β-catenin in GFAP+ NSCs and Mash1+ TAPs in the dorsolateral, striatal (lateral), and ventral SVZ along the antero-posterior axis in young adult mice. That work led me to focus on the anterior striatal (lateral) SVZ (lSVZ), where Gal-3 expression and nuclear β-catenin were highest amongst SVZ regions examined. I also found that Gal-3 null mice did not display altered subcellular localisation of β-catenin in NSCs and TAPs (data not shown). Similarly, Gal-3 knockout mice did not demonstrate changes in subcellular expression patterns of transcriptionally active phospho-Serine 552 β-catenin expression in TAPs (data not shown). In addition, SVZ expression of β-catenin at both mRNA and protein levels was not different in Gal-3 null mice from wild-type controls (data not shown). The expression of active and inactive phosphorylated forms of β-catenin was also intact in Gal-3 nulls (data not shown). Contrary to what I expected, Gal-3 knockout mice did

not compensate for Gal-3 loss by increasing the levels of other SVZ-expressed Galectins 1, 8, or 9 (data not shown).

As a result of these studies, I focused my subsequent studies to investigate Gal-3's function in acute settings wherein cellular responses can be monitored while possibly circumventing potential compensatory mechanisms, which are still unknown to me. To interrogate Gal-3's functions acutely, I chose in vivo electroporation as means to manipulate Gal-3 levels and simultaneously report Wnt/β-catenin signalling activity. For reasons discussed below in Section 3.3.2, I limited the study to the plSVZ. In summary, this preliminary body of work enabled me to refine my research questions and focus them on studying the functional and molecular regulation of plSVZ lineage progression by Gal-3.

In this chapter I aimed to answer the following questions: How does Gal-3 expression relate to β-catenin expression and signalling in the aSVZ lineage? Is the plSVZ comparable to the young adult lSVZ in respect to Gal-3 and β-catenin co-expression? Does Gal-3 regulate Wnt/β-catenin signalling in the plSVZ? If so, what is the nature of this regulatory relationship? And finally, how does Gal-3 gain-of-function influence the niche? This study is the first to investigate the role of Gal-3 in regulating SVZ lineage progression in the pSVZ. In tackling my research questions, I discovered a novel regulatory relationship between Gal-3 and the Wnt/β-catenin signalling pathway. In contrast to its positive effects in cancer cells, Gal-3 decreased Wnt signalling in the SVZ. After conducting detailed analysis of the proliferation dynamics in the SVZ niche after Gal-3 gain-of-function, I described a previously unknown function of Gal-3 in regulating cell cycle exit. Overall, this study provides novel

insight into the roles of Gal-3 in regulating postnatal SVZ lineage progression, proliferation, and Wnt/β-catenin signalling.

3.2 Results

3.2.1 Galectin-3 and β-catenin were co-expressed in the SVZ niche

Gal-3 is co-expressed with, and binds to β-catenin in several cancer cell lines (Funasaka et al., 2013; Kim et al., 2010; Shimura et al., 2004). To assess whether Gal-3 is co-expressed with β-catenin in the SVZ neurogenic lineage, I used fluorescent immunohistochemistry on brain sections from young adult mice (4-6 weeks of age). GFAP staining was used to label a subset of NSCs (type-B cells), Mash1 (Ascl1) to label TAPs (type-C cells), and Dcx to label neuroblasts (type-A cells). I found that Gal-3 and β-catenin were co-expressed in a subset of GFAP+ cells (Figures 3.1A, 3.2A-C). β-catenin expression was either nuclear (Figures 3.1A and 3.2B), or cytoplasmic (Figures 3.1B, 3.2A). Of note, nuclear localisation of β-catenin is the hallmark of Wnt/β-catenin signalling, and has been used as a readout of transcriptional activity (Durak et al., 2014; Fang et al., 2007). Similarly, Mash1+ cells co-expressed Gal-3 and β-catenin, and β-catenin expression was localised in the nucleus (Figure 3.1B) or the cytoplasm (Figure 3.1B and 3.2D). A subset of GFAP+ and Mash1+ cells did not express Gal-3 (Figure 3.2C-D). In preliminary work I found that 28.72 ± 3.24% and 12.57 ± 0.74% of SVZ GFAP+ and Mash1+ cells, did not express β-catenin, respectively (Figure 3.1E). In contrast to TAPs and NSCs, and consistent with Comte et al. (Comte et al., 2011), all Dcx+ neuroblasts in the SVZ did not express Gal-3, and β-catenin expression was non-nuclear (Figure 3.1C). Interestingly, when

neuroblasts migrated out of the RMS into the OB, they lost β-catenin expression (Figure 3.2E). I next quantified the percentage of SVZ cells that expressed Gal-3 or nuclear β-catenin. Gal-3 was expressed in 47.6% and 58.6% in GFAP+ and Mash1+ cells, respectively. Nuclear β-catenin was detected in 48.3% and 11.9% of β-catenin+ GFAP+ and β-catenin+ Mash1+ cells, respectively. Neither Gal-3 nor nuclear β-catenin were observed in any Dcx+ cell examined in the SVZ and RMS (Figure 3.1D). Notably, almost all Gal-3+ cells quantified expressed β-catenin. In sum, Gal-3 and β-catenin were co-expressed in a subset of NSCs and TAPs, and both were downregulated in more differentiated neuroblasts.

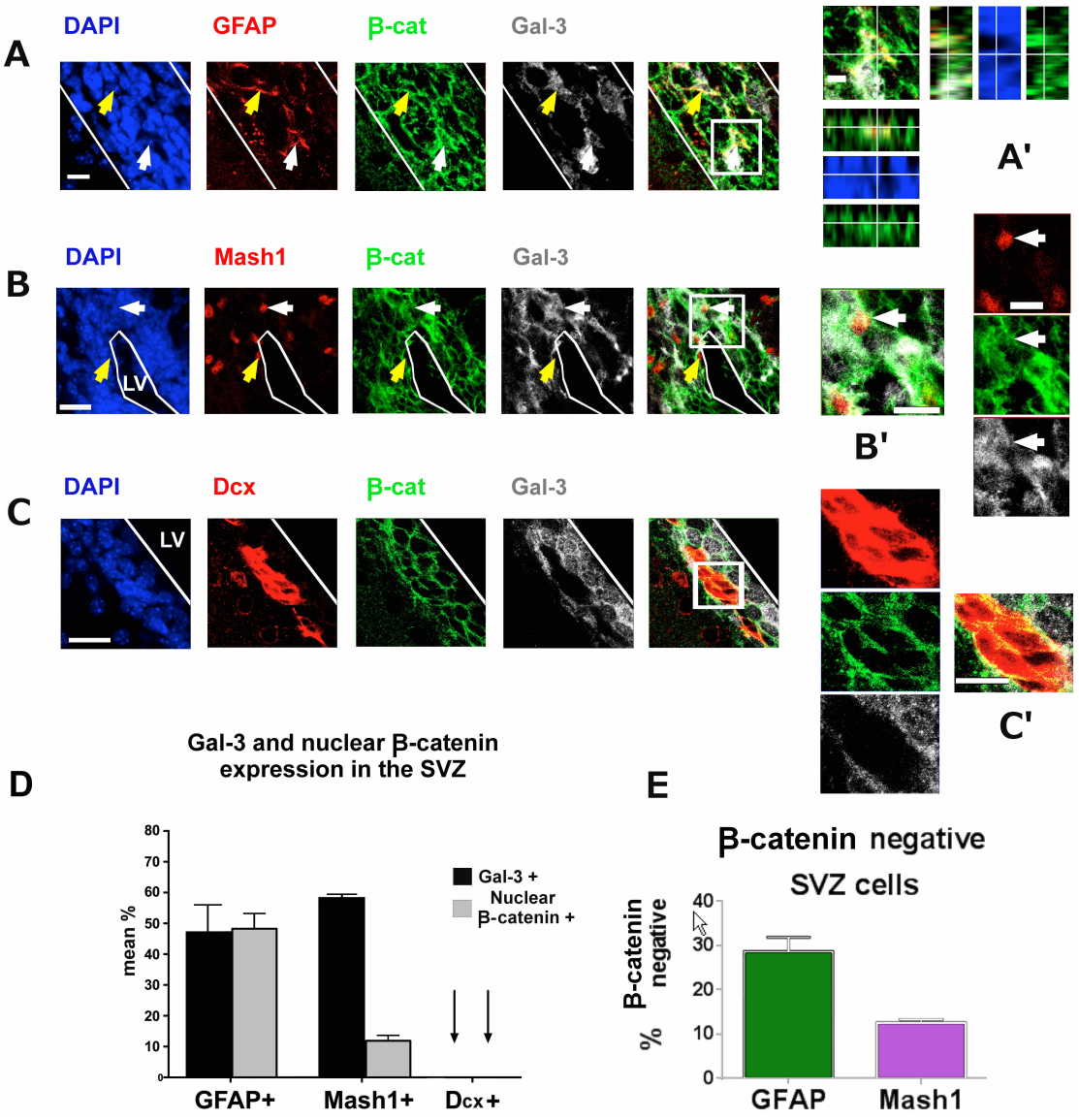


Figure 3.1 Gal-3 and β-catenin co-expression in the aSVZ lineage

(A) Both Galectin-3 (Gal-3) and β-catenin are expressed in subventricular zone (SVZ) GFAP+ cells. The white arrow shows a GFAP+ cell that expresses Gal-3 and nuclear β-catenin, the yellow arrow shows a GFAP+ cell that labels with Gal-3 and cytoplasmic β-catenin. **A',** shows an orthogonal view of the boxed area in A.
(B) Gal-3 and nuclear β-catenin are co-expressed in Mash1+ cells. The white arrow shows a Mash1+ cell positive for Gal-3 and nuclear β-catenin, and expanded view is shown in **B'**. The yellow arrow points to a cell that expresses Gal-3 and non-nuclear β-catenin.
(C) Dcx+ neuroblasts express non-nuclear β-catenin but not Gal-3. An enlarged view of the boxed area is shown in **C'**.
Scale bars measure 20μm in A,B,C, 5μm in A', and 10μm in B', C'. Panels in A, B, C, B', and C' are single confocal optical planes.
(D) Quantification of Gal-3 expression in SVZ subtypes and proportion of nuclear β-catenin expression in β-catenin+ SVZ cells. Note that Dcx+ neuroblasts expressed neither nuclear β-catenin nor Gal-3. The proportion of GFAP+ β-catenin- and Mash1+ β-catenin- cells is quantified in (**E**). The data is presented as mean ± SEM.

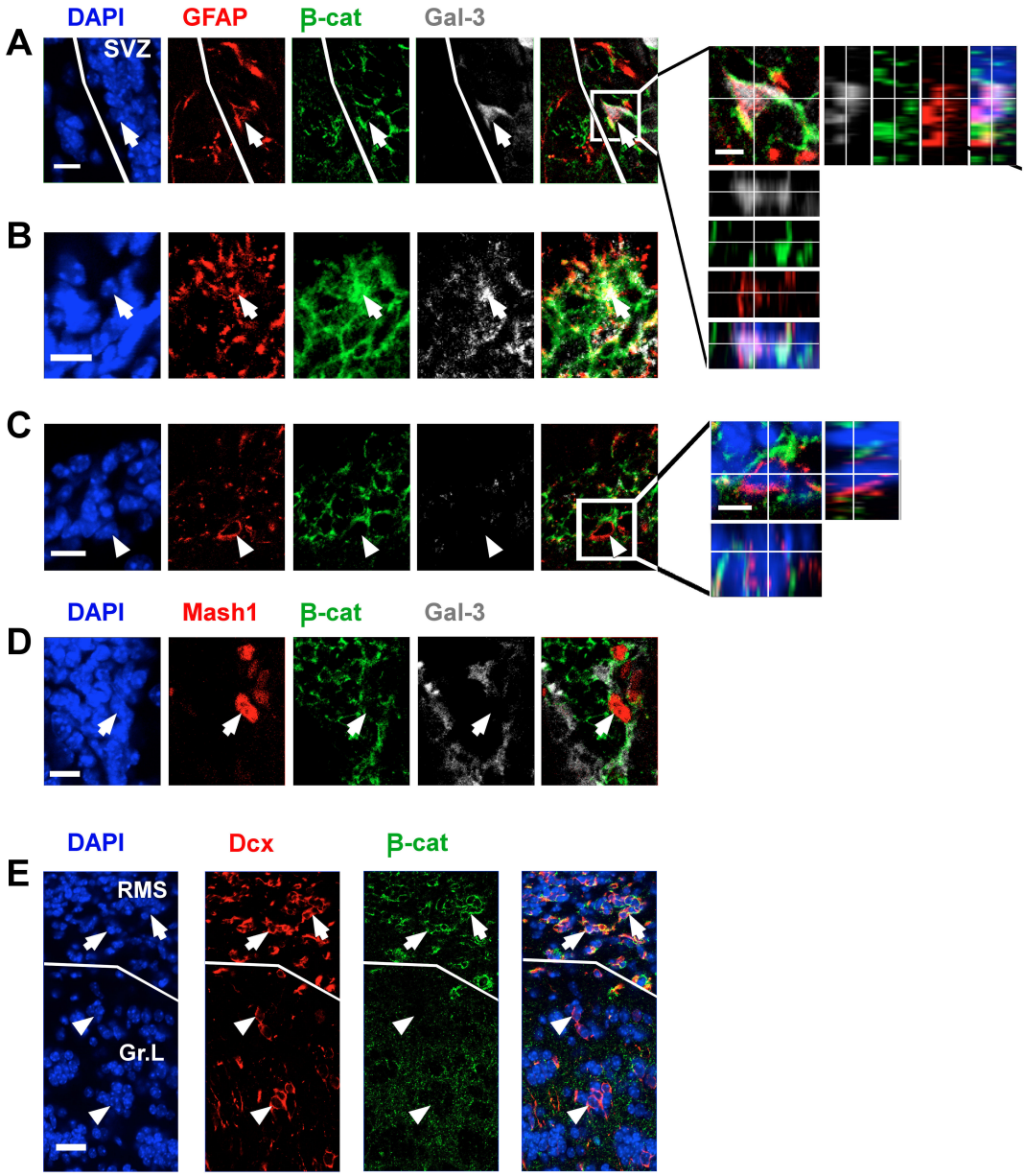


Figure 3.2 Gal-3 and β-catenin co-expression patterns in the aSVZ

(A-E) Confocal images of β-catenin (green), Galectin-3 (Gal-3; grey), DAPI (blue), and GFAP **(A-C)**, Mash1 **(D)**, or Dcx **(E)** (red) in the subventricular zone (SVZ) **(A-D)** and olfactory bulb (OB) **(E)**.
(A) The arrow shows a GFAP+ cell that expressed cytoplasmic β-catenin and Gal-3. The boxed area is shown as an orthogonal view.
(B) The arrow indicates GFAP+ nuclear β-catenin+ Gal-3+ cell.
(C) The arrowhead denotes a GFAP+ Gal-3- β-catenin- cell. The boxed area is shown as an orthogonal view.
(D) The arrow shows a Mash1+ cell that expressed cytoplasmic β-catenin but not Gal-3.
(**A-D**) Scale bars: 10μm for main panels and 5μm for orthogonal panels.
(E) Arrows point to Dcx+ β-catenin + cells in rostral migratory stream (**RMS**), whereas arrowheads point to Dcx+ β-catenin – cells in the granule cell layer (**Gr.L**). Scale bar: 20μm

3.2.2 Galectin-3 was complexed with β-catenin in the aSVZ

Whether Gal-3 binds β-catenin in the SVZ has not been previously addressed. To determine if these molecules bind each other in the SVZ, I immunoprecipitated Gal-3 from total lSVZ protein using a specific monoclonal antibody and then immunoblotted for β-catenin (Figure 3.3A). Gal-3 immunoprecipitated with β-catenin, indicating they coexisted in a protein complex. In the cell membrane compartment, β-catenin is sequestered in the AJ's and is subject to phosphorylation by various pathways (reviewed in (Nelson and Nusse, 2004)). To test if Gal-3 bound β-catenin in the cell membrane compartment, I first enriched the lSVZ membrane protein fraction, immunoprecipitated Gal-3, then immunoblotted for β-catenin (Figure 3.3B). Gal-3 again showed strong interaction with β-catenin. Immunoprecipitating Gal-3 from SVZ soluble-protein enriched fraction also showed positive interaction with β-catenin (n=2, data not shown). Therefore, the results show that Gal-3 was complexed β-catenin in total, membrane-enriched, and soluble SVZ protein.

To confirm binding of Gal-3 to β-catenin, I immunoprecipitated β-catenin from the lSVZ membrane protein fraction with a monoclonal antibody, then blotted for Gal-3 (Figure 3.3C). A band roughly measuring 68kDa probably corresponding to the dimeric form of Gal-3 was detected. Of note, this band was observed after boiling the immunoprecipitated protein samples at 95°C for 5 minutes. Without boiling, brighter bands appeared approximately between 120 and 75kDa (Appendicular Figure A3A). These bands disappeared after boiling giving rise to the band observed in Figure 3.3C. And

when Gal-3 was pulled down from SVZ protein and blotted for FGFR1, a similar band pattern was observed, supporting the presence of Gal-3 oligomers in the SVZ (Appendicular Figure A3B). This is consistent with previously described Gal-3 protein interactions, whereby immunoprecipitation of Elastin from breast carcinoma cells and blotting for Gal-3 showed dimeric Gal-3 forms (Ochieng et al., 1999). This data indicates that Gal-3 was complexed with β-catenin in the membrane compartment-enriched protein fraction of the lSVZ, and this binding involved dimeric and/or higher order oligomeric forms of Gal-3.

Since both Gal-3 and β-catenin are expressed in ependymal cells (Comte et al., 2011), the binding described here could have been primarily due to their co-expression in ependymal cells and not NSCs and TAPs. To verify binding in NSCs and TAPs, I isolated protein from growing tertiary neurospheres, immunoprecipitated Gal-3, and then blotted for β-catenin (Figure 3.3E). Ultrastructural analysis of secondary to quaternary neurospheres revealed the absence of ependymal cells (Gil-Perotin et al., 2013). The results showed that Gal-3 was bound to β-catenin in neurosphere protein. Therefore, these results indicate that Gal-3 interacted with β-catenin in NSCs and TAPs.

I next addressed whether the Gal-3-β-catenin interaction is activation-state specific. To address this question, I blotted for different phosphorylated β-catenin forms after Gal-3 immunoprecipitation from lSVZ membrane protein (Figure 3.3D). β-catenin phosphorylated (p-β-catenin) at Serine residues 33/37/45 and Threonine 41 is targeted for proteasomal degradation (Clevers and Nusse, 2012). Conversely, p-β-catenin at Serine 552 (Fang et al., 2007)

or 675 (Hino et al., 2005; Taurin et al., 2006) is transcriptionally active. The results showed that Gal-3 was bound to both active and inactive p-β-catenin species. Overall, Gal-3 was bound to β-catenin in both active and inactive states.

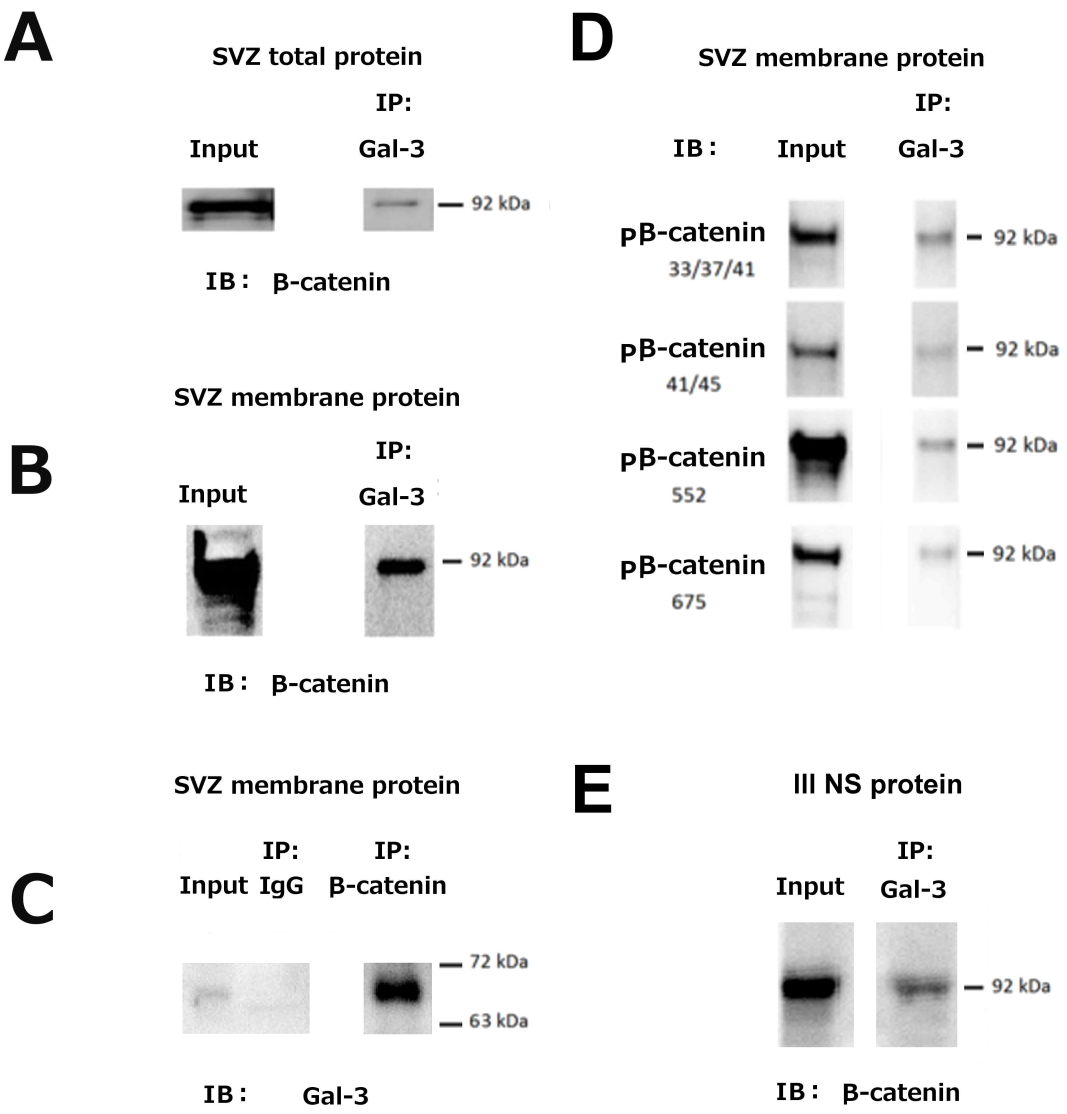


Figure 3.3 Gal-3 was bound to β-catenin in the SVZ

(**A-E**) Co-immunoprecipitation shows that Gal-3 bound to β-catenin in the lSVZ; from both SVZ total (**A**) and membrane-enriched protein fractions (**B**). The binding was confirmed in reverse co-immunoprecipitation (**C**). Note that the band detected measured ~68kDa, likely a dimeric Gal-3 form. Gal-3 bound to various phosphorylated β-catenin (pβ-catenin) forms (**D**). Gal-3 was also bound to β-catenin form tertiary neurospheres protein (**III NS**) (**E**).

3.2.3 In vivo brain electroporation as means to manipulate Gal-3 levels and report Wnt/β-catenin in the postnatal SVZ

Given the co-expression and binding, I hypothesised that Gal-3 regulated β-catenin function in the SVZ. To test this hypothesis, I decided to test the impact of Gal-3 overexpression and knockdown on Wnt/β-catenin signalling in the SVZ. To address this, I constructed appropriate tools and utilised a suitable delivery method into the SVZ as I explain below.

3.2.3.1 Gal-3 overexpression and knockdown constructs

I first constructed Gal-3 overexpression (Gal-3 OE) and knockdown (shGal-3) plasmids (see Sections 2.4.4 – 2.4.6). I then tested whether these constructs efficiently upregulated and downregulated Gal-3 levels in vitro in HEK293T cells transfected with the plasmid combination shown in Figure 3.4A. After 72 hours, the cells were harvested and lysed for western blot analysis of Gal-3 and the loading control β-Actin protein levels. DNA-free Lipofectamine, GFP plasmid, and non-targeting shRNA (shNT) plasmid were used as controls. At baseline, HEK293T cells expressed very little Gal-3, which proved useful in testing overexpression and knockdown of overexpressed Gal-3. Firstly, the Gal-3 OE plasmid significantly increased Gal-3 levels from baseline. Secondly, from 4 shGal-3 plasmids (V1-4), V1 was determined to be most efficient in knocking down Gal-3 protein levels. For all knockdown experiments thereafter, I used shGal-3 V1 (called shGal-3 hereafter). To test whether these plasmids worked efficiently in cultured NSCs, I nucleofected NSCs from tertiary neurospheres with control, shGal-3, and Gal-3 OE

plasmids and cultured the cells for 48 hours before harvesting them for protein analysis (Figure 3.4F). Gal-3 OE efficiently increased Gal-3 protein levels compared to control, while shGal-3 decreased it. Altogether, these data demonstrate that, in vitro, Gal-3 OE and shGal-3 plasmids sufficiently upregulated and downregulated Gal-3 levels, respectively.

3.2.3.2 In vivo electroporation

Testing the effects of Gal-3 level manipulation on Wnt/β-catenin signalling in the SVZ first requires delivering the plasmids into the SVZ niche, and second, verifying timely overexpression and knockdown of Gal-3 levels. In vivo electroporation of plasmid DNA delivered into the LV of the forebrain is an increasingly popular method to target RGCs in the pSVZ (Boutin et al., 2008; Chesler et al., 2008; Fernandez et al., 2011; Platel et al., 2010) and to a lesser extent NSCs in adults (Barnabe-Heider et al., 2008). Our laboratory's experience with postnatal electroporation showed a higher success rate and better survival when the procedure targeted mice pups compared to adults; therefore, I chose to use electroporation to target the lSVZ of P2 pups and test Gal-3 OE and shGal-3 plasmids in vivo (Figure 3.4B-E). I electroporated the pSVZ with the plasmid combinations shown in Figure 3.4B, and sacrificed the pups 3 days post electroporation (DPE). I next used fluorescent immunohistochemistry to determine whether overexpression and knockdown of Gal-3 correlated with its detected levels in the lSVZ (Figure 3.4B,D). All labelled cells expressed mCherry, and I verified that almost all mCherry+ cells overexpressed or downregulated Gal-3 expression, in Gal-3 OE and shGal-3 groups, respectively. Quantification of Gal-3 mean fluorescent intensity (MFI)

normalised to mCherry revealed that Gal-3 OE significantly increased Gal-3 by approximately 2.5 fold of control levels, whereas knockdown of Gal-3 reduced its levels to approximately half of the control levels (Figure 3.4E). Thus, Gal-3 OE and shGal-3 plasmids efficiently overexpressed and knocked down Gal-3 levels in vivo 3 DPE, respectively.

To address the biological questions presented in the following chapters, I included two additional cohorts of mice that were sacrificed at 7 and 17 DPE (Figure 3.4C). Of note, both Gal-3 OE plasmids used in this study equally overexpressed Gal-3 in vivo and in vitro; pCAG-Gal-3 (in vivo; Figure 3.4D. In vitro; Figure 6.9) and pCAG-Gal-3-IRES-GFP (In vivo; Appendicular Figure A1A. In vitro; Figure 3.4A). I also confirmed that Gal-3 remained persistently upregulated in both later time-points in the OB neuroblasts and differentiated neurons (Appendicular Figure A1B-C). Of note, control non-targeting shRNA co-electroporated with the Wnt/β-catenin reporter plasmid (Mutch et al., 2009) did not alter Gal-3 expression levels compared to Wnt reporter only; hence, these groups were pooled and used as controls.

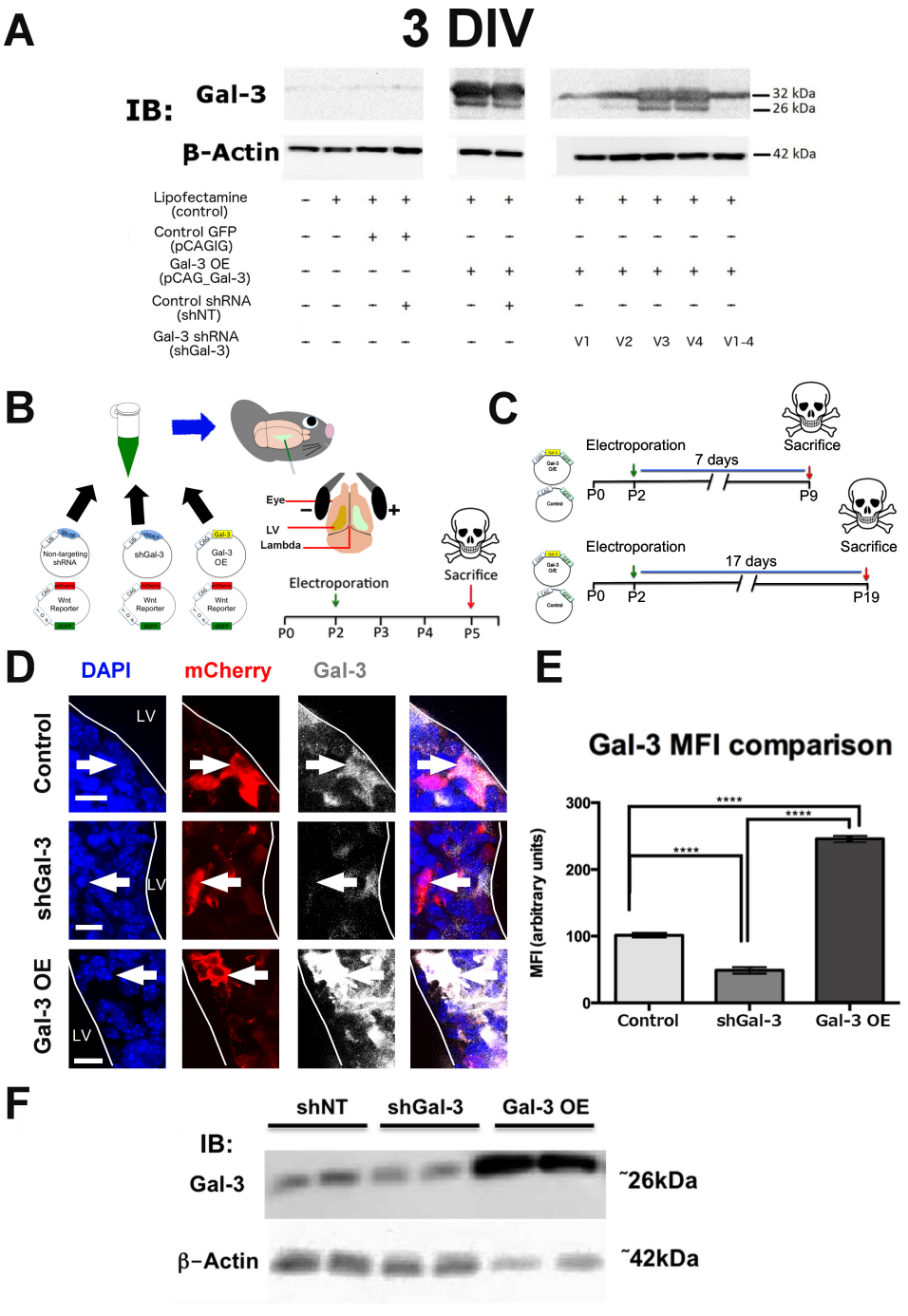


Figure 3.4 Gal-3 construct validation

(**A**) Western blot analysis of protein samples from HEK293T cells transfected with the detailed plasmid combinations and analysed 3 days after transfection in vitro (3DIV).
(**B**) Schematic illustration of in vivo electroporation procedure and scheme used in (**D**). Plasmid combinations were mixed, injected into the lateral ventricle (LV), and electroporated. Mice were sacrificed 3, 7, or 17 days post electroporation (DPE) (**B-C**).
(**D**) Shows a representative confocal image for mCherry (red) and Galectin-3 (Gal-3; grey) in the subventricular zone (SVZ) 3 DPE with Wnt reporter plus control shRNA, Gal-3 knockdown (shGal-3), or Gal-3 overexpression (Gal-3 OE) plasmids. Note the different Gal-3 staining intensity in the 3 groups. All images were acquired using the same settings. Scale Bars: 10µm.
(**E**) Quantification of D; Normalised Gal-3 mean fluorescent intensity (MFI) to mCherry MFI in arbitrary units. Data is shown as mean ± SEM. Statistical significance was determined using One-Way ANOVA, Kruskal-Wallis test for multiple comparisons. N=4. ****: $p < 0.0001$.
(**F**) Western blot analysis of protein samples from neurosphere cultures nucleofected with control (shNT), shGal-3, or Gal-3 OE and analysed 2 days later.

3.2.4 Wnt signalling and Galectin-3 expression were downregulated with SVZ lineage progression

Since I demonstrated that in vivo electroporation can be used to modulate Gal-3 levels in the plSVZ, I next aimed to ascertain whether Gal-3 was expressed in cells actively signalling in Wnt/β-catenin pathway in the plSVZ. Also I aimed to verify if Gal-3 expression and Wnt/β-catenin signalling were downregulated in more differentiated plSVZ cells. To tackle these questions a bicistronic Wnt/β-catenin reporter plasmid was electroporated into the plSVZ of P2 mice (Figure 3.5A). All labelled cells expressed mCherry, but only cells with active Wnt/β-catenin signalling expressed GFP. Mice were sacrificed 3 DPE. I examined Gal-3 and GFP expression in labelled mCherry+ cells at different points along the antero-posterior axis (Figure 3.5B). At the anterior SVZ level, a subset of labelled cells co-expressed Gal-3 and GFP, confirming postnatal Gal-3 expression and Wnt/β-catenin signalling in a subset of plSVZ cells (Figure 3.5C). At posterior and anterior RMS levels, mostly neuroblast descendants of labelled SVZ NSCs and TAPs could be observed. At these rostral levels, almost none of the labelled cells expressed Gal-3 or GFP (Figure 3.5D-E). These data confirmed the expression of Gal-3 in a subset of NSCs and TAPs targeted by in vivo electroporation of the plSVZ. Furthermore, the data verified that Gal-3 expression and Wnt/β-catenin signalling were downregulated in cells that progressed through the lineage and migrated out of the SVZ.

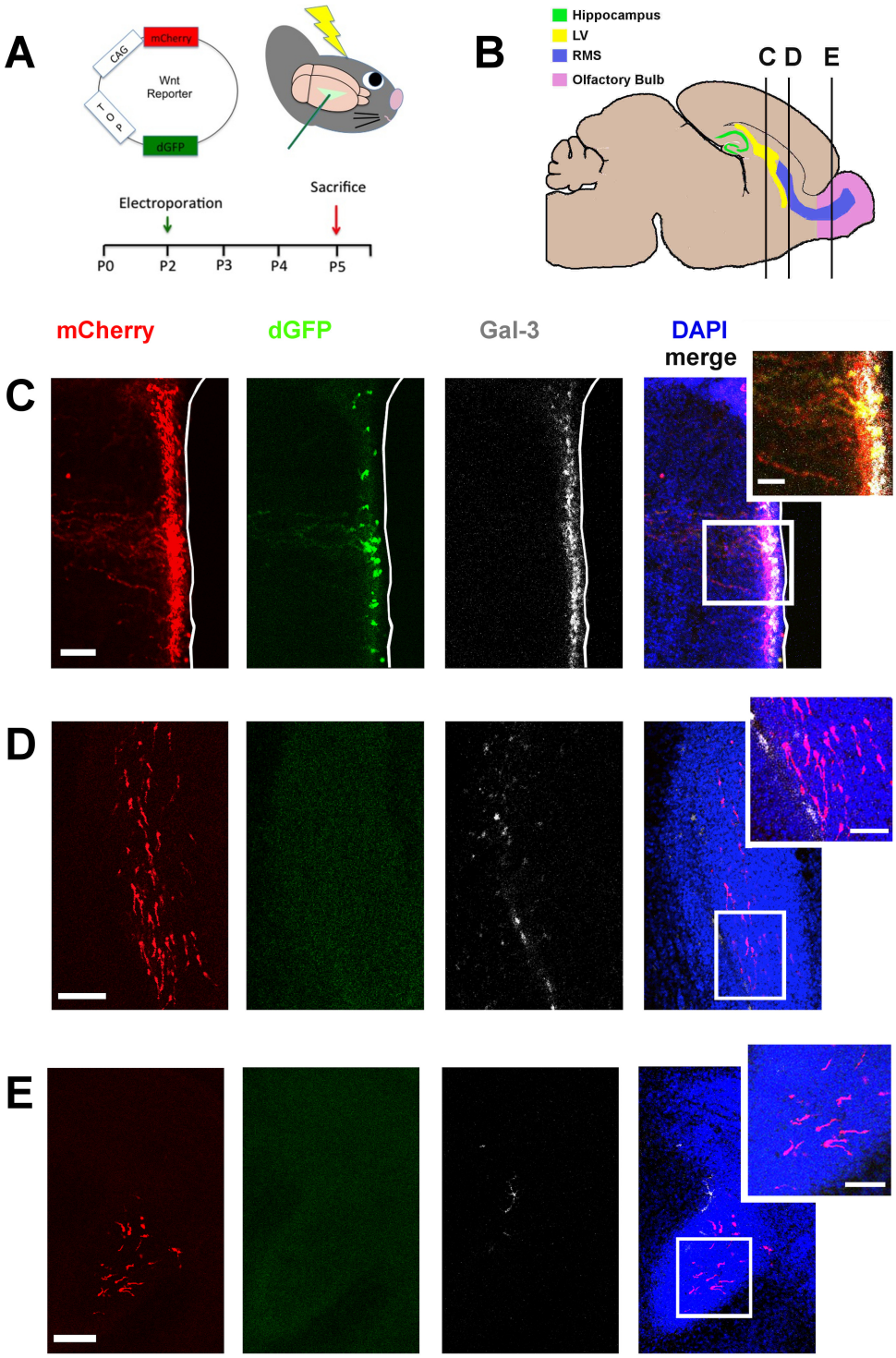


Figure 3.5 Gal-3 and Wnt/β-catenin signalling were downregulated with plSVZ lineage progression

(A-B) Cartoon depictions of the structure of Wnt reporter plasmid and *in vivo* brain electroporation scheme (**A**), and the approximate anatomical locations of panels C,D, and E (**B**). All labelled cells express mCherry, and only cells with active Wnt signalling express GFP. **(C-E)** Single optical planes from confocal microscopy of fluorescent immunohistochemistry showing that Wnt signalling is active in labelled stem and progenitor cells in the lateral subventricular zone (**C**). Galectin-3 (Gal-3) is expressed in a subset of those cells. Neuroblasts in the proximal RMS (**D**) and distal RMS (**E**) do not express Gal-3 and down-regulate Wnt signalling. Scale bars measure 100μm in main panels and 50μm in insets.

3.2.5 Galectin-3 regulated Wnt signalling in the plSVZ in vivo

I next set out to investigate if manipulation of Gal-3 levels altered Wnt/β-catenin signalling. To that end, I co-electroporated the Wnt reporter plasmid with Gal-3 OE, shGal-3, or control shRNA (shNT) constructs, into the lSVZ of P2 mice and then sacrificed the mice 3 DPE (Figure 3.6A). The percentage of GFP+ labelled cells was used as a readout for Wnt/β-catenin signalling in the plSVZ. Labelled cells either significantly upregulated Gal-3 in the Gal-3 OE group, or downregulated it in the shGal-3 group, compared to control (Figure 3.4D-E). Qualitatively, GFP intensity was higher in shGal-3 and lower in Gal-3 OE groups. Quantitatively, I found more GFP+ labelled cells in the shGal-3 group, and fewer in the Gal-3 OE group, compared to control (Figure 3.6B). Gal-3 level manipulation significantly altered the percentage of GFP+ labelled cells in the SVZ (One way-ANOVA; $F(2,20) = 21.27$, $p < 0.0001$). More specifically the percentage of Wnt signalling was 35.3 ± 2.4% in Gal-3 OE (n=7) and 53.7 ± 1.2% in shGal-3 (n=7) compared to 43.3 ± 1.9% in control (n=9) (p values: Control vs Gal-3 OE = 0.0183, control vs shGal-3 = 0.0025, and Gal-3 OE vs shGal-3 < 0.0001)(Figure 3.6C). These findings indicate that Gal-3 negatively regulated Wnt/β-catenin signalling in vivo in the plSVZ.

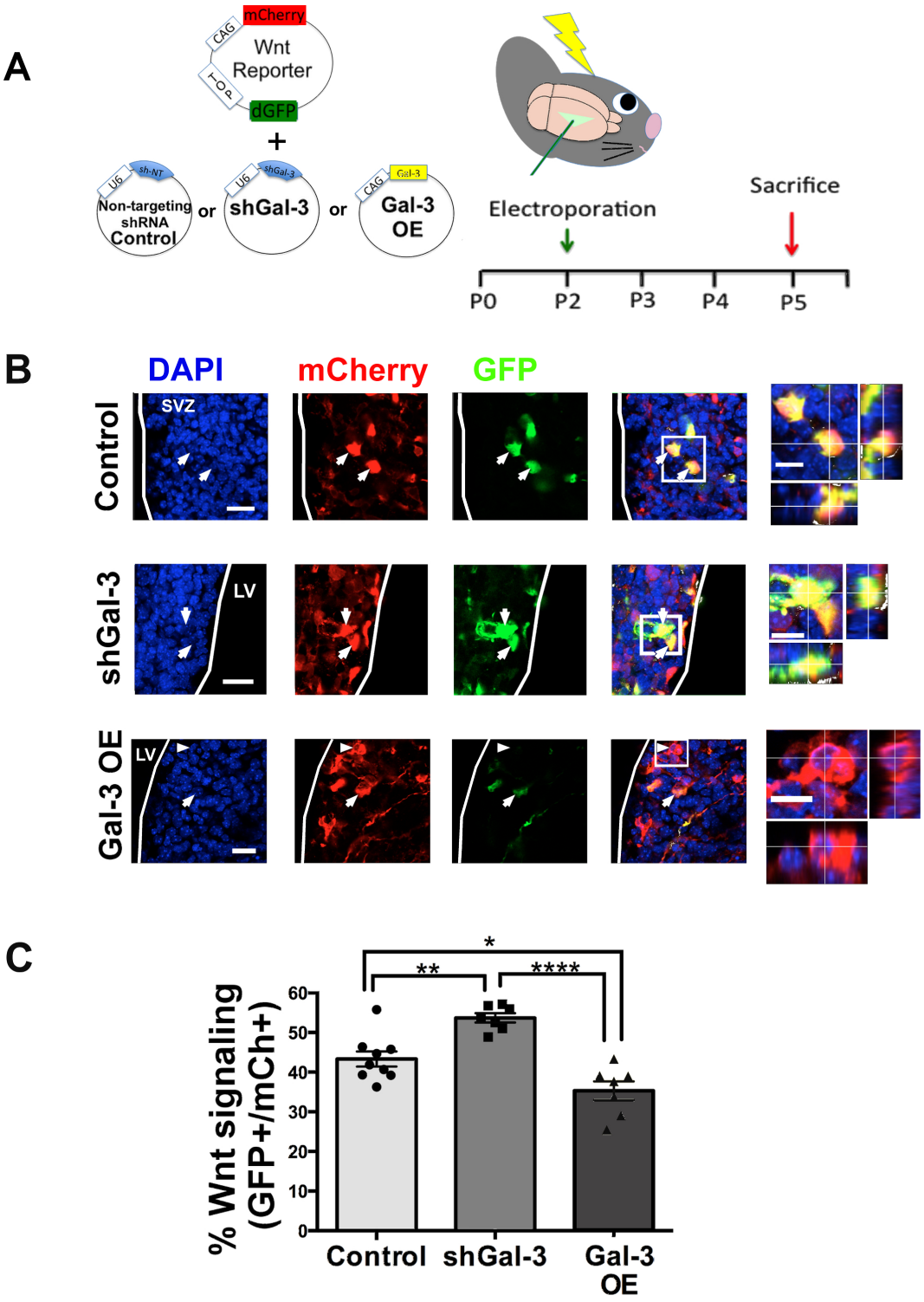


Figure 3.6 Gal-3 regulated Wnt/β-catenin signalling in vivo

(A) Cartoon depiction of in vivo brain electroporation scheme.
(B) Confocal images of Fluorescent Immunohistochemistry analysis of GFP (green; positive in cells with active Wnt signalling) and mCherry (red; positive in all labelled cells) in control non-targeting shRNA, Galectin-3 (Gal-3) knockdown (shGal-3), and Gal-3 overexpression (Gal-3 OE) groups. Orthogonal views of boxed areas are shown on next to the respective panels**.** Arrows indicate mCherry+GFP+ and arrowheads mCherry+GFP- cells. Scale bars measure 20μm in B and 10μm in insets.
(**C**) Quantification of B. n=9 for control group and 7 for shGal-3 and Gal-3 OE groups. Statistical significance was calculated using One-Way ANOVA, Tukey's test for multiple comparisons.

3.2.6 Galectin-3 regulated Wnt/β-catenin signalling in NSCs in vitro

To ascertain if the relationship between Gal-3 and Wnt/β-catenin signalling was preserved in vitro, I cultured pISVZ-derived NSCs as floating neurospheres in vitro, and passaged them to tertiary neurospheres before they were co-nucleofected with the Wnt reporter and Gal-3 OE, shGal-3, or control plasmids. I allowed the cells to grow in suspension at a density of $1x10^5$ cells/ml for 24 hours in growth media containing EGF and FGF before flowcytometric (FACS) analysis (Figure 3.7A). I used forward scatter (FSC) and side scatter (SSC) to gate out debris, FSC and pulse width to gate on single cells, and Live/Dead® Fixable Violet Kit (Life Technologies) to gate on live cells (Appendicular Figure A2A-C). Flowcytometry controls are shown in Appendicular Figure A2D. The percentage of labelled cells that expressed GFP or high GFP (defined as GFP signal intensity > 10^2) was used as a readout for Wnt/β-catenin signalling. Qualitatively, labelled cells in Gal-3 OE showed fewer cells with high GFP expression compared to control, whereas shGal-3 showed the opposite effect (Figure 3.7B). Quantitatively, FACS analysis showed that the percentage of GFP+ labelled cells was not significantly altered (93.6 ±3.4% and 99.81 ± 4.4% of control, p=0.155 and 0.968, for Gal-3 OE and shGal-3, respectively, n=4; Figure 3.7C). However, compared with control, Gal-3 OE significantly reduced the overall percentage of GFP-high+ labelled cells (81.1 ± 3.2% of control, p=0.0099) and the proportion of GFP-high+ cells amongst GFP+ cells (86.8 ± 3.3% of control, p=0.0267). In contrast, knockdown of Gal-3 displayed an opposite trend without reaching statistical significance; increasing GFP-high+ labelled cells (116.4 ± 6.8% of control, p=0.0953) and GFP-high between GFP+ cells (115.9

± 7.2% of control, p=0.1137) compared to control (Figure 3.7D-E). In sum, this data supports the in vivo results and show that Gal-3 levels negatively regulated Wnt/β-catenin signalling in the plSVZ NSCs in vitro.

Notably, when cells survived longer in culture, Wnt/β-catenin signalling dynamics changed. This was apparent in the sizeable reduction in the proportion of cells with active Wnt/β-catenin signalling at 3 days post nucleofection (3DIV) compared to that at 1DIV (Figure 3.8). To elaborate, Wnt/β-catenin signalling was active in 63.79 ± 6.18%, 64.27 ± 8.9%, and 59.32 ± 4.84 % of nucleofected cells in control, shGal-3 and Gal-3 OE, respectively, at 1DIV. This dropped 3DIV to 21.28%, 23.77%, and 21.97% in control, shGal-3, and Gal-3 OE, respectively. In addition, there was no qualitative difference in GFP signal intensity as determined by visual assessment of experimental groups under epifluorescence microscopy at 20 and 40X magnification (n=3 experiments) before FACS analysis (n=2 experiments). The latter did not reveal any significant differences in Wnt/β-catenin signalling between the test groups. Therefore, these data indicate that firstly, Wnt/β-catenin signalling was downregulated with increased survival of NSCs cultured at high density in growth media. Secondly, the effects of Gal-3 level manipulation were acute and were lost with increased survival in culture.

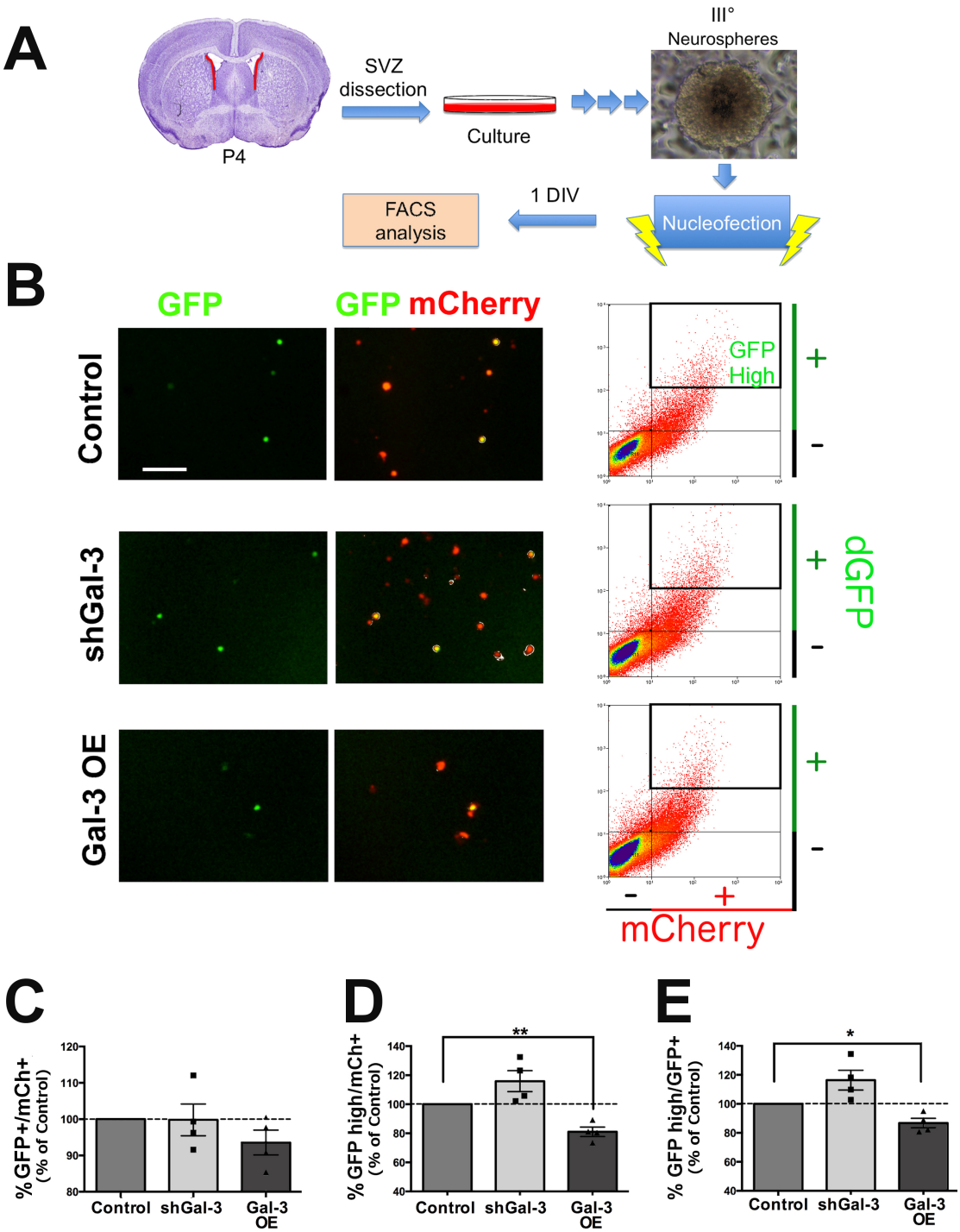


Figure 3.7 Gal-3 regulated Wnt/β-catenin signalling in vitro

(A) Cartoon depiction of in vitro culture of lateral ventricular wall subventricular zone (SVZ) tissue (area lined with red), followed by nucleofection with the same conditions in Figure 3.6A. Flowcytometry (FACS) analysis was done 1 day after nucleofection.
(B) Epifluorescence images of nucleofected conditions (Left side) just before FACS Analysis (right side). The boxed area in FACS panel defines GFP high population with active Wnt/β-catenin signalling. Scale bar: 100μm
(C-E) Quantification of B. Data is shown as percentage of control. n=4 independent experiments. Statistical significance was calculated using One-sample *t*-test. Data is shown as mean ± SEM. *p* values: * < 0.05, ** < 0.01.

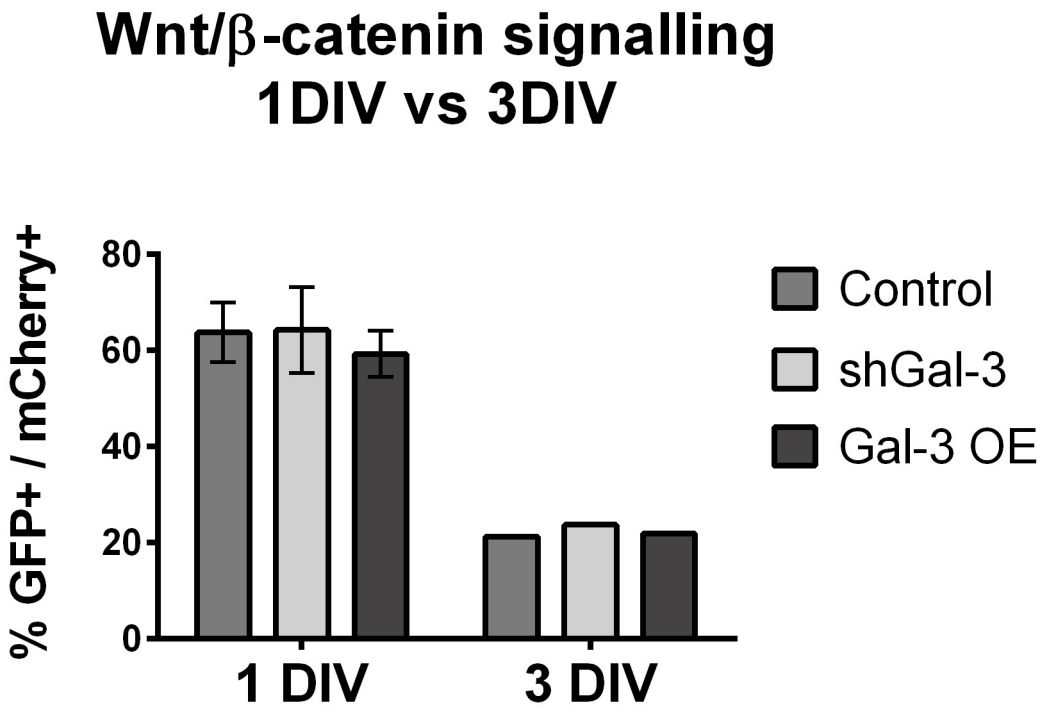


Figure 3.8 Wnt/β-catenin signalling was downregulated with increased survival in vitro

Comparison between Wnt/β-catenin signalling in NSC/TAPs nucleofected with Gal-3 overexpression (Gal-3 OE), Gal-3 knockdown (shGal-3) and non-targeting shRNA (Control) 1 and 3 days after nucleofection in vitro (DIV). n=4 for 1DIV and 2 for 3 DIV. Data is shown as mean ± SEM. Error bars were not shown for 3DIV groups because n=2.

3.2.7 Overexpression of Galectin-3 reduced proliferation and increased cell cycle exit in the plSVZ

β-catenin activation and canonical Wnt signalling have been shown to promote adult NSC symmetric division (Piccin and Morshead, 2011), maintenance (Qu et al., 2010), and TAP amplification (Adachi et al., 2007). In light of the findings presented above demonstrating the negative regulation of Wnt/β-catenin signalling by Gal-3, I investigated whether cell proliferation was altered after Gal-3 level manipulation. Co-electroporation was done as above (Figure 3.6A), and the percentage of labelled cells expressing the mitotic marker phospho-Histone-3 (PHi3) was used as a readout for cell proliferation (Figure 3.8A). To statistically compare the PHi3 expression in the experimental groups, I used Kruskal-Wallis test (One-way ANOVA for non-parametric data) and found they were significantly different (Kruskal-Wallis statistic = 6.012, n=3 groups, p=0.0398). More specifically, post-hoc analysis revealed that Gal-3 OE significantly reduced the percentage of PHi3+ labelled cells compared to control (2.60 ± 0.76%, n=3, Gal-3 OE; 8.34 ± 1.5% control, n=5, p=0.0416). In contrast, increased Wnt/β-catenin signalling in Gal-3 knockdown was not accompanied by a commensurate increase in proliferation (7.42 ± 1.1%, n=3, p > 0.99; Figure 3.8C). These findings indicate that Gal-3 gain-of-function, but not loss-of-function, reduced proliferation in the plSVZ 3 DPE.

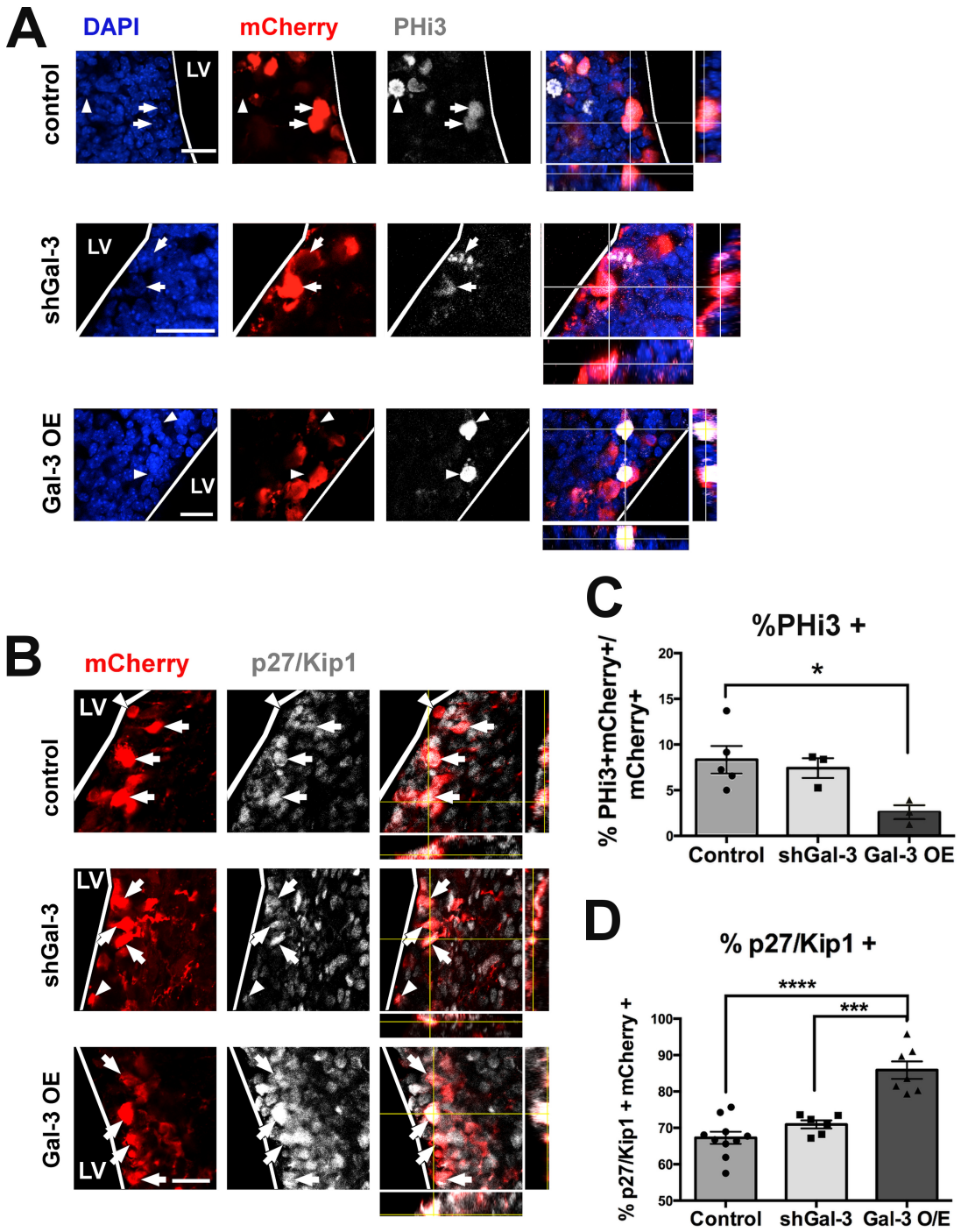


Figure 3.9 Gal-3 OE reduced plSVZ proliferation

(A-B) Confocal images show mCherry (labelled cells; red) and mitotic marker phospho-Histone-3 (PHi3) in **A**, and cell cycle exit marker p27/Kip1 in **B**, shown in grey. Merged images also show orthogonal views. Scale bars: 20µm
Arrows indicate double-labelled cells. Arrowheads show mCherry- PHi3+ cells in **(A)** and mCherry+ p27/Kip1-low/negative cells in **(B)**.
(C) Quantification of A, n=5 for control, and 3 for shGal-3 and Gal-3 OE. Statistical significance was calculated using Kruskal-Wallis test with Dunn's test for multiple comparisons. (Groups were compared to control group).
(D) Quantification of B. Only p27/Kip1-high cells were counted, n=9 for control and 7 for shGal-3 and Gal-3 OE. Statistical significance was calculated using One-Way ANOVA, Tukey's test for multiple comparisons.
Data is shown as mean ± SEM. *p* values: * < 0.05, *** < 0.001, **** <0.0001.

β-catenin loss-of-function was previously shown to induce cell cycle exit in embryonic cortical precursors (Chenn and Walsh, 2002; Machon et al., 2007; Woodhead et al., 2006). Thus, I set out to determine if the alteration in Wnt/β-catenin signalling induced by Gal-3 level manipulation caused plSVZ cell cycle exit. To tackle this question, I immunostained electroporated brain sections for p27/Kip1, a cyclin-dependent kinase inhibitor that supresses the G_1/S-phase transition and promotes cell cycle exit (Doetsch et al., 2002b) (Figure 3.8B). I then used One-way ANOVA to determine whether the experimental groups were different in p27/Kip1 expression. I found that p27/Kip1 expression in labelled cells in the lSVZ was significantly different after Gal-3 level manipulation 3 DPE ($F(2, 20) = 28.46$, $p < 0.0001$). Post-hoc analysis revealed that while Gal-3 knockdown failed to alter the percentage of p27/Kip1+ labelled cells (70.96 ± 1.11%, n=7, p=0.3654) compared to control (67.28 ± 1.67%, n=9), Gal-3 OE significantly increased p27/Kip1 expression (85.88 ± 2.38%, n=7, $p < 0.0001$; Figure 3.8D). Therefore, these data support that Gal-3 upregulation increased p27/Kip1 expression in the lSVZ, indicative of increased cell cycle exit.

I next postulated that If Gal-3 increased cell cycle exit, then more SVZ cells would progress through the lineage and give rise to neuroblasts, which will subsequently migrate through the RMS to the OB. To test this hypothesis, I quantified labelled cell density in the RMS 3 DPE of Gal-3 OE, shGal-3, and control plasmids. I examined the RMS distal to the tip of the LV; where neuroblasts are confined in a cylindrical stream all the way to the OB. Next, Kruskal-Wallis test was used to statistically compare the experimental groups. In concert with the p27/Kip1 data, I found that the test groups were

significantly different (Kruskal-Wallis statistic = 7.395, n=3 groups, p=0.0109). Post-hoc analysis showed significantly more labelled cells in the RMS of Gal-3 OE compared with control (123,464 ± 8,448 cells/mm^3, n=4, Gal-3 OE; 41,363 ± 12,581 cells/mm3, n=5, control, p=0.0442). In contrast, Gal-3 knockdown showed no difference from control (45,150 ± 17,166 cells/mm^3, n=3, p >0.99; Figure 3.10). These results indicate that Gal-3 upregulation increased neuroblast density in the RMS 3 DPE, which supports the data presented previously showing increased cell cycle exit after Gal-3 OE. These data cast doubt on my original hypothesis, which contended that downregulation of Gal-3 levels may be required to allow plSVZ lineage progression. Finding neuroblasts in the RMS after Gal-3 OE indicate that Gal-3 downregulation was not necessary to allow lineage progression. Taken together, upregulation of Gal-3 increased p27/Kip1 expression in the plSVZ, supporting a model whereby Gal-3 upregulation increased cell cycle exit and reduced proliferation 3 DPE in the plSVZ. The fact that Gal-3 upregulation increased cell density in the RMS lends further support to that model, and rules out the hypothesis that Gal-3 downregulation might have been required to allow plSVZ lineage progression.

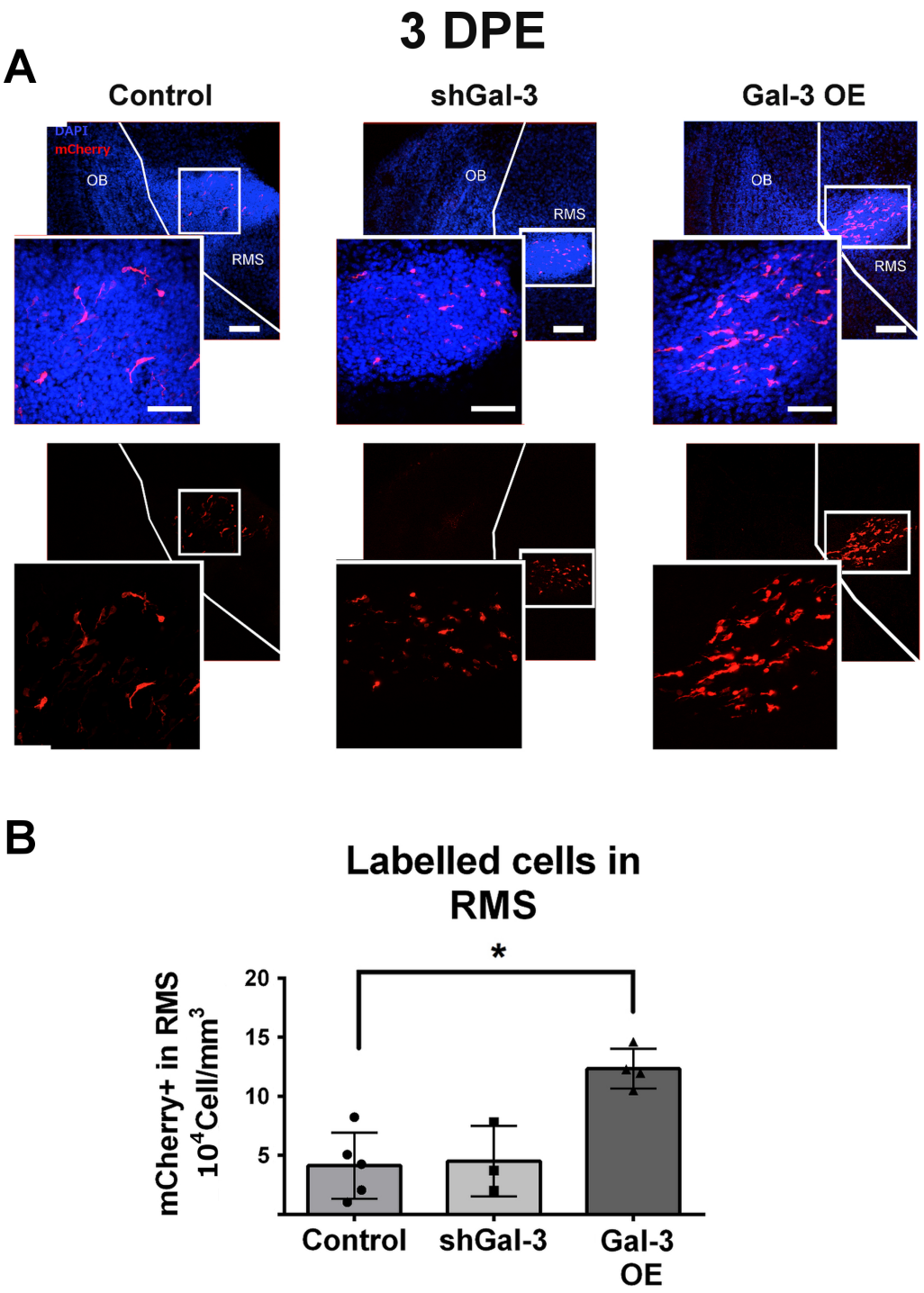


Figure 3.10 More Gal-3 overexpressing neuroblasts reached the RMS

(A) Confocal images of the distal rostral migratory stream (RMS) at the level of the caudal Olfactory bulb (OB) 3 DPE of Wnt reporter plus control shRNA, Gal-3 knockdown (shGal-3), or Gal-3 overexpression (Gal-3 OE) plasmids, as in **figure 3.6A**. Labelled cells are mCherry+ (red) and nuclei stain with DAPI (blue). The boxed area is enlarged in the insets. Scale bars: 100µm for main panels and 50µm for insets.
(B) Quantification of (**A**). Cell density as mCherry+ cells/mm^3 is shown. Statistical significance was calculated using One-Way ANOVA, Kruskal Wallis test, Dunn's test for multiple comparisons (with control group). n=5 for control, 3 for shGal-3, and 4 for Gal-3 OE. Data is shown as Mean ± SEM. *p* value: * < 0.05

To further verify the reduction in proliferation induced by Gal-3 OE, and to determine at which point Gal-3 OE triggered cell cycle exit, I employed a double-thymidine analogue-labelling paradigm. This allowed me to label a subset of actively proliferating plSVZ cells with BrdU, and determine the proportion of these cells that re-entered the cell cycle 24hours later. In addition, it would serve to verify the proliferation phenotype in Gal-3 OE using a different cell cycle label. The experimental plan is shown in Figure 3.10A. Briefly, P2 mice were electroporated with Gal-3 OE or GFP control plasmids. Next, the pups received one pulse of BrdU 2 DPE, and a pulse of EdU 24 hours afterwards (2 hours before sacrifice)(Figure 3.10A). I then stained for GFP, BrdU, and EdU (Figure 3.10B) and quantified the proportion of GFP-labelled cells in the lSVZ that expressed BrdU, EdU, or both. The proportion of BrdU+GFP+ cells from the total GFP+ population was used as a readout for proliferation at 2 DPE (24hour proliferation in Figure 3.10C), and the proportion of EdU+GFP+ cells as an indicator for proliferation 3 DPE (2hour proliferation in Figure 3.10D). The cells that re-entered the cell cycle expressed both BrdU and EdU (Figure 3.10E). The ratio of those BrdU+EdU+GFP+ over BrdU+GFP+ cells signifies cell-cell re-entry. Mann-Whitney test was used to compare the test groups. In line with the PHi3 data, Gal-3 OE significantly reduced the percentage of labelled cells that took up both BrdU 2 DPE (26.94 ± 1.87%, n=5, Gal-3 OE; 43.64 ± 3.21% control, n=4, p=0.0159) and EdU 2 hours before sacrifice (3DPE) (21.62 ± 2.18% Gal-3 OE; 35.1 ± 2.16% control, p=0.0159; Figure 4G-H). Consistently, the percentage of BrdU+ EdU+ labelled cells, which re-entered the cell cycle, was proportionately reduced (16.58 ± 0.84% Gal-3 OE; 24.57 ± 2.44% control, p=

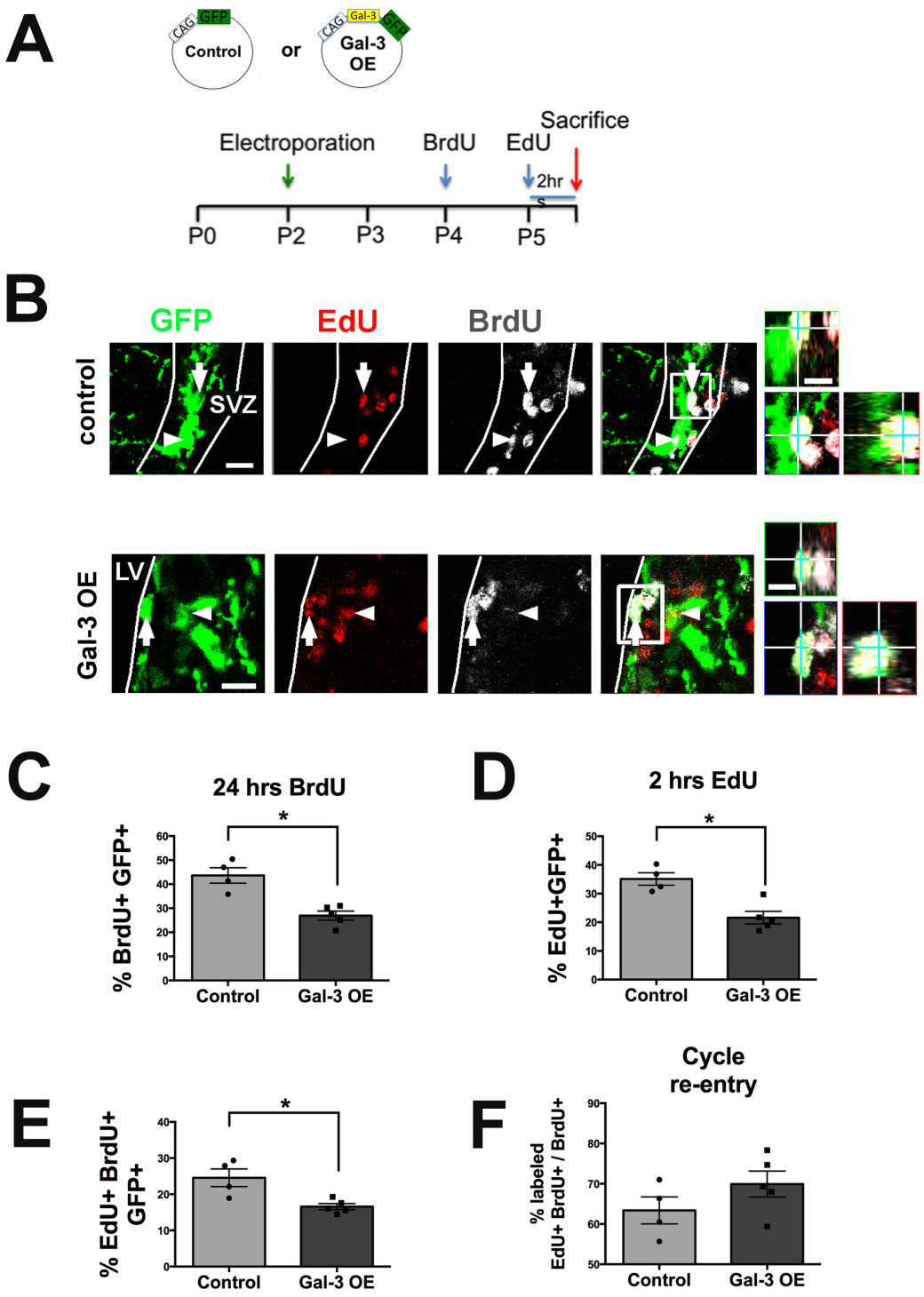


Figure 3.11 Proliferation dynamics after Gal-3 OE

(**A**)Cartoon illustration of in vivo electroporation and double-Thymidine analogues labelling paradigm (BrdU/EdU).
(B) Confocal images showing GFP (green), BrdU (grey), and EdU (red). Arrows indicate BrdU+ EdU+ labelled cells, Arrowheads indicate BrdU+EdU- labelled cells in control and EdU+BrdU- cells in Gal-3 OE. The boxed area is shown in an orthogonal view. Scale bars: 10μm for main panels and 5μm for orthogonal views.
(C-F). Quantification of D, n=4 for control and 5 for Gal-3 OE. Statistical significance was calculated using Mann-Whitney test. Data is shown as Mean ± SEM. *p* values: * < 0.05.

0.0317; Figure 4I). However, cell cycle re-entry, represented by the ratio of BrdU+ EdU+ GFP+ / total BrdU+ GFP+ population, was not significantly altered (69.93 ± 3.24% Gal-3 OE; 63.38 ± 3.35% control, p=0.2857; Figure 4J). Together these data indicate that Gal-3 gain-of-function reduced proliferation 2 and 3 DPE without altering cell cycle re-entry of labelled proliferative cells. Moreover, the data suggests that Gal-3 OE promoted cell cycle exit earlier than 2 DPE; acutely reducing the population growth fraction.

3.2.8 Gal-3 did not increase cell death in the lSVZ

Cell death could reduce the amount of proliferative cells detected, potentially accounting for the results observed. To rule out increased apoptosis as a possible cause for reduced plSVZ proliferation after Gal-3 OE, immune-labelling for activated caspase-3 in electroporated brains was conducted (Figure 3.11A). The results showed no significant change in apoptosis in the labelled cells (One-way ANOVA, $F(2,12)=1.26$, $p=0.3187$, $n=5$). However, Gal-3 OE significantly decreased the total (labelled and unlabelled) number of apoptotic SVZ cells compared to control (1.03 ± 0.21 Gal-3 OE; 2.97 ± 0.59 control, $p=0.0233$). On the other hand, Knockdown of Gal-3 did not alter cell death (2.6 ± 0.49, $p > 0.99$; Figure SG). The data indicates that Gal-3 OE increased survival 3 DPE in a cell non-autonomous fashion. Thus, increases cell death cannot be the cause of reduced number of proliferating cells observed after Gal-3 OE. I next examined if Gal-3 altered cell death at later time points (7 and 17 DPE). I found Gal-3 OE did not alter activated caspase-3 positivity of both labelled and unlabelled cells 7 and 17 DPE (Figure 3.12B,D-E). Therefore, these data indicate that Gal-3 upregulation had an

acute cell non-autonomous pro-survival effect that did not persist 7 and 17 DPE.

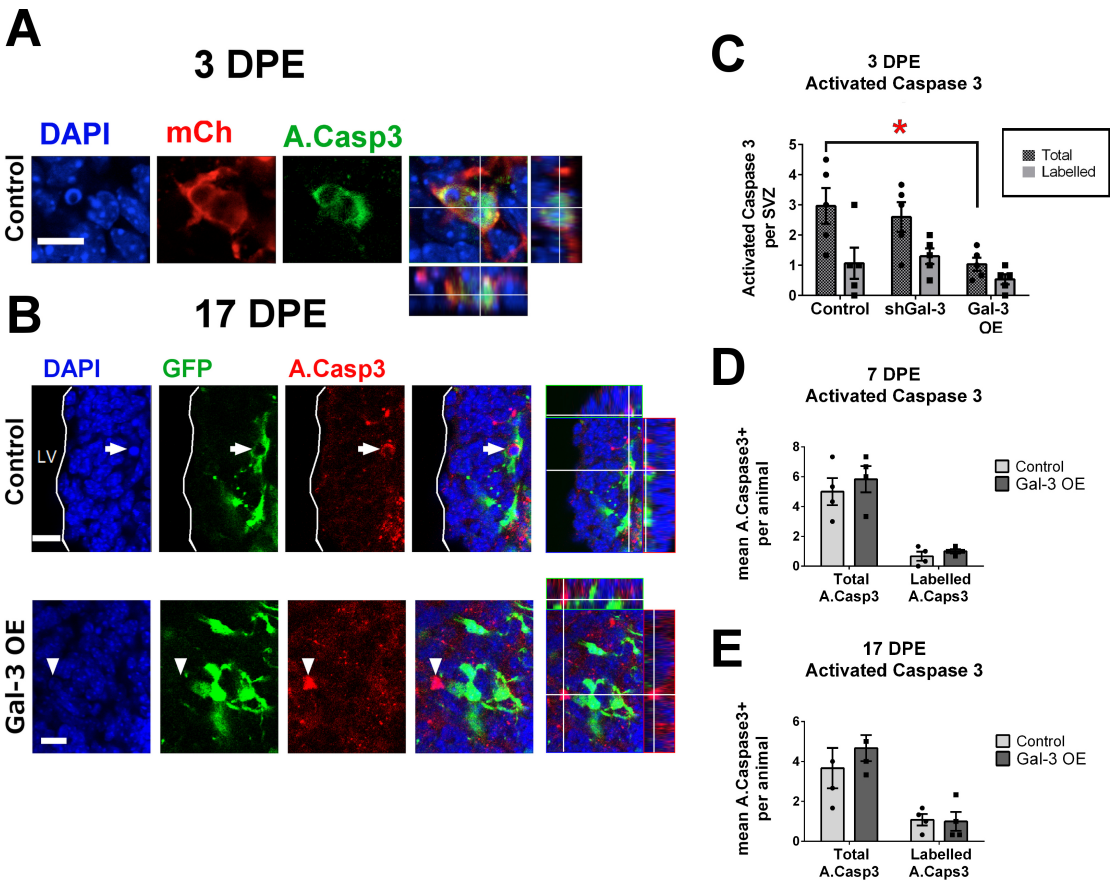


Figure 3.12 Acute cell non-autonomous anti-apoptotic effects of Gal-3

(**A**) Shows a representative confocal image for mCherry (mCh; red) and activated caspase-3 (A.Casp3) and DAPI (blue) of a control animal 3 days post electroporation (DPE). The merged panel also displays an orthogonal view. Note both mCh+ cells express A.Casp3, and the cell on the right also shows a pyknotic nucleus. Scale bar: 20μm.
(**B**) Confocal image showing labelled cells (GFP+; green), activated caspase-3 (A.Casp3; red), and nuclei (DAPI; blue) from control and Gal-3 overexpression (Gal-3 OE) animals. The arrow indicates a GFP+A.Casp3+ cell, whereas the arrowhead indicates a GFP-A.Casp3+ cell. Orthogonal views of the indicated cells are shown on the left. Scale bars: 10μm.
(**C**) Quantification of A. A.Casp3+mCh+ reveal no significant difference between experimental groups. However, total activated caspase-3 was significantly reduced in Gal-3 OE compared to control. Statistical significance was calculated using One-Way ANOVA.
(D-E) Quantification of lSVZ cell survival 7 and 17 DPE. Statistical significance was determined using Mann-Whitney test.
Data is shown as mean ± SEM. *: $p < 0.05$.

3.3 Discussion

3.3.1 Gal-3 and β-catenin are co-expressed in the adult lSVZ

The expression and functions of β-catenin have been thoroughly examined in the developing forebrain prenatally (Chenn, 2008; Mutch et al., 2009; Mutch et al., 2010; Noles and Chenn, 2007; Wrobel et al., 2007; Zhang et al., 2010). In the aSVZ, β-catenin's functions in context of Wnt signalling are increasingly being explored and will be discussed in Section 3.3.3. Moreover, β-catenin is commonly used as a marker for the cell-boundaries in wholemount preparation of the lateral ventricular wall (Comte et al., 2011; Mirzadeh et al., 2010a; Mirzadeh et al., 2010b; Mirzadeh et al., 2008). In these preparations, the ventricular wall is seen en face, and β-catenin facilitates the discrimination between ependymal cells, organised in pinwheel structures, and NSCs, which fall in the centre of the pinwheel (Mirzadeh et al., 2008). However, data about the expression of β-catenin in the postnatal and adult SVZ lineages in coronal sections are scattered in the literature and proved difficult to track down. First, Cleary et al showed co-localisation between GFAP and β-catenin, as well as PSA-NCAM and β-catenin (Cleary et al., 2006). Second, Adachi et al. documented the expression of β-catenin in the lSVZ, without identifying the subtypes of cells expressing it (Adachi et al., 2007). Third, Mirzadeh et al. described β-catenin expression in ependymal cells and a subset of NSCs using the wholemount assay (Mirzadeh et al., 2008). Lastly, expression in NSCs and TAPs was inferred from BAT-GAL and Axin2-GFP reporter mice (Adachi et al., 2007; Piccin and Morshead, 2011). The results presented in this chapter support those in the aforementioned literature. More specifically, I

demonstrated co-expression of β-catenin with GFAP, Mash1, and Dcx, markers of NSCs, TAPs, and neuroblasts in the lSVZ, respectively. Altogether, I confirmed the expression of β-catenin in the lSVZ neurogenic lineage of young adult mice.

In order to study Wnt/β-catenin activity in the adult lSVZ, I examined the subcellular expression of β-catenin. Nuclear translocation of β-catenin is downstream to canonical Wnt signalling (Ring et al., 2014), and that has been employed to report the signalling pathway's activity (Adachi et al., 2007; Durak et al., 2014; Fang et al., 2007). To the best of my knowledge, this is the first study to quantify nuclear β-catenin expression in the SVZ lineage. I found that approximately half of GFAP+ cells in the SVZ, a subset of which include bona fide NSCs, expressed nuclear β-catenin. Conversely, nuclear β-catenin was present in just under 12% of Mash1+ TAPs and none of the neuroblasts. These data indicate that Wnt/β-catenin signalling, as determined by nuclear β-catenin expression, was downregulated with aSVZ lineage progression. Notably, neuroblasts in the RMS core of the OB completely abolished β-catenin expression when they migrated out the RMS into OB layers. I observed a similar pattern of β-catenin expression loss in the rare neuroblasts that exited the SVZ/RMS near the LV (data not shown). This data suggests that β-catenin expression was characteristic of cells within the SVZ-RMS niche, and was lost when cells exited the niche.

In concert with data describing Gal-3 expression in the aSVZ lineage (Comte et al., 2011), I confirmed that Gal-3 was expressed in a subset of GFAP+ NSCs and Mash1+ TAPs, but not neuroblasts. More specifically, I showed that Gal-3 is expressed in 47.6% and 58.6% of GFAP+ cells and

Mash1+ TAPs, respectively. These data indicate that Gal-3 expression, like Wnt/β-catenin signalling, was present in NSCs and TAPs, but was abolished in more differentiated neuroblast. Interestingly, almost all Gal-3+ NSCs and TAPs examined in this study expressed β-catenin.

Co-expression of Gal-3 and β-catenin does not prove functional interaction or binding. Thus, I investigated whether the two proteins were complexed together in the lSVZ. I demonstrated that Gal-3 was bound to β-catenin in the total, soluble, and membrane-enriched fractions of lSVZ protein. I also specifically showed that the interaction is present in NSCs and TAPs cultured from plSVZ. Moreover, the data indicates that Gal-3 was bound to β-catenin in both the soluble and membrane protein fractions, and to both active and inactive p-β-catenin. Together, these findings support the hypothesis that Gal-3 might regulate Wnt/β-catenin signalling in the lSVZ, and that Gal-3-β-catenin interaction may not be dependent on β-catenin activation or inhibition. That being said, and given the co-expression patterns of Gal-3 and β-catenin, I hypothesised that downregulation of Gal-3 expression may be required to allow SVZ lineage progression.

3.3.2 Gal-3 expression and Wnt/β-catenin signalling were downregulated with postnatal lSVZ lineage progression

In order to test the hypotheses presented in the previous section above, I used validated molecular tools to overexpress and knockdown Gal-3 as well as a Wnt/β-catenin signalling reporter to monitor the pathway's activation (Mutch et al., 2009), and then employed in vivo electroporation of the LV to deliver the constructs into NSCs and TAPs in the plSVZ of P2 mice. However,

for the hypotheses generated from aSVZ data to be tested in the pSVZ, I had to first confirm the main premise; that Gal-3 levels and Wnt/β-catenin signalling were downregulated with lineage progression in the plSVZ. Therefore, I first demonstrated that Gal-3 is expressed in a subset of lSVZ NSCs/TAPs with active Wnt/β-catenin signalling. I also showed that Gal-3 expression and Wnt/β-catenin signalling were lost in more differentiated neuroblasts. Notably, this data is consistent with that found by Adachi et al. in the adult lSVZ, when only GFAP+ and Mash1+ but not Dcx+ cells were marked in Axin-d2EGFP Wnt reporter mice (Adachi et al., 2007). In contrast, previous work from BAT-Gal (Marinaro et al., 2012) and $Axin2^{CreERT2}$;$R26R^{mTmG}$ (Bowman et al., 2013) Wnt reporter mice showed some Wnt activity in Dcx+ neuroblasts. However, both β-Gal (Gonda et al., 1989) and GFP (Corish and Tyler-Smith, 1999) have long half-lives exceeding 24 hours, which makes these proteins potentially heritable to daughter cells; hence, they might not reflect Wnt/β-catenin activity in neuroblasts. On the other hand, the Wnt/β-catenin reporters employed in Adachi el al. and this study used destabilised GFP (dGFP) (Adachi et al., 2007; Mutch et al., 2009) with a half-life of approximately 2 hours (Reya et al., 2003). Therefore, cells expressing GFP were unlikely to have inherited it from mother cells, and instead were actively signalling with Wnt/β-catenin at the time of tissue fixation. Therefore, I contend that the main premise of the hypotheses in question- that Gal-3 expression and Wnt/β-catenin signalling were downregulated with plSVZ lineage progression, was satisfied. Further work to investigate whether Gal-3 regulated Wnt/β-catenin signalling and lineage progression was limited to the plSVZ niche.

In vivo electroporation is a powerful technique that allows accurate targeting of different SVZ regions based on the orientation of the electroporation electrodes (Fernandez et al., 2011). I chose to target the lSVZ for the following reasons. Firstly, the area of the lSVZ is larger than other regions, reducing the margin for experimental error in electrode positioning. Secondly, in a prelude to this body of work, I discovered that the lSVZ displayed the highest proportion of Gal-3 expression in Mash1+ and GFAP+ cells compared to other adult SVZ regions. Thirdly, and more importantly, little is known about the gliogenic potential of the plSVZ, as I will demonstrate in the next 2 chapters. Furthermore, Wnt/β-catenin signalling has been more thoroughly studied in the pdSVZ (Azim et al., 2014a), but was shown to be active in the plSVZ (Bowman et al., 2013). Altogether, the plSVZ was suitable to study the interaction between Gal-3 and Wnt/β-catenin signalling in postnatal SVZ lineage progression.

3.3.3 Gal-3 negatively regulated Wnt/β-catenin signalling in the plSVZ

Gal-3 and β-catenin were shown to interact in numerous cancer cell lines. For example, Shimura et al. first used breast carcinoma cell lines to show that N-terminal of β-catenin binds the C-terminal of Gal-3, in a CRD dependent manner (Shimura et al., 2004). The authors also demonstrated that Gal-3 positively regulated Wnt/β-catenin signalling. Furthermore, this interaction was confirmed in gastric (Kim et al., 2010), colorectal (Song et al., 2009), pancreatic (Kobayashi et al., 2011), and tongue squamous cell carcinomas (Wang et al., 2013; Zhang et al., 2013). These studies support a model

whereby Gal-3 positively regulates Wnt/β-catenin signalling activity in various cancer cell lines.

When I started my thesis, there was no data available about Gal-3-β-catenin interaction in the pSVZ. I tested the hypothesis that Gal-3 might regulate Wnt/β-catenin signalling in the plSVZ by increasing or decreasing Gal-3 levels while reporting Wnt/β-catenin signalling activity. Intriguingly, the evidence supported that Gal-3 overexpression reduced the proportion of cells actively signalling via the Wnt/β-catenin pathway in vivo, as well as the level of Wnt/β-catenin signalling in vitro, while Gal-3 knockdown displayed an opposite trend. Thus, Gal-3 levels negatively regulated Wnt/β-catenin signalling in the plSVZ in vivo and in vitro.

This negative regulatory relationship is in sharp contrast to the case in all cancer cell lines tested so far, where Gal-3 positively regulates Wnt/β-catenin signalling. It is tempting to speculate on the potential reasons for this contrast. One explanation for this discrepancy lies in the difference in the tissues of origin. For instance, the studies detailed above used adult human cancer cell lines from breast, colorectal, pancreatic, gastric, and squamous epithelial tongue tissues, whereas in this study I used lSVZ cells from postnatal murine brains. It is possible to find differences in cellular response to Gal-3 levels across species, ages, and between different organs. Another possibility is that cancerous cells might respond to Gal-3 level manipulation in a manner distinct from untransformed NSCs. This is conceivable given the variety of genetic alteration cancerous tissues take advantage of during the process of transformation. One important example comes from colorectal cancer, where several components of Wnt/β-catenin signalling pathway, like

APC, β-catenin, and Axin are commonly mutated (Kolligs et al., 2002). Given the fact that Gal-3 is known to interact with β-catenin and Axin (Shimura et al., 2005; Shimura et al., 2004), one can hypothesise that Gal-3's may regulate Wnt/β-catenin differently if some the Wnt/β-catenin signalling components were mutated. Other regulatory components of Wnt/β-catenin pathway are also implicated in carcinogenesis. For instance, GSK3β can function as a tumour suppressor of breast tumours, and its inactivation promotes mammary oncogenesis through Wnt/β-catenin activation. This was additionally detected in epidermal squamous cell carcinoma (Luo, 2009). Moreover, CKI has been incriminated in breast and colorectal carcinomas (Knippschild et al., 2005). Interestingly, both CKI and GSK3β were found to phosphorylate Gal-3, potentially regulating its activity (Liu and Rabinovich, 2005; Shimura et al., 2004). In fact, CKI phosphorylation of Gal-3 at Serine residue 6 has been shown to promote its anti-apoptotic activity (Liu and Rabinovich, 2005). Thus, it is possible that Gal-3 activity or binding abilities, hence its function, might be different in cancerous states as opposed to untransformed pSVZ tissue. Finally, one can argue that technical variations might account for the observed differences in Gal-3's effects on Wnt/β-catenin signalling. For example, Gal-3 overexpression constructs utilised in some of the aforementioned studies (Kim et al., 2010; Wang et al., 2013) used a CMV promoter, which is less efficient in overexpressing Gal-3 than the CAG promoter I used in my experiments, giving rise to Gal-3 protein level differences which can potentially confound the comparison (Chen et al., 2011). Overall, the disparities in the Gal-3 of effects in regulating Wnt/β-catenin signalling between the cancer cell lines

and the plSVZ may be attributed to differences between species, age, tissue of origin, technical aspects, and/or malignant transformation status.

Wnt/β-catenin signalling activity has been recorded in the growing aSVZ neurosphere cultures. For example, Piccin et al. used adult BAT-gal mice to demonstrate that Wnt/β-catenin signalling was active in aSVZ-derived NSCs and promoted self-renewal (Piccin and Morshead, 2011). These findings are consistent with my results showing Wnt/β-catenin signalling was active in plSVZ NSCs cultures in vitro.

Strikingly, I showed that the proportion of plSVZ-derived NSCs that were actively engaged in Wnt/β-catenin signalling dropped from roughly two thirds to one fifth between the first and third days in vitro, respectively. This decrease corresponded with the expansion phase of neurosphere growth, whereby numbers of NSCs and progenitors increase coinciding with the growing neurosphere size. Notably, neurospheres are dynamic structures that consist of not only NSCs and progenitors, but also differentiated progeny (Pastrana et al., 2011). That being said, it is possible that the reduction of the percentage of cells actively signalling with Wnt/β-catenin coincided with increased differentiated progeny. These more differentiated cells will have progressed through the lineage, hence downregulated Wnt/β-catenin signalling, as I showed in vivo. Alternatively, with growing neurosphere size, it is possible that additional cells may engage in forming adherent junctions, thereby sequestering β-catenin in the cell junctions and dampening its transcriptional activity. This was observed in classical contact inhibition demonstrated in cancer-derived spheroids transfected with E-Cadherin (St Croix et al., 1998). Taken together, Wnt/β-catenin signalling was active in

NSCs cultured from the plSVZ, and its activity was dampened with increased growth in culture, which could be explained by increased lineage progression and differentiation, increased contact inhibition, or both.

It is important to remember that the reduction in the level of Wnt/β-catenin signalling documented after Gal-3 upregulation in vitro was transient. It is unclear why that was the case. In Section 6.2, I aim to explain why the effects of Gal-3 on proliferation, survival, and Wnt/β-catenin signalling were short-lived.

3.3.4 Gal-3 upregulation reduced proliferation of plSVZ cells and induced cell cycle exit.

The role of Gal-3 in controlling pSVZ proliferation is not well characterised. Our laboratory did not find an effect for Gal-3 loss on aSVZ neurogenic lineage proliferation at baseline (Comte et al., 2011), after stroke (Young et al., 2014), TMEV viral model of multiple sclerosis, Cuprizone-induced demyelination, or traumatic brain injury (Szele lab unpublished data). However, none of these studies examined the plSVZ or utilised Gal-3 gain-of-function. Here, I demonstrated evidence to support that Gal-3 upregulation reduced proliferation in the plSVZ. Firstly, I demonstrated that Gal-3 reduced PHi3 expression in the labelled population 3 DPE, indicating that fewer cells were in the M-phase of the cell cycle after Gal-3 upregulation. Secondly, fewer labelled cells took up BrdU 2 DPE, suggesting that fewer cells were in the S-phase at that point after Gal-3 overexpression. Thirdly, I also showed that scarcer labelled cells were marked with EdU administered 2 hours before sacrifice, 3 DPE, indicating that fewer cells were in the S-phase at that time after Gal-3 gain-of-function. Concomitantly, there was a proportionate

reduction in BrdU and EdU double-labelled cells, however, the ratio of labelled BrdU+ cells that re-entered the cell cycle was not changed by Gal-3 OE. These data support a model whereby Gal-3 gain-of-function reduced the growth fraction, i.e. proliferation, reduced length of the S-phase in the cell cycle, or both.

I will attempt to next address whether Gal-3 gain-of-function reduced the growth fraction or the cell cycle length. As this study did not aim to measure the length of the cell cycle, the data was insufficient to rule out changes in cell cycle length. That being stated, I posit that Gal-3 upregulation was more likely to have, at least in part, reduced the growth fraction in the plSVZ for the following reasons. Firstly, cell cycle length is controlled at the transitions between G_1 to S, and S to G_2 phases (Cheffer et al., 2013), while G_2 and M phases are relatively constant in length throughout embryonic development (Takahashi et al., 1995). Of note, the early pSVZ was determined to be similar to embryonic VZ with respect to proliferative dynamics (Tramontin et al., 2003), thus I contend that G_2 and M phases may well retain embryonic length. I found reduced PHi3 expression, a marker of the M-phase, thus, if the cell cycle length was shorter in Gal-3 OE while the growth fraction and growth rate were not altered, PHi3 expression should not have been reduced under these conditions. On the contrary, shortening of the cell cycle at the G_1 phase was associated with increased proliferation and cell cycle re-entry (Hodge et al., 2004; Zhang et al., 2006). Secondly, given the reduction in labelled BrdU+ cells detected in Gal-3 OE, and assuming that only the cell cycle length and not the growth fraction or rate was reduced, then a smaller fraction of these labelled BrdU+ would have taken up EdU. This is

because fewer BrdU+ labelled cells in the Gal-3 OE group would have been in the S-phase when EdU was bioavailable. That translates into a greater reduction in labelled BrdU+EdU+ cells than would be predicted by the initial reduction in BrdU uptake 2 DPE. However, this was not the case, as there was a proportionate reduction BrdU+EdU+ labelled cells in Gal-3 OE, arguing against a reduced cell cycle length. Thirdly, the rate at which labelled BrdU+ cells re-entered the cell cycle was not altered by Gal-3 upregulation, suggesting that equal fractions of BrdU+ labelled cells in both Gal-3 OE and control animals were in the S-phase when EdU was bioavailable. This argues against both reduced cell cycle length and changes in the growth rate, as equal fractions of plSVZ cells re-entered the cell cycle in both Gal-3 and control animals. Finally, Gal-3 OE increased the cell cycle exit marker p27/Kip1 expression in the lSVZ, which was reported to inhibit proliferation (Andreu et al., 2015; Doetsch et al., 2002b; Li et al., 2009; Qiu et al., 2009), denoting a reduction in the growth fraction. Taken together, these data indicate that while changes in cell cycle length cannot be ruled out, Gal-3 gain-of-function reduced the proliferative growth fraction and increased cell cycle exit in the plSVZ 3 DPE.

There are alternative explanations for the reduced growth fraction, although they are less likely. One viewpoint argues that reduction in proliferation may be attributed to increased cell death. However, I demonstrated that Gal-3 gain-of-function actually reduced cell death in a cell non-autonomous fashion. Therefore, increased cell death cannot account for the reduction in proliferation after Gal-3 overexpression. Notably, the cell non-autonomous pro-survival effect of Gal-3 overexpression, like Wnt/β-catenin

signalling in vitro, was short-lived. Another argument posits that the reduction in proliferation observed in the SVZ may be accounted for by increased migration of proliferative cells out of the SVZ. Indeed, I observed increased density of labelled cell in the RMS 3 DPE. However, I contend that this increment was related to increased cell cycle exit, which is supported by increased p27/Kip1 expression after Gal-3 OE. I will present further evidence to argue against increased net migration when labelled cells were followed to the OB 7 and 17 DPE in chapter 5, where I will discuss the topic of migration in more detail. Significantly, the fact that neuroblasts were produced and indeed migrated through the RMS after Gal-3 upregulation argues against the postulate that Gal-3 downregulation might be necessary to allow plSVZ lineage progression. I will present additional evidence in the next two chapters to further debunk the hypothesis. That aside, I contend that the reduced proliferative fraction of labelled plSVZ cells 3 DPE was not attributed to increased cell death or migration outside the SVZ, but rather to increased cell cycle exit and subsequent shrinkage of the growth fraction. Intriguingly, it appears that Gal-3 acutely induced cell cycle exit possibly within the first 1-2 days following overexpression. This is manifested in an overall reduction in growth fraction with preservation of cell cycle re-entry rates of BrdU-labelled cells 2 DPE after Gal-3 overexpression (which is balanced against cell cycle exit rates). However, p27/Kip1 expression was increased 3 DPE, indicating that cell cycle exit had occurred in a subpopulation of labelled cells. Taken together, these data suggest that Gal-3 overexpression induced cell cycle exit in a fraction of the labelled population before they could be labelled with BrdU 2 DPE, possibly within the 1-2 days after electroporation.

3.3.5 Downregulation of Wnt/β-catenin signalling might account for the reduction in proliferation after Gal-3 upregulation.

Wnt/β-catenin signalling plays a pivotal role in controlling cell cycle re-entry during the early embryonic neurogenic period, whereby aberrant over-activation leads to increased cell cycle re-entry, expanding the progenitor population (Chenn and Walsh, 2002, 2003; Woodhead et al., 2006). It was also shown to control the choice of intermediate cortical progenitors to exit the cell cycle and differentiate (Mutch et al., 2009; Mutch et al., 2010). Moreover, depletion of Wnt/β-catenin signalling promoted RGC cell cycle exit and differentiation prenatally (Woodhead et al., 2006). In the aSVZ, Wnt/β-catenin signalling has been shown to promote symmetric NSC division (Piccin and Morshead, 2011), TAP cell cycle re-entry (Adachi et al., 2007), and NSC maintenance (Qu et al., 2010). Moreover, studies of Wnt pathway inhibitors like Dickkopf 3 (Dkk3) implicate Wnt/β-catenin signalling in promoting neurogenesis (Zhu et al., 2014). In addition, Wnt/β-catenin signalling is activated after stroke and is required for post-injury neurogenesis, as well as SVZ regeneration after ARA-C ablation of proliferative cells (Adi Shruster, 2012; Piccin and Morshead, 2011). Furthermore, abolishment of Wnt/β-catenin signalling prevented post-stroke SVZ neurogenesis (Lei et al., 2008). Thus, the roles of Wnt/β-catenin signalling in regulating aSVZ proliferation are evident.

On the other hand, Wnt/β-catenin signalling was shown to promote oligodendrocytic fate and differentiation (Azim and Butt, 2011; Azim et al., 2014a). Interestingly, it has been proposed that Wnt/β-catenin signalling

activity can promote proliferation, or discourage it in favour of differentiation depending on the presence of environmental factors; like Shh and FGF2 (Viti et al., 2003), and expression of endogenous factors like homeodomain interacting protein kinase 1 (Hipk1) (Marinaro et al., 2012). In addition, Wnt/β-catenin signalling has been shown to be pro-proliferative in early embryonic neurogenesis, and pro-differentiation in late neurogenesis (Hirabayashi and Gotoh, 2005). One must be reminded that these studies evaluated Wnt/β-catenin signalling in adult and embryonic settings, but not postnatally. Therefore, Wnt/β-catenin signalling can induce pro-proliferative or pro-differentiation responses depending on environmental, cell-autonomous, and/or temporal factors. In summary, these data stress the temporally diversified roles of Wnt/β-catenin signalling in controlling SVZ proliferation or differentiation.

In light of the roles of Wnt/β-catenin signalling in proliferation discussed above, it is likely that the reduction in proliferation after Gal-3 overexpression could be related to the decrease in Wnt/β-catenin signalling. I argue that the reduction in the proportion of labelled cells actively engaged in Wnt/β-catenin signalling was conveniently paired with the reduced growth fraction; i.e. with fewer cells to proliferate, fewer cells would activate the pro-proliferative Wnt/β-catenin pathway. Unexpectedly, Gal-3 knockdown did not alter cell proliferation despite increasing Wnt/β-catenin signalling. The fact that shGal-3 failed to alter proliferation is consistent with Gal-3 null mice not experiencing changes in proliferation (Comte et al., 2011). It is possible that Wnt/β-catenin signalling is necessary for maintaining the proliferative potential, such that reduction in signalling levels as seen in Gal-3 OE would reduce proliferation.

However, activating Wnt/β-catenin signalling on its own might not be sufficient to commit cells to proliferate. In other words, additional growth signals might be needed before cells can overcome the checks on progressing through the cell cycle. In support of this, Piccin et al. showed that lateral ventricular infusion of the Wnt agonist SB216763 was not accompanied by increased aSVZ proliferation despite increasing Wnt/β-catenin signalling (Piccin and Morshead, 2011). In addition, Marinaro et al. showed that stabilization of β-catenin by splicing out the third exon actually reduced proliferation in the aSVZ and promoted lineage progression (Marinaro et al., 2012). This contrasts with the previously discussed studies highlighting the pivotal role for Wnt/β-catenin signalling in controlling proliferation. In these studies, variability stemming from mice strains, ages, and different ways to activate Wnt/β-catenin signalling like truncated ΔN90-β-catenin, GSK3β inhibitors (Adachi et al., 2007), and Wnts (Qu et al., 2010; Yu et al., 2006) can confound the comparison.

Another possible explanation for why increased Wnt/β-catenin signalling after Gal-3 knockdown failed to increase proliferation is that activation of Wnt/β-catenin signalling might require more time to promote proliferation. For instance, increased proliferation in the aSVZ was recorded 5 days (Adachi et al., 2007) but not 4 days (Piccin and Morshead, 2011) after Wnt/β-catenin activation. Alternatively, Gal-3 knockdown might have upregulated an unknown anti-proliferative agent that counteracted Wnt/β-catenin signalling influence on proliferation. In sum, Gal-3 overexpression acutely reduced plSVZ proliferation, possibly through dampening Wnt/β-

catenin signalling, while increased signalling activity accompanying Gal-3 loss-of-function was not sufficient to increase proliferation.

3.4 Conclusion

Galectin-3 is a multifunctional protein that has diverse functions in inflammation, migration, and angiogenesis. Although Gal-3 expression and function in the aSVZ niche has been previously described, whether it can regulate the neurogenic lineage progression postnatally remained an unanswered question. Here, I tackled this question by examining the interaction of Gal-3 with β-catenin, a pillar of the pro-proliferative Wnt/β-catenin signalling pathway. I found in the aSVZ that Gal-3 was co-expressed with and bound to β-catenin in a subset of NSCs and TAPs, but not neuroblasts. I verified that Gal-3 expression and Wnt/β-catenin signalling were downregulated as cells progressed in the neurogenic lineage in the plSVZ. Importantly, Gal-3 levels negatively regulated Wnt/β-catenin signalling in the plSVZ niche in vivo and in vitro. Additionally, Gal-3 upregulation induced a reduction in the proliferative growth fraction and increased cell cycle exit in a subset of plSVZ cells. However, the increase in Wnt/β-catenin signalling activity after Gal-3 downregulation did not bring about a proliferative response. Contrary to my expectation, Gal-3 downregulation was not necessary to allow lineage progression. In summary, I discovered a novel regulatory relationship whereby Gal-3 upregulation acutely and negatively regulated Wnt/β-catenin signalling in the plSVZ, which was accompanied by a commensurate reduction in proliferation.

Chapter 4

Upregulation of Galectin-3 did not alter stemness in the postnatal SVZ

4.1 Introduction *132*

4.2 Results *135*

4.3 Discussion *154*

4.4 Conclusion *164*

4 Upregulation of Galectin-3 did not alter stem cell behaviour in the postnatal SVZ

4.1 Introduction

The majority of what is known about Gal-3 comes from studies in cancer (Song et al., 2014) and inflammation (Henderson and Sethi, 2009). The role of Gal-3 in the brain is increasingly being explored, mainly focusing on injury models in the adult setting. For instance, work from the Szele laboratory revealed a role for Gal-3 in regulating neuroblast migration (Comte et al., 2011). Also, Gal-3 loss prevented post-stroke angiogenesis in the ischemic penumbra, but not the SVZ (Young et al., 2014). Our group showed that one and two weeks after stroke, Gal-3 was upregulated in the SVZ, and by reactive and not resting striatal astrocytes. However, Gal-3 loss-of-function did not influence microglial infiltration or activation. In contrast, using Gal-3 null mice, others demonstrated a specific role for Gal-3 in acute activation and proliferation of resident microglia ameliorating damage in the stroked striatum (Lalancette-Hebert et al., 2007; Lalancette-Hebert et al., 2012). Surprisingly, whereas Gal-3 was acutely increased in a murine model of neonatal hypoxia/ischemia, its loss conferred protection to the postnatal hippocampus and striatum (Doverhag et al., 2010). Again in the adult setting, Gal-3 was enriched in FACS-sorted adult NSC compared to diencephalic astrocytes (Beckervordersandforth et al., 2010), and was shown to promote oligodendrocytic differentiation (Hoyos et al., 2014; Pasquini et al., 2011). These findings highlight age-dependent, temporally tuned, and cell-specific differences in functions mediated by Gal-3. Despite the aforementioned

advances, the effects of chronic Gal-3 upregulation in the plSVZ niche are unknown, and therefore warrant investigation.

Development of the murine brain proceeds in the pSVZ, with continued neural and glial cell production into adulthood (Lois and Alvarez-Buylla, 1994; Luskin, 1993; Merkle et al., 2004). Astrocytogenesis is most pronounced in the first two weeks after birth, while oligodendrocyte production peaks after the second postnatal week and continues into adulthood (Levison et al., 1993; Levison and Goldman, 1993; Lyck et al., 2007; Menn et al., 2006; Sauvageot and Stiles, 2002). Wnt/β-catenin signalling is active in the lSVZ during the postnatal period (Bowman et al., 2013) and is necessary for NSC maintenance in both the embryo (Kalani et al., 2008) as well as the adult (Piccin and Morshead, 2011). Moreover, this signalling pathway regulates differentiation (Marinaro et al., 2012) and oligodendrocytic fate choices (Azim et al., 2014a). In chapter 3 I showed that Gal-3 upregulation reduced Wnt/β-catenin signalling, and whether this influenced NSC function, lineage progression, and differentiation will be discussed thoroughly.

In this chapter, I set out to address two key questions; first, whether Gal-3 overexpression altered NSC function in the plSVZ, and second, whether it hindered or influenced lineage progression in that domain at longer time points of survival. In doing so, I investigated the developmental changes surrounding ongoing neuronogenesis and gliogenesis in the plSVZ. To the best of my knowledge, most of what is known regarding postnatal neurogenesis was described in the anterior or dorsolateral SVZ (Brazel et al., 2003a; Levison et al., 1993; Levison and Goldman, 1993; Luskin and McDermott, 1994; Suzuki and Goldman, 2003). The striatal or lSVZ was most

studied for its robust olfactory neuronogenesis (Doetsch F et al., 1999), while its gliogenic potential is less well-characterised. Thus, this study allowed me to describe the developmental changes that occur in the lSVZ during the first 3 weeks of life, and shed light on the temporal changes that characterise the neuronogenic and gliogenic processes taking place. Finally, I detailed how Gal-3 overexpression impacted upon these developmental events, and discuss that in light of the literature and previous data.

Noteworthy, I limited the analysis to Gal-3 gain-of function and excluded Gal-3 loss-of-function. This is because, in the prelude to this work, I characterised Gal-3 null mice and found that Gal-3 loss did not influence neurogenesis in adult mice. Moreover, I attempted to characterise conditional Gal-3 knockout mice, however, that was met with technical difficulties, and the data is preliminary. Therefore, analysing the effects of acute Gal-3 loss-of-function are beyond the scope of this thesis.

4.2 Results

4.2.1 SVZ NSC proliferation is not affected by prolonged Gal-3 gain-of-function

To determine if Gal-3 upregulation changed stem cell function in the SVZ niche, I carried out immunohistochemical staining on brain tissue electroporated with Gal-3 overexpression and control GFP plasmids to assess whether NSC proliferation in the plSVZ was altered. I examined 2 cohorts of mice allowed to survive for 7 and 17 DPE (Cohorts 2 and 3, detailed in Section 2.2). GFAP staining was used to label NSCs and Ki67 to mark proliferative cells (Figures 5.1-2). GFAP+Ki67+ cells were likely activated NSC cells that were in the cell cycle. Firstly, I found that Gal-3 OE did not change the overall proportion of Ki67+ proliferative cells 17 DPE (24.2 ± 1.5%, Gal-3 OE; 24.24 ± 2.69% control, n=4, p=0.6571; Figure 4.1B) and 7 DPE (23.63 ± 4.16%, n=4, Gal-3 OE; 15.21 ± 4.15%, n=3, control, p=0.40; Figure 4.2B). Secondly, Gal-3 OE did not change the proportion of GFAP+ labelled cells that expressed Ki67 17 PDE (25.24 ± 3.49% control, 16.11 ± 3.95% Gal-3 OE, n=4, p=0.20)(Figure 4.1A,D). On the other hand, there was a trend suggesting Gal-3 OE increased labelled GFAP+Ki67+ cells 7 DPE (7.4 ± 3.92% control, n=3, 19.66 ± 5.48%; Gal-3 OE, n=4, p=0.1143; Figure 4.2A,D). Thirdly, the proportion of GFAP+ labelled cells was not changed after Gal-3 upregulation 17 DPE (56.04 ± 4.66% control; 58.72 ± 3.97% Gal-3 OE, p=0.6286; Figure 4.1C) or 7 DPE (43.37 ± 6.93% control; 41.98 ± 6.67% Gal-3 OE, p=0.6286; Figure 4.2C). Notably, total (GFP-labelled and unlabelled cells) Ki67 expression was not altered by Gal-3 OE 7 DPE (156.2 ± 11.87

cells/animal, control; 173 ± 30.3 cells/animal, Gal-3 OE; p > 0.99). These data indicate that the plSVZ niche overall proliferative fraction, NSC proportion, or activation were not changed by Gal-3 upregulation 7 and 17 days after overexpression.

Gal-3 upregulation reduced the proliferative fraction 2 and 3 DPE in the postnatal lSVZ. I next asked whether the proliferative capability of RGC labelled during the first 2 days of Gal-3 overexpression was reduced 7 DPE. This would determine if NSC proliferative behaviour was persistently altered by Gal-3 upregulation. To tackle this question, I labelled a subset of electroporated RGC by giving BrdU 1 and 2 DPE, the time during which Gal-3 reduced proliferation. I then allowed a washout period of 5 days to allow proliferative TAPs and neuroblasts labelled by BrdU in the SVZ to differentiate and migrate out, such that 5 days after the last BrdU injection, only labelled RGCs and their differentiated progeny remained in the plSVZ (Figure 4.3A-B). To label proliferative cells 7DPE, EdU was administered 2 hours before sacrifice. I used the proportion of BrdU+ labelled cells that re-entered the cell cycle and took up EdU as a readout for NSC activation. Firstly, I found that the ratio of EdU+ labelled cells was not different in Gal-3 OE compared to control (12.93 ± 0.8%, n=4, Gal-3 OE; 10.87 ± 2.1%, n=3, control, p=0.4; Figure 4.3F). Secondly, the proportion of labelled BrdU+ cells was not different between Gal-3 OE and control (26.4 ± 7.49%, control; 30 ± 2.93%, Gal-3 OE; p > 0.99). Thirdly, the proportion of BrdU+ labelled cells that expressed EdU from the total labelled population (% re-entrant EdU+BrdU+GFP+/GFP+) was not changed by Gal-3 overexpression (7.1 ± 0.52%, control; 9.52 ± 1.71%, Gal-3 OE; p=0.5174)(Figure 4.3E). In addition,

the proportion of those labelled re-entrant cells from labelled BrdU+ cells (EdU+BrdU+GFP+/BrdU+GFP+) was not altered by Gal-3 overexpression (31.67 ± 9.18%, control; 30.92 ± 3.8%, Gal-3 OE; p=0.7143; Figure 4.3H). Of note, labelled cell density between Gal-3 OE and control was never different in the plSVZ for this and all other experiments 3, 7 and 17 DPE (Figure 4.5C). Finally, Gal-3 upregulation did not change total (labelled and unlabelled) EdU or BrdU expression (Figure 4.3C-D), indicating that it did not change proliferation in a cell non-autonomous fashion. Together, these data confirm that Gal-3 gain-of-function did not change plSVZ proliferation cell autonomously or non-autonomously, nor did it alter NSC activation 7 DPE.

Next, I examined the possible effects of developmental age on GFAP expression in the plSVZ (Figure 4.2E). I used 2-way ANOVA, with experimental group and developmental age (analysis time-point) as main factors. Analysis revealed that GFAP expression was significantly influenced by age ($F(2,18) = 11.63$, $p=0.0006$). This was reflected by post-hoc analysis, which showed that GFAP expression 17 DPE was significantly higher than that 3 DPE (37.41 ± 4.37% control, $p=0.0313$, and 33.13 ± 1.28% Gal-3 OE, $p=0.0019$). Moreover, compared to 7 DPE, GFAP expression 17 DPE was higher in Gal-3 OE ($p=0.0488$), but not in control ($p=0.1987$). Finally neither control nor Gal-3 OE exhibited significant variance between 3 and 7 DPE ($p=0.7936$ for control, and 0.4283 for Gal-3 OE). Thus, together these data indicate that more cells in the plSVZ became GFAP+ with increasing developmental age.

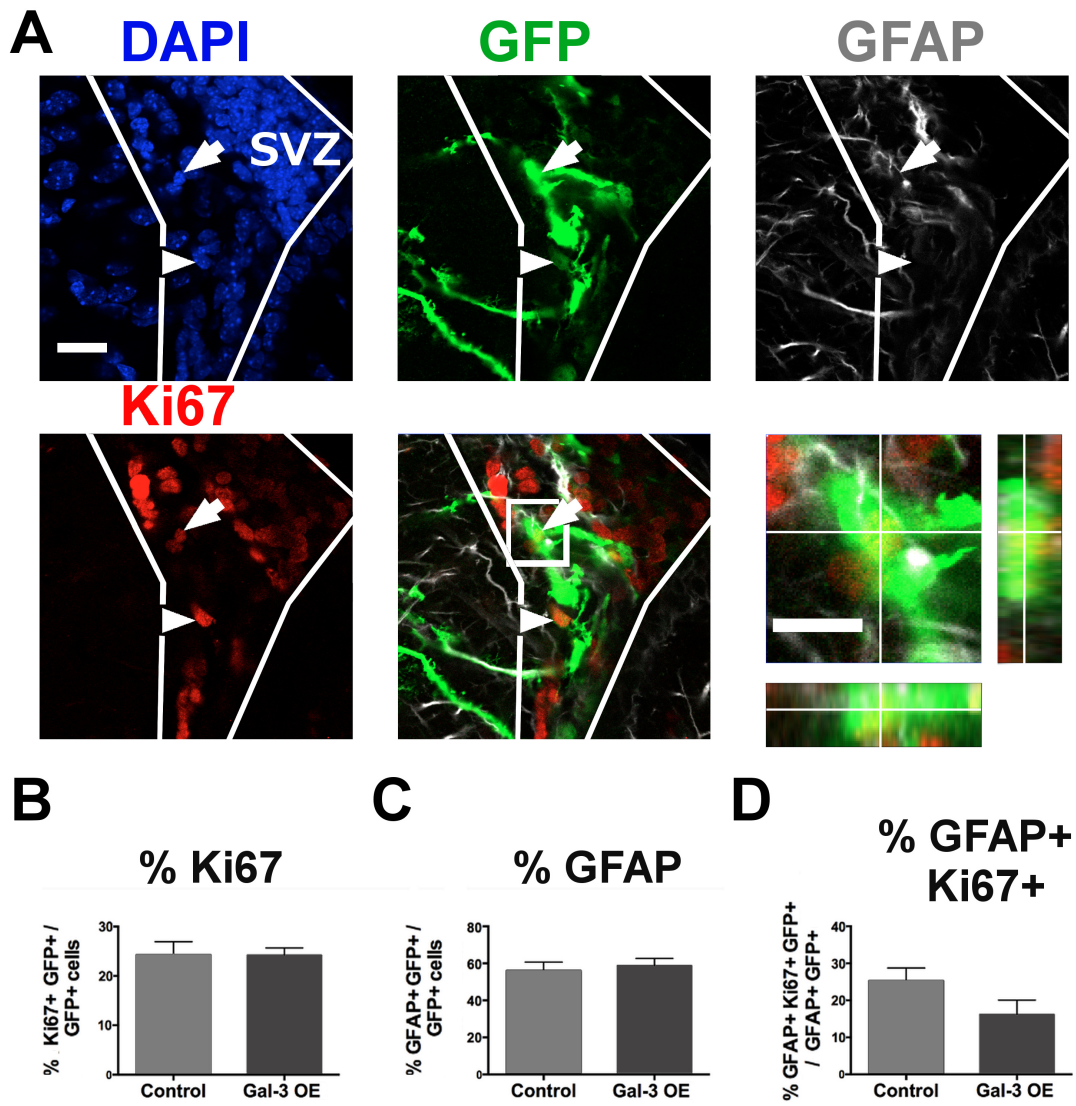


Figure 4.1 Chronic Gal-3 upregulation did not alter NSC activation or SVZ cell proliferation 17 DPE

(A) Shows a representative confocal image for GFP (green), GFAP (grey), Ki67 (red) and DAPI (blue) of a control animal 17 days post electroporation. The white contour outlines the SVZ, the arrow shows a GFP+GFAP+ Ki67+ cell and the arrowhead indicates a GFP+GFAP- Ki67+ cell. The boxed area is magnified in an orthogonal view. Scale bars: 20µm for main panels and 10µm for orthogonal view.
(B-D) Quantification of A. The percentage of labelled cells that were Ki67+ (**B**), GFAP+ (**C**), or GFAP+Ki67+/GFAP+ (**D**) was not significantly different between the control and Galectin-3 (Gal-3) overexpression (Gal-3 OE) groups. n=4. Statistical significance was calculated using Mann-Whitney test.

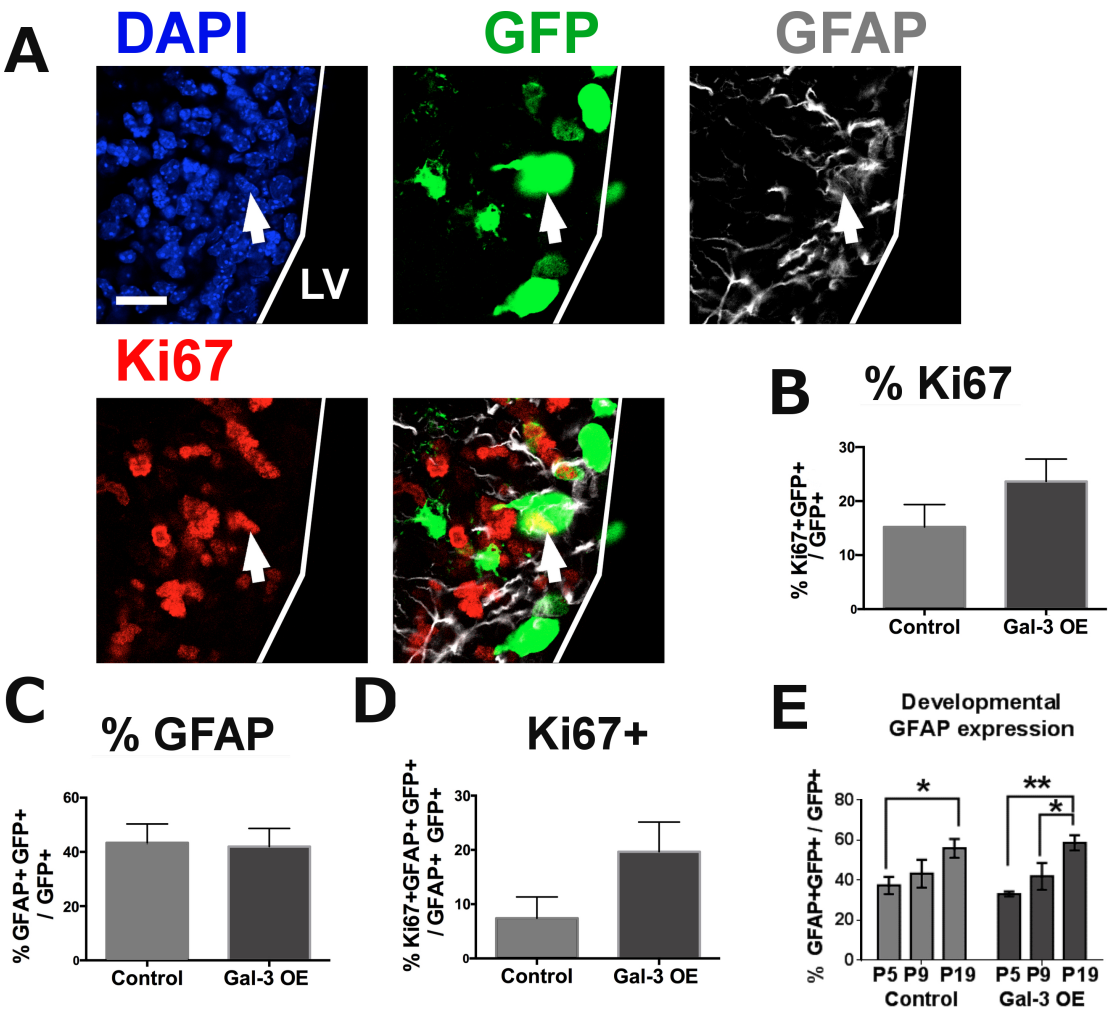


Figure 4.2 Gal-3 overexpression did not alter NSC activation or SVZ cell proliferation 7 DPE

(A) Shows a representative confocal image for GFP (green), GFAP (grey), Ki67 (red) and DAPI (blue) of a control animal 7 days post electroporation. The arrow shows a GFP+GFAP+ Ki67+ cell. Scale bar: 20µm

(B-D) Quantification of A. The percentage of labelled cells that were Ki67+ (**B**), GFAP+ (**C**), or GFAP+Ki67+/GFAP+ (**D**) was not significantly different between the control and Galectin-3 (Gal-3) overexpression (Gal-3 OE) groups. n=3 for control and 4 for Gal-3 OE. Statistical significance was calculated using Mann-Whitney test.

(**E**) Developmental expression of GFAP in control and Gal-3 OE groups 3, 7, and 17 DPE (P5, 9, and 19, respectively). 2-way ANOVA Tukey's test for multiple comparisons. * : $p < 0.05$, ** : $p < 0.01$.

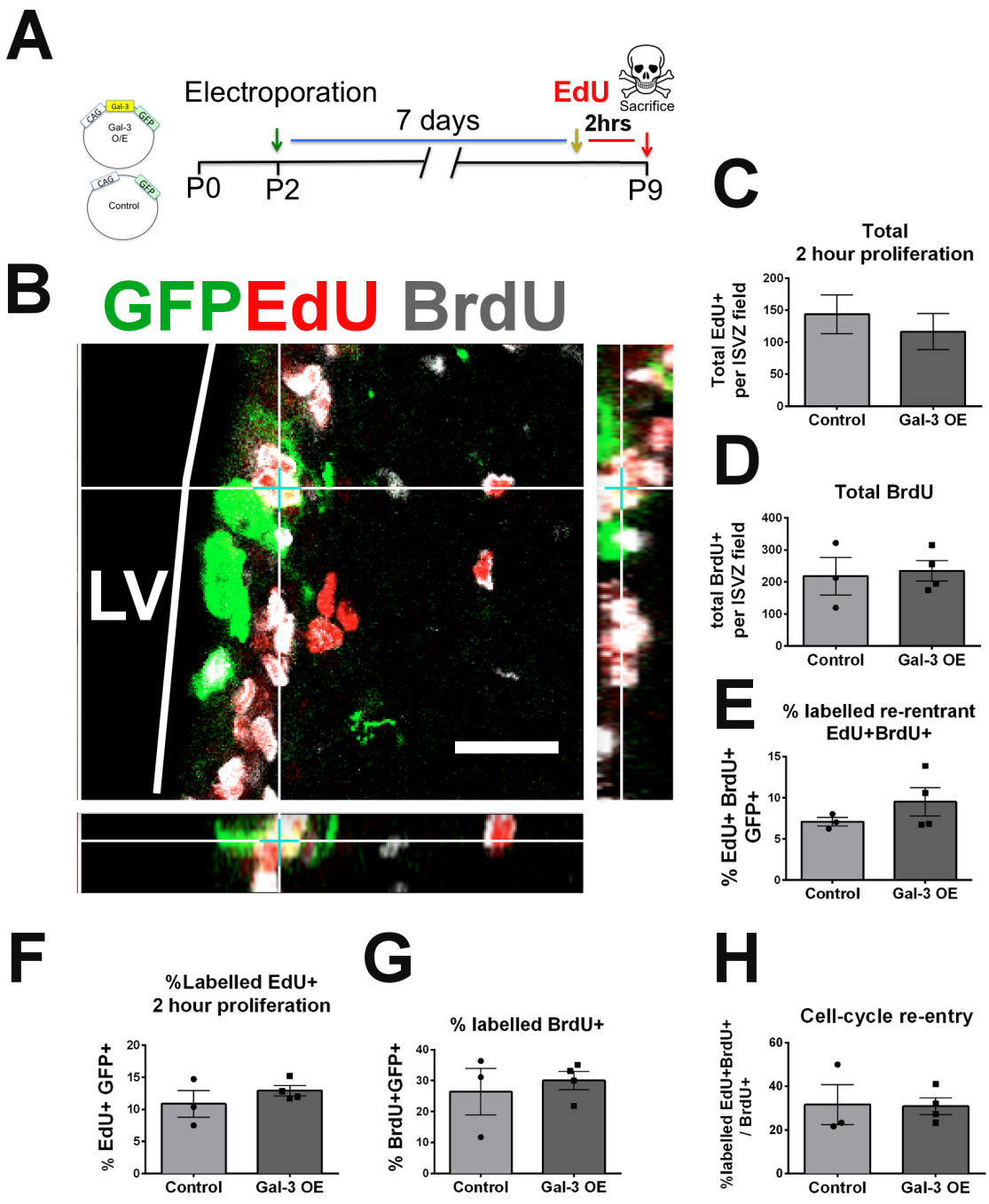


Figure 4.3 Proliferation and cell cycle re-entry were not altered by Gal-3 overexpression 7 DPE.

(**A**) Electroporation and thymidine analogue labelling scheme.
(**B**) Representative control confocal orthogonal image showing labelled cells (GFP; green) BrdU (grey), and EdU (red). LV: lateral ventricle. Scale bar: 20μm.
(**C-H**) Quantification of B. Statistical significance was determined using Mann-Whitney test, n=4 Gal-3 OE, 3 for control. Data is shown as mean ± SEM.

4.2.2 Sox2 expression was not changed by Galectin-3 upregulation

To further assess SVZ stem cell function after Gal-3 overexpression, I carried out immunohistochemical labelling for Sox2, which is expressed in NSCs and is required for proliferation (Ferri et al., 2004). I quantified the proportion of GFP-labelled Sox2+ cells both at 7 and 17 DPE (Figure 4.4A). The data showed that Gal-3 OE did not change Sox2 expression compared to controls 7 DPE (48.4 ± 4.09% control, 47.28 ± 5.5% Gal-3 OE, n=4, $p > 0.99$) and 17 DPE (38.97 ± 2.03% control, 40.18 ± 2.69% Gal-3 OE, n=4, $p > 0.8286$; Figure 4.3B-C). These data suggest that NSC function as determined by Sox2 expression was not altered by Gal-3 gain-of-function.

4.2.3 Galectin-3 overexpression did not alter NSC morphology

Contrasted to non-neurogenic astrocytes, SVZ type-B NSCs protrude a primary cilium into the ventricular lumen, and extend a basal process radially in the opposite direction, which often terminates on blood vessels (Mirzadeh et al., 2008). This gives NSCs a typical radial morphology reminiscent of their RGC counterparts, a subset of which gives rise to type-B NSCs postnatally (Merkle et al., 2004). I hence used radial morphological features to define SVZ NSCs 17 DPE (P19) and investigated if Gal-3 upregulation altered NSC number or morphology (Figure 4.4A). I found that the percentage of labelled cells with radial morphology did not differ after Gal-3 overexpression (17.23 ± 3.19% Gal-3 OE, 19.79 ± 2.49% control, n=4, $p=0.8286$; Figure 4.4B-C). Qualitatively, no overt morphological differences in labelled radial-like cells between the 2 groups were detected (Figure 4.4A-insets). Overall, these data

suggest that Gal-3 gain-of-function did not alter NSC proportion or morphology.

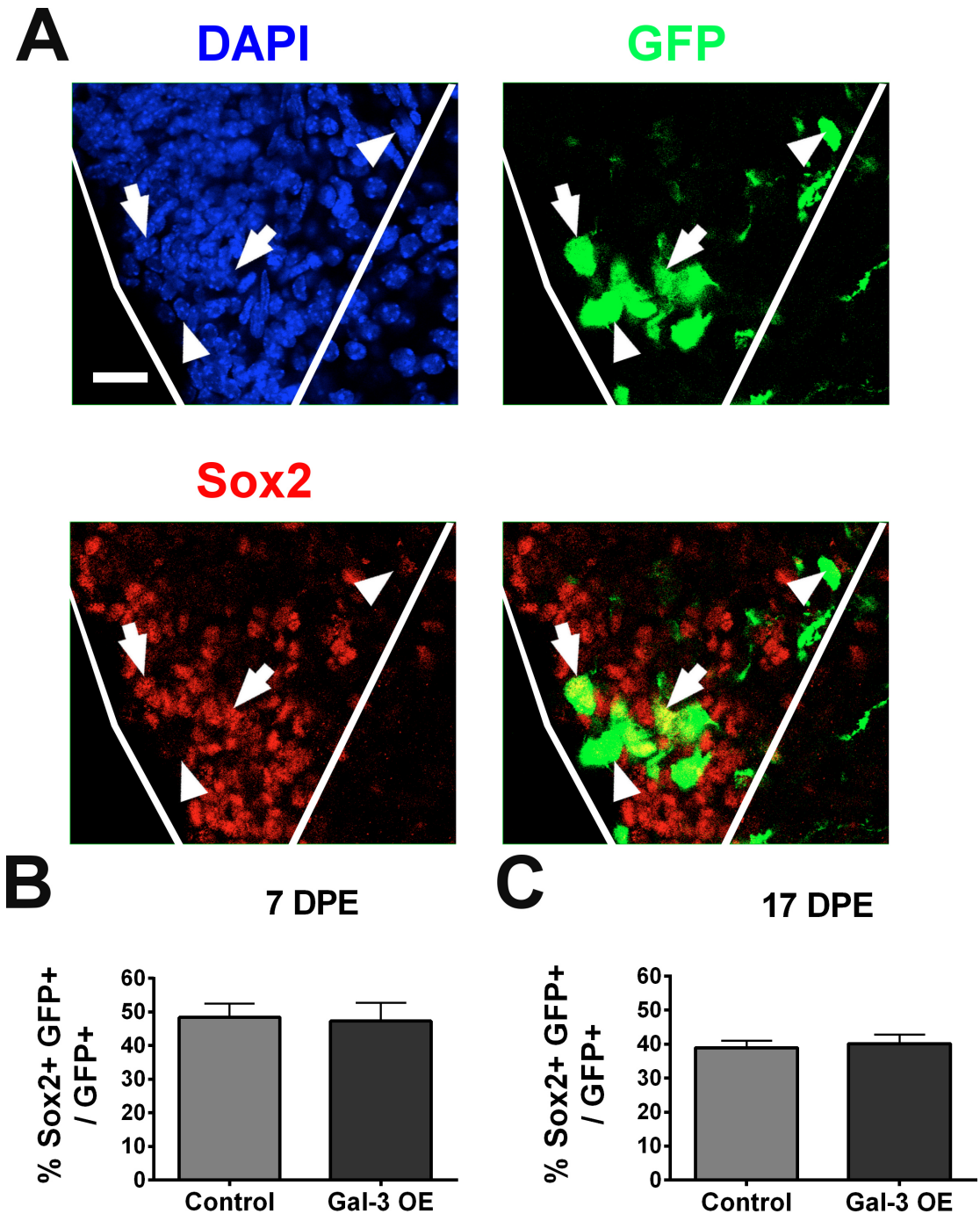


Figure 4.4 Sox2 expression is not influenced by Gal-3 overexpression

(A) Representative confocal images from control brain sections 17 DPE showing labelled cells (GFP+; green), (Sox2; red), and nuclei (DAPI; blue). Arrows indicate GFP+ Sox2+ cells while arrowheads indicate GFP+ Sox2- cells. Scale bar: 20μm
(B-C) Quantification of the percentage of GFP labelled cells that co-expressed Sox2 7 (B) and 17 DPE. Statistical significance was calculated using Mann-Whitney test. Data is shown as Mean ± SEM.

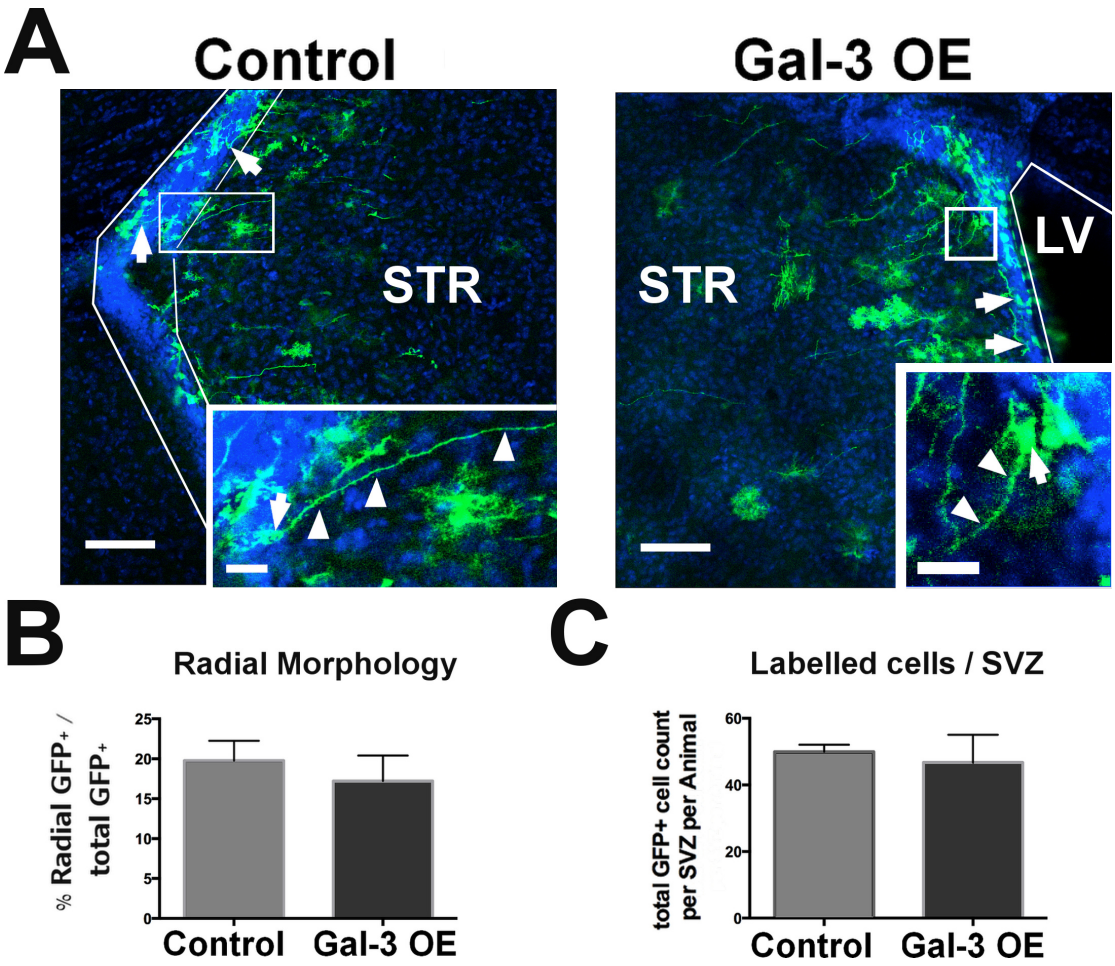


Figure 4.5 Gal-3 upregulation did not change the proportion of cells with radial morphology

(A) Shows representative confocal images from control and Galectin-3 overexpression (Gal-3 OE) 17 DPE. The SVZ and the lateral ventricle (LV) are outlined and the striatum (STR) is indicated. Examples of GFP+ cells with radial morphology are shown in the boxed areas, which are enlarged in the insets. Scale bars: in main panels 100µm, in insets 20µm.
(B-C) Quantification of the percentage of cells with radial morphology per SVZ (B) and total GFP+ cells per SVZ (C). Statistical significance was calculated using Mann-Whitney test. Data is shown as Mean ± SEM.

4.2.4 SVZ transit amplifying progenitors were unaffected by Galectin-3 gain-of-function

To test stem cell function I examined the direct progeny of NSCs; the transit amplifying progenitors (TAPs; type-C cells in P19). TAPs express Mash1, and a subset of these progenitors also expresses Olig2 (Parras et al., 2004), which specifies oligodendrocytic fate (Meijer et al., 2012). To assess whether Gal-3 upregulation alters stem cell function through influencing TAPs, I co-labelled electroporated brain sections for Mash1 and Olig2 3, 7, and 17 DPE (Figure 4.6A). Compared to controls, Gal-3 OE did not change the proportion of GFP-labelled cells that co-expressed Mash1, Olig2, or both, at any of the time-points examined (Figure 4.6B-D). This suggests that Gal-3 OE did not change the proportion of SVZ TAPs or Olig-2+ oligodendrocytic precursors in the labelled population.

Next, I compared the developmental expression of Mash1 and Olig2 across the three time-points examined, to reveal developmental themes that might be affected by Gal-3 overexpression. To that end, I performed a 2-way ANOVA with experimental group and developmental age (analysis time-point) as main factors. First, I found that Mash1 expression in the labelled population did not vary with the time-points examined ($F(2,18) = 0.9397$, $p=0.41$; Figure 4.6B). To elaborate, 12.93 ± 2.61%, 7.96 ± 2%, and 11.62 ± 2.35% of labelled cells were Mash1+ in control animals at 3, 7, and 17 DPE, respectively. Similarly, 12.87 ± 2.85%, 12.11 ± 0.56%, and 13.51 ± 1.57% of GFP+ cells were labelled with Mash1 at 3, 7, and 17 DPE in Gal-3 OE, respectively. On the other hand, developmental age had a significant effect on Olig2 expression ($F(2,18) = 7.055$, $p=0.0059$). On post-hoc analysis, Olig2 co-

labelling was significantly lower 7 DPE compared to 3 DPE in Gal-3 OE (7.13 ± 2.26% vs 13.14 ±1.12%, p=0.0358), and there was a similar trend in controls (5.94± 2.05% vs 11.57 ± 1.62%, p=0.0626; Figure 4.6C). In addition, developmental age exerted a similar effect of on Mash1+Olig2+ oligodendrocytic progenitors ($F(2,18) = 4.293$, p=0.0289). However, post-hoc analysis failed to reveal any significance in both control (2.24 ± 1.29% vs 5.53 ± 1.60%, p=0.1370) and Gal-3 OE (3.67± 0.88% vs 7.05 ± 0.75%, p=0.1015; Figure 4.6D). Thus, the data suggests that the labelled stem cells retained the ability to produce TAPs and Olig2+ progenitors regardless of Gal-3 upregulation. Moreover, it suggests that the SVZ's oligodendrocytic output was reduced with increasing developmental age.

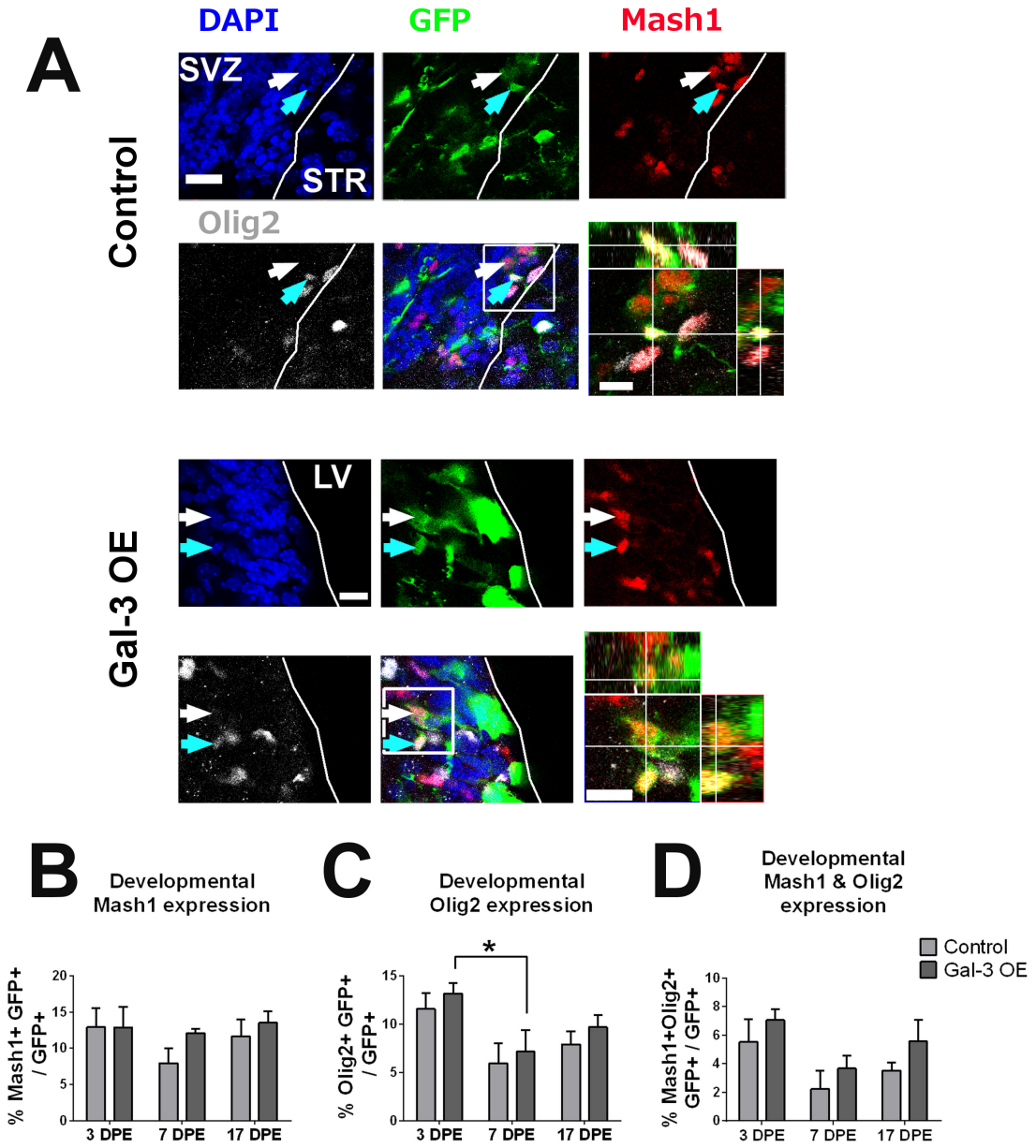


Figure 4.6 Gal-3 OE did not change Mash1 or Olig2 expression

(A) Representative confocal images from control and Galectin-3 overexpression (Gal-3 OE) 17 DPE stained for GFP (green), Mash1 (red), Olig2 (grey) and nuclei (DAPI; blue). White arrows indicate GFP+Mash1+Olig2- cells and blue arrows point to GFP+Mash1+Olig2+ cells. The subventricular zone (SVZ) and striatum (STR) are outlined in the control image, and the lateral ventricle (LV) in Gal-3 OE. The boxed area is enlarged in an orthogonal view. Scale bars: control: 20µm for main panels and 10µm for inset. Gal-3 OE: 10µm for main panels and inset.
(B-D) Quantification of Mash1 (B), Olig2 (C), and Mash1 and Olig2 co-expression in GFP labelled cells 3, 7 and 17 days post electroporation (DPE). Statistical significance was calculated using 2-way ANOVA Tukey's test. Data is shown as Mean ± SEM. * : $p < 0.05$.

4.2.5 Galectin-3 Overexpression did not change neuroblast production

Neuroblasts are the descendants of TAPs and they migrate from different loci along the SVZ axes to reach the RMS and then the OB. Assessing neuroblast production is a direct readout of the neurogenic potential of the SVZ niche. To investigate whether the SVZ's neurogenic potential is changed by Gal-3 overexpression, I carried out immunohistochemical staining for Dcx, a marker of neuroblasts in the SVZ (Figure 4.7A). I found that Gal-3 overexpression did not change neuroblast production in the SVZ both 7 (21.08 ± 3.39% control, 28.57 ± 1.97% Gal-3 OE, n=4, p=0.8286) and 17 DPE (11.47 ± 4.04% control, 17.07 ± 7.72% Gal-3 OE, n=4, p=0.1143).

I next examined the developmental Dcx expression between 7 and 17 DPE. 2-way ANOVA with developmental age and experimental group as main factors showed that age significantly altered Dcx expression in the labelled population ($F(1,12) = 4.899$, $p=0.047$). However, post-hoc analysis failed to show significant differences between the time-points examined for control ($p=0.327$) and Gal-3 OE ($p=0.2148$). Consequently, the data indicates that SVZ neurogenesis was not altered by Gal-3 overexpression. Moreover, the neurogenic potential of labelled cells was reduced with increasing developmental age, regardless of Gal-3 upregulation.

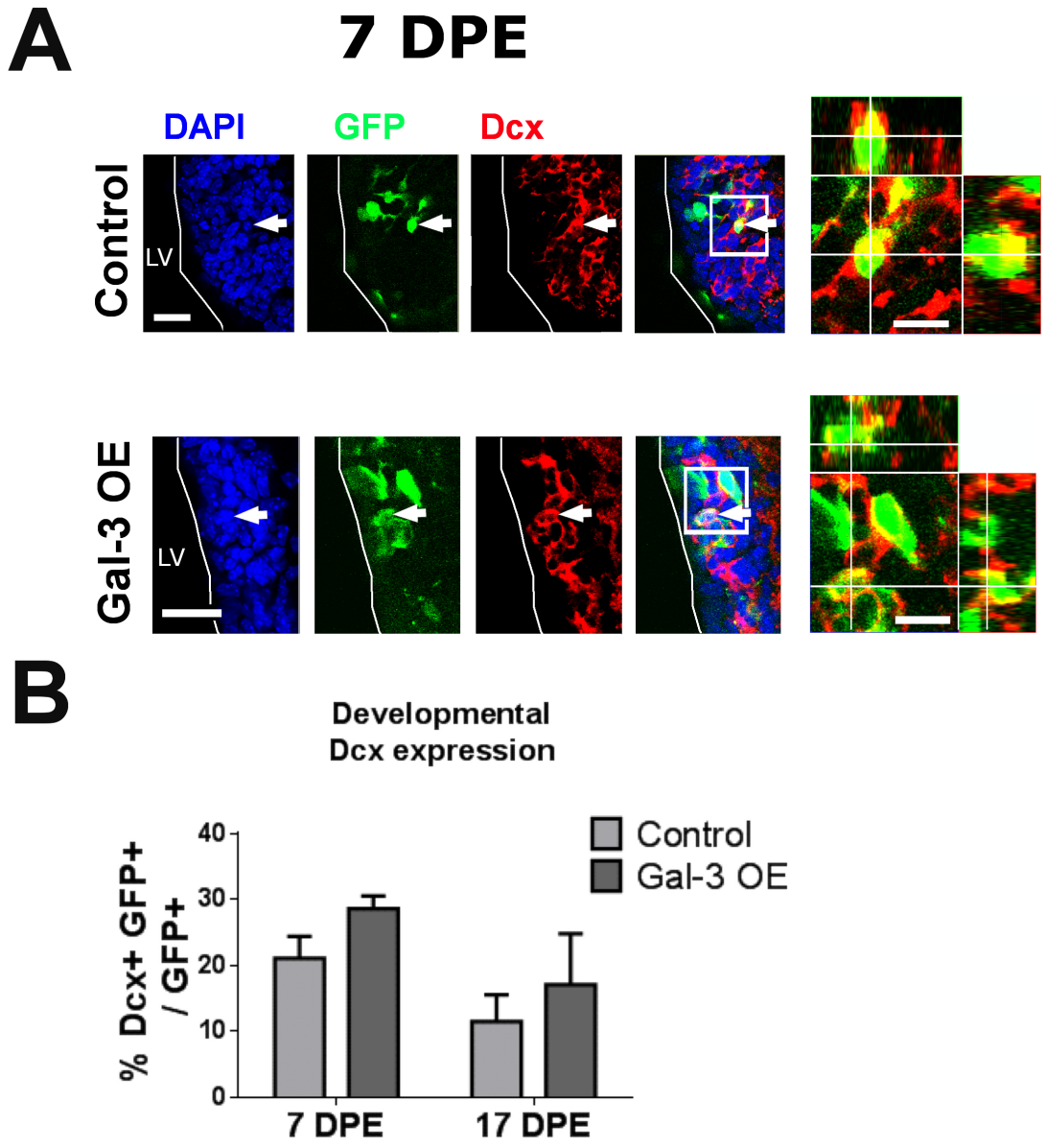


Figure 4.7 Neuroblast production was unimpeded by Gal-3 upregulation

(A) Representative confocal images showing GFP (green), Dcx (red), and nuclei (DAPI; blue) from a control and Galectin-3 overexpression (Gal-3 OE) in the SVZ 7 days post electroporation (DPE). Arrows indicate GFP+Dcx+ cells. The boxed area is enlarged in an orthogonal view. Scale bars: 20µm main panels and 10µm for insets.
(**B)** Quantification of the proportion of Dcx+GFP+ cells 7 and 17 DPE revealed no significant difference. Statistical significance was determined using Mann-Whitney test. Data is shown as Mean ± SEM.

4.2.6 Clonal neurosphere assay showed preserved NSC function after Gal-3 upregulation

To further verify that NSC function was not affected by Gal-3 overexpression, I investigated the effects of Gal-3 gain-of-function on clonal neurosphere forming capacity and self-renewal in vitro. I nucleofected NSCs from tertiary neurospheres with Gal-3 overexpression or control plasmids, then cultured them at clonal density (10 cells/µl) for 7 days before analysis or passage, subsequent culture for 7 more days, and analysis (Figure 4.8). The test plates were not handled except for at the time of analysis or subculture. This minimises the chance of sphere fusion (Coles-Takabe et al., 2008). Thus, it is reasonable to assume that neurospheres were derived from single NSCs. At analysis, I found that upregulation of Gal-3 did not change primary neurosphere forming capacity. Furthermore, NSC self-renewal, as determined by secondary neurosphere formation, was not affected by Gal-3 upregulation (Figure 4.8B). However, the diameter of primary neurospheres was consistently lower after Gal-3 overexpression (87.92 ± 3.37% of control, n=4, p=0.0337). The size effect was not replicated in secondary neurospheres (73.67 ± 11.26% of control, n=3, p=0.1443). This data indicates that Gal-3 OE did not change stemness or self-renewal in vitro.

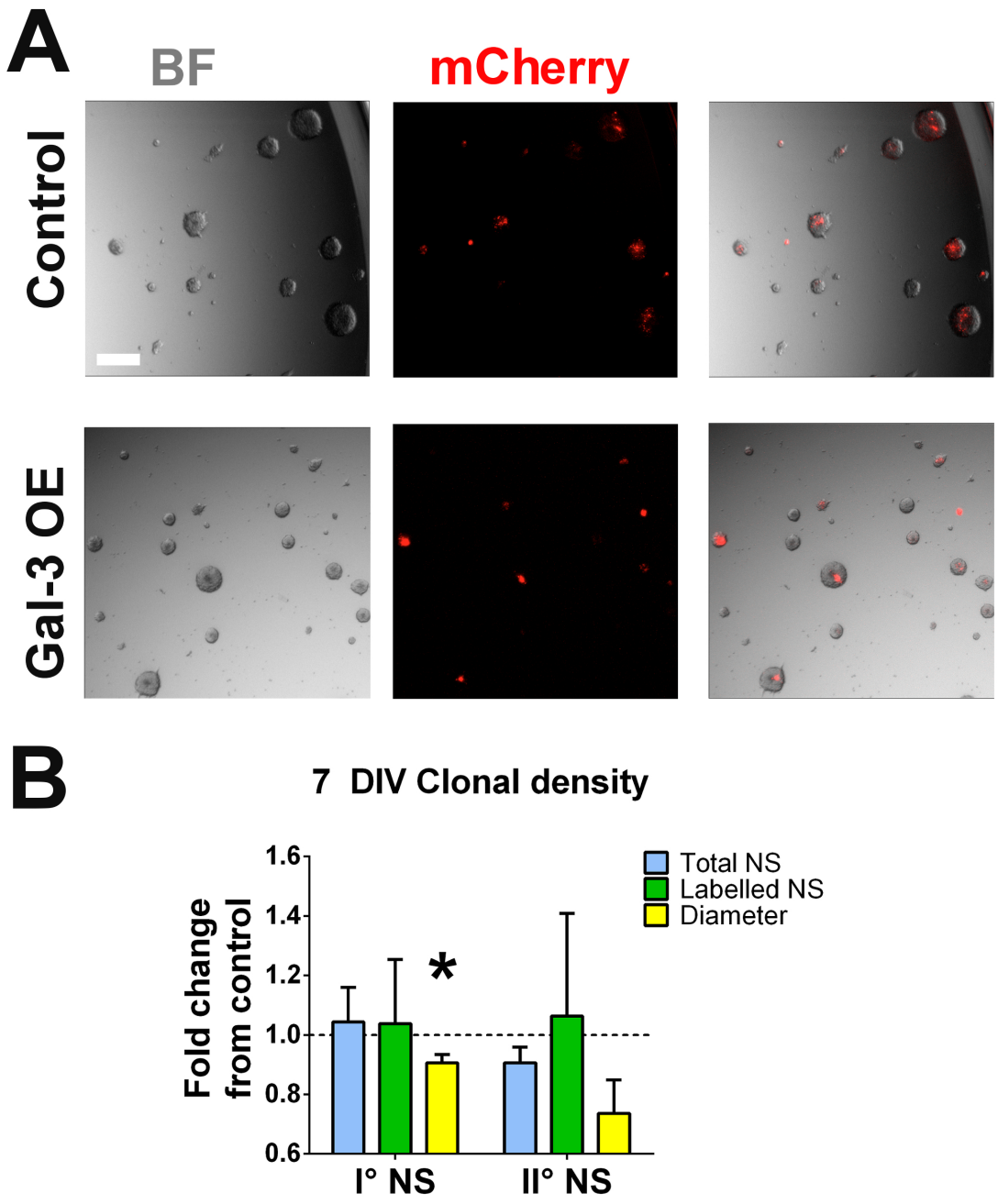


Figure 4.8 Gal-3 overexpression did not influence stemness or self-renewal in vitro

(**A**) Representative bright field (BF) and fluorescence images of nucleofected tertiary NSC's 7 days in vitro (DIV). mCherry (red) labels nucleofected cells. Scale bar: 200µm.
(**B**) Quantification of A. Total and labelled primary (I°) and secondary (II°) neurosphere (NS) formation was not significantly different in Gal-3 OE. However, NS diameter was significantly lower for I° NS. The data is shown as fold change compared to control, total of n=4 independent experiments. Statistical significance was calculated using one-sample t-test. Data is shown as Mean ± SEM. *p* value: * < 0.05.

4.2.7 Other SVZ cells were not overtly affected by Gal-3 overexpression

Gal-3 has been shown to play a role in microglial activation (Lalancette-Hebert et al., 2012) and ependymal ciliary function (Comte et al., 2011). Therefore, I set out to determine if postnatal Gal-3 OE affected microglia or ependymal cells. First, I used CD45 to label microglia and performed a blinded qualitative assessment of microglial morphology (Figure 4.9). The criteria for this assessment included microglial morphology (ramified, semi-activated, or amoeboid), staining intensity, and relative microglial numbers. Four blinded observers performed the analysis and the same conclusion was reached. We found that microglia were not different morphologically and semi-quantitatively after Gal-3 upregulation 3, 7, and 17 DPE in the plSVZ and neighbouring parenchyma (Figure 4.9A-C). In addition, with increasing developmental age, CD45+ microglia assumed a more ramified morphology indicative of quiescence (Figure 4.9C). Therefore, I concluded that Gal-3 gain-of-function did not alter microglial activation at the time-points examined. This was an important control because it also suggested that Gal-3 OE does not induce inflammation, which could have confounded results.

Next, I examined whether Gal-3 OE altered the expression of S100β, a marker of ependymal cells (Spassky et al., 2005), in the cells abutting the lateral ventricle (Figure 4.10A) 17DPE. I found that 50.18 ± 9.02% and 38.01 ± 4.94% of labelled cells expressed S100β in control and Gal-3 OE, respectively (Figure 4.10B), which was not statistically significant ($p=0.3429$). Qualitative examination of S100β expression by two blinded observers did not highlight differences between the groups in staining intensity, regions stained, and morphology of labelled cells. Therefore, the data indicates that S100β

expression in the SVZ was not affected by Gal-3 upregulation, suggesting that Gal-3 OE did not quantitatively or qualitatively affect ependymal cells 17 DPE. More detailed experimentation to assess ependymal function was outside the scope of this thesis.

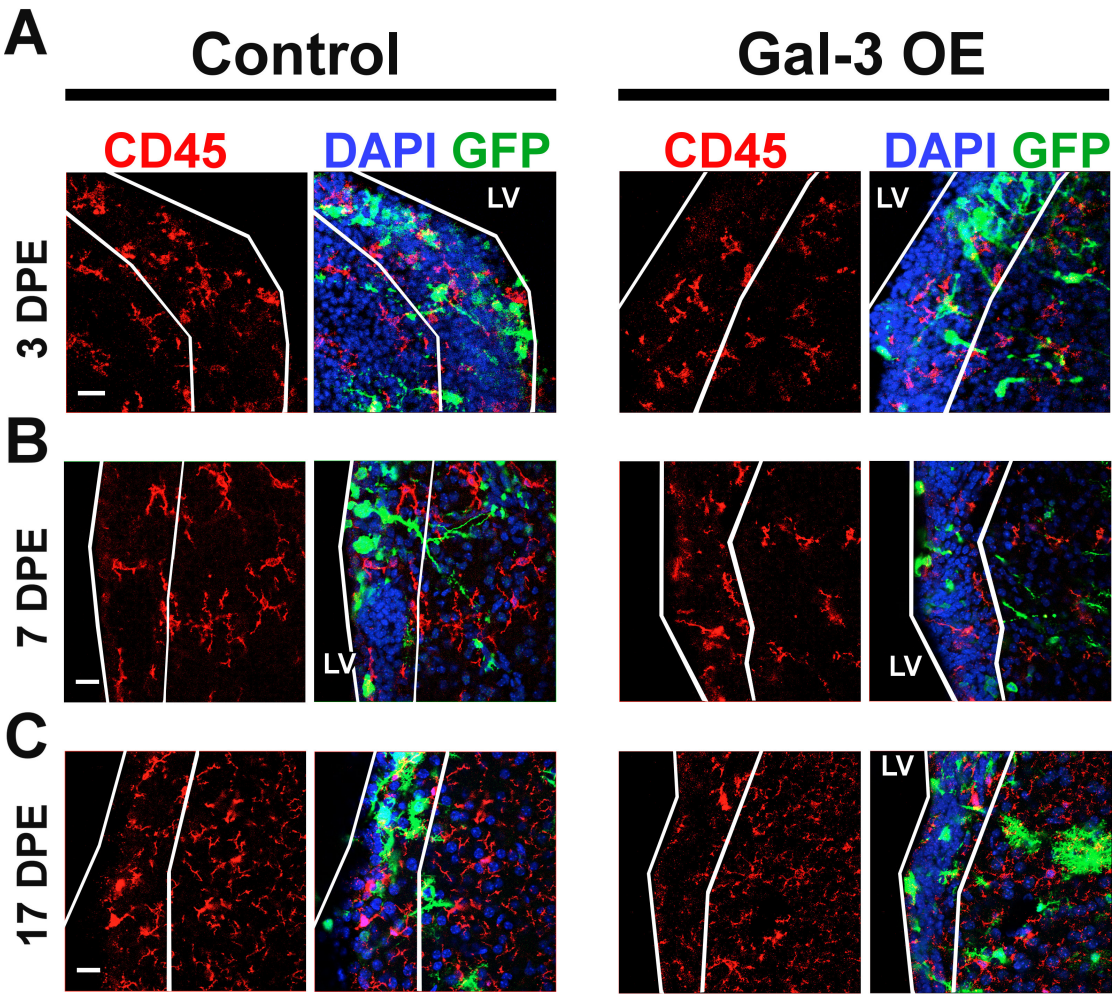


Figure 4.9 Developmental CD45 expression was not influenced by Gal-3 upregulation

(A-C) Representative confocal images showing microglial marker CD45 (red), GFP (green), and nuclei (DAPI; blue) from controls and after Galectin-3 overexpression (Gal-3 OE) in the SVZ 3, 7, and 17 days post electroporation (DPE). The subventricular zone (SVZ) is outlined and lateral ventricle (LV) is indicated. Scale bars: 20μm.

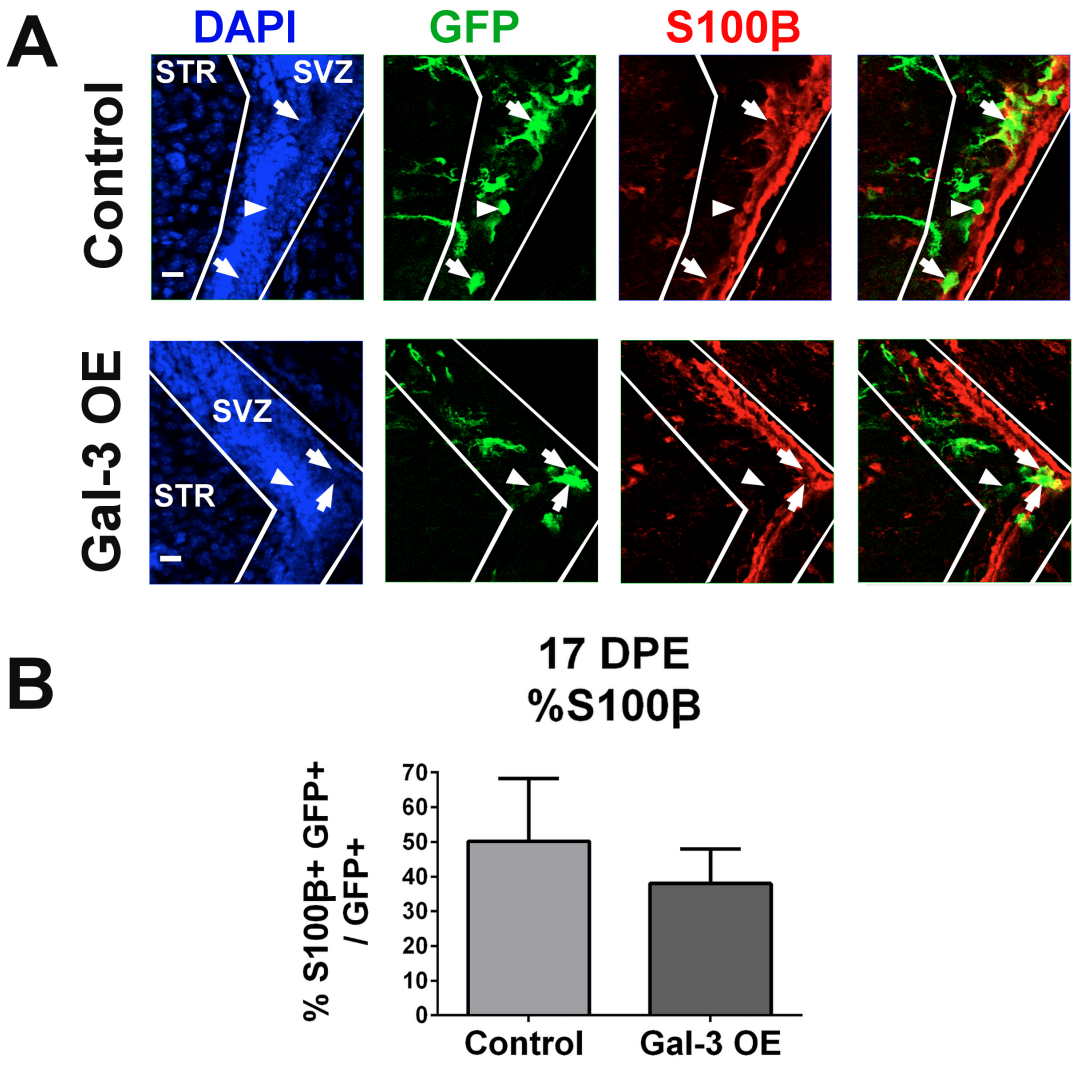


Figure 4.10 Ependymal S100β expression did not vary after Gal-3 overexpression

(A) Representative confocal images showing S100β (red), GFP (green), and nuclei (DAPI; blue) from a control and Galectin-3 overexpression (Gal-3 OE) in the SVZ 17 days post electroporation (DPE). The subventricular zone (SVZ) is outlined and striatum (STR) is indicated. Arrows show S100β+GFP+ cells and arrowheads indicate GFP+S100β- cells. Scale bars: 20μm

(B) Quantification of the proportion of GFP+S100β+ cells shown in A. n=4. Statistical significance was calculated using Mann-Whitney test. Data is shown as Mean ± SEM.

4.3 Discussion

The plSVZ is a dynamic region with robust neuronogenic and gliogenic potentials. The role of Gal-3 upregulation in the plSVZ was yet to be uncovered in functional studies before I commenced my thesis. In this study, I investigated the effects of Gal-3 gain-of-function on NSC activation and lineage progression in the plSVZ. I found Gal-3 did not affect NSC activation, neurogenesis, or lineage progression. However, Gal-3 overexpression underscored a novel developmental theme in the plSVZ, in which oligodendrogenesis decreased over the first 2 postnatal weeks. I also discovered that Gal-3 enhanced the acquisition of the glial character in the lSVZ without influencing neuroblast production.

4.3.1 Galectin-3 overexpression did not chronically change proliferation, NSC activity, or lineage progression in the plSVZ

In chapter 3, I presented evidence to support that Gal-3 gain-of-function acutely reduced proliferation and induced cell cycle exit in the plSVZ. Henceforth, it was important to address whether this proliferation phenotype persisted after the initial decrease in plSVZ growth fraction. I showed that Gal-3 gain-of-function did not persistently alter proliferation 7 or 17 DPE. In support of that I demonstrated that Ki67 expression in the plSVZ was not different after Gal-3 overexpression 7 and 17 DPE. Ki67 is expressed throughout the cell cycle, therefore, the proportion of positive labelled cells denote the growth fraction (Ponti et al., 2013). Moreover, I showed that proliferation as detected by EdU administered 2 hours before sacrifice was not altered by Gal-3 upregulation 7 DPE. Notably, total GFP unlabelled and

labelled EdU+ cells were not significantly different in Gal-3 OE compared to control, indicating that overexpression of Gal-3 did not cell non-autonomously affect proliferation 7 DPE in the plSVZ. Together these data indicate that the growth fraction and proliferation dynamics in the plSVZ were not changed by Gal-3 upregulation.

Next, I addressed whether Gal-3 upregulation persistently altered NSC function in the plSVZ. I presented data to support that NSC activation was not affected by Gal-3 expression status 7 and 17 DPE (P9 and 19). Firstly, I examined the NSCs labelled with BrdU in the period when Gal-3 reduced proliferation i.e. the first two days after overexpression. I determined that the proportion of these cells that re-entered the cell cycle was not altered by Gal-3 upregulation 7 DPE. Moreover, there was no change in total or labelled BrdU expression, indicating that NSCs and their differentiated progeny were not quantitatively different after Gal-3 OE. Secondly, the proportion of labelled GFAP+ Ki67+ cells, presumably the activated NSCs, was not affected by Gal-3 upregulation 17 PDE. On the other hand, Gal-3 OE showed a trend for increasing labelled GFAP+Ki67+ cells 7DPE, despite not reaching statistical significance. Thirdly, the proportion of labelled cells 17 DPE (P19) that retained radial morphology, which represent SVZ type-B NSCs (Merkle et al., 2004; Ventura and Goldman, 2007), was not affected by Gal-3 gain-of-function either. Fourthly, TAP and neuroblast production- the progeny of activated NSCs, was comparable between Gal-3 OE and control groups. Finally, clonal neurosphere forming capacity and self-renewal, features of bona fide NSCs (Pastrana et al., 2011), were not affected by Gal-3

overexpression. Taken together, these data strongly suggest that NSC activation was not affected by Gal-3 gain-of-function.

Of note, GFAP is also expressed in niche astrocytes (Doetsch F et al., 1999; Mirzadeh et al., 2008), which have been reported to proliferate in the aSVZ in earlier reports (Doetsch et al., 1997). On the other hand, Garcia et al. demonstrated that proliferative GFAP+ cells were predominantly unipolar or bipolar in morphology, thus it was more likely for NSCs than niche astrocytes to be the GFAP+ proliferative cells in the aSVZ (Garcia et al., 2004). It is unknown whether niche astrocytes proliferate in the postnatal SVZ. Therefore, I cannot exclude the possibility that GFAP+Ki67+ cells included a subset of proliferative niche astrocytes, in addition to activated NSCs. Another important point is that Gal-3 OE showed a trend for increasing GFAP+Ki67+ 7DPE despite not reaching statistical significance. Reducing the noise by increasing the technical replicates per animal, and increasing the power through increasing the total number of animals per group will prove crucial in determining whether this effect is real. If that were the case, it would explain the increased striatal gliogenesis phenotype presented in Chapter 5.

Noteworthy as well is that in the clonal neurosphere assay I found that Gal-3 reduced the mean diameter of labelled primary neurospheres, and there was a similar trend in the secondary neurospheres. This may reflect the acute effects of Gal-3 gain-of-function on reducing proliferation, such that fewer cells made up smaller Gal-3 overexpressing neurospheres. One has to remember that neurosphere forming capacity is not a readout for how many stem cells are there, instead it may reflect the potential of cells to exhibit proliferative SC-like traits, and their responsiveness to mitogens (Pastrana et al., 2011). In

addition, neurosphere size reduction in Gal-3 OE may be related to increased adhesiveness induced by Gal-3 (James, R. and Szele unpublished observations). Therefore, caution is warranted when interpreting the neurosphere size data with respect to stem cell numbers or functions.

In chapter 3, I demonstrated that Gal-3 was complexed with β-catenin, and that these molecules were co-expressed and downregulated with lineage progression. I then hypothesised that this downregulation may have been important to allow lineage progression. I further showed that acute overexpression of Gal-3 did not prevent neuroblast production or migration to the OB, indicating that Gal-3 downregulation was not necessary for lineage progression. Here, I show that chronic upregulation of Gal-3 in the plSVZ did not hinder neurogenesis either. RGCs and then type-B NSCs continued to produce TAPs and neuroblast at P9 and 19, with no detectable effect of Gal-3 on the rate of neurogenesis. This further supports that Gal-3 has little influence on lineage progression. Considering the aforementioned discourse, I conclude that plSVZ neurogenesis and lineage progression were not influenced by Gal-3 gain-of-function.

4.3.2 Retained neurogenic potential in the plSVZ

Neurogenesis was consistently shown to continue in the postnatal (Altman, 1969; Luskin, 1993) and adult SVZ niches (Altman, 1969; Lois and Alvarez-Buylla, 1994). Newborn neuroblasts express the microtubule-associated protein Dcx (Yang et al., 2004), and predominantly migrate through the RMS to reach the OB. The SVZ produces most of the olfactory neurons in the first 3 postnatal weeks (Bandeira et al., 2009; Bayer, 1983). Afterwards,

neurogenesis slows down with increasing age (Kishi, 1987; Lewis and Lai, 1974; Lyck et al., 2007). I found that the labelled population in the plSVZ continued to produce neuroblasts, and the production rate slowed down from P9 to P19 (7 to 17 DPE). Furthermore, Gal-3 gain-of-function had little effect on the rate of neuroblast production. These findings are in agreement with the aforementioned studies; and highlight yet another developmental theme in the postnatal lSVZ, whereby neurogenesis slows down in the first postnatal month. This can be explained by the multiple fates RGCs adopt postnatally (Kriegstein and Alvarez-Buylla, 2009). Some transform into type-B NSCs (Merkle et al., 2004), astrocytes (Merkle et al., 2004; Noctor et al., 2008), and ependymal cells (Spassky et al., 2005). Therefore, fewer RGC-like NSCs were present at P19, potentially offering an explanation to the findings at hand.

Nonetheless, caution is warranted in the interpretation of the differences in neuroblast proportions quantified in coronal sections; as these cells migrate along the rostro-caudal axis of the lateral ventricle (Goldman, 2003), which can confound the results. For this reason, I was careful not to include the dlSVZ in my analysis, as it represents the major rostro-caudal migratory route, as opposed to the dorso-ventral migration prevalent in the striatal or lSVZ (Goldman, 2003; Kakita and Goldman, 1999). That being said, to achieve higher confidence in interpretation of the aforementioned Dcx data, one must consider it in light of analysing the differences in labelled cells in OB between control and Gal-3 OE groups. I will tackle this issue in the chapter 5.

4.3.3 The postnatal SVZ niche is gliogenic

The gliogenic potential of the postnatal SVZ manifests itself in the progressive production of astrocytes and oligodendrocytes. These glial cells migrate from the SVZ to populate the surrounding white and grey matter (Levison and Goldman, 1993; Luskin, 1993; Merkle et al., 2004; Ventura and Goldman, 2007). SVZ astrocyte production begins in the late embryonic period as early as E14 (Parnavelas, 1999), accelerates after neurogenesis slows down (E18) (Levers et al., 2001), peaks at P0-2 (Sauvageot and Stiles, 2002) but decelerates after P14 (Levison et al., 1993; Lyck et al., 2007; Parnavelas, 1999), and continues throughout adulthood (Sohn et al., 2015). Thus, whether Gal-3 overexpression during the postnatal gliogenic period had an effect on gliogenic potential or differentiation is important to tackle. I found that GFAP expression was not affected quantitatively or qualitatively by Gal-3 overexpression 3, 7, and 17 DPE (P 5, 9, and 19, respectively). This is interesting because Gal-3 nulls exhibited increased SVZ GFAP-immunoreactivity and disrupted glial tubes in the SVZ and RMS, but showed no apparent alteration in GFAP expression elsewhere in the brain (Comte et al., 2011). I speculate that Gal-3 may be involved in regulating the function of GFAP, especially given that GFAP is glycosylated (Korolainen et al., 2005), allowing potential Gal-3 binding. Alternatively, potential compensatory effects in Gal-3 nulls may have had an indirect effect on GFAP expression. It is also possible that Gal-3 exerts level-specific effects on GFAP expression that were manifested in Gal-3 null mice but might not be apparent in the Gal-3 gain-of-function model employed in this study.

Comparison of GFAP expression in labelled cells in the plSVZ across different postnatal age groups revealed that GFAP expression was upregulated with increasing age in both control and Gal-3 overexpression groups. It is possible that Gal-3 may instruct astrocytic differentiation in the SVZ, potentially through accelerating the implementation of astrocytic differentiation programmes induced by BMP, Notch, CNTF, LIF, or IL-6 (Kanski et al., 2014). However, there is little evidence to support that is the case in the SVZ. Assessing gliogenesis in the neighbouring striatum, which will be addressed in chapter 5, will shed more light on this issue. Overall, these findings are in agreement with earlier studies that described gradual accumulation of astrocytes in the postnatal brain until P21 and progressive increase in GFAP staining intensity in the SVZ during the first 2 postnatal weeks (Lyck et al., 2007; Peretto et al., 2005; Tramontin et al., 2003).

The developmental increase in GFAP expression could be a result of an increase in either GFAP+ niche astrocytes or NSCs. One obstacle to addressing this question is that niche astrocytes are defined by their multipolar morphology and location on the striatal side of the SVZ away from the ventricle (Doetsch et al., 1997; Doetsch F et al., 1999; Mirzadeh et al., 2008). Unfortunately, the crowded nature of labelled cells in the postnatal SVZ made identifying complex morphologies a difficult task. Another hindrance lies in the lack of a specific marker for niche astrocytes. For instance, S100β, labels both ependymal cells and mature astrocytes, but it showed a relative specificity to ependymal cells in the cohort examined; as only few cells were observed where niche astrocytes should be present, and staining intensity was relatively weak. In addition, the temporal dynamics of niche astrocyte

development and marker expression are a relatively unexplored field, and further studies are warranted to address this matter.

4.3.4 The fleeting oligodendrogenesis in the postnatal lateral SVZ

Wnt signalling has been shown to promote oligodendrocytic fate in the postnatal dorsal SVZ (pdSVZ) (Azim et al., 2014a; Azim et al., 2014b; Ortega et al., 2013). In chapter 3, I presented data to support that Gal-3 negatively regulated Wnt/β-catenin signalling in the plSVZ. Whether the oligodendrocytic lineage was affected in the plSVZ after Gal-3 gain-of-function is an important question to address. In addition, little is known about the postnatal oligodendrogenic potential of the lSVZ or the temporal expression patterns of Olig2 in the plSVZ; since almost all studies focus on the dSVZ or dlSVZ (Kakita and Goldman, 1999; Levison and Goldman, 1993, 1997; Luskin and McDermott, 1994; Marshall and Goldman, 2002; Marshall et al., 2003; Merkle et al., 2004). Therefore, I evaluated the temporal patterns of Olig2 expression in plSVZ after Gal-3 overexpression during the first 3 weeks of postnatal life.

The data presented in this chapter does not support an effect for Gal-3 upregulation on the expression of the oligodendrocytic-lineage marker Olig2 in the plSVZ at P5, 9 and 19. Nevertheless, it emphasised a novel developmental theme in the plSVZ; whereby Olig2 expression was downregulated with increasing developmental age. 2-way ANOVA analysis showed that developmental age exerted a significant main effect on Olig2 downregulation in the plSVZ. Post-hoc analysis showed Olig2 immunopositivity was downregulated in the plSVZ from 3 (P5) to 7 DPE (P9) after Gal-3 upregulation. However, the same trend was present in the control

group without reaching statistical significance. Together, the data highlight a novel developmental theme whereby oligodendrogenesis is dampened in the plSVZ with increasing developmental age.

The oligodendrogenic potential for NSCs in the dSVZ increases from P2 to P14 (Levison et al., 1993; Parnavelas, 1999). Compared to the dSVZ, previous reports documented a smaller oligodendrogenic potential in the lSVZ, which is preserved in the aSVZ (Azim et al., 2014a; Menn et al., 2006; Ortega et al., 2013). Moreover, postnatal oligodendrogenesis increasingly shifts towards the dorsal Emx1 domain from the lateral Gsh2 domain, reducing the contribution of the plSVZ to oligodendrogenesis (Kessaris et al., 2006). Since the prenatal Gsh2 oligodendrogenic wave is overtaken by the postnatal Emx1-driven progenitors, it is conceivable to postulate that oligodendrogenesis slows down in the lSVZ. This hypothesis is supported by the observed temporal dampening of Olig2 expression in the plSVZ.

An alternative interpretation of the data contends that the observed theme is a technical by-product of labelling a proliferative population. To clarify, lateral ventricular electroporation targets stem and progenitor cells in the SVZ. It may be argued that the higher percentage of Olig2+ labelled cells observed 3 DPE is a result of directly targeting thus labelling these progenitors, and by 7 DPE, these cells differentiate and exit the SVZ leaving it only with Olig2+ descendants of labelled resident NSCs. Although this may be true, it is unlikely due to the following reasons. First, postnatal electroporation of the lateral ventricle specifically targets RGCs (Boutin et al., 2008; Fernandez et al., 2011). Furthermore, the 3-day survival before analysis (3 DPE) would probably dilute out the rapidly proliferative intermediate

progenitors, which will have differentiated, and their progeny would have been en route to their final destinations. Accordingly, labelled TAPs and Olig2+ progenitors are more likely to be descendants of labelled resident NSCs as opposed to having been directly labelled. Second, Olig2+ Mash1+ double-labelled progenitors were reduced with age, whereas the proportion of labelled Mash1+ progenitors did not vary with age, making it more plausible to posit that the observed pattern was lineage specific. In summary, oligodendrocytic progenitors were specifically reduced from the plSVZ with increasing developmental age from P5 to P9, a novel developmental pattern emphasised by Gal-3 upregulation.

4.3.5 SVZ microglia were not affected by Galectin-3

Microglia that reside in the aSVZ are semi-activated (Goings et al., 2006) and do not express Gal-3 at baseline (Comte et al., 2011). Gal-3 nulls showed defective microglial activation and proliferation after stroke (Lalancette-Hebert et al., 2012); however, we did not find that to be the case in our stroke model (Young et al., 2014). So, I asked whether Gal-3 overexpression changed microglial activation postnatally. I discovered that Gal-3 upregulation did not change microglial activation in the plSVZ and neighbouring parenchyma. On the contrary, in both control and Gal-3 OE groups, SVZ and parenchymal microglia progressively became more branched, reminiscent of the mature ramified microglia resident in the brain parenchyma. This is consistent with reports documenting the gradual change from amoeboid to ramified morphology in the first postnatal month (Sato, 2015). At all time-points examined, some CD45+ microglia in the SVZ displayed brighter staining, and

fewer but thicker processes. This agrees with the findings of Goings et al. (2006) in finding morphologically semi-activated microglia in the SVZ, and in this study, I add that the aforementioned findings were detected in the postnatal setting.

4.4 Conclusion

The murine plSVZ is a dynamic structure that transitions from embryonic to adult state during the first three weeks of postnatal life. During this transition, the niche displays robust gliogenic and neuronogenic potentials. In this chapter, I addressed whether Gal-3 overexpression alters NSC activation and lineage progression. I found that Gal-3 gain-of-function did not change NSC activation, proliferation, or lineage progression. In addition, this chapter underscored the developmental changes that dominated the lSVZ during the first three postnatal weeks; whereby the lSVZ increasingly acquired astrocytic features and dampened its oligodendrogenic potential. The differentiation of the progeny of the plSVZ into the OB and neighbouring striatum will be investigated in chapter 5.

Chapter 5

Galectin-3 regulated fate choices in the postnatal SVZ

5.1 Introduction *166*

5.2 Results *169*

5.3 Discussion *189*

5.4 Conclusion *209*

5 Galectin-3 regulated fate choices in the postnatal SVZ

5.1 Introduction

Murine forebrain development is a dynamic process that persists after the foetus is born. During early development, NSCs residing in the wall of the developing neural tube give rise to cortical and subcortical neurons (Kriegstein and Alvarez-Buylla, 2009). This neurogenic period in the VZ continues from E11-18, peaking at E14, and is thought to slow down after E18. Cortical projection neurons are formed in an inside out fashion with neurons radially migrating into deep layers before superficial layers, with the exception of the outermost layer, which develops early on with the deep layers. On the other hand, interneurons originate from the ventrally located MGE and LGE. They migrate tangentially and dorsally around the ventricular cavity, and fan out to reach their destinations in the forebrain (Brazel et al., 2013; Kriegstein and Alvarez-Buylla, 2009; Price et al., 1997; Tan et al., 1998). The striatum develops between E12 and P2 primarily from the LGE and MGE; with the majority of projection neurons being contributed by the LGE (Bayer, 1984; Bayraktar et al., 2014; Brazel et al., 2013; Halliday and Cepko, 1992; Tan et al., 1998). At approximately E16, astrogliogenesis commences providing the developing forebrain with the first astrocytes (Qian et al., 2000). This process continues postnatally until the second or third postnatal week, with a peak around P0-2 (Sauvageot and Stiles, 2002). Oligodendrogenesis primarily occurs postnatally and continues well into adulthood (Brazel et al., 2013; Lyck et al., 2007).

Postnatal neurogenesis involves a complex balance of neuronal, astrocytic, and oligodendrocytic cell production, migration, and differentiation. Most of what is known about gliogenesis comes from characterising cortical gliogenesis (Brazel et al., 2003b; Goldman, 2003; Kakita and Goldman, 1999; Levison et al., 1993; Levison and Goldman, 1993, 1997; Levison et al., 1999; Luskin and McDermott, 1994; Parnavelas, 1999). These and other studies provided valuable insights into the cellular and molecular mechanisms of gliogenesis. For example, it is now known that RGCs transform into parenchymal astrocytes during the first week or so of postnatal life (Noctor et al., 2008; Voigt, 1989). In addition, another subset of astrocytes originates from glial progenitors in the pSVZ, which migrate in the first month of life into the grey and white matter tissues of the brain (Brazel et al., 2003b; Levison et al., 1993; Levison and Goldman, 1993, 1997; Luskin and McDermott, 1994; Luskin et al., 1993; Magavi et al., 2012). Moreover, many of these progenitors divide before differentiating, which increases the size of glial clones (Ge et al., 2012). However, little is known about the temporal dynamics of striatal gliogenesis, or the lineage relationships between striatal glia and NSCs in the pSVZ.

Very little is known about whether Gal-3 plays a role in prenatal or postnatal neural development. The majority of the studies focusing on Gal-3 functions used Gal-3 Knockout mice (Colnot et al., 1998). The Szele laboratory characterised adult Gal-3 null mice and found no apparent defects in neural development, but did find significantly decreased neuroblast migration and dystrophic SVZ glial tubes (Comte et al., 2011). Others have found reduced myelin integrity in the white matter of these mice, and defective

remyelination after Cuprizone-induced demyelination (Hoyos et al., 2014; Pasquini et al., 2011). However, whether Gal-3 influences postnatal neuronogenesis or gliogenesis from the lSVZ is still unknown. I chose Gal-3 gain-of-function as a means of addressing these gaps in the literature and deepening our understanding of postnatal neurogenesis.

In chapter 4, I showed that Gal-3 did not influence NSC activation, TAP and neuroblast production, or oligodendrocytic marker expression in the plSVZ. I then showed that the plSVZ progressively acquired astrocytic features and downregulated its oligodendrocytic output during the first three weeks of life. In light of these findings, I asked the following questions: In what way does Gal-3 gain-of-function affect fate choices in the plSVZ? Particularly, how does Gal-3 gain-of-function influence olfactory neuronogenesis? And could it alter the positional identity of plSVZ NSCs? In other words, could Gal-3 OE respecify SVZ-derived olfactory neurons to adopt different OB positions? And how does Gal-3 upregulation impact upon striatal oligodendrogenesis and astrocytogenesis? And finally, what are the molecular underpinnings of the phenotype brought about by Gal-3 upregulation? In order to address these questions, I characterised the neurogenic, oligodendrocytic, and astrocytic output of the plSVZ after Gal-3 upregulation. I demonstrated a previously unexamined contribution of the plSVZ to striatal gliogenesis, whereby more SVZ-derived astrocytes than oligodendrocytes populate the striatum in the third postnatal week. I also discovered novel functions for Gal-3 in regulating the gliogenic fate choices of the plSVZ progeny, such that it increased the preference for the astrocytic rather than oligodendrocytic fate choice. Finally, I reveal a novel regulatory function for Gal-3 on BMP

signalling, whereby Gal-3 positively regulated BMP signalling activity, which may account for the observed phenotype.

5.2 Results

5.2.1 Olfactory neuronogenesis was not altered by Galectin-3 overexpression

The plSVZ is responsible for robust olfactory neuronogenesis (Doetsch F et al., 1999; Luskin, 1993). The majority of these neuroblasts migrate to the OB where they differentiate into olfactory interneurons. To determine if Gal-3 overexpression altered postnatal olfactory neuronogenesis, I examined P9 and 19 OB sections from brains electroporated with Gal-3 OE and control plasmids at P2 (Figure 5.1 and 5.2). First, the mean numbers of labelled cells present in the OB layers 7 and 17 DPE (P9 and 19) were compared (Figure 5.1B and 5.2C). I found that Gal-3 OE had no significant influence on the numbers of neuroblasts that migrated into the OB 7 DPE (83.92 ± 22.19 cells/OB section, n=4, control; and 82.33 ± 16.18 cells/OB section, n=3, Gal-3 OE; p=0.8571), or neurons that settled in OB 17 DPE (48.71 ± 12.06 cells/OB section, control; and 33.96 ± 7.1 cells/OB section, Gal-3 OE; n=4, p=0.3143). I next asked whether Gal-3 OE influenced neuronal maturation. To address this question, immuno-staining of OB sections for the neuronal differentiation marker NeuN was conducted 7 (Figure 5.1A,C) and 17 DPE (Figure 5.2B,D). The proportion of NeuN+ labelled cells was used as a readout for neuronal differentiation. The results showed no significant difference in the ratio of labelled cells that co-expressed NeuN 7 DPE (10.69 ± 2.4%, n=4, control; 10.92 ± 1.14%, n=3, Gal-3 OE; p > 0.99) and 17 DPE (81.58 ± 1.99%, control;

83.08 ± 2.85%, Gal-3 OE; n=4, $p > 0.99$). These data indicate that Gal-3 OE did not induce premature neuronal differentiation at P9, nor did it influence neuronal maturation at P19.

Gal-3 is known to interact with Nkx2.1, a TF activated in response to Shh signalling (Dumic et al., 2006). Nkx2.1 activity was shown to be active in vSVZ NSCs, and their progeny primarily adopted deep granular localisation in the OB (Ihrie et al., 2011). To address whether Gal-3 OE altered olfactory neuronal layer-specificity, I examined the distribution of labelled cells in OB layers. I found that the distribution of labelled cells both 7 and 17 DPE (Figure 5.1E and 5.2E, respectively), and labelled mature neurons 17 DPE (Figure 5.2F) in the OB layers was not altered after Gal-3 overexpression. These data indicate that Gal-3 upregulation did not change the layer-specificity of differentiating neurons in the OB. To further confirm neuronal differentiation was not changed by Gal-3 overexpression, qualitative morphological examination of labelled neuronal morphology 17 DPE was done. Assessment of labelled olfactory neuronal morphology 17 DPE by two observers blinded to experimental conditions revealed no discernible differences in neuronal morphology. In addition, I did not detect GFP+ cells with glial morphology in the OB. Thus, Gal-3 had no identifiable effect on neuronal morphology. Taken together, the data suggests that Gal-3 gain-of-function had no influence on olfactory neuronogenesis.

I next used activated caspase-3 labelling to examine whether Gal-3 overexpression altered survival of labelled neuroblasts 7 DPE (data not shown). I detected no activated caspase-3+ labelled cells 7 DPE in either group. Of note, there was no significant difference between the experimental

groups in total (GFP labelled and unlabelled) activated caspase-3+ cells in the OB 7 DPE (7.75 ± 0.76 cells/animal, n=4, control, and 10.72 ± 2.36 cells/animal, n=3, Gal-3 OE; p=0.4; Figure 5.1D). Therefore, I conclude that Gal-3 gain-of-function did not influence survival in the OB 7 DPE.

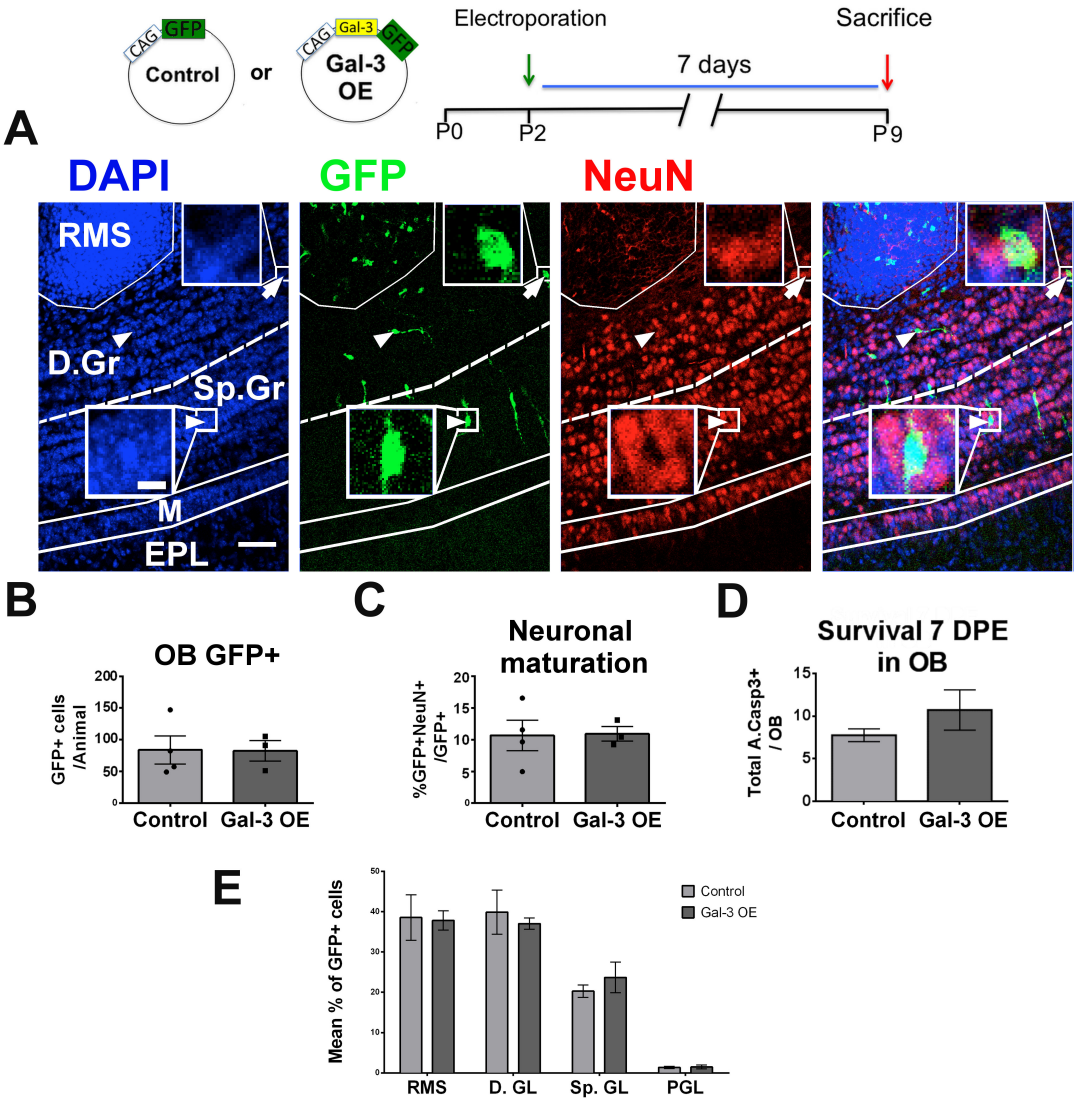


Figure 5.1 Gal-3 did not alter olfactory neuronogenesis 7 DPE

(**A**) Cartoon depiction of the experimental scheme is shown in the top. Confocal images of a control olfactory bulb (OB) 7 DPE displaying labelled GFP+ cells (green), NeuN (red), and nuclei (DAPI; blue). The arrow points to a NeuN+GFP+ cell in the deep granule layer (**D.Gr**) and arrowheads indicate NeuN-GFP+ cells in the D.Gr. and superficial granule layer (**Sp.Gr**). Boxed areas are enlarged in the inset. Rostral migratory stream (**RMS**), mitral cell layer (**M**), external plexiform layer (**EPL**). Scale bars: main panels 50µm and inset 10µm.
(**B-C**) Quantification of A. The mean number of GFP+ cells per OB section per animal is shown in **B**, and the percentage of GFP+ NeuN+ cells is quantified in **C**.
(**D**) Quantification of activated caspase-3 (A.casp3)+ cells in OB of control and Gal-3 OE. (**E**) Percent distribution of GFP+ cells in OB layers.
Statistical significance was calculated using Mann-Whitney test (**B-D**) and 2-way ANOVA (**E**). Data is shown as Mean ± SEM.

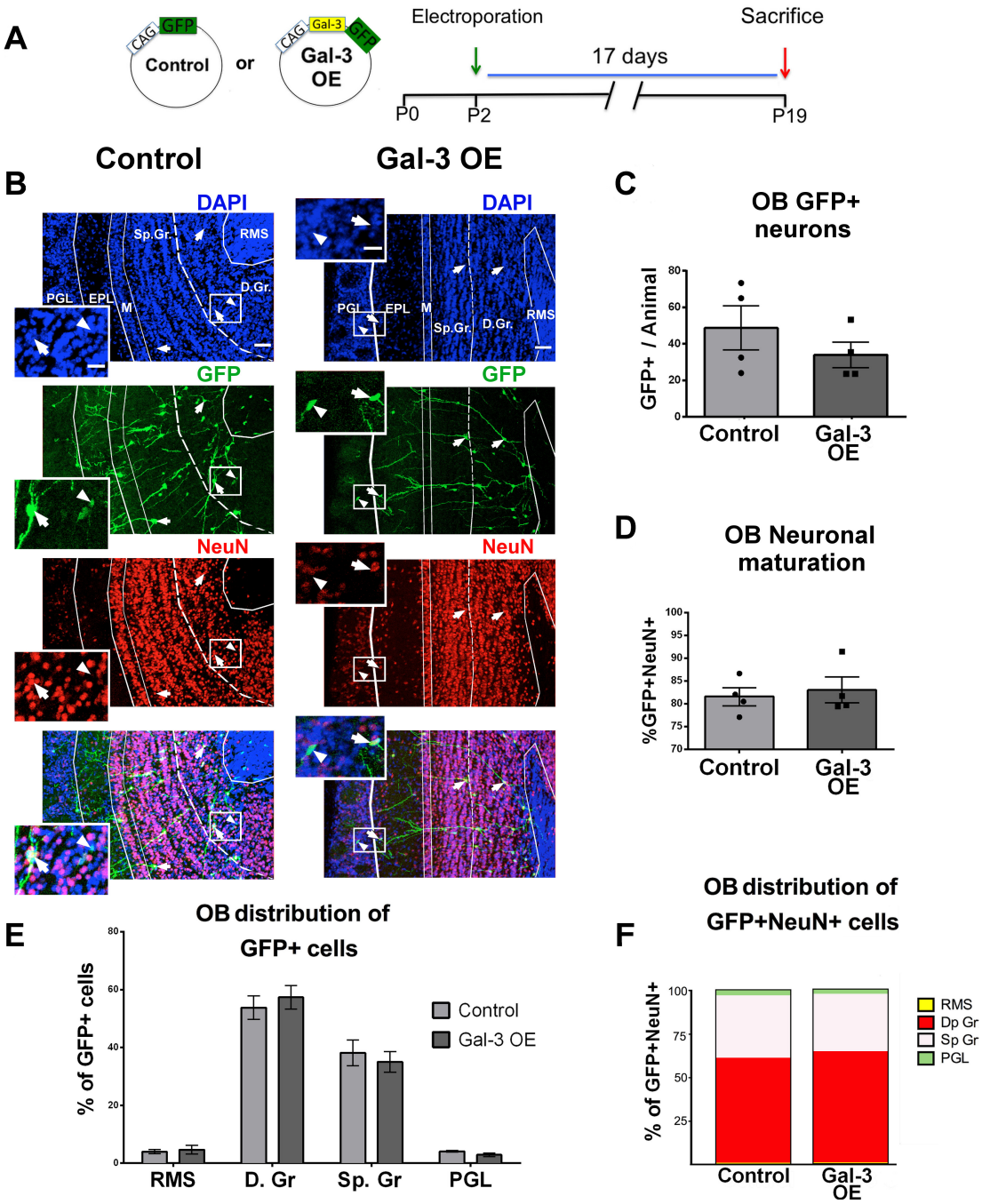


Figure 5.2 Olfactory neuronal differentiation was not affected by Gal-3 OE 17 DPE

(A) Cartoon depiction of the experimental scheme.
(B) Collapsed confocal *z*-stacks acquired from olfactory bulb (OB) sections 17 DPE of control and Gal-3 OE plasmids. Fluorescent Immunohistochemistry shows GFP (green), NeuN (red), and nuclei (DAPI; blue). GFP+NeuN+ (arrows) and GFP+NeuN- (arrowheads) cells are shown in OB layers demarcated by solid lines. Interrupted line marks the estimated boundary between deep and superficial Granule layers (**D.Gr** and **Sp.Gr**, respectively). Boxed areas are magnified in insets. **RMS**, rostral migratory stream, **M**, mitral layer, **EPL**, external plexiform layer, **PGL**, periglomerular layer. Scale bars: 50µm main panels and 20µm insets.
(C-F) Quantification of B. The mean number of GFP+ cells/OB section/animal is shown in **C**, and the percentage of GFP+NeuN+ cells is shown in **D**. The percent distribution of GFP+ and GFP+NeuN+ cells in OB layers is shown in **E** and **F**, respectively. n=4. Statistical significance was calculated using Mann-Whitney tests in B and C, and 2-way ANOVA in D and E. Data is shown as Mean ± SEM.

5.2.2 The plSVZ rarely gave rise to striatal neurons

I next asked whether RGCs labelled in the plSVZ at P2 could give rise to neurons in the dorsal or ventral striatum. To address that, I examined brain sections of mice 17 DPE for GFP+ cells in the striatum. In both control and Gal-3 OE groups, the majority of labelled cells in the striatum exhibited glial-like morphology, and only rarely were cells with neuronal morphology found (Figure 5.3A-B). Morphologically, glial-like cells had thick, branched processes (arrows in Figure 5.3A), and some showed signs of radial glial transformation; namely RGC displacement from the SVZ into the striatum and basal radial process retraction away from the cortical surface (arrowhead in Figure 5.3A). On the other hand, neuronal-like cells were morphologically characterised by large round cell bodies with long slender processes reminiscent of interneurons (Figure 5.3B-E). When sections were immunohistochemically stained for the glial markers GFAP and S100β, neuronal-like cells lacked expression of these markers (Figure 5.3C-E). Unfortunately, the observed neuronal cells were too few to allow comparison between experimental groups. Therefore, the conclusion from this data is that the plSVZ contributes to limited neuronogenesis in the striatum. Further experiments to better characterise this process fall outside the scope of this thesis.

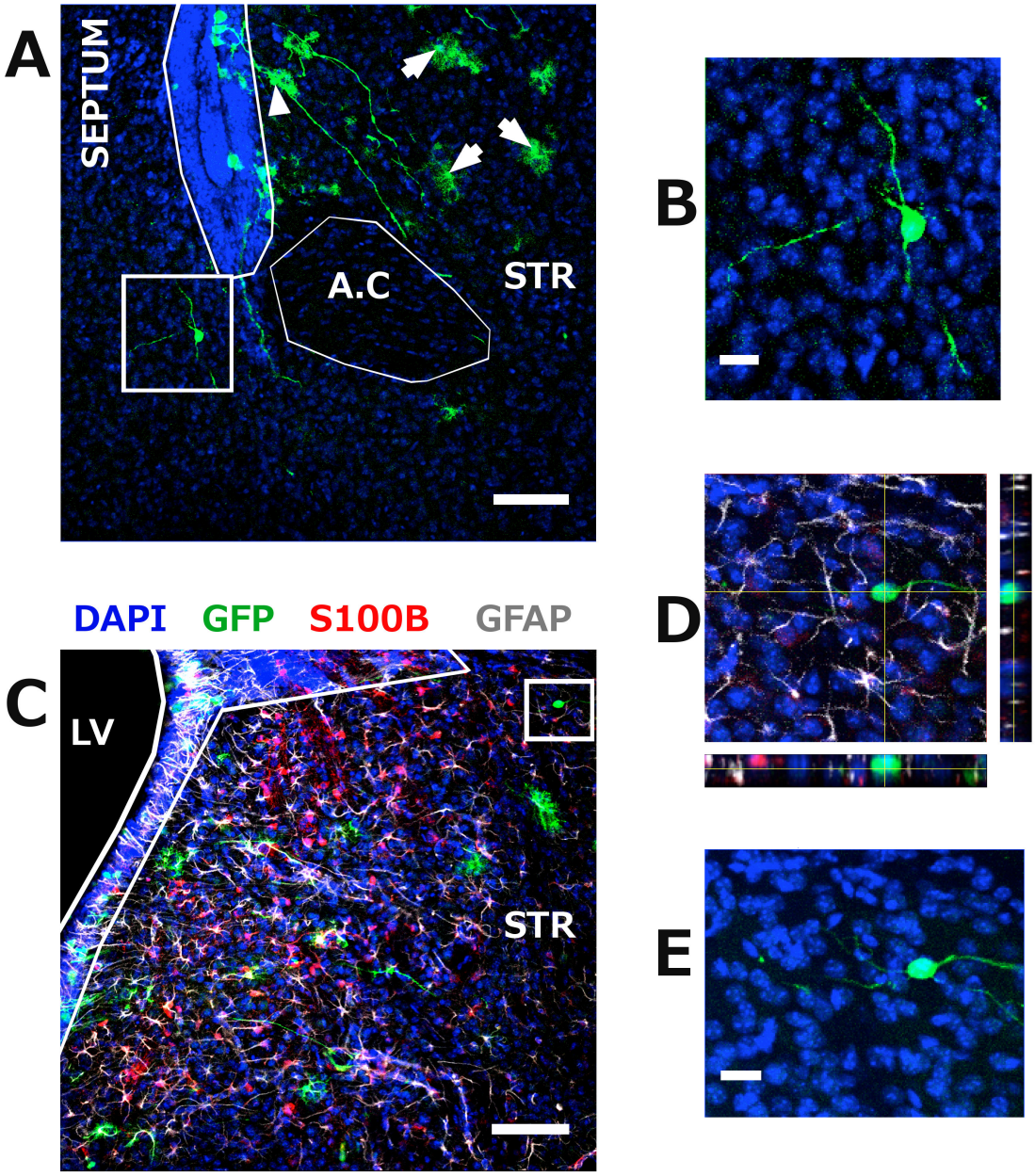


Figure 5.3 limited Pallidal neuronogenesis from the plSVZ

(A-B) Confocal image showing the ventral part of the SVZ 17 DPE acquired from a Gal-3 OE animal. Fluorescent Immunohistochemistry labelled GFP (green) and nuclei (DAPI; blue). The arrows indicate cells with glial morphology; the arrowhead points to a transforming radial glial cell. The boxed area contains a cell with neuronal morphology, and is enlarged in (**B**).
(**C-E**) Confocal image of a Gal-3 OE section 17 DPE. GFP (green), S100β (red), GFAP (grey), and nuclei (DAPI; blue) are shown. The boxed area is shown as an orthogonal view in (**D**) and collapsed z-stack (**E**)
(A-E) The white lines demarcate the subventricular zone (SVZ). Striatum (STR), lateral ventricle (LV), anterior commissure (A.C).
Scale bars: 100μm for A and C, and 20μm for B, D, and E.

5.2.3 Striatal gliogenesis from the plSVZ was increased by Gal-3 gain-of-function

I noticed that many GFP+ cells with glial morphology appeared in the striatum of the Gal-3 OE cohort. To evaluate whether Gal-3 gain-of-function influenced glial differentiation into the striatum, I quantified the percentage of GFP-labelled cells in the striatum from the total labelled cell population in the lSVZ and striatum in P9 and P19 (7 and 17 DPE) brain sections (Figure 5.4A-B). At P19, I found that Gal-3 OE increased the proportion of labelled cells in the striatum by more than 1.7 fold (30.78 ± 1.87% Gal-3 OE; 17.29 ± 1.32% control, n=4, p=0.0286; Figure 5.4D) without changing the total number of labelled cells in the lSVZ (Figure 5.4C). In contrast, this effect was not present at P9 (10.02 ± 5.61%, n=3, control; 10.19 ± 1.61%, n=4, Gal-3 OE). Of note, the majority of cells were detected in the medial striatum, although sporadic cells could be observed in more lateral regions of the striatum. These findings indicate that Gal-3 upregulation increased glial cell differentiation from the plSVZ into the striatum.

In the first two weeks after birth, glial progenitors migrate into the white and grey matter, and continue to divide before terminal differentiation (Levison and Goldman, 1993). I observed that some labelled striatal glial cells occurred in clusters (Figure 5.5A). I therefore postulated that this increase in striatal gliogenesis might result from increased proliferation of glial cells in the striatum. To test this hypothesis, I stained control and Gal-3 OE brain sections for the proliferative marker Ki67 and quantified the proportion of GFP-labelled cells that co-expressed Ki67 both at 7 and 17 DPE. At both time-points, minimal co-labelling of GFP and Ki67 in the striatum did not permit a statistical

comparison. Thus, increased striatal gliogenesis was not likely to be due to increased proliferation in the striatum at 7 or 17 DPE.

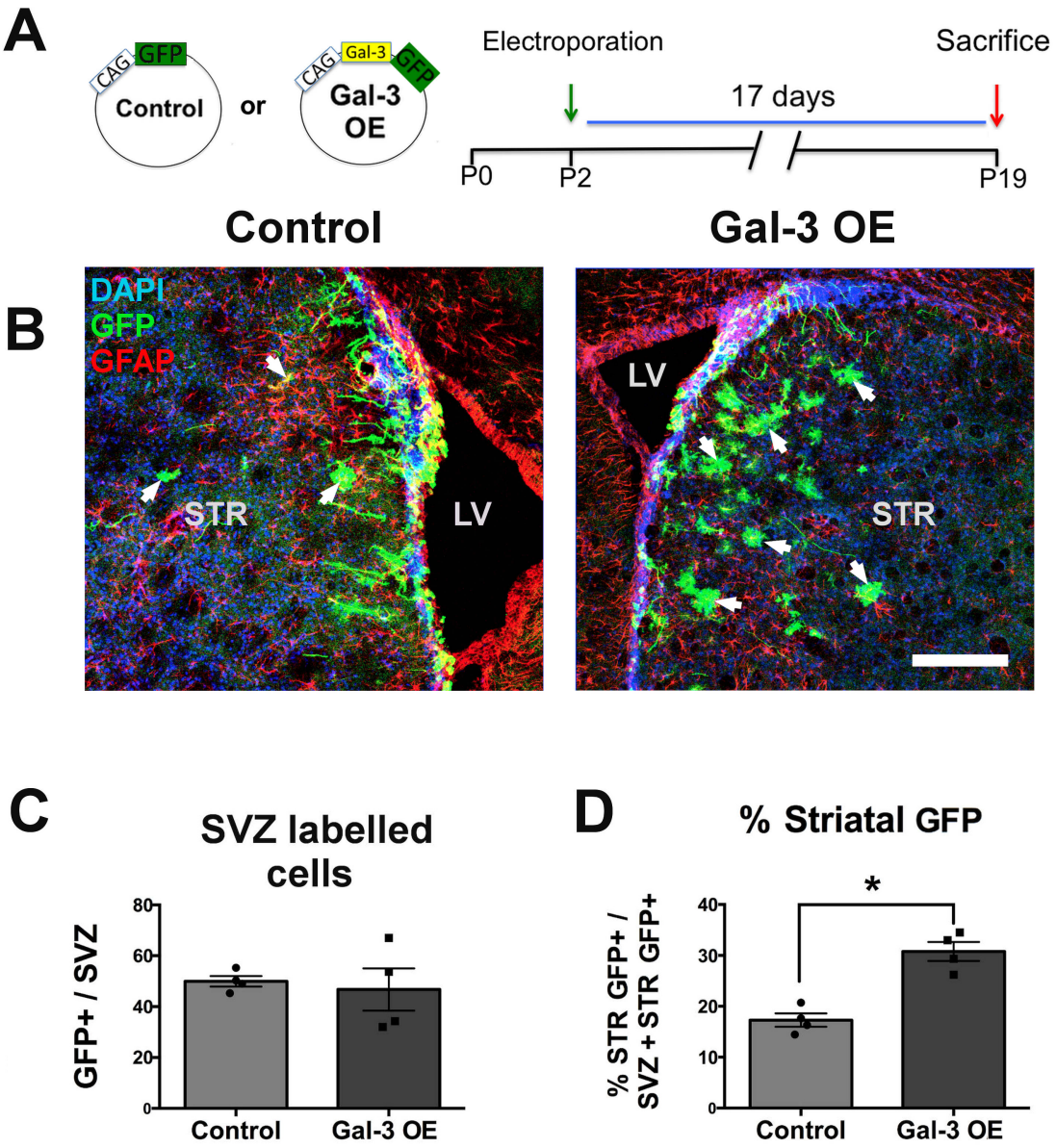


Figure 5.4 Gal-3 upregulation increased striatal gliogenesis from the plSVZ

(A) Cartoon depiction of the structure of plasmids and *in vivo* brain electroporation scheme for control (GFP) and Galectin-3 overexpression (Gal-3 OE) experimental groups. Labelled cells expressed GFP.
(B) Representative confocal images from brain sections at the level of the rostral lateral ventricle (LV) showing the subventricular zone (SVZ) and striatum (STR). Nuclei (DAPI; blue), GFP (green), and GFAP (red) are shown. Notice the increased number of labelled cells in the STR in Gal-3 OE group. Scale bar: 200µm
(C-D) Quantification of B. GFP+ labelled cells were counted in the lSVZ excluding the dorsolateral horn. There was no significant difference between the two groups (**C**). The proportion of labelled cells in the STR from total labelled cells in the SVZ and STR was quantified. Significantly more labelled cells were found in the STR in Gal-3 OE compared to control (**D**). Data is shown as mean ± SEM. *p* values: * < 0.05, n=4. Statistical significance was calculated using Mann-Whitney tests.

5.2.4 Gal-3 increased striatal astrocytic maturity

Labelled striatal cells adopted various morphologies reminiscent of protoplasmic astrocytes. In order to verify the glial identity and determine the state of maturity of these cells, I performed immunohistochemical staining for Vimentin, S100β, and GFAP on P19 sections. Vimentin labels young astrocytes, whereas GFAP and S100β are expressed in more mature astrocytes (Eliasson et al., 1999; Wang and Bordey, 2008). I found that Gal-3 OE reduced the proportion of striatal cells that co-labelled with Vimentin (66.47 ± 6%, control; 34.14 ± 1.94%, Gal-3 OE; n=4, p=0.0286; Figure 5.5A,C). This data suggests that Gal-3 OE reduced the proportion of immature astrocytes that were generated in the SVZ and migrated into the striatum. On the other hand, I discovered that Gal-3 gain-of-function increased the percentage of GFAP+ GFP-labelled cells in the striatum (81.89 ± 2.28%, control; 93.25 ± 2.55%, Gal-3 OE; n=4, p=0.0286; Figure 5.5B,D). Moreover, Gal-3 OE increased the proportion of S100β+ GFP-labelled striatal cells (52.43 ± 3.29%, control; 78.33 ± 3.22%, Gal-3 OE; n=4, p=0.0286; Figure 5.5B,E). Furthermore, the proportion of S100β+GFAP+ double-labelled cells was correspondingly increased in the Gal-3 OE group (44.48 ± 4.25%, control; 75.88 ± 2.81%, Gal-3 OE; n=4, p=0.0286). Taken together, these data suggest that Gal-3 upregulation increased striatal astrocytic identity and maturation.

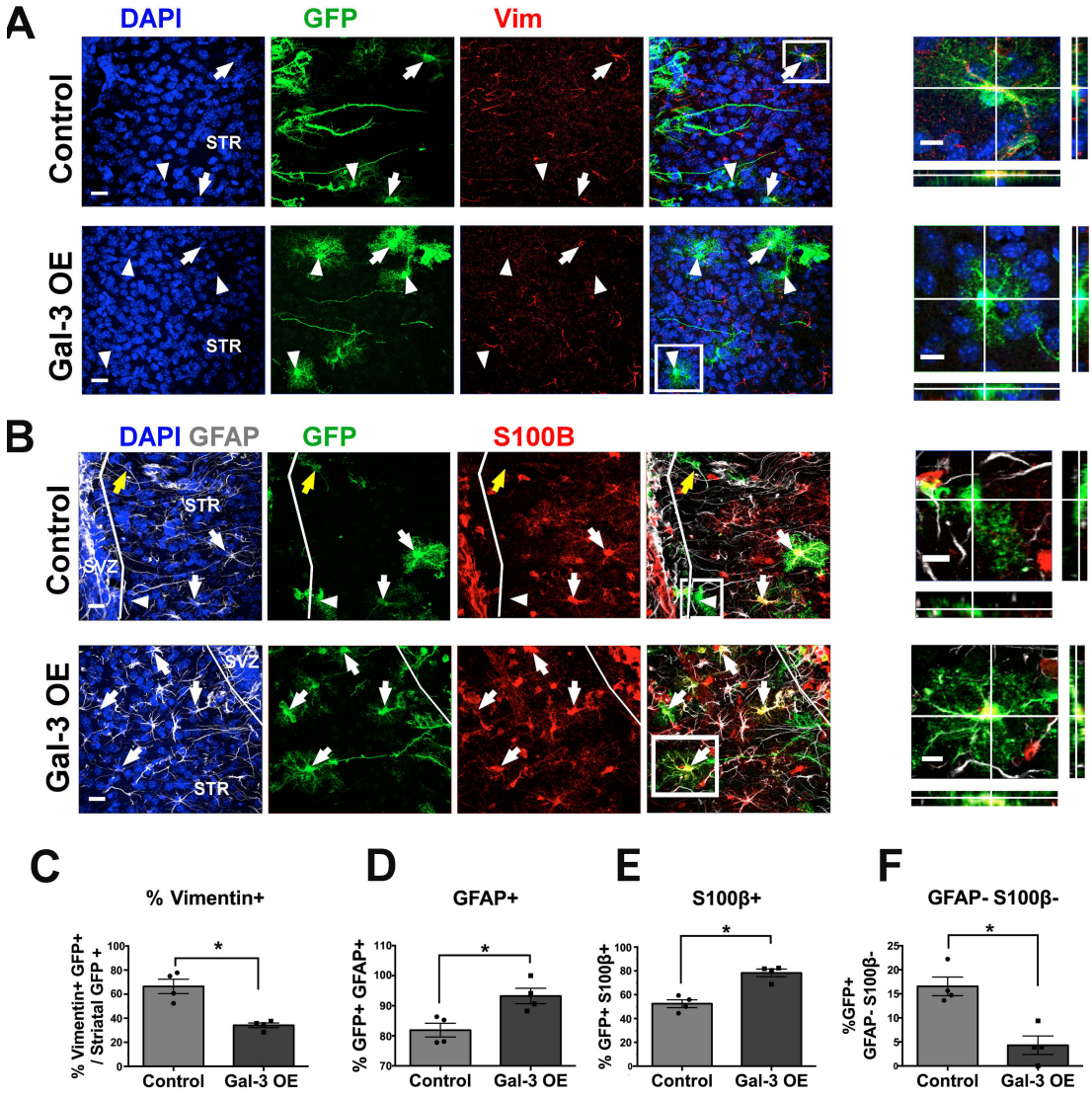


Figure 5.5 Gal-3 overexpression increased astrocytic differentiation and fate-choice

(A-B) Collapsed confocal *z*-stack (5μm) showing **(A)** DAPI (blue), GFP (green), and Vimentin (Vim; red). The arrows point to GFP+Vim+ and arrowheads to GFP+Vim- cells in the striatum (STR). **(B)** Shows DAPI (blue), GFP (green), S100β (red), and GFAP (Grey). The white arrows point to GFP+GFAP+S100β+, yellow arrow to GFP+GFAP+S100β-, and arrowhead to GFP+GFAP-S100β- cells in the STR. The white line demarcates the SVZ. The boxed area is enlarged in the inset on the right.
Scale bars: 20μm for main panels and 10μm for insets
(C-F) The percentages of striatal GFP+ cells that were positive for Vim **(C)**, GFAP **(D)**, S100β **(E)**, or negative for GFAP and S100β **(F)**, were quantified and compared.
Data is shown as mean ± SEM. *p* values: * < 0.05, n=4. Statistical significance was calculated using Mann-Whitney tests.

5.2.5 Gal-3 overexpression reduced the oligodendrocytic output from the plSVZ

To determine whether striatal oligodendrogenesis was influenced by Gal-3 upregulation, I first quantified the proportion of GFAP- S100β- labelled striatal cells. These cells lacked the molecular markers for astrocytes, and were therefore more likely to be oligodendrocytes or oligodendrocytic precursors. While the majority of labelled cells in the striatum expressed GFAP, S100β, or both in the Gal-3 OE group, labelled GFAP-S100β- striatal cells were significantly reduced compared to control (16.55 ± 1.93%, control; 4.31 ± 1.93%, Gal-3 OE; n=4, p=0.0286; Figure 5.5B,F). This data suggests that striatal oligodendrocytes were reduced after Gal-3 OE. To further validate the reduction in oligodendrocytic output into the striatum after Gal-3 OE, I performed immunostaining for the pan-oligodendrocytic lineage marker Olig2 (Lu et al., 2002) (Figure 5.6A). I found that Gal-3 upregulation significantly reduced the proportion of Olig2+ labelled striatal cells (37.04 ± 5.34%, control; 13.16 ± 2.74%, Gal-3 OE; n=3, p=0.0446; Figure 5.6B). Together, these data indicate that gain-of-function reduced the oligodendrocytic lineage output from the plSVZ.

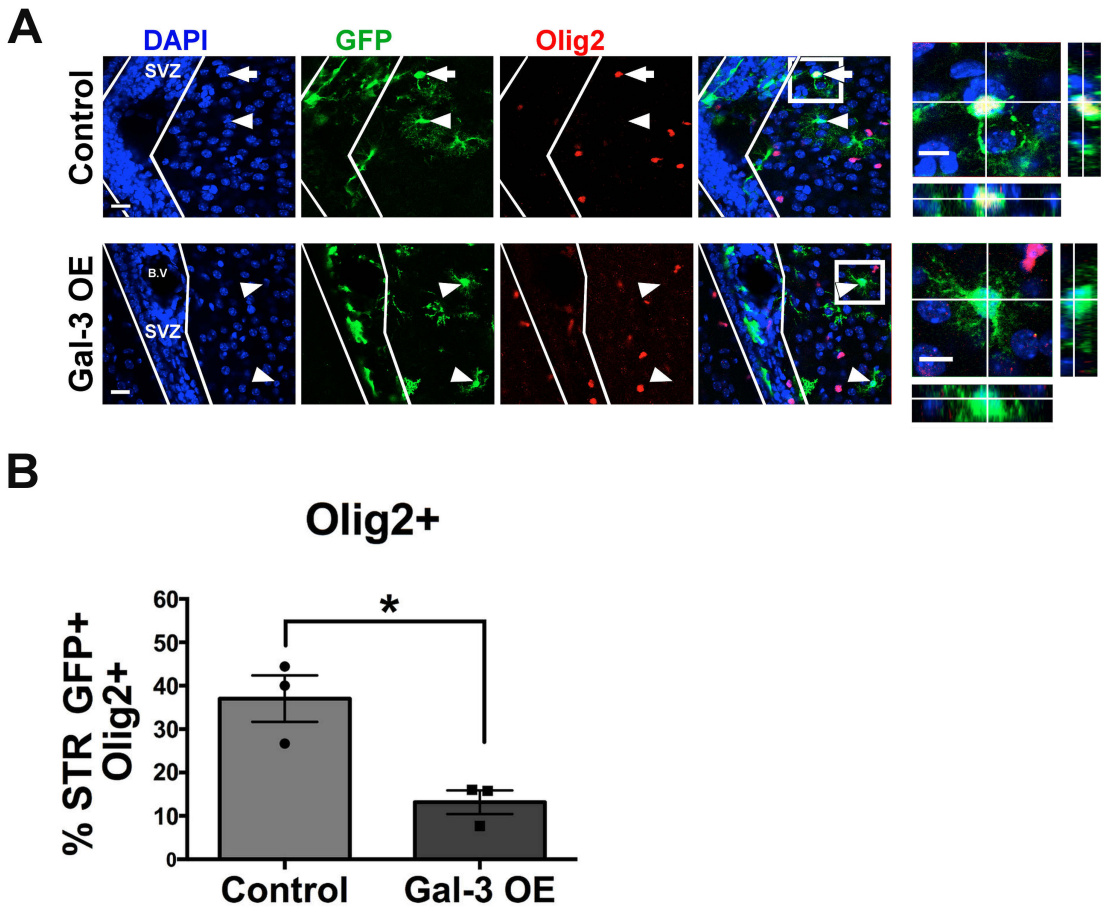


Figure 5.6 Gal-3 overexpression reduced striatal oligodendrocytic fate-choice from the plSVZ

(**A**) Single confocal planes showing nuclei (DAPI; blue), GFP (green), Olig2 (red) in the subventricular zone (SVZ) of control and Gal-3 OE 17 DPE. Arrowheads point to GFP+Olig2- cells and the arrow in control shows a GFP+Olig2+ cell in the striatum (STR). B.V: blood vessel.
Scale bars: 20µm for main panels and 10µm for insets.
(**B**) The percentage of striatal GFP+ cells that were positive for Olig2 was quantified.
Data is shown as mean ± SEM. *p* values: * < 0.05, n=3. Statistical significance was calculated using Mann-Whitney test.

5.2.6 Galectin-3 gain-of-function increased BMP signalling in vivo

BMP signalling in the SVZ has been shown to reduce proliferation and oligodendrogenesis, while promoting astrocytogenesis and astrocyte differentiation (Gomes et al., 2003). I postulated that Gal-3 might regulate BMP signalling in the SVZ, possibly contributing to the gliogenic effect observed in the striatum. Thus, I asked if BMP signalling was altered after Gal-3 overexpression. To address this question, I performed immunohistochemistry for phosphorylated-Smad/1/5/8 (pSmad1/5/8) on brain sections from P5 pups 3 DPE of Gal-3 overexpression, knockdown, or control plasmids (Figure 5.7). These Smad proteins are phosphorylated upon canonical BMP signalling in the SVZ (Colak et al., 2008). Labelled cells that were successfully electroporated with control plasmids or Gal-3 OE construct expressed mCherry in this experiment. The proportion of mCherry labelled cells that co-expressed pSmad1/5/8 was used to report BMP signalling in the plSVZ. I found that upregulation of Gal-3 more than doubled the percentage of pSmad1/5/8+ labelled cells in the SVZ 3 DPE, but knockdown of Gal-3 was similar to controls (12.19 ± 0.93% for control; 14.04 ± 1.03% for knockdown; and 27.31 ± 1.49% for Gal-3 OE, $p < 0.0001$; Figure 5.7B). This data suggests that Gal-3 positively regulated BMP signalling in the plSVZ.

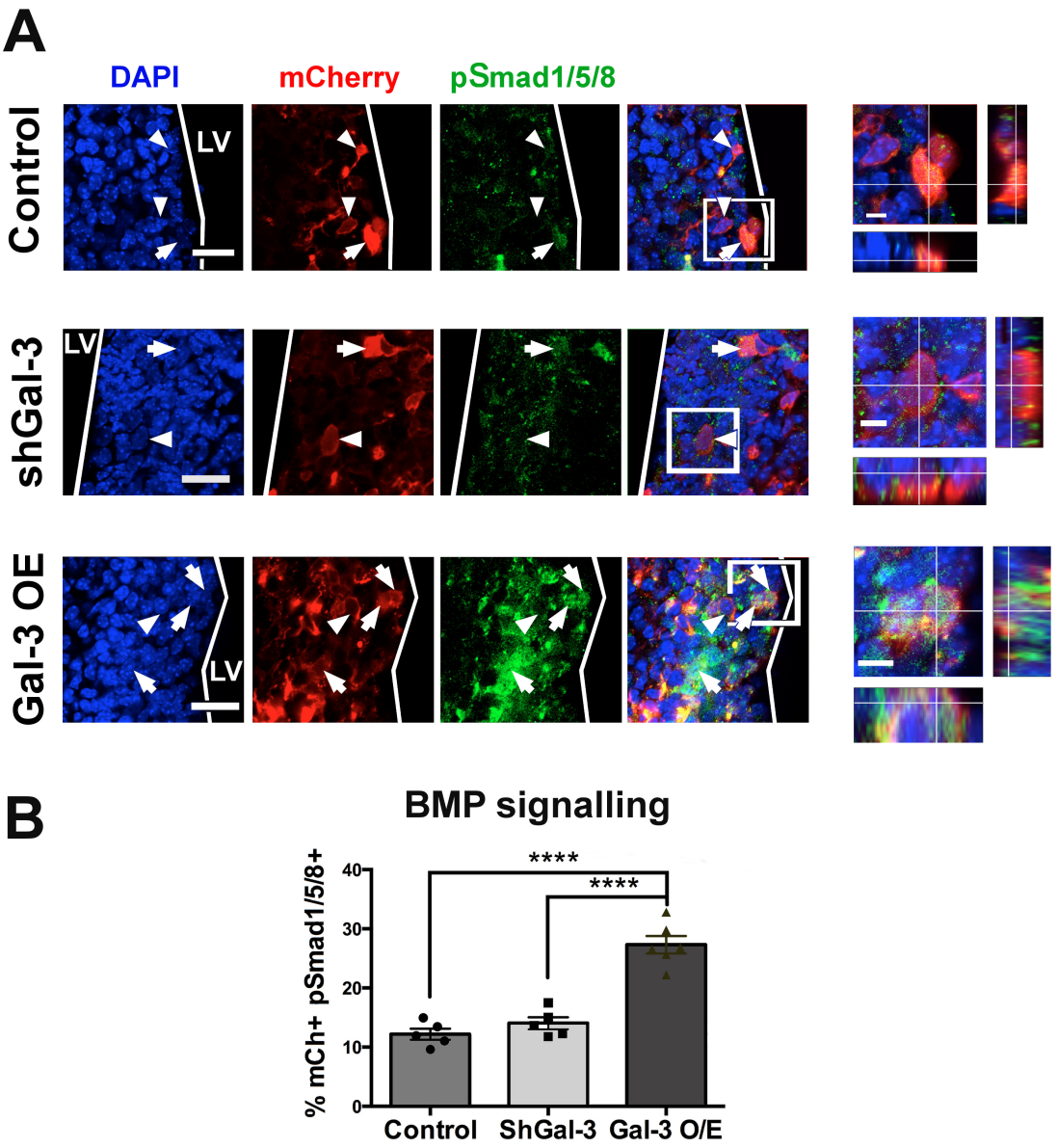


Figure 5.7 Gal-3 overexpression increased Smad1/5/8 phosphorylation in vivo

(A) Confocal images from P5 brain sections 3 DPE with control, Galectin-3 (Gal-3) knockdown (shGal-3), and Gal-3 overexpression (Gal-3 OE) at the level of the rostral lateral ventricle (LV). Labelled cells (mCherry+; red), nuclei (DAPI; blue), and phosphorylated Smad1/5/8 (pSmad 1/5/8; green) are shown. Arrows and arrowheads point to pSmad1/5/8+ and pSmad1/5/8- labelled cells, respectively. Boxed areas are enlarged as orthogonal views. Scale bars: 20μm for main panels and 5μm for insets.
(B) Quantification of **A**. The percentage of labelled cells (mCherry+; mCh) positive for pSmad1/5/8 was compared. n=5 for control and shGal-3 and 6 for Gal-3 OE. Statistical significance was calculated using one-way ANOVA, Tukey's test for multiple comparisons.

5.2.7 Galectin-3 upregulation increased BMP signalling in vitro

In order to assess whether Gal-3 regulated BMP signalling in vitro, I utilised a BMP signalling reporter (BRE-Luciferase) to gauge BMP signalling activity after overexpression or knockdown of Gal-3. I nucleofected NSCs from tertiary neurospheres with control, Gal-3 OE, and shGal-3 plasmids, along with a 20:1 ratio of BRE-Firefly-Luciferase: CMV-Renilla-Luciferase. The Renilla-Luciferase, driven by a CMV promoter, served as a nucleofection control to allow comparison between different nucleofection conditions. I then cultured the nucleofected NSCs for two days before cell harvesting cells for protein extraction. Next, I measured Firefly and Renilla Luciferase activities using the Promega Dual-Luciferase Assay kit®, and normalised the averages of Firefly Luciferase readings to Renilla Luciferase activities. The experiment was replicated four times and BMP signalling activity in Gal-3 OE and shGal-3 groups was expressed as a fold change from control (Figure 5.8A). Consistent with my pSmad1/5/8 in vivo results, Gal-3 OE increased baseline BMP signalling activity by 1.44 ± 0.14 fold compared to control ($p=0.0484$), whereas knockdown showed a trend towards reducing BMP signalling (0.61 ± 0.15 fold, $p=0.0921$). This data showed that Gal-3 overexpression increased baseline BMP signalling in vitro, whereas knockdown possibly decreased it.

I next set out to determine if Gal-3 retained its regulatory role on BMP signalling after increasing BMP4 concentration. The rationale was that stimulating the culture system with BMP might exaggerate and thus confirm the effects observed at baseline. To that effect, the experiment was conducted as previously described, but with the addition of 5ng/ml of recombinant mouse BMP4 to the media 24 hours before cell harvest and

protein isolation. The results were normalised and presented as fold change from control as before (Figure 5.8B). BMP4 treatment increased BRE-Luciferase activity in all experimental conditions (mean fold change from untreated controls: 14.65 ± 5.34 in control, 112.5 ± 64.10 in shGal-3, and 15.2 ± 6.34 in Gal-3 OE). As expected, I found that Gal-3 overexpression increased BRE-Luciferase activity compared to control by 1.94 ± 0.22 fold (n=4 independent experiments, p=0.0233). Surprisingly, Gal-3 knockdown displayed a trend for increasing in BRE-Luciferase activity by 5.44 ± 1.62 fold (p=0.0711). Thus, the data indicates that Gal-3 upregulation increased BMP signalling in cultured NSCs/TAPs upon BMP stimulation in vitro. Interestingly, Gal-3 knockdown possibly increased BMP signalling in that setting as well.

Canonical Wnt/β-catenin signalling has been reported to both inhibit BMP signalling (Nakashima et al., 2005), and prolong depending on the context (Fuentealba et al., 2007). I hypothesised that increasing Wnt/β-catenin signalling may regulate BMP pathway activation in cultured NSCs. To evaluate whether Wnt signalling regulated BMP pathway activity, and whether Gal-3 levels affected that relationship, I treated the nucleofected NSCs (conditions as above) with 5mM LiCl for 24 hours before cell harvest for protein isolation and subsequent Luciferase activity measurement (Figure 5.8C). The experiment was replicated three times. LiCl inhibits the GSK3β leading to activation of Wnt/β-catenin signalling (Wexler et al., 2008), and a concentration of 5mM was sufficient to increase proliferation of cultured hippocampal NSCs (Kim et al., 2004). 2-way ANOVA with the experimental group and LiCl treatment as main factors was used to statistically determine if LiCl treatment changed BRE-Luciferase activity. Compared to no treatment

controls, 5mM LiCl did not significantly alter BRE-Luciferase activity for any of the nucleofected conditions ($F(1,4) = 0.3762$, $p=0.5728$). Together, these data show that 5mM LiCl treatment for 24 hours had no effect on BMP signalling in cultured NSCs.

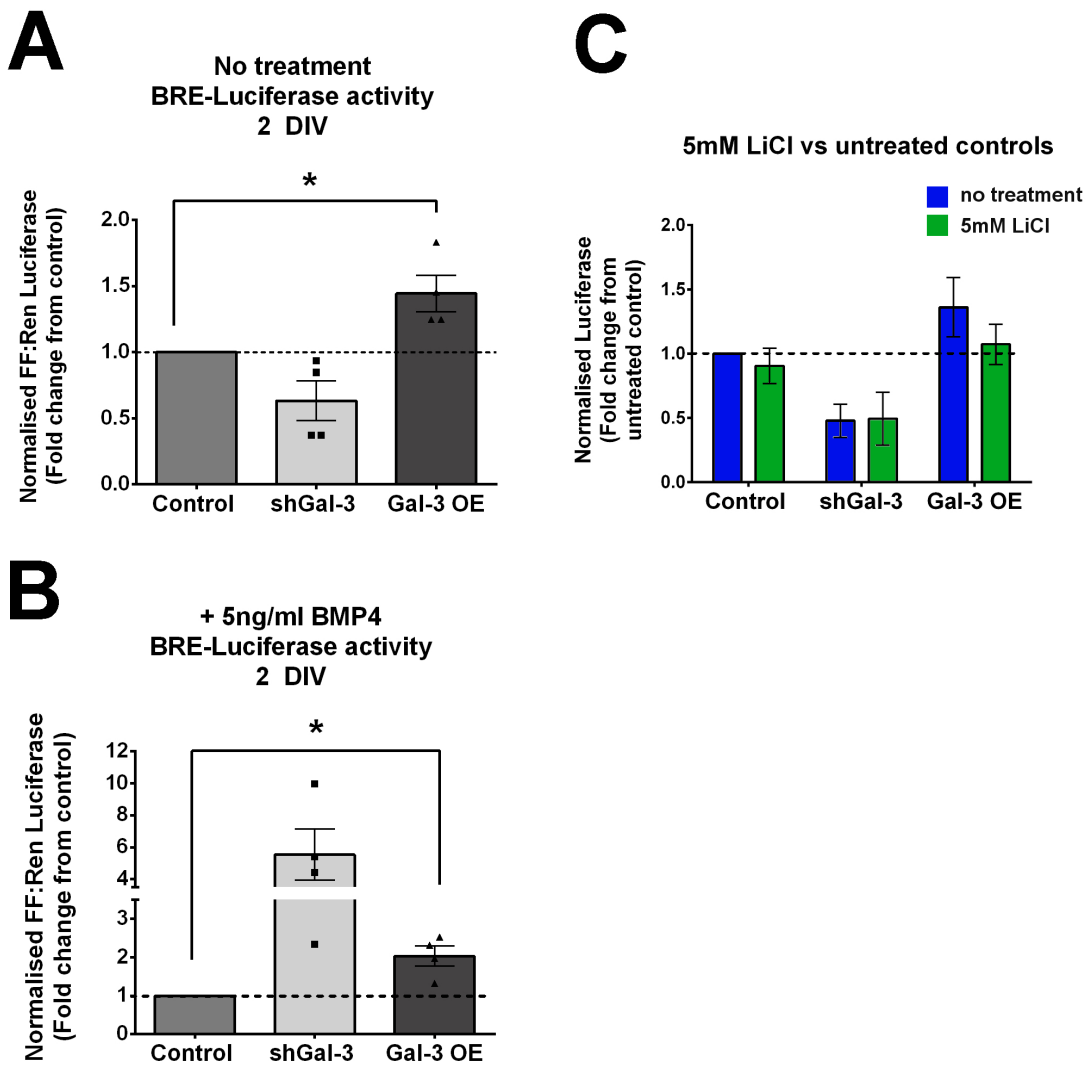


Figure 5.8 In vitro Gal-3 upregulation increased BMP signalling

(**A-C**) Normalised Firefly to Renilla Luciferase activity was measured and expressed as fold change from control. 24 hours post-nucleofection, cultures were either treated with control media (**A**) or 5ng/ml BMP4 (**B**) or 5mM LiCl (**C**) for 24 hours before analysis. The data is presented as mean ± SEM fold change from control in **A-B**, and untreated control in **C**. Individual points represent biological replicates (n=4 independent experiments for **A-B**, and 3 for **C**). Statistical significance was calculated using one-sample t-test in A-B, and 2-way ANOVA in C. * : $p < 0.05$

5.2.8 Gal-3 regulated phosphorylation of Smads 1/5/8

The increase in Luciferase activity could be due to increased Smad protein content or phosphorylation and subsequent transcriptional activity. To determine the cause of the increase in BMP activity in vitro, I examined protein samples from both BMP treated and untreated nucleofected NSCs/TAPs detailed in Section 5.2.7. I immunoblotted for pSmad1/5/8 to report BMP signalling activity, total Smads 1, 5 and 4 to control for Smad protein content, Gal-3 to verify its overexpression or knockdown, and β-actin to serve as a loading control (Figure 5.9A). When pSmad1/5/8 was normalised to β-actin then to shNT control, the data showed that downregulation of Gal-3 reduced pSmad1/5/8 in untreated NSCs cultures (0.58 ± 0.09 fold, n=4, p=0.0192; Figure 5.9B). On the other hand, Gal-3 OE did not significantly alter β-actin-normalised pSmad1/5/8 band intensity in untreated samples (1.61 ± 0.4 fold, n=4, p=0.22; Figure 5.9B). More appropriately, when pSmad1/5/8 band intensities were normalised to Smad 1 or Smad5, the effects of Gal-3 OE were more apparent (Figure 5.9D,E). Gal-3 OE significantly increased Smad5-normalised pSmad1/5/8 band intensities compared to shGal-3 in untreated NSCs, and there was a trend when compared to shNT control (Figure 5.9E). After BMP4 treatment, Gal-3 OE significantly increased Smad1 and Smad5-normalised pSmad1/5/8 band intensities (Figure 5.9D,E). In contrast, shGal-3 failed to alter Smad1 and Smad5-normalised pSmad1/5/8 band intensities in BMP4-treated NSCs (Figure 5.9D,E). Finally, total levels of Smads 1, 4, and 5 were not different between experimental conditions per treatment. These data indicate that Gal-

3 levels regulated BMP signalling by changing the phosphorylation of pSmad1/5/8 without altering total Smad protein content.

Of note, BMP treatment caused a notable increase in Gal-3 levels in both control (shNT) and shGal-3 conditions (Gal-3 rows in Figure 5.9A). When β-Actin-normalised Gal-3 band intensities from control, shGal-3 and Gal-3 OE were compared before and after BMP4 treatment, an interesting pattern arose. Whereas Gal-3 levels were not significantly altered by BMP treatment in Gal-3 OE, they were significantly increased in shGal-3 by 3.1 ± 0.43 fold ($p=0.0398$), and by 1.72 ± 0.48 fold in the control without reaching significance ($p=0.073$; n=3 independent biological samples; Figure 5.9C). Taken together, the data suggests that BMP treatment may have induced Gal-3 expression, but additional experiments are required to validate this.

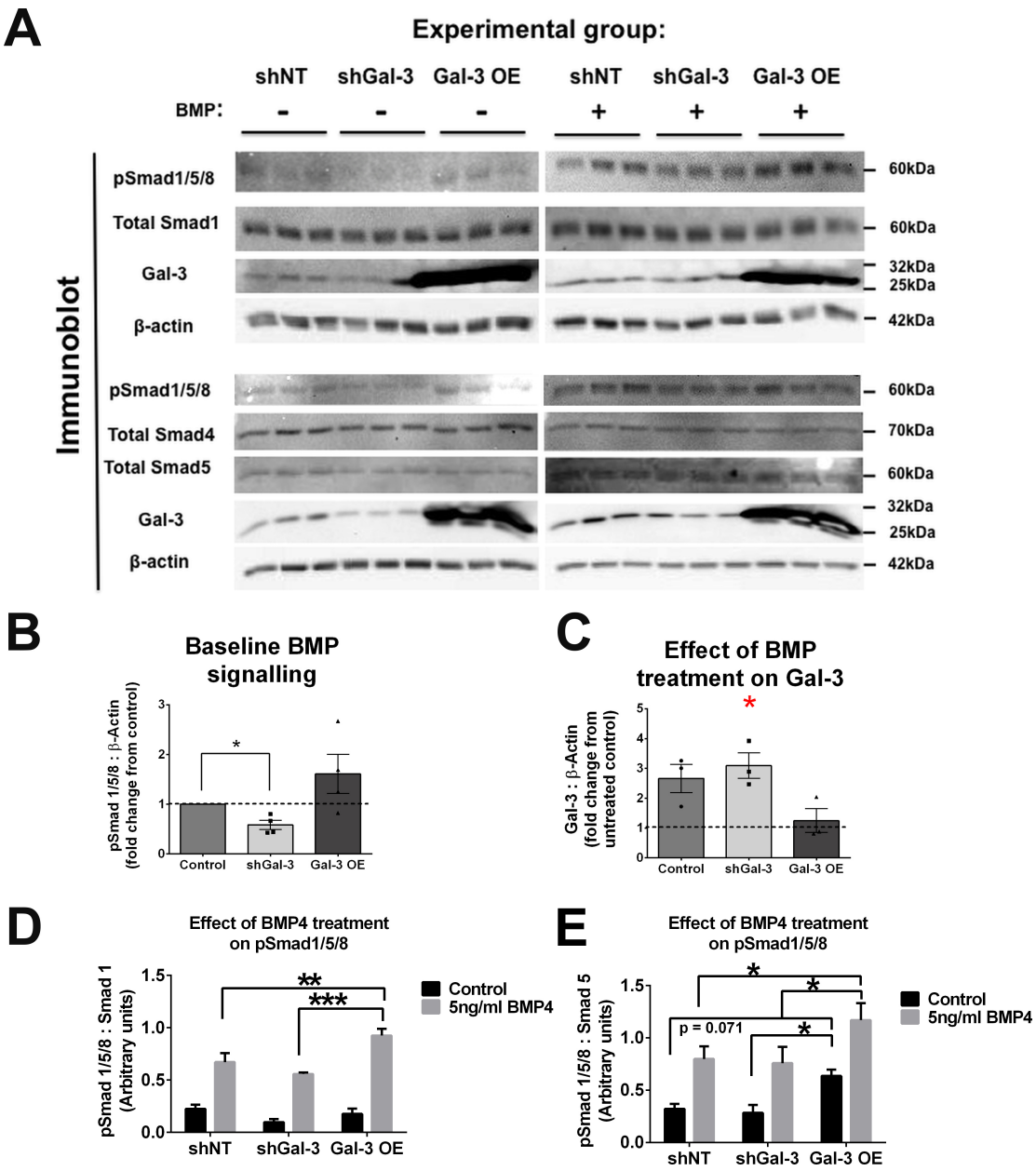


Figure 5.9 Gal-3 regulated Smad phosphorylation

(**A**) Western Blot analysis from two independent experiments, to show pSmad1/5/8, total Smad1, Gal-3, and β-Actin from one experiment, and pSmad1/5/8 total Smad 4, 5, Gal-3, and β-Actin from another. Three technical replicates are shown per condition. The approximate sizes in kDa are shown on the left. Samples were either treated with control media or 5ng/ml BMP4 as indicated above. β-Actin was used as a loading control. Note that Gal-3 OE greatly increased and shGal-3 moderately reduced Gal-3 levels. The effect of knockdown on Gal-3 levels was ameliorated in BMP treated samples, and Gal-3 levels were increased after BMP treatment.
(B) Quantification of β-Actin-normalised pSmad1/5/8 band intensities from 4 experiments, expressed as a fold change from control.
(C) Quantification of β-Actin-normalised Gal-3 band intensities from n=3 experiments, expressed as fold change from untreated conditions.
(**D-E**) pSmad1/5/8 band intensities from (A) were normalised to total Smad 1 (D) and total Smad 5 (E) and compared. (**B-E**) Data is shown as mean ± SEM. *p* values: * < 0.05, ** < 0.01, *** < 0.001.

5.3 Discussion

5.3.1 Gal-3 gain-of-function did not influence olfactory neuronogenesis and maturation

In the chapter 4, I showed that the proportion of labelled Dcx+ cells in the plSVZ was not altered by Gal-3 overexpression 7 and 17 DPE. Here, I tracked the progeny of plSVZ NSCs to their primary destination- the OB, and examined their differentiation dynamics. After they are born, neuroblasts undergo divisions en route to the OB (Menezes et al., 1995), where they switch from tangential to radial migration, entering the layers of the OB (Kishi, 1987; Luskin and Boone, 1994). Neuroblasts can be seen in the RMS core of the OB as early as 3 days after being born, and once they arrive in the OB, they begin to differentiate into Gr-Ns or PGCs (Kishi, 1987; Lois and Alvarez-Buylla, 1994; Luskin, 1993). As neuroblasts start differentiation, young neurons begin to express the nuclear antigen NeuN, and replace the leading process with apical dendrites that branch into the external plexiform layer, where they establish synaptic connections with mitral and tufted cells (Kishi, 1987; Petreanu and Alvarez-Buylla, 2002). This process is almost complete approximately 15-22 days after birth of these cells. Interestingly, a wave of apoptosis occurs 15-45 days after birth of these neurons, after they have established synaptic contact with mitral and tufted cells. This is governed by receiving proper input in the olfactory circuitry, ensuring the right number and localisation of young neurons that will integrate into the olfactory circuitry (Petreanu and Alvarez-Buylla, 2002).

Examination of P9 OB sections 7 days after labelling RGCs with control or Gal-3 overexpression plasmids showed that most labelled cells were localised either in the RMS core or in deep granule layer. This indicates that a

large proportion of these cells had not yet reached the final destination. In addition, the majority of these cells retained the morphology of migratory neuroblast, with an elongated body, long leading process and occasional shorter trailing process (Kakita and Goldman, 1999; Kishi, 1987; Luskin, 1993; Luskin and Boone, 1994), suggesting their on-going radial migration in the OB. In addition, approximately only 10% of labelled cells in the OB acquired NeuN positivity, confirming that these cells had not yet acquired differentiated neuronal characteristics. This is consistent with previous literature, supporting that only a minority of neuronal precursors had begun to differentiate 7 days after labelling (Kishi, 1987; Luskin, 1993; Luskin and Boone, 1994; Petreanu and Alvarez-Buylla, 2002). Importantly, upregulation of Gal-3 had no effect on labelled cell localisation in the OB and neither did it change the proportion of NeuN+ labelled OB cells. Thus, the data indicates that Gal-3 gain-of-function did not induce premature or delayed olfactory neuronal differentiation 7 DPE.

Gal-3 has been shown to play a role in neuroblast migration. Comte et al showed that neuroblasts accumulated in the RMS, and their tangential migration into the OB was reduced in Gal-3 null mice (Comte et al., 2011). The authors described slower, more exploratory, and inefficient neuroblast migration in the RMS of Gal-3 nulls. Radial migration was not examined but might have been affected by Gal-3 loss. Had Gal-3 OE increased net neuroblast migration, as suggested by the increase in labelled cells in the RMS 3 DPE after Gal-3 OE, more labelled cells would reach the OB 9 DPE. On the contrary, I found that upregulation of Gal-3 did not increase total neuroblast migration into the OB or induce radial migration into OB layers 7 or 17 DPE. To elaborate, firstly, Gal-3 overexpression did not change total GFP+

cell numbers in the OB at 7 and 17 DPE. Secondly, there was no significant change in the proportion of labelled cells in the RMS core of the OB at 7 and 17 DPE, arguing against increased tangential migration. Finally, there was no redistribution of labelled cells form the OB RMS core to more superficial OB layers. That would have been the case had Gal-3 OE increased radial migration; i.e. encouraged efflux of cells out of the RMS into OB layers. Thus, these findings argue against a role for exogenously overexpressed Gal-3 in increasing tangential neuroblast migration to the OB, or radial migration of neuroblasts out of the RMS core into OB layers. One caveat, however, is that Comte et al. used 6-8 week old mice, whereas I examined mice at the postnatal stage. It is possible that Gal-3 OE may increase neuroblast migration in the adult setting, when glial tubes are fully formed. On the other hand, the glial tubes in the RMS are fully formed only from the fourth postnatal week (Peretto et al., 2005). Therefore, if Gal-3 maintained neuroblast migration by functioning via the glial tubes in the adult setting as suggested by Comte el al., then the current study is not suited to address the role of Gal-3 in neuroblast migration in the postnatal setting.

Of note, I found almost no apoptotic labelled cells in the OB 7 DPE, as determined by activated caspase-3 positivity. However, Gal-3 upregulation did not change the survival of unlabelled OB cells. This is consistent with what I observed in the lSVZ both at 7 and 17 DPE, where Gal-3 OE did not alter survival. Together these findings support that Gal-3 reduced apoptosis only acutely in a cell non-autonomous fashion, and these effects are lost when test animals were followed for longer survival times. Evaluating long-term survival of labelled neurons in the OB was not the aim of this study. However, it would

be interesting to test if Gal-3 upregulation influenced neuronal survival; which would require further follow up of test animals into the period of maximal vulnerability to apoptosis: 15-45 days after birth. This would also serve as an indirect readout of neuronal integration, which is a main determinant of survival of olfactory interneurons (Petreanu and Alvarez-Buylla, 2002).

Examining OB sections from control and Gal-3 OE animals 17 DPE revealed that <5% of the labelled population in the OB was located in the RMS core, and only a minor subset of neuroblasts retained migratory morphology. This is consistent with previously published data showing that labelled neuroblasts almost completely exit the RMS by 3 weeks after birth (Kishi, 1987; Petreanu and Alvarez-Buylla, 2002). The fact that migratory neuroblasts were detected in the RMS core and more superficial layers of the OB 17 DPE indicates that labelled plSVZ NSCs retained their neurogenic potential at longer survivals, as shown in chapter 4. On the other hand, most OB labelled cells were localised in the deep (53.76 ± 4.1%) and superficial (38.14 ± 4.47%) granule layers, with less than 5% settling in the glomerular layer. This is in line with the fact that the lSVZ has been reported to produce more deep than superficial Gr-N, and has limited potential for PGC production (Merkle et al., 2007). In addition, most cells adopted a more differentiated morphology, with long apical processes and branched basal dendrite. Also, NeuN was expressed in ~80% of OB labelled cells. These data support the notion that labelled OB cells differentiated into olfactory interneurons at P19 (17 DPE). Of note, Gal-3 OE did not change the proportion of NeuN+ labelled OB cells, plus, there was no apparent morphological difference induced by Gal-3 OE. Together, these data indicate that upregulation of Gal-3 did not

influence neuronal differentiation, which is in contrast to its effects on glial differentiation (see section 5.3.4 below).

Olfactory neuronal layer-specificity is intrinsically determined by the location of parent NSCs, and this positional identity is not readily changed by environmental factors in both neonates and adults. For example, cells born in the vSVZ primarily give rise to calbindin+ deep and fewer superficial Gr-N or PGCs, whereas cells born in the dSVZ preferentially differentiate into superficial Gr-N and tyrosine hydroxylase+ PGCs (Kohwi et al., 2007; Merkle et al., 2007; Ventura and Goldman, 2007; Young et al., 2007). Because Gal-3 was shown to bind the TF Nkx2.1 and increase its transcriptional activity in thyroid cancer (Paron et al., 2003), and because Nkx2.1 is downstream to Shh signalling which specifies ventral (deep granular) neuronal identity, I hypothesised that Gal-3 OE might change the layer-specificity of newborn neurons from the lSVZ. However, in both controls and Gal-3 OE, olfactory neurons adopted deep and superficial positions in the granule layer, and Gal-3 upregulation did not change the distribution of total or NeuN+ labelled cells in OB layers at P19. This indicates that Gal-3 gain-of-function did not alter olfactory neuronal layer-specificity, i.e. Gal-3 overexpression was not sufficient to re-specify olfactory neurons, or change their inherited positional identity. Altogether, I conclude that Gal-3 upregulation did not influence the olfactory neuronal fate, differentiation, or OB layer-specificity in plSVZ precursors.

5.3.2 Striatal neuronogenesis is limited postnatally

Neurogenesis continues postnatally in the olfactory bulbs and hippocampus, but not in other brain structures. In spite of that consensus, postnatal continuation of limited neocortical and striatal neurogenesis has been reported (Levison et al., 1993; Levison and Goldman, 1993; Malatesta et al., 2003). In support of that, I showed that the plSVZ rarely gave rise to striatal neurons from precursors labelled as late as P2, as defined by morphology and lack of glial marker expression. Rare neocortical neurons were also present in sections where the dSVZ was inadvertently labelled. Therefore, I conclude from this preliminary evidence that limited neuronogenesis continued in the plSVZ in the striatum and ventral forebrain.

5.3.3 Striatal gliogenesis from the plSVZ

In the developing embryo, neuronogenesis in striatal structures occurs primarily prenatally, between embryonic days E12 and P2 and peaking around E15 (Brazel et al., 2003a; Halliday and Cepko, 1992). Gliogenesis on the other hand, occurs primarily postnatally, and was most extensively studied in the rat dlSVZ (Brazel et al., 2003b; Goldman, 2003; Kakita and Goldman, 1999; Levison et al., 1993; Levison and Goldman, 1993, 1997; Levison et al., 1999; Luskin and McDermott, 1994; Parnavelas, 1999). The focus of these early studies was primarily on oligodendrogenesis from the dlSVZ into the corpus callosum and neocortex, with limited attention given to the striatum. For example, in a study by the Goldman laboratory, the authors examined P28 rat brains after retroviral labelling of the dlSVZ at P0-1, and found that

43.8% and 48.3% of the labelled cells in the striatum were astrocytes and oligodendrocytes, respectively (Kakita and Goldman, 1999). This was similar to results from previous studies from the same group, where approximately 43% of the progeny of rat dlSVZ labelled at P2 differentiated into astrocytes in the striatum, while the remainder were identified as oligodendrocytes (Levison et al., 1993; Levison and Goldman, 1993). Moreover, the preference for the astrocytic fate decreased to 12% when dlSVZ progeny was labelled at P14, with the majority of the cells adopting oligodendrocytic morphologies, indicating that astrocytogenesis slows down over the first two postnatal weeks (Levison et al., 1993). Additional follow up revealed further reduction in the proportion of astrocytes in labelled striatal clones with increasing age (Levison et al., 1999). In the previously published studies, the proportion of labelled cells that differentiated into the striatum was less than 15% of total labelled cells from the dlSVZ. Together, these studies show that postnatal striatal gliogenesis takes place in the first two postnatal weeks before slowing down. Moreover, the dlSVZ plays a minor role in striatal gliogenesis, shifting from providing astrocytic precursors before P14 to oligodendrocytic precursors afterwards.

Only a handful of studies tackled postnatal gliogenesis from the lSVZ in mice. For instance, Merkle et al. briefly examined striatal gliogenesis from the P0 murine dlSVZ and lSVZ by injecting Adeno:Cre virus into the ventro-lateral striata of Z/EG mice (Merkle et al., 2004). The authors documented postnatal birth of striatal astrocytes and oligodendrocytes without detailing the dynamics of this gliogenic process. A more recent study traced the birth of postnatal astrocytes in the septum, cortex, and lateral as well as ventral striatum to

radial glia residing in the medial, dorsal, dorsolateral, and ventral LV, respectively (Tsai et al., 2012). The authors concluded that astrocytes are born along the trajectories of their RGC ancestors, and do not migrate tangentially across RG territories. However, no details were provided about astrocytes born into the medial striatum, or the contribution of the lSVZ to striatal gliogenesis. Another example comes from studying postnatal cortical gliogenesis, where Magavi et al. briefly alluded to finding striatal but not cortical astrocytes labelled along with both cortical and striatal interneurons after low-rate recombination induced in Thy1.2-Cre:Z/EG reporter mice, which mark the neuronal progeny (Magavi et al., 2012). This is consistent with the finding of a common subpallial Dlx2+ precursor for a subset of postnatal glia and interneurons (Marshall and Goldman, 2002). Of note, studying cortical gliogenesis provided the field with valuable insights into contribution of local proliferation into gliogenesis (Ge et al., 2012; Magavi et al., 2012). Overall, these studies reinforce an emerging concept in understanding gliogenesis, whereby postnatal astrocytes are born according to the segmental blueprint laid down by ancestor RGCs, which are diversified in their progeny based on their molecular and temporo-spatial signatures (Bayraktar et al., 2014; Kriegstein and Alvarez-Buylla, 2009). Moreover, the aforementioned arguments highlight a gap in the literature, where striatal gliogenesis remains an open topic for exploration. This study therefore provides a novel insight into the temporal dynamics of postnatal gliogenesis in the striatum.

Here, I labelled RGCs with CAG-IRES-GFP or pCAG-Gal-3-IRES-GFP plasmid using in vivo electroporation of the LV at P2, and followed their progeny in the striatum at P9 and P19. Whereas labelled cells and their

progeny did not leave the SVZ/RMS at P5 (3 DPE), approximately 10% of the control labelled population was located in the medial striatum at P9 (7 DPE). These cells were well positioned to supplement the neighbouring striatum with glial cells. At P19 (17 DPE), numerous glial cells could be identified in the medial striatum, amounting to 17.3% of the control labelled cells. These findings support that plSVZ was actively involved in the gliogenic process in the medial striatum. Immunohistochemical analysis of control newborn striatal glia at P19 revealed that approximately one sixth to one third of the plSVZ progeny was of oligodendrocytic lineage- as suggested by the proportion of GFAP- S100β- (~16%) and Olig2+ (~37%) striatal cells. The remainder of the cells were identified as astrocytes by virtue of GFAP and/or S100β expression. Together, these findings provide a novel insight into the role the plSVZ in striatal gliogenesis, which, in contrast to the dlSVZ, was more competent for astrocytogenesis.

It is attractive to speculate on the possible reasons why the fate choices and molecular profile of glia born in lSVZ differ from those of born in the neighbouring dlSVZ. As previously presented, the dlSVZ is progressively more oligodendrogenic in the first two postnatal weeks and thereafter, whereas I showed that the plSVZ is more astrocytogenic. One possible explanation is the different embryonic origin of these regions; the plSVZ derives from RGCs in the ventricular wall of LGE (Malatesta et al., 2003; Young et al., 2007) whereas the dlSVZ has mixed origins from ventral Dlx+ precursors that migrate dorsally from the MGE (Brazel et al., 2003b; Marshall and Goldman, 2002) in addition to cortical and striatal SVZ derivatives (Young et al., 2007). The former ventrally derived Dlx2+ precursors are known to be

highly oligodendrogenic (Kessaris et al., 2006), possibly accounting for the increased oligodendrogenic competence of the dlSVZ. Another possible explanation hinges around the distinct molecular signatures of the dlSVZ and lSVZ. To be more precise, the dlSVZ comprises a mixture of cells that express the TFs Dbx1, Emx1, and Gsh2, whereas lSVZ cells express Gsh2 and little Nkx2.1 (Young et al., 2007). Both Nkx2.1 and Emx1 expressing progenitors have been described to have robust prenatal and postnatal oligodendrocytic potential, respectively (Kessaris et al., 2006). In addition, the regional/molecular segmentation of SVZ NSCs translates into differential production of distinct OB neuronal subtypes (Kohwi et al., 2007; Merkle et al., 2007; Ventura and Goldman, 2007; Young et al., 2007). One can see correlates of this phenomenon potentially applying to gliogenesis in light of recent discoveries about the regional restriction of astrocytogenesis in the spinal cord and forebrain (Tsai et al., 2012). Finally, I contend that cells in the dlSVZ are farther from the ventricular lumen than those in the lSVZ. As a result, the dlSVZ might enjoy different availability of patterning morphogens such as BMP Shh, Wnts, and FGFs, which may translate into morphogenetic gradients similar to those observed during development. In summary, the differences between the fate choices of dlSVZ and lSVZ descendants may be explained by differences in embryonic origin, molecular signature, and/or environmental factors.

5.3.4 Upregulation of Gal-3 was accompanied by increased striatal astrocytic fate and maturity at the expense of oligodendrogenesis

In this chapter, I showed the important finding that Gal-3 played a central role in the postnatal striatal gliogenic scene. Firstly, I demonstrated that Gal-3 overexpression increased striatal gliogenesis 17 DPE. On first analysis, compared to control, upregulation of Gal-3 did not change the proportion of labelled striatal cells at P9, but it did increase that proportion in the striatum by 1.7 fold (30.8% of labelled cells) at P19, without altering the number of labelled cells in the plSVZ. These findings indicate that Gal-3 overexpression increased striatal gliogenesis from the plSVZ, probably in the period between P9 and P19. Secondly, I showed that fewer striatal cells expressed Olig2 and scarcer cells were negative for GFAP and S100β after Gal-3 OE, marking a reduction in the oligodendrocytic fate by almost two thirds. Conversely, more cells expressed GFAP and/or S100β, indicating an increase in the astrocytic fate. Thus, Gal-3 gain-of-function favoured the astrocytic over oligodendrocytic fate during striatal gliogenesis from the plSVZ. Thirdly, fewer striatal glia overexpressing Gal-3 expressed Vimentin, a marker of immature astrocytes (Pixley and Devellis, 1984), and more cells expressed S100β and GFAP, which mark mature astrocytes (Eliasson et al., 1999; Wang and Bordey, 2008). Thus, Gal-3 overexpression increased astrocytic maturity in the striatum. These findings are reminiscent of that found by Bonaguidi et al. The authors showed that ectopic upregulation of BMP4 increased astrocytogenesis in the hippocampus. Also, it induced astrocytic maturity by reducing Vimentin and increasing GFAP expression (Bonaguidi et al., 2005). Altogether, these data revealed novel functions for Gal-3 in promoting striatal gliogenesis from the plSVZ, favouring the astrocytic fate choice over oligodendrogenesis, and increasing astrocytic maturity.

How did these glial cells end up in the striatum and how did Gal-3 increase gliogenesis in the striatum? One possibility is that Gal-3 may have increased the proportion of plSVZ RGCs that transformed into parenchymal astrocytes. This is unlikely to be the only explanation despite having recorded transforming RGCs in both controls and Gal-3 OE. Had that been the only explanation, fewer labelled NSCs would retain radial morphology in the lSVZ after Gal-3 OE at P19. The correlate of increased RGC transformation would be a reduction in NSC activity in the plSVZ at P19. In contrast, I showed that Gal-3 PE did not change the proportion of labelled cells with radial morphology or the activity of NSCs 17 DPE. Another possible explanation for the accumulation of striatal glial cells posits that the plSVZ increased its supply of GRPs to the striatum. This can be achieved by increased GRPs proliferation, enhanced migration of these cells into the striatum, or augmented survival of striatal glia. I will attempt to tackle these possibilities below.

Firstly, I found that proliferation of plSVZ cells both at P9 and P19 was unchanged by Gal-3 upregulation. Also, proliferation of labelled cells in the striatum was minimal at both time points. Therefore, it is unlikely that Gal-3 OE increased striatal gliogenesis by augmenting the proliferative potential of lSVZ-derived GRPs, at least at P9 and P19. However, I cannot exclude the possibility that labelled cells in the lSVZ or striatum increased their proliferation between P9 and P19. This seems plausible because there was no difference between controls and Gal-3 OE in the proportion of labelled striatal cells at P9; however, the difference was apparent at P19. Also some of the labelled striatal glia occurred in clusters, indicative of local propagation as

previously described for cortical glia (Brazel et al., 2003b; Luskin et al., 1993; Voigt, 1989). Furthermore, Cate et al. showed that BMP-induced differentiating astrocytes can proliferate in vitro (Cate et al., 2010) One can speculate that the GRPs present at the medial edge of the striatum at P9 migrated deeper into the striatum, where they underwent more rounds of cell division in the Gal-3 OE, and then they differentiated at P19, when they dampened their proliferative potential. With data lacking for the period between P9 and P19, a more detailed study into the temporal dynamics of striatal gliogenesis after Gal-3 OE is required to address this possibility.

Secondly, Gal-3 upregulation may have enhanced the migration of the striatal precursors from the lSVZ. Given that exogenous Gal-3 promoted migration of neuroblasts from postnatal RMS explants (Comte et al., 2011), it is possible that Gal-3 may increase migration of glial precursors as well. Additional experiments are required to confirm this conjecture.

Finally, Gal-3 might have enhanced the survival of the striatal GRPs. I found a cell non-autonomous effect for acute Gal-3 upregulation on increasing survival of plSVZ cells, however, this effect was lost at P9 and P19. It is still a feasible possibility that Gal-3 OE may have increased survival in the striatum, however, very few activated caspase-3+ labelled cells in the striatum were detected, which did not permit a statistical comparison. In summary, Gal-3 overexpression increased postnatal striatal gliogenesis from the lSVZ possibly through affecting proliferation, migration, survival of glial progenitors, or a combination of the aforementioned processes.

The profile of striatal glia originating from the plSVZ was different after Gal-3 gain-of-function. I showed that fewer labelled cells in the striatum were

Olig2+ or GFAP-S100β- after Gal-3 overexpression, highlighting a reduction in the oligodendrocytic fate. Concomitantly, more cells expressed GFAP, S100β, or both in Gal-3 OE, underscoring an increase in astrocytic fate. These data indicate that Gal-3 upregulation induced a shift from oligodendrocytic to astrocytic fate in striatal glia generated in the plSVZ. This fate shift is interesting to consider in light of previous reports indicating Gal-3 loss reduced oligodendrocytic fate in vitro, altered oligodendrocyte differentiation, and impeded proper myelination (Pasquini et al., 2011). It is possible that Gal-3 exerts a level-dependent influence on the fate adopted by differentiating progenitors; such that baseline levels are required for oligodendrocytic fate and differentiation, but higher protein levels cause a shift towards the astrocytic fate. However, the authors of the previous paper did not replicate their findings in vivo; thus, prudence is required in interpreting these results bearing in mind that Gal-3 overexpression suppressed the oligodendrocytic fate in vivo. Intriguingly, fewer striatal astrocytes in Gal-3 OE expressed the immature astrocytic marker Vimentin, and more expressed the mature astrocytic markers GFAP and S100β, indicating that Gal-3 increased astrocytic maturity. Taken together, Gal-3 assumed a central role in promoting astrocytic fate and maturity while suppressing the oligodendrocytic fate from the plSVZ.

Remarkably, 80% and 90% of newborn striatal glia form the lSVZ expressed GFAP in control and Gal-3 OE, respectively. This is in contrast to approximately 50% of newborn striatal astrocytes from the dlSVZ expressing GFAP (Levison and Goldman, 1993). The authors also reported that almost all astrocytes were positive for S100β, whereas I found that roughly one half

and three quarters of the striatal astrocytes from lSVZ were S100β+ in control and Gal-3 OE, respectively. The abovementioned discrepancies further emphasise the differences between the dlSVZ and lSVZ discussed above, and underscore the emerging concept of astrocyte heterogeneity. Together, these findings highlight the unique molecular signature of plSVZ-derived striatal astrocytes, which was accentuated by Gal-3.

5.3.5 BMP signalling was regulated by Gal-3

BMP signalling has been implicated in fate choice regulation throughout development and postnatal life. During early development, suppression of BMP signalling is required for neural induction, while intermediate levels of signalling instruct the formation of the neural crest, and subsequent adrenergic sympathetic neuronal differentiation. Later on in the embryonic neurogenic period, BMP signalling directs the differentiation of several types of neuronal populations from the spinal cord, midbrain, cerebellum, septum, hippocampus, and neocortex (reviewed in (Hegarty et al., 2013)).

After birth, BMP signalling is poised to fine-tune the neuronogenic and gliogenic processes from the SVZ niche. This is supported by expression of BMP 2, 4 and 7, Noggin, as well as BMPRIa, Ib and II in the pSVZ (Colak et al., 2008; Lim et al., 2000; Mabie et al., 1999; Soderstrom et al., 1996). More specifically, NSCs and TAPs expressed BMP2, BMP4, BMPRIa, and BMPRII, neuroblasts expressed BMPRIb and BMPR II, whereas ependymal cells expressed the BMP antagonist Noggin (Lim et al., 2000). Importantly, BMP signalling has been demonstrated to exert level-dependent functions on NSC differentiation. For instance, loss of Smad4, which is downstream of BMP pathway activation, decreased neurogenesis while increasing the

oligodendrocytic fate (Colak et al., 2008). In contrast, increased BMP signalling levels inhibited neurogenesis (Gajera et al., 2010; Lim et al., 2000), augmented astrocytic fate choice preference over the oligodendrocytic fate, and increased astrocytic differentiation and GFAP expression (Gomes et al., 2003; Gross et al., 1996). In addition, activation of BMP signalling has been shown to reduce SVZ cell proliferation, induce cell cycle exit, and increase survival (Coskun et al., 2001; Lim et al., 2000; Mabie et al., 1999; Mercier and Douet, 2014). Finally, baseline BMP signalling in cultured NSCs and TAPs without BMP supplementation was previously described and attributed to endogenous BMP production by NSC/TAPs (Bonaguidi et al., 2005; Gross et al., 1996). These data suggest that BMP signalling in the SVZ can regulate both proliferation and fate choices in a context-dependant manner.

In this study, I showed that Gal-3 gain-of-function in the plSVZ acutely reduced proliferation, increased striatal astrocytic fate choice at the expense of oligodendrogenesis, and augmented striatal astrocytic maturity and GFAP expression. These findings are reminiscent of the effects of BMP signalling in the pSVZ detailed above. Thus, I hypothesised that Gal-3 may regulate BMP signalling in the plSVZ, and used pSmad1/5/8 as a readout for BMP signalling in vivo (Bonaguidi et al., 2008; Colak et al., 2008). In a nutshell, I found that Gal-3 positively regulated BMP signalling in the plSVZ, and I supported this finding using both in vivo and in vitro data. However, I shall discuss below a few caveats that are worth considering in order to fully appreciate the data.

First, I showed that Gal-3 OE increased pSmad1/5/8 expression in the lSVZ in vivo at P5 (3 DPE), while knockdown of Gal-3 had no effect. On the other hand, the in vitro BRE-luciferase assay showed that Gal-3 upregulation

and downregulation increased and likely decreased baseline BMP signalling, respectively. These data indicated that while Gal-3 overexpression retained its positive effect on BMP signalling in vivo and in vitro, while Gal-3 knockdown likely reduced BMP signalling only in vitro. I contend that the apparent discrepancy between in vivo and in vitro Gal-3 loss-of-function effects on BMP signalling bears two possible explanations. Firstly, one must remember that the in vivo data were collected 3 days post knockdown, while in vitro results were collected 2 days after nucleofection. I posit that the influence Gal-3 has on BMP signalling may be level dependent, and Gal-3 protein levels in labelled cells might be different between 2 and 3 days after knockdown, in vitro and in vivo, respectively. It is possible that by the time the animals were sacrificed, labelled SVZ cells compensated for any change in BMP signalling brought about by Gal-3 knockdown by an unknown mechanism, and this might not have been detected after 2 days in vitro. Secondly, the SVZ niche might contain a factor that compensated for potential reduction in BMP signalling induced by loss of Gal-3 in vivo, while this proposed factor might not be available in vitro. This is particularly important to consider when interpreting the results because the in vitro culture environment is considerably different from SVZ niche. This is exemplified by the in vitro culture lacking ependymal and endothelial cells, a ventricle transporting diffusible signals across the brain-CSF barrier and from the choroid plexus, blood vessels delivering systemic signals, extracellular matrix components, and innervation, all of which are key components of the SVZ niche and can regulate its function (Ihrie and Alvarez-Buylla, 2011). On the other hand, NSCs are maintained in vitro in the presence of EGF and FGF, both of which

potentially modulate BMP signalling (Fuentealba et al., 2007; Martynoga et al., 2013). Dissecting the influence of niche components on BMP signalling in NSCs requires further study and falls out of the scope of this thesis. In summary, differences between in vivo and in vitro data inform the overall interpretation of the data and underscore the importance of the SVZ niche in shaping the response of NSCs to environmental factors.

Second, I showed that Gal-3 upregulation increased pSmad1/5/8 expression in vivo, however, the effect could be demonstrated in vitro only after treating the cultures with BMP4 but not at baseline. This is in contrast to the BRE-Luciferase data that showed a positive effect of Gal-3 on BMP signalling both at baseline and after BMP4 treatment. One way to resolve this apparent conflict lies in appreciating the difference in sensitivity and specificity between western blotting and Luciferase reporter systems. The dual-Luciferase assay system controls for nucleofection efficiency by utilising the CMV-driven Renilla-luciferase co-nucleofected with BRE-Luciferase, allowing for more specific representation of labelled cells. On the other hand, western blotting results are less specific for targeted cells because proteins from both nucleofected and non-nucleofected cells are intermixed when analysed by western blotting. This dilutes proteins from nucleofected cells, especially given that the nucleofection efficiency ranged from 15-25%. In addition, Promega™ technical resources document that the Dual Luciferase system has a sensitivity of ≤ 0.1 femtograms (10^{-16}g), which is at least one order of magnitude more sensitive than the reported sensitivity for enhanced chemi-luminescence detection method used in western blotting, which was in the mid-femtogram range as reported by EMD Millipore™. Thus, BRE-Luciferase

activity can more sensitively and specifically reflect the BMP signalling activity in the labelled cells, whereas pSmad1/5/8 signal intensity measured using western blotting might not detect a potentially diluted effect resulting from mixing of proteins from both labelled and unlabelled cells. Reassuringly, the effect Gal-3 had on BMP signalling became more apparent after treating the cultures with BMP4, as detected by Luciferase activity and pSmad1/5/8 signal intensity in western blotting. Considered together, these findings confirm that Gal-3 upregulation increased BMP signalling.

Third, the Luciferase assay reported increased BMP signalling activity in BMP-treated cultures after Gal-3 knockdown, whereas immunoblotting for pSmad1/5/8 showed no change from control levels. These data are puzzling when compared to the response of untreated cultures after Gal-3 knockdown, which demonstrated a strong trend for reduced BMP signalling activity in both pSmad1/5/8 signal intensity and BRE-luciferase activity. The most apparent factor that might have confounded these results is that Gal-3 levels were increased by BMP treatment, in both controls and Gal-3 knockdown cultures. Thus, it is difficult to interpret the effects of BMP4 treatment on the BMP signalling in Gal-3 knockdown cultures when the knockdown effect was overturned by BMP4 treatment itself. Alternatively, it is possible that BMP signalling was increased after BMP treatment in Gal-3 knockdown cultures due to interactions with other signalling pathways. Since I previously showed that Gal-3 knockdown increased Wnt signalling activity in vivo and in vitro, I posit that this effect might influence BMP signalling. Fuentealba et al. demonstrated that activation of Wnt/β-catenin pathway increased the duration of BMP signalling in vitro (Fuentealba et al., 2007). Conceivably, the increase

in Wnt/β-catenin signalling induced by Gal-3 knockdown might have prolonged BMP signalling as reflected in the luciferase results, but the effect may have been diluted in the western blotting data. However, increasing Wnt/β-catenin signalling in vitro by LiCl treatment failed to increase BMP signalling. Thus, an alternative explanation may be more valid. Given that Gal-3 levels after knockdown were rescued by BMP4 treatment in vitro, perhaps other methods of blocking Gal-3 function can be employed to address this question. For instance, small molecule inhibitors have been employed to block Gal-3 function in cancer cell lines (Lin et al., 2009); using such a method can counteract the increase in Gal-3 levels induced by BMP treatment. In summary, these data encourage further experimentation to resolve the apparent incongruity manifested in evaluating the effect of Gal-3 knockdown on BMP signalling activity between BMP-treated and untreated NSC cultures.

Finally, I investigated the potential interaction between BMP and Wnt signalling in NSCs cultured from the plSVZ, to specifically determine if Gal-3's effects on BMP signalling were connected to its influence on the Wnt/β-catenin pathway. As previously mentioned, BMP and Wnt pathways interact in a context dependant manner. I attempted to increase Wnt signalling using the commonly GSK3β inhibitor; LiCl at a 5mM concentration, which has been shown to induce a proliferative effect in cultured hippocampal cells (Kim et al., 2004; Wexler et al., 2008). The results did not show significant interactions between the two pathways. It is possible that a higher concentration of LiCl is required to induce a response reflected in BMP signalling. In addition, I did not validate that LiCl increased Wnt signalling at that concentration and time in

vitro. In spite of the previous discourse, the data indicates that potential activation of Wnt signalling by 5mM LiCl failed to alter BMP signalling, regardless of Gal-3 expression status. Further investigation is required to evaluate the interaction between Wnt and BMP signalling pathways before meaningful conclusions can be drawn, perhaps trying different LiCl concentrations and Wnt agonists may address this point.

5.4 Conclusion

The first three weeks of postnatal life witness gradual transition of the postnatal SVZ into adult status, a process accompanied by dramatic changes in structure and output of this stem cell niche. During this period, robust neuronogenesis contributes to the majority of the olfactory interneurons. Moreover, gliogenesis reaches its peak providing oligodendroglia and astrocytes to surrounding grey and white matters. In this chapter, I described the temporal dynamics of striatal gliogenesis from the lSVZ, a region often forgotten in the gliogenesis literature. I showed that this region is more astrogliogenic than oligodendrogenic postnatally. I also revealed novel functions for Gal-3 in promoting the astrocytic identity and maturation over oligodendrogenesis from the lSVZ, without altering neuronogenesis. Finally, I showed that Gal-3 positively regulated BMP signalling in the postnatal lSVZ, providing a potential mechanism to account for Gal-3's gliogenic functions.

Chapter 6

General Discussion

6.1 Galectin-3 regulates postnatal lSVZ lineage progression: Towards a molecular model *212*

6.2 Limitations *223*

6.3 Future directions *227*

6 General Discussion

This thesis aimed to interrogate the molecular regulation of plSVZ lineage progression by Gal-3. In tackling this overarching question, I discovered novel functions for Gal-3 in regulating pSVZ lineage progression. In chapter 3, I showed that Wnt/β-catenin signalling was downregulated with lineage progression, as was the case with Gal-3 expression. I then demonstrated that Gal-3 was complexed with β-catenin in NSCs and TAPs, and it negatively regulated Wnt signalling. That was accompanied with an acute reduction in the proliferative growth fraction in the plSVZ. In chapter 4, I followed the long-term effects of chronic Gal-3 overexpression on lineage progression in the plSVZ. This led me to discover that the effects of Gal-3 on proliferation were no longer seen after persistent upregulation of Gal-3. Population dynamics in the lSVZ niche were not influenced by prolonged Gal-3 overexpression, such that NSC activation and neurogenesis were unimpeded. In chapter 5, I showed that Gal-3 gain-of-function increased striatal gliogenesis. More specifically, it induced a fate shift from oligodendrocytic to astrocytic fate choices and increased striatal astrocytic maturation. Moreover, I discovered that the plSVZ was more astrogliogenic than oligodendrogenic, and lSVZ-derived astrocytes had a distinctive glial marker expression profile. Finally, I showed that Gal-3 positively regulated BMP signalling in the lSVZ that. These molecular and cellular responses to Gal-3 upregulation are summarised in Figure 6.1. The potential involvement of Wnt/β-catenin and BMP signalling in mediating Gal-3's cellular responses provided additional insights into neurogenesis in the plSVZ niche and suggests that this protein can simultaneously regulate and therefore contribute to the coordination of two

key signalling pathways. In the next section, I will attempt to link the aforementioned findings, and propose a model to explain Gal-3's molecular and cellular effects in the plSVZ.

6.1 Galectin-3 regulates postnatal lSVZ lineage progression: Towards a molecular model

The phenotype observed after Gal-3 overexpression in the plSVZ was twofold. First were the molecular events manifested themselves in the negative and positive regulation of Wnt/β-catenin and BMP signalling pathways, respectively. Second were the temporally separated cellular events: an early reduction in the proliferative growth fraction and a delayed increase in striatal astrogliogenesis at the expense of oligodendrogenesis.

The molecular and cellular events might have been mechanistically, spatially, and/or temporally segregated, i.e. the mechanism through which Gal-3 reduced proliferation could be distinct from that responsible for astrogliogenesis. Moreover, Gal-3 may have reduced proliferation in a subset of cells, and caused a fate shift in another spatially separate subset. Another possibility is that the effects of Gal-3 may be temporally regulated, such that acute upregulation caused reduced proliferation, and chronic overexpression induced the observed fate shift. In contrast, the described molecular events following Gal-3 overexpression might not be related at all to the observed cellular responses, i.e. Gal-3 might have mediated its proliferative and gliogenic influences independently of Wnt/β-catenin and BMP signalling, possibly through different molecular pathways. In the following sections, I will explore these possibilities en route to formulating an inclusive model that accounts for the effects of Gal-3 on both the molecular and cellular levels.

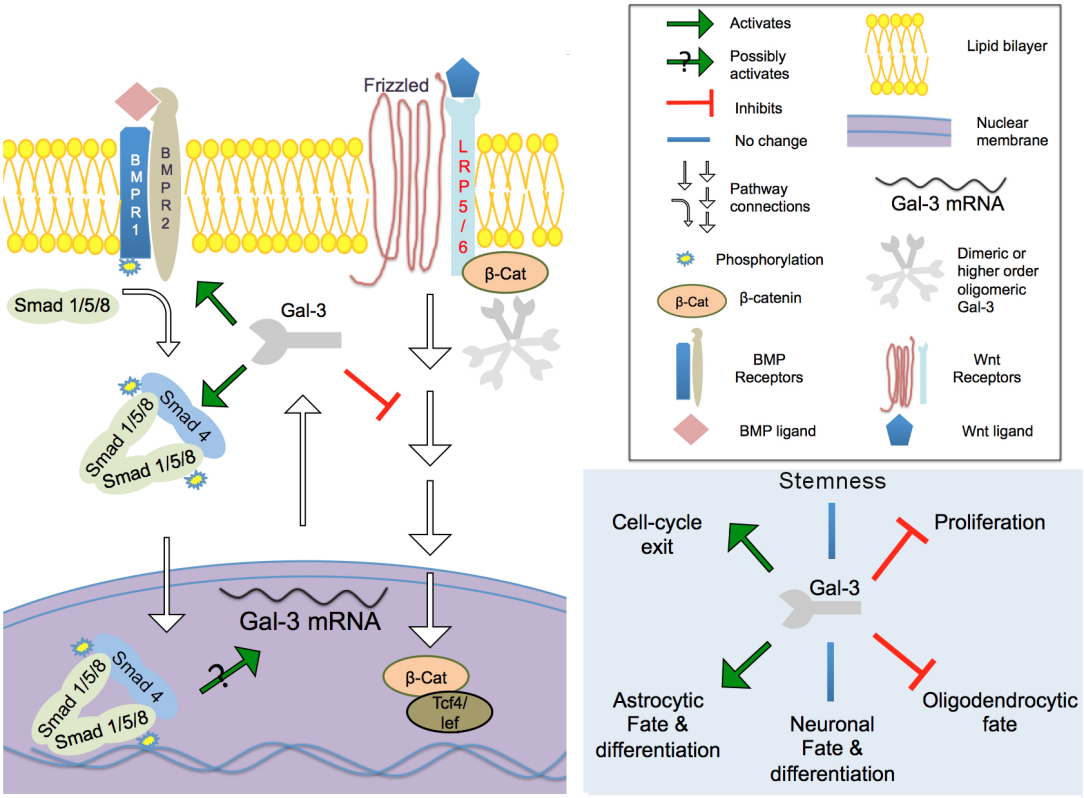


Figure 6.1 Summary of Gal-3's role in regulating plSVZ neurogenesis.

Galectin-3 (Gal-3) is central to both Wnt/β-catenin and BMP signalling pathways; inhibiting the former, and inducing the latter. BMP ligand binding to BMP receptors (BMPR1 and 2) causes phosphorylation of BMPR1, recruitment and subsequent phosphorylation of R-Smad 1,5 or 8, binding to Co-Smad4, transport to nucleus, and finally, transcription. Gal-3 induces BMP signalling either at the level of the receptor or intracellular signalling machinery culminating in phosphorylation of R-Smads. BMP signalling increases Gal-3 protein levels, possibly at the mRNA level. Concurrently, Gal-3 binds to β-catenin and attenuates its signalling through the Tcf/lef transcriptional pathway. This translates into reduced proliferation and increased cell cycle exit. Moreover, increased striatal astrocytic fate choice and differentiation is observed in the striatum, with concurrent reduction of striatal oligodendrogenesis. However, olfactory bulb neuronogenesis and differentiation is not affected. Decreased Wnt/β-catenin signalling and increased BMP signalling may possibly bring about this phenotype.

6.1.1 The link between the molecular and cellular effects of Gal-3 upregulation

This thesis suggests, although it cannot causally prove, that the molecular and cellular events induced by Gal-3 were related. Section 6.2 aims to explain why causality cannot be supported. An alternative viewpoint assumes that the cellular responses after Gal-3 overexpression were not related to the molecular responses Gal-3 induced. A brief recount of the processes regulated by Wnt/β-catenin and BMP signalling pathways will show that this viewpoint is unlikely. Firstly, Wnt/β-catenin signalling was shown to regulate SVZ cell proliferation (Wisniewska, 2013), promote oligodendrocytic fate choice (Azim et al., 2014a; Azim et al., 2014b), control the embryonic switch from neuronogenesis to astrocytogenesis (Draganova et al., 2015), and reduce differentiation of adult as well as postnatal SVZ-derived NSCs into GFAP+ astrocytes in vitro (Yu et al., 2006). Together, these examples demonstrate that Wnt/β-catenin signalling, which itself was regulated by Gal-3, controls processes similar to those described in this thesis to be modulated by Gal-3 in the plSVZ. Secondly, BMP signalling has well-established roles in decreasing proliferation and suppressing oligodendrogenesis, while increasing astrocytogenesis and astrocyte maturity (Coskun and Luskin, 2002; Gomes et al., 2003; Gross et al., 1996; Mehler et al., 2000). Furthermore, upregulation of BMP signalling by overexpression of BMPRIa did not alter SVZ neurogenesis (Coskun et al., 2001). These functions mediated by BMP signalling are reminiscent of the effects of Gal-3 overexpression in the plSVZ. Therefore, I propose that Gal-3 overexpression, by virtue of reducing Wnt/β-catenin activity and/or increasing BMP signalling,

brought about the early cell cycle exit and the delayed oligodendrocytic to astrocytic fate shift.

As well as Wnt/β-catenin and BMP signalling, other pathways like LIF, CNTF, and Notch may have also contributed to mediating the cellular effects of Gal-3 gain-of-function. This is likely possible because Gal-3 overexpression did not alter NSC activation, neurogenic potential, neurosphere forming capacity, or self-renewal in vitro. Considering the recent evidence showing Gal-3 binding to Notch1 in human fetal osteoblast cells (Nakajima et al., 2014), it is conceivable that NSC function after Gal-3 OE was maintained through a pathway other than Wnt/β-catenin or BMP, possibly Notch. On the other hand, both BMP signalling activation and Wnt/β-catenin signalling suppression reduce NSC function, which manifests as reduced neurogenesis in vivo and self-renewal in vitro (Bonaguidi et al., 2005; Faigle and Song, 2013; Lim et al., 2000; Piccin and Morshead, 2011). Therefore, this thesis supports a model whereby Gal-3 overexpression brought about the previously described cellular events by virtue of, but perhaps not fully through, its regulatory actions on Wnt/β-catenin and BMP signalling pathways in the plSVZ.

Of note, the mechanism through which Gal-3 regulated Wnt/β-catenin and BMP signalling is still unknown. It is possible that Gal-3 indirectly inhibited Wnt/β-catenin signalling through regulating other pathways like JAK-STAT or BMP. I showed that Gal-3 was complexed with β-catenin in the membrane-enriched SVZ protein fraction, and that Gal-3 was bound to both active and inactive p-β-catenin forms, which indicates that Gal-3 binding to β-catenin was not activation state-specific. Therefore, this thesis contends that Gal-3 might

sequester β-catenin in the membrane compartment, physically preventing its nuclear translocation thereby inhibiting Wnt/β-catenin signalling. Still, additional studies are required to test this hypothesis. How Gal-3 enhanced BMP signalling is also unknown. The data presented in this thesis suggests that Gal-3 increased the phosphorylation of Smads 1, 5, and 8, as opposed to increasing their protein levels. In addition, preliminary data did not reveal changes in the levels of BMPRIa or BMPRII after Gal-3 overexpression (Data not shown). Together, these data support that Gal-3 may mediate its actions upstream of Smad1/5/8 phosphorylation, by either potentiating signalling through the receptors, enhancing Smad phosphorylation by BMPRI, or stabilising pSmad1/5/8 by delaying dephosphorylation. Again, further experiments are required to elucidate this regulatory relationship.

6.1.2 A potential Gal-3-responsive subpopulation in the plSVZ

Cells in the plSVZ may be homogeneous or heterogeneous with respect to Gal-3 responsiveness. I posit that the former possibility is unlikely due to the following reasons. Firstly, I showed that Gal-3 was expressed in a subset, but not all, of NSCs and TAPs. Secondly, when Gal-3 was overexpressed, Wnt/β-catenin signalling was lost in approximately 18% of the labelled population. Similarly, BMP signalling was increased from 12.2% to 27.3% of the labelled populations. These data indicate that not all cells responded to Gal-3 overexpression by reducing or increasing Wnt/β-catenin or BMP signalling, respectively. Thirdly, the ability of BrdU labelled lSVZ cells 2 DPE to re-enter the cell cycle was not influenced by Gal-3 expression. This indicates that a subpopulation of proliferative cells did not exit the cell cycle after Gal-3 OE,

indicating it was not responsive to Gal-3's anti-proliferative influences. Together these results support a model where plSVZ cells are heterogeneous in their Gal-3 responsiveness.

Gal-3-responsive lSVZ cells may show homogeneity or heterogeneity in terms of displaying early and/or delayed cellular responses. In other words, all Gal-3-responsive cells might exit the cell cycle and switch fates afterwards. Conversely, Gal-3-responsive cells might display heterogeneous responses with a cohort of cells exiting the cell cycle, shifting fates, and/or shifting fates as well as exiting the cell cycle. Unfortunately, this thesis cannot definitively address these possibilities. However, given that neuroblasts that overexpressed Gal-3 did not abandon the olfactory neuronal fate, it is more prudent to propose that the cellular responses to Gal-3 overexpression were heterogeneous. Overall, this thesis posits that, first, plSVZ cells are heterogeneous with regards to whether or not they are Gal-3-responsive, and second, plSVZ cells are varied with respect to the nature of their response to Gal-3; with cohorts of cells exiting the cell cycle, switching fates, or both after Gal-3 upregulation.

6.1.3 A possible molecular basis for the temporally diversified plSVZ responses to Gal-3 upregulation

It is possible that early and delayed cellular responses, being temporally separated, might be mediated by independent molecular events. This requires that Gal-3 first induced cell cycle exit, then -through a different mechanism and at a later point in time- promoted the observed fate shift. However, this explanation is less parsimonious than the model proposed below, which argues that both early and delayed cellular events were mediated, at least

partially, by Gal-3's early actions on Wnt/β-catenin and BMP pathways. This is supported by the fact that only brief exposures to BMP agonists are sufficient to induce early cell cycle exit, and late suppression of oligodendrocytic as well as increased astrocytic fate and maturation (Bonaguidi et al., 2005; Gross et al., 1996; Mabie et al., 1997; Mehler et al., 2000).

Alternatively, Gal-3 may have instilled a sustained molecular change that in early stages reduced proliferation, and in later stages induced a fate shift. Whether Gal-3 persistently altered Wnt/β-catenin and BMP signalling in vivo was not determined. However, I showed that Gal-3's effect on Wnt/β-catenin was transient in vitro, and because in vitro findings were in line with in vivo data, it is possible that Gal-3's influenced Wnt/β-catenin signalling transiently in vivo. It is also possible that Gal-3 may have chronically upregulated BMP signalling such that it induced late astrogliogenesis, and may have contributed to the early reduction in proliferation, possibly in conjunction with Wnt/β-catenin signalling. However, further experiments are required to determine whether Wnt/β-catenin and BMP signalling were chronically influenced in vivo. In summary, while this thesis cannot rule out that persistent Wnt/β-catenin and BMP signalling in vivo possibly mediating early and delayed cellular responses separately, It does support a model in which Gal-3 upregulation promoted anti-proliferative and astrogliogenic effects in the plSVZ by regulating Wnt/β-catenin and BMP signalling early on after overexpression.

6.1.4 A molecular model to explain Gal-3's cellular effects on the plSVZ

Considering the previous discussion, the model proposed by this thesis argues that plSVZ is heterogeneous in its Gal-3 responsiveness and only a specific Gal-3-responsive subpopulation in the plSVZ reacted to Gal-3 upregulation; displaying varied responses in different cells. On the molecular level, this thesis posits that Gal-3 mediated anti-proliferative and astrogliogenic effects in the plSVZ early on after upregulation, at least partially through downregulation and upregulation of Wnt/β-catenin and BMP signalling, respectively. From these premises two possible scenarios arise (summarised in Figure 6.2).

Firstly, long-term Gal-3 upregulation in the plSVZ might not have been compensated for. In this scenario, the potential Gal-3-responsive subpopulation in the plSVZ reacted to Gal-3 overexpression by exiting the cell cycle, switching to an astrocytic fate, or both; but was depleted afterwards. Other Gal-3-unresponsive lSVZ cells may have compensated for the potentially reduced neurogenic output after the depletion of the Gal-3-responsive subpopulation. Secondly, the alternative scenario contends that the effects of Gal-3 overexpression may have been compensated for by a factor that negated Gal-3's influence on both NSCs and their progeny. In that case, a fraction of the acutely Gal-3-responsive subpopulation exited the cell cycle, switched to an astrocytic fate, or both; however, contrary to the first scenario, that subpopulation was not depleted. Instead, they may have compensated for Gal-3 overexpression and behaved like the remainder of the lSVZ afterwards.

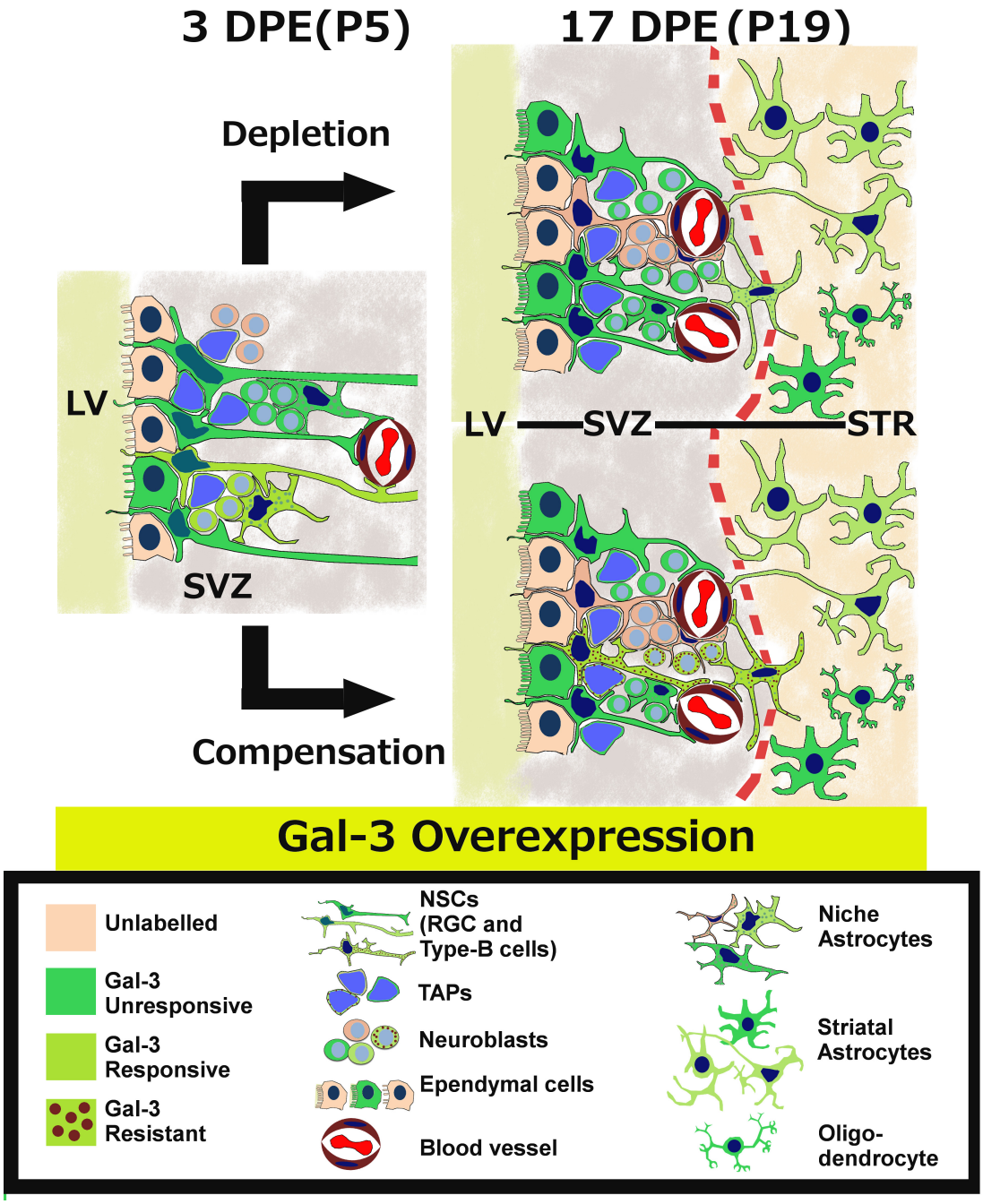


Figure 6.2 A model to explain Gal-3's effects on the plSVZ

A cartoon depiction of the model proposed in this thesis. In the postnatal lateral SVZ, a Galectin-3 (Gal-3) responsive subpopulation exists, and reacts to Gal-3 overexpression by exiting the cell cycle, shifting from oligodendrocytic to astrocytic fates, or both. This Gal-3-responsive subpopulation might be either depleted after chronic Gal-3 overexpression, and Gal-3 unresponsive cells might compensate for that loss; or the subpopulation loses its Gal-3 responsiveness and becomes Gal-3-resistant, possibly through upregulation of a Gal-3 antagonist or a heritable epigenetic modification that counteracts Gal-3's anti-proliferative effects. LV: Lateral ventricle, STR: striatum, NSC: neural stem cell, RGC: radial glial cell, TAP: transient amplifying progenitor.

The nature of this potential compensation is elusive; long-term Gal-3 upregulation perhaps stimulated the secretion of an unknown Gal-3 antagonist. Instead, Gal-3 upregulation may have brought about a heritable epigenetic modification that negated its actions. For example, the levels or activity of kinases that regulate Gal-3's activity, like CKI or GSK3β, might have been modified to reduce Gal-3 phosphorylation, hence its affinity to target glycoproteins. Instead, the levels or activity of glycosylating enzymes, which modify Gal-3 target glycoproteins to allow them to bind Gal-3, may have been reduced, thereby reducing the binding of Gal-3 to its targets. Importantly, this thesis cannot determine which of these proposed scenarios is more likely and additional data is required to answer these questions.

The obvious question that stems from this model is: what is the nature of the Gal-3-responsive subpopulation? In other words, at which stage in the lineage did Gal-3 induce its anti-proliferative and astrogliogenic effects? Unfortunately, I am unable to answer this question decisively before additional data is collected. Co-labelling studies for SVZ lineage markers and Ki67 or p27/Kip1 might shed light on the identity of the cells that exited the cell cycle. Examining the proliferative response of FACS-sorted NSCs, TAPs, and neuroblasts will also be beneficial. Alternatively, live imaging of NSCs nucleofected or transduced with Gal-3 overexpression constructs can reveal whether NSCs, TAPs, or neuroblasts exited the cell cycle. However, I speculate that neuroblasts were unlikely to have been the cells that gave rise to striatal astrocytes. In support of this, Colak et al. showed that neuroblasts were not active in BMP signalling (Colak et al., 2008), and Coskun et al. reported that BMPRIa-overexpressing neuroblasts, which exhibited

heightened BMP signalling, did not alter their fate compared to neuroblasts that expressed dominant negative BMPRIa (Coskun and Luskin, 2002). Importantly, p27/Kip1 was shown to regulate TAPs proliferation and numbers in the SVZ (Cheffer et al., 2013; Doetsch et al., 2002b; Qiu et al., 2009). In addition, loss of Smad4 resulted in a fate shift at the level of Dlx+ TAPs and reduced neurogenic potential at the level of NSCs. The authors also demonstrated that BMP signalling directs fate choices at the level of NSC/TAPs (Colak et al., 2008). Hence, this thesis posits that Gal-3 gain-of-function may have specifically acted on a subset of NSCs and TAPs to cause cell cycle exit and a shift from oligodendrocytic to astrocytic fates.

Finally, one of the most interesting findings this thesis described was the fact that Gal-3 levels were increased after BMP4 treatment. This suggests that BMP signalling and Gal-3 might be involved in a positive feedback loop. Additional experiments are required to further validate this finding. Intriguingly, Gal-3 has been described to participate in a positive feedback loop to sustain the alternative macrophage activation (M2 phenotype associated with chronic and fibrotic stages of inflammation) (Henderson and Sethi, 2009). The authors described a model wherein Gal-3 was induced after IL-4/IL-13 activation of IL-4Rα (IL-4 and IL-13 common receptor). This increased CD98 and Integrin mediated signalling culminating in PI3K and pAkt activation, eventually perpetuating alternative macrophage activation and Gal-3 expression. Here, I showed that Gal-3 was upregulated at the protein level, which could be secondary to enhanced transcription of Gal-3 mRNA or increased stability of the mRNA or protein. Interestingly, we found a Smad1 binding site in the LGALS3 promoter, suggesting a possible regulation at the level of

transcription. In light of this, experiments are underway to further examine this exciting finding.

6.2 Limitations

Despite my best efforts to address my research questions, I recognise the limitations discussed below that could be addressed to provide a more complete outlook of the molecular regulation of Gal-3 in lineage progression of the plSVZ. I will now aim to explore these limitations and propose plans to guide addressing them in future studies.

Firstly, the effects of Gal-3 loss-of-function on lineage progression have not been fully addressed in this study. Despite characterising the acute effects of Gal-3 loss on Wnt/β-catenin and BMP signalling, long-term effects on the plSVZ population dynamics, neuronogenesis, and gliogenesis have not been determined. It is possible that Gal-3 loss-of-function may alter oligodendrocytic fate choice and differentiation. In support of that, Pasquini et al. showed that in vitro Gal-3 knockout neurospheres were less able to give rise to oligodendrocytes upon differentiation, and Gal-3 loss hampered oligodendrocytic myelination functions in vivo (Pasquini et al., 2011). However, the authors did not verify these fate-choice findings in vivo. Therefore, investigation of plSVZ lineage progression after Gal-3 loss may potentially reveal additional functions for Gal-3 in regulating oligodendrocytic fate and differentiation. Currently, experiments aiming to investigate the effects of acute Gal-3 loss in the stem/progenitor population of conditional Gal-3 knockout mice are underway. In fact, I have already begun to address the roles of Gal-3 loss-of-function in the plSVZ using in vivo electroporation of

Cre recombinase into Gal-3$^{fl/fl}$ mice, but this data is still preliminary. Thus, additional work will verify whether Gal-3 loss affects oligodendrocytic fate and differentiation, or gliogenesis in vivo. In summary, this study was short of addressing the affects of Gal-3 loss on plSVZ lineage progression, and additional studies will reveal whether acute Gal-3 loss alters oligodendrocytic fate and differentiation.

Secondly, this thesis mainly dealt with the cell-autonomous effects of Gal-3 gain-of-function; however, I cannot rule out that, at least partially, some of the effects were mediated through a cell non-autonomous mode of action. This is because several lines of evidence indicate that Gal-3 is secreted despite lacking an endoplasmic reticulum targeting sequence, possibly via a non-classical mechanism (Dumic et al., 2006; Hughes, 1999). We discovered that Gal-3 was present in exosomes isolated from NSC-conditioned media (O'Neill, E and Szele, F, unpublished). This is consistent with a previous report in which Gal-3 was detected in dendritic cell derived exosomes (Thery et al., 2001). Thus, Gal-3 could have cell non-autonomously influenced lSVZ labelled and/or unlabelled SVZ cells. Furthermore, because SVZ NSCs have access to the LVs (Mirzadeh et al., 2008), secreted Gal-3 may have diffused throughout the neuraxis; possibly altering the behaviour of distant cells. In support of cell non-autonomous effects of Gal-3, I showed that its upregulation reduced cell death in a cell non-autonomous manner 3 DPE. In contrast, total proliferation in unlabelled cells in the plSVZ, as determined by Ki67 and 2-hour EdU administration, was not affected by Gal-3 overexpression 7 DPE. Given that proliferation in labelled cells was not altered in Gal-3 OE at that point, one cannot rule out cell non-autonomous

effects on proliferation. Perhaps verifying the effects on proliferation in unlabelled cells 3 DPE when Gal-3 reduced the proliferative growth fraction would be more suitable. Therefore, this study was not suited to fully address cell non-autonomous effects of Gal-3.

Related to this point; this study cannot determine whether Gal-3 mediated its effects from the intracellular or extracellular compartment. My main purpose in investigating labelled, but not unlabelled, cells was that the former cells overexpressed Gal-3 intracellularly, and if those cells displayed an altered behaviour, the effects would be likely attributed to intracellular Gal-3, which interacts with intracellular proteins (Liu et al., 2012; Shimura et al., 2004). However, it is possible Gal-3 could have exerted its influences from outside the cell, modulating cellular responses by interacting with membrane proteins like growth factor receptors (Partridge et al., 2004). It is also conceivable that secreted Gal-3 may localise to the extracellular matrix (ECM), binding various ECM proteins and soluble growth factors (Ochieng et al., 2004). Extracellular Gal-3 can exert functions distinct from, and sometimes in contrast to, intracellular function; for instance, extracellular Gal-3 can mediate apoptosis, while intracellular Gal-3 protects against it (Dumic et al., 2006). Similarly, this study cannot determine whether Gal-3's action had been mediated by cleaved or full-length, monomeric or oligomeric Gal-3. I showed that dimeric or higher order oligomeric Gal-3 bound β-catenin in the membrane-enriched protein fraction of the lSVZ. In spite of that, oligomerisation may have occurred after protein isolation, since Gal-3 was shown to form oligomers even in the presence of sodium dodecyl sulfate (SDS) or in non-reducing conditions (Henderson and Sethi, 2009). Perhaps

tagging the Gal-3 protein with a fluorophore may potentially identify its extracellular localisation, but even then teasing out intracellular as opposed to extracellular modes of action would be difficult. This is because the SVZ niche is crowded with cells, and appreciating the extracellular space is difficult. Unfortunately, a method to retain Gal-3 within cells seems elusive given the absence of a classical export signal and alternative secretion through exosomes. Similarly, administration of exogenous Gal-3 may not rule out intracellular modes of actions, since Gal-3 can bind to cell-surface receptors (Markowska et al., 2011; Partridge et al., 2004) and regulate their trafficking (Liu et al., 2012). This means that Gal-3 may be internalised, hence making separating extracellular from intracellular functions more difficult. In summary, this study cannot address whether Gal-3's effects were mediated, at least partially, in a cell non-autonomous fashion. Perhaps using a function-blocking antibody can antagonise extracellular functions of Gal-3, allowing focused study of its intracellular roles. Furthermore, whether monomeric or oligomeric, intracellular or extracellular Gal-3 promoted the observed effects are questions this study cannot address.

An important consideration is that while Gal-3 regulated Wnt/β-catenin and BMP signalling, and at the same time reduced proliferation and increased astrocytic fate choice, causality cannot by supported by this study. In other words, Gal-3 was indeed responsible for the observed phenotypes, however, data is lacking to support that for example, the reduction in Wnt/β-catenin signalling after Gal-3 overexpression caused a reduction in proliferation, or the increased BMP signalling increased astrocytic fate. In order to prove causality, rescue experiments are required. For example, to prove that Gal-3

overexpression reduced proliferation through suppressing Wnt/β-catenin signalling, proliferation must be measured after Gal-3 overexpression and rescue of β-catenin loss-of-function. Additionally, to causally relate astrocytic fate shift to increased BMP signalling, Gal-3 overexpression should be accompanied by inhibition of BMP signalling before astrocytic fate is assessed. In fact, I have already taken steps to investigate the causal relationship between BMP signalling and astrocytic differentiation. To that end, I electroporated Gal-3 overexpression or control plasmids, along with Cre recombinase construct, into the pISVZ of BMPRIa$^{fl/fl}$ conditional knockout mice. However, these results are still preliminary and require further analysis. I also attempted to rescue β-catenin function by electroporating an EF1α-ΔN90-β-catenin, an active form of β-catenin resistant to degradation; however, the construct failed to overexpress β-catenin in vivo. That being said, Gal-3 could reduce proliferation via a Wnt/β-catenin-independent manner, or it may promote astrocytic fate shift independent of BMP signalling, possibly inhibiting or activating other pathways as discussed above. Overall, while this study demonstrated that Gal-3, directly or indirectly, dampened Wnt/β-catenin signalling, increased BMP signalling, reduced proliferation, and increased the astrocytic fate choice, a causal relationship between the molecular events and the respective cellular responses is suggested but is yet to be proven.

6.3 Future directions

Asides from the aforementioned limitations, which can be addressed in future studies, I envisage a number of future paths this project may take in the

future. For example, I showed that Gal-3 increased striatal astrocytic fate choice and differentiation. It remains to be determined whether Gal-3 overexpressing striatal astrocytes can behave like NSCs after injury. This is an important question to address in light of recent findings demonstrating that striatal neurogenesis continues in adulthood in humans (Ernst et al., 2014) and rats (Dayer et al., 2005). The SVZ was suggested to be the origin of the newborn striatal interneurons; however, other origins could not be excluded. A recent report form the same group demonstrated that striatal astrocytes might become neurogenic and give rise to neurons upon Notch inhibition, artificially or in response to stroke (Magnusson et al., 2014). Thus, astrocytes may possibly give rise to neurons in the striatum. Interestingly, Gal-3 has been shown to bind to and promote signalling of Notch1 in human fetal osteoblast cells (Nakajima et al., 2014). Therefore, an additional question to ask next is whether the Gal-3 overexpressing striatal astrocytes retain neurogenic competence in producing neurons after injury. In other words, does Gal-3 promote Notch1 signalling in striatal astrocytes? Also, are these astrocytes less neurogenic after injury, because of their Gal-3 expression? These are exciting questions to tackle, and knowledge of the signalling pathways that Gal-3 regulates can serve to better address these questions.

Another path this project can take involves investigating the role of Gal-3 in postnatal lineage progression of other SVZ regions, especially the dSVZ. This is thought-provoking because, compared to the lSVZ, the dSVZ has higher Wnt/β-catenin signalling activity, and gives rise to a specific progeny of olfactory glutamatergic interneurons as well as callosal oligodendrocytes (Azim et al., 2014a). It is interesting to test whether Gal-3 gain-of-function may

inhibit Wnt/β-catenin signalling in the dSVZ, similar to what it did in the lSVZ. Will Gal-3 also increase BMP signalling after upregulation? Will Gal-3 gain-of-function respecify oligodendrocytic precursors to astrocytic fate? Will the dSVZ retain its neuronogenic and oligodendrogenic potentials after Gal-3 gain-of-function and loss-of-function? These are questions that merit being addressed given the regulatory function Gal-3 has on Wnt/β-catenin signalling.

It is tempting to ask whether, and if so how, Gal-3 regulates Wnt/β-catenin and BMP signalling in Glioblastoma Multiforme (GBM). GBM is the most aggressive primary brain tumour in adults, and is thought to be related to the SVZ, at least with respect to survival (Jafri et al., 2013; Modrek et al., 2014). Notably, several mouse models of GBM involve transforming SVZ NSCs into GBM-like tumours (Modrek et al., 2014). However, the relationship between Gal-3 and GBM is far from defined. For example, Gal-3 levels were shown to significantly correlate with astrocytic tumour grade in one study, but the opposite was shown by another report (Le Mercier et al., 2010). I showed that Gal-3 negatively regulated Wnt/β-catenin signalling in the plSVZ, which is contrasted with the positive regulatory function Gal-3 exerts in various cancers (Song et al., 2014). In what way does Gal-3 regulate Wnt/β-catenin signalling in GBM? Is the negative regulatory relationship between Gal-3 and Wnt/β-catenin signalling detected in the plSVZ preserved in GBM? Or does GBM behave like other tumours with respect to Wnt/β-catenin-Gal-3 interaction? How does BMP signalling relate to Gal-3 expression and Wnt/β-catenin signalling in GBM? In fact, I have started delving into these questions; for example, I found that Gal-3 negatively regulated Wnt/β-catenin signalling

in that LN-18 GBM cell line. Further experiments are required to confirm this relationship in other GBM cell lines as well as in primary cultures of GBM cells derived from GBM patients. Moreover, we already began collecting human brain samples from GBM cases and controls to facilitate investigating the aforementioned questions in human GBM tissue sections. These are questions that have stemmed from this thesis and fortunately I will see them being answered.

A final thought provoking question, given the roles of Gal-3 in mediating fibrotic reactions in the lungs, kidneys, heart, and liver (Henderson and Sethi, 2009), could this pro-fibrotic action be comparable to the gliogenic effects of Gal-3? Is it possible that Gal-3 employs the same molecular machinery to induce fibrosis in the aforementioned organs, and gliogenesis in the brain? Is it possible to inhibit this gliogenic process in contexts where it is considered harmful as in stroke and spinal cord injury? More interestingly, is it possible to inhibit gliogenesis by inhibiting Gal-3? These are exciting questions presented by my thesis, and hopefully, the scientific community will address these in the future.

7 Appendices

7.1 Additional work not included in thesis

7.1.1 C1orf103 project

In the first year of my DPhil, I was in the laboratory of Prof. Lars Fugger in the Weatherall institute for Molecular Medicine (WIMM), where I investigated a novel gene; C1orf103. Single nucleotide polymorphisms in this gene were found to be associated with multiple sclerosis and inflammatory bowel disease. I worked on revealing the sequence of its mRNA variants, which proved challenging. I managed to uncover its 3' sequence; however, its 5' end proved elusive to assess. Before I joined to the Szele laboratory in October 2012, I enriched C1orf103 mRNA and managed to sequence almost the entire gene product.

7.1.2 Investigating the role of Galectin-3 in neurogenesis after stroke in mice

Between October and December 2012, I worked in the Szele laboratory on previous project led by Dr. Chris Young, a previous Szele laboratory DPhil student. I evaluated whether Gal-3 loss influenced angiogenesis in the SVZ, and whether loss of Gal-3 after stroke altered olfactory neurogenesis. My contribution was acknowledged as a shared second author of the resultant publication (Young et al., 2014).

7.1.3 Characterization of nuclear β-catenin Gal-3 knockout mice

During the initial part of my DPhil project in the Szele laboratory, I set out to determine the binding partners of Gal-3 in the SVZ. I showed that Gal-3 was bound to FGFR1, Laminin, and β-catenin, but not Ezh2, EGFR, or NCAM. Binding to PSA-NCAM was not replicated by reverse CoIP, and

may be artifact. I then evaluated whether Gal-3 loss influenced β-catenin subcellular localisation in the aSVZ. To that end, I characterised nuclear β-catenin in GFAP+ and Mash1+ cells across the dorso-ventral and antero-posterior axes of the aSVZ. I found that Gal-3 loss did not influence nuclear lation of β-catenin in GFAP+ or Mash1+ cells. Moreover, qPCR of β-catenin from Gal-3 null SVZ revealed no difference from WT SVZ. Next, I evaluated whether activated β-catenin phosphorylated at residue Ser552 was affected by Gal-3 loss in Mash1+ SVZ cells and came to the same conclusion; that Gal-3 had no influence on phospho-β-catenin expression. Gal-3 knockout animals did not show any alteration in β-catenin or different phospho- β-catenin expression in the SVZ as determined by WB. I then evaluated whether Gal-3 loss in the knockout animals was compensated for by upregulation of other Galectins in the SVZ. I found that Gal-1, 8, and 9 were not increased in Gal-3 nulls.

7.1.4 Evaluating the effects of the cancer-related IDH1 R132H on the brain

I worked with Dr. Chiara Bardella from Prof. Ian Tomlinson's laboratory to evaluate the effects of a knockin IDH R132H mutation on the brain. I provided Dr. Bardella with training in free-floating immunohistochemistry and in vitro NSC culture techniques. I also planned experiments to assess the effect of the mutation on SVZ neurogenesis. Together, we found that knockin mice had increased SVZ proliferation and ectopic migration in the corpus callosum and the striatum. For my contribution, I will be second author on the paper in preparation.

7.2 Appendix: Solutions and recipes

- **Cryoprotectant**
  - 300g Sucrose
  - 300ml Ethylene glycol
  - Up to 1L PB 0.1M

- **Paraformaldehyde (PFA) 4%w/v**
  - 20g Paraformaldehyde
  - Up to 500ml PBS 0.1M
  - Heat to 70C in Chemical fumehood on magnetic stirrer.
  - When clear, adjust pH to 7.4 using 10mM NaOH

- **Phosphate Buffer (PB) 0.1 M**
  - Monobasic solution A (0.2M):
    - 27.8g Sodium phosphate monobasic (NaH_2PO_4)
    - Up to 1L Distilled water
  - Dibasic solution B (0.2M):
    - 28.4g Sodium phosphate dibasic anhydrous (Na_2HPO_4)
    - Up to 1L Distilled water
  - Add 140mls of Solution A to 360mls of Solution B and 500ml of distilled water (final volume 1L)
  - Adjust pH to 7.4

- **Phosphate buffered saline (PBS) 10X (1M)**
  - 80g Sodium chloride (NaCl)
  - 2.0g Potassium choloride (KCl)
  - 2.4g Potassium dihydrogen phosphate (KH_2PO_4)
  - 14.4g Sodium phosphate dibasic anhydrous (Na_2HPO_4)
  - Up to 1L Distilled water
  - Adjust pH to 7.4
  - Use at 1X (0.1M)

- **TAE buffer 50X**
  - Tris-base
  - 242g Tris-Base
  - 57.1ml Glacial acetic acid
  - 100ml EDTA 0.5 M
  - Up to 1L Distilled water
  - Dilute to 1X in Distilled water before use

- **Triton-X lysis buffer:**
  - 150 mM NaCl
  - 1% Triton X-100,
  - 50mM Tris HCl (pH 8.0)

- **TBS 10X 20mM**
  - 88g Sodium chloride (NaCl)
  - 24g Tris-base Distilled
  - Up to 1L distilled water

- Adjust pH to 7.4
- Use at 1X

- **Running buffer 10X**
  - 30.3 g Tris-base (250mM)
  - 144.1g Glycine (1.92M)
  - 10g SDS (1%) – add last
  - Up to 1L Distilled water
  - Use at 1X (can recycle)

- **Transfer buffer 10X**
  - 30.3 g Tris-HCl (250mM)
  - 144.1g Glycine (1.92M)
  - Up to 1L Distilled water
  - For 1X:
    - 100ml of 10X transfer buffer
    - 150ml Methanol
    - 750ml Distilled water
- **Stripping buffer:**
  - 15g Glycine
  - 1g SDS
  - 10 ml Tween20
  - Adjust pH to 2.2
  - Up to 1L with Distilled water.
    - 15 minutes incubation in 15ml stripping buffer/Membrane at room temperature
    - 2X 5-minutes PBS washes
    - 2X 5 minutes TBST
    - Dry membrane or re-block

- **Co-immunoprecipitation elution buffer (SDS gel loading buffer)**:
  - 50mM Tris-HCl (pH 6.8)
  - 50mM DTT
  - 1% SDS
  - 0.005% Bromophenol blue
  - 10% glyercol

- **SDS-PAGE gel:**

  - **Resolving gel (8mls)**

Reagent	Volume (8% gel)	Volume (10% gel)
Distilled water	3.7ml	3.2ml
30% Acrylamide	2.13ml	2.67ml
1.5 M Tris pH 8.8	2ml	2ml
10% SDS	80µl	80µl
10% Ammonium persulfate (APS)	80µl	80µl
Tetramethylethylenediamine (TEMED)	8µl	8µl

- **Stacking gel (5mls)**

6%	
Reagent	Volume
Distilled water	2.6ml
30% Acrylamide	1ml
0.5 M Tris pH 6.8	1.25ml
10% SDS	50µl
10% APS	50µl
TEMED	5µl

7.3 Appendicular figures

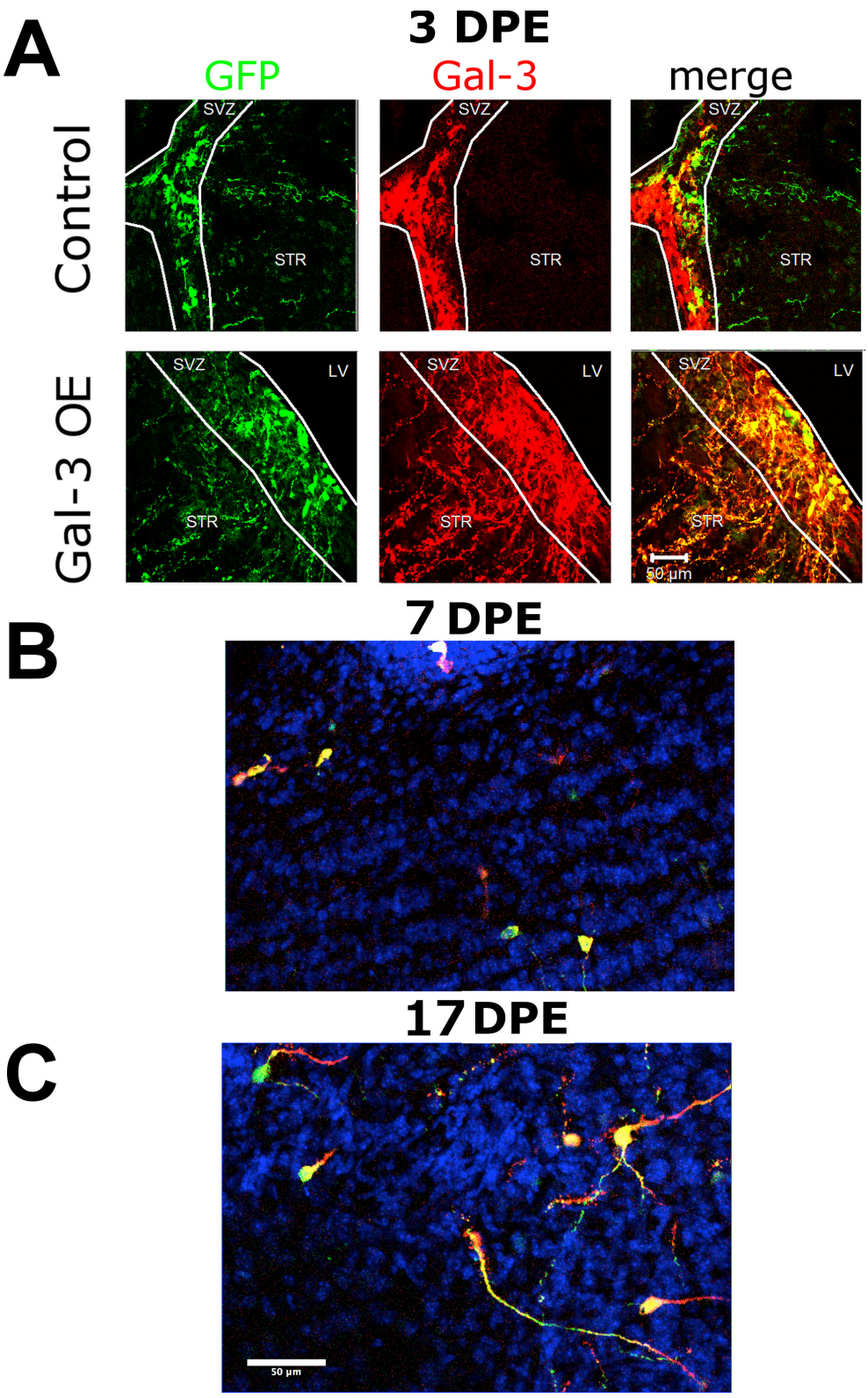


Figure A 1. Gal-3 overexpression constructs in vivo

(**A**) Confocal images showing that pCAG-Gal-3-IRES-GFP overexpressed Gal-3 (red) in GFP+ (green) SVZ cells. (**B-C**) DAPI (blue), Gal-3 (red) remains to be expressed in most GFP+ (green) neuroblasts and neurons 7 and 17 days post electroporation (DPE). Scale Bars: 50µm.

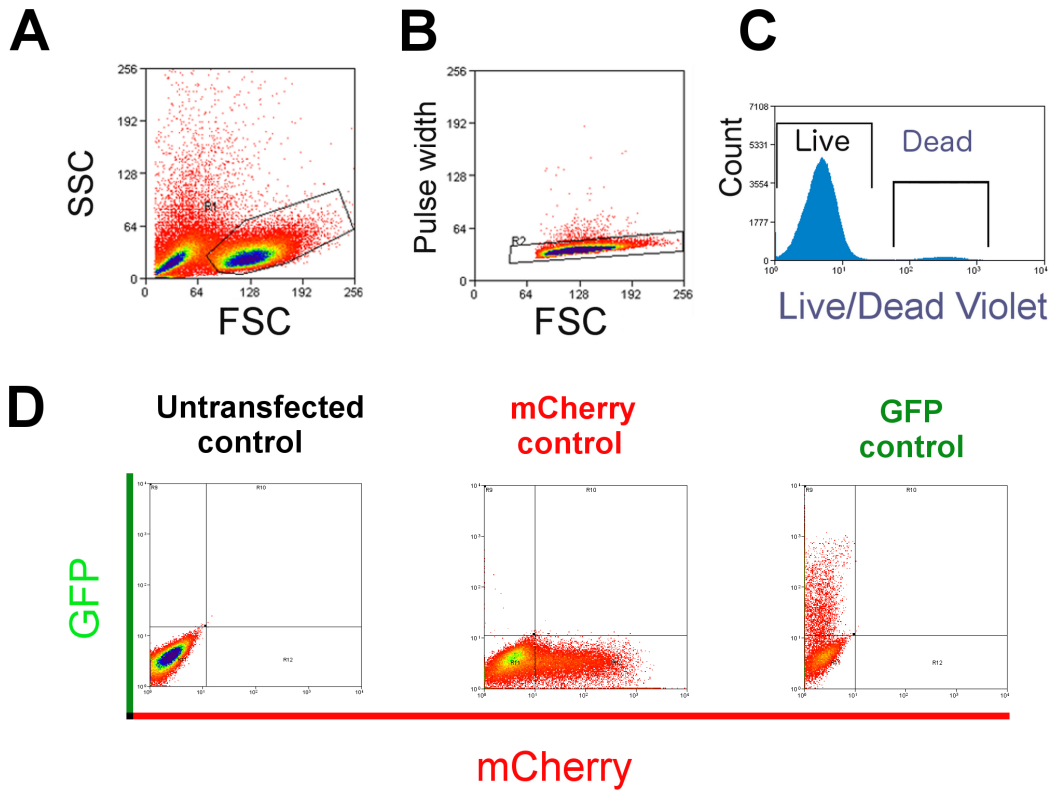


Figure A 2. Flowcytometry control

(A-C) Show Flowcytometry gating procedure. **(A)** Forward scatter (FSC) and side scatter (SSC) were used to gate out cell debris. **(B)** Doublets were gated out using FSC and FSC-Pulse width. **(C)** Live cells were gated on using Violet Live/Dead stain.
(D) Shows Flowcytometry controls. Un-nucleofected, mCherry only, and GFP only controls are shown. Voltages were set to cluster negative cells in the first decade.

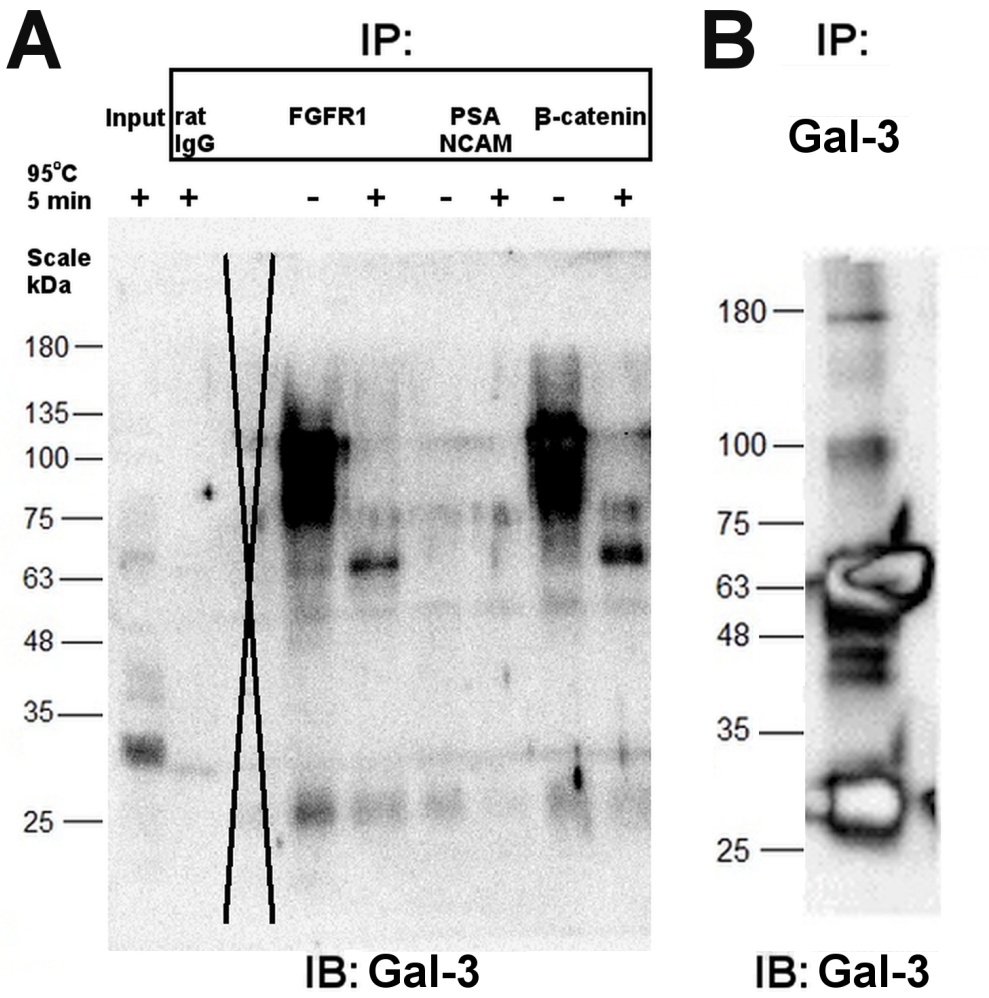


Figure A 3. Reverse co-IP

(**A**) Reverse co-immunoprecipitation (IP) of lSVZ membrane proteins with anti-β-catenin monoclonal antibody, anti-FGFR1, anti-PSA-NCAM, or control rat IgG, and Immunoblotting (IB) for Gal-3. Protein samples were boiled at 95°C dor 5 minutes or not. Note FGR1 and β-catenin bind Gal-3 in oligomeric forms that reduce down to dimeric forms after boiling.
(**B**) Pull down of Gal-3 from SVZ whole tissue lysates with a rat monoclonal antibody was followed by immunoblotting for Gal-3 with a rabbit polyclonal Antibody. The samples were boiled for 5 minutes at 95°C. The molecular weight standard ladder is shown on the left.

7.4 References

Adachi, K., Mirzadeh, Z., Sakaguchi, M., Yamashita, T., Nikolcheva, T., Gotoh, Y., Peltz, G., Gong, L., Kawase, T., Alvarez-Buylla, A.*, et al.* (2007). Beta-catenin signaling promotes proliferation of progenitor cells in the adult mouse subventricular zone. Stem Cells *25*, 2827-2836.

Adi Shruster, T.B.-Z., Eldad Melamed, Daniel Offen (2012). Wnt Signaling Enhances Neurogenesis and Improves Neurological Function after Focal Ischemic Injury. PloS one.

Aguirre, A., Rubio, M.E., and Gallo, V. (2010). Notch and EGFR pathway interaction regulates neural stem cell number and self-renewal. Nature *467*, 323-327.

Akahani, S., Nangia-Makker, P., Inohara, H., Kim, H.R., and Raz, A. (1997). Galectin-3: a novel antiapoptotic molecule with a functional BH1 (NWGR) domain of Bcl-2 family. Cancer research *57*, 5272-5276.

Altman, J. (1969). Autoradiographic and histological studies of postnatal neurogenesis. IV. Cell proliferation and migration in the anterior forebrain, with special reference to persisting neurogenesis in the olfactory bulb. The Journal of comparative neurology *137*, 433-457.

Alvarez-Buylla, A., and Ihrie, R.A. (2014). Sonic hedgehog signaling in the postnatal brain. Seminars in cell & developmental biology *33*, 105-111.

Alvarez-Buylla, A., and Lim, D.A. (2004). For the long run: maintaining germinal niches in the adult brain. Neuron *41*, 683-686.

Andreu, Z., Khan, M.A., Gonzalez-Gomez, P., Negueruela, S., Hortiguela, R., San Emeterio, J., Ferron, S.R., Martinez, G., Vidal, A., Farinas, I.*, et al.* (2015). The cyclin-dependent kinase inhibitor p27 kip1 regulates radial stem cell quiescence and neurogenesis in the adult hippocampus. Stem Cells *33*, 219-229.

Arvidsson, A., Collin, T., Kirik, D., Kokaia, Z., and Lindvall, O. (2002). Neuronal replacement from endogenous precursors in the adult brain after stroke. Nature medicine *8*, 963-970.

Azim, K., and Butt, A.M. (2011). GSK3beta negatively regulates oligodendrocyte differentiation and myelination in vivo. Glia *59*, 540-553.

Azim, K., Fischer, B., Hurtado-Chong, A., Draganova, K., Cantu, C., Zemke, M., Sommer, L., Butt, A., and Raineteau, O. (2014a). Persistent Wnt/beta-Catenin signaling determines dorsalization of the postnatal subventricular zone and neural stem cell specification into oligodendrocytes and glutamatergic neurons. Stem Cells.

Azim, K., Rivera, A., Raineteau, O., and Butt, A.M. (2014b). GSK3beta regulates oligodendrogenesis in the dorsal microdomain of the subventricular zone via Wnt-beta-catenin signaling. Glia.

Bandeira, F., Lent, R., and Herculano-Houzel, S. (2009). Changing numbers of neuronal and non-neuronal cells underlie postnatal brain growth in the rat. Proceedings of the National Academy of Sciences of the United States of America *106*, 14108-14113.

Barnabe-Heider, F., Meletis, K., Eriksson, M., Bergmann, O., Sabelstrom, H., Harvey, M.A., Mikkers, H., and Frisen, J. (2008). Genetic manipulation of adult mouse neurogenic niches by in vivo electroporation. Nature methods *5*, 189-196.

Basak, O., Giachino, C., Fiorini, E., Macdonald, H.R., and Taylor, V. (2012). Neurogenic subventricular zone stem/progenitor cells are Notch1-dependent in their active but not quiescent state. The Journal of neuroscience : the official journal of the Society for Neuroscience *32*, 5654-5666.

Bayer, S.A. (1983). 3H-thymidine-radiographic studies of neurogenesis in the rat olfactory bulb. Experimental brain research Experimentelle Hirnforschung Experimentation cerebrale *50*, 329-340.

Bayer, S.A. (1984). Neurogenesis in the rat neostriatum. International journal of developmental neuroscience : the official journal of the International Society for Developmental Neuroscience *2*, 163-175.

Bayraktar, O.A., Fuentealba, L.C., Alvarez-Buylla, A., and Rowitch, D.H. (2014). Astrocyte Development and Heterogeneity. Cold Spring Harbor perspectives in biology.

Beckervordersandforth, R., Tripathi, P., Ninkovic, J., Bayam, E., Lepier, A., Stempfhuber, B., Kirchhoff, F., Hirrlinger, J., Haslinger, A., Lie, D.C.*, et al.* (2010). In vivo fate mapping and expression analysis reveals molecular hallmarks of prospectively isolated adult neural stem cells. Cell stem cell *7*, 744-758.

Bonaguidi, M.A., McGuire, T., Hu, M., Kan, L., Samanta, J., and Kessler, J.A. (2005). LIF and BMP signaling generate separate and discrete types of GFAP-expressing cells. Development *132*, 5503-5514.

Bonaguidi, M.A., Peng, C.Y., McGuire, T., Falciglia, G., Gobeske, K.T., Czeisler, C., and Kessler, J.A. (2008). Noggin expands neural stem cells in the adult hippocampus. The Journal of neuroscience : the official journal of the Society for Neuroscience *28*, 9194-9204.

Boscher, C., Dennis, J.W., and Nabi, I.R. (2011). Glycosylation, galectins and cellular signaling. Current opinion in cell biology *23*, 383-392.

Boscher, C., Zheng, Y.Z., Lakshminarayan, R., Johannes, L., Dennis, J.W., Foster, L.J., and Nabi, I.R. (2012). Galectin-3 protein regulates mobility of N-cadherin and GM1 ganglioside at cell-cell junctions of mammary carcinoma cells. The Journal of biological chemistry *287*, 32940-32952.

Boutin, C., Diestel, S., Desoeuvre, A., Tiveron, M.C., and Cremer, H. (2008). Efficient In Vivo Electroporation of the Postnatal Rodent Forebrain. PloS one *3*.

Bowman, A.N., van Amerongen, R., Palmer, T.D., and Nusse, R. (2013). Lineage tracing with Axin2 reveals distinct developmental and adult populations of Wnt/beta-catenin-responsive neural stem cells. Proceedings of the National Academy of Sciences of the United States of America.

Bradl, M., and Lassmann, H. (2010). Oligodendrocytes: biology and pathology. Acta neuropathologica *119*, 37-53.

Brazel, C.Y., Alaythan, A.A., Felling, R.J., Calderon, F., and Levison, S.W. (2013). Molecular Features of Neural Stem Cells Enable their Enrichment Using Pharmacological Inhibitors of Survival-Promoting Kinases. J Neurochem.

Brazel, C.Y., Romanko, M.J., Rothstein, R.P., and Levison, S.W. (2003a). Roles of the mammalian subventricular zone in brain development. Progress in neurobiology *69*, 49-69.

Brazel, C.Y., Romanko, M.J., Rothstein, R.P., and Levison, S.W. (2003b). Roles of the mammalian subventricular zone in brain development. Progress in neurobiology *69*, 49-69.

Butti, E., Cusimano, M., Bacigaluppi, M., and Martino, G. (2014). Neurogenic and non-neurogenic functions of endogenous neural stem cells. Frontiers in neuroscience *8*, 92.

Calzolari, F., Michel, J., Baumgart, E.V., Theis, F., Gotz, M., and Ninkovic, J. (2015). Fast clonal expansion and limited neural stem cell self-renewal in the adult subependymal zone. Nature neuroscience *18*, 490-492.

Cate, H.S., Sabo, J.K., Merlo, D., Kemper, D., Aumann, T.D., Robinson, J., Merson, T.D., Emery, B., Perreau, V.M., and Kilpatrick, T.J. (2010). Modulation of bone morphogenic protein signalling alters numbers of astrocytes and oligodendroglia in the subventricular zone during cuprizone-induced demyelination. J Neurochem *115*, 11-22.

Cheffer, A., Tarnok, A., and Ulrich, H. (2013). Cell Cycle Regulation During Neurogenesis in the Embryonic and Adult Brain. Stem cell reviews.

Chen, C.M., Krohn, J., Bhattacharya, S., and Davies, B. (2011). A comparison of exogenous promoter activity at the ROSA26 locus using a PhiiC31 integrase mediated cassette exchange approach in mouse ES cells. PloS one *6*, e23376.

Chen, S., Lewallen, M., and Xie, T. (2013). Adhesion in the stem cell niche: biological roles and regulation. Development *140*, 255-265.

Chenn, A. (2008). Wnt/beta-catenin signaling in cerebral cortical development. Organogenesis *4*, 76-80.

Chenn, A., and Walsh, C.A. (2002). Regulation of cerebral cortical size by control of cell cycle exit in neural precursors. Science *297*, 365-369.

Chenn, A., and Walsh, C.A. (2003). Increased neuronal production, enlarged forebrains and cytoarchitectural distortions in beta-catenin overexpressing transgenic mice. Cereb Cortex *13*, 599-606.

Chesler, A.T., Le Pichon, C.E., Brann, J.H., Araneda, R.C., Zou, D.J., and Firestein, S. (2008). Selective gene expression by postnatal electroporation during olfactory interneuron nurogenesis. PloS one *3*, e1517.

Ciceroni, C., Mosillo, P., Mastrantoni, E., Sale, P., Ricci-Vitiani, L., Biagioni, F., Stocchi, F., Nicoletti, F., and Melchiorri, D. (2010). mGLU3 metabotropic glutamate receptors modulate the differentiation of SVZ-derived neural stem cells towards the astrocytic lineage. Glia *58*, 813-822.

Citri, A., and Yarden, Y. (2006). EGF-ERBB signalling: towards the systems level. Nature reviews Molecular cell biology *7*, 505-516.

Cleary, M.A., Uboha, N., Picciotto, M.R., and Beech, R.D. (2006). Expression of ezrin in glial tubes in the adult subventricular zone and rostral migratory stream. Neuroscience *143*, 851-861.

Clevers, H., Loh, K.M., and Nusse, R. (2014). Stem cell signaling. An integral program for tissue renewal and regeneration: Wnt signaling and stem cell control. Science *346*, 1248012.

Clevers, H., and Nusse, R. (2012). Wnt/beta-catenin signaling and disease. Cell *149*, 1192-1205.

Codega, P., Silva-Vargas, V., Paul, A., Maldonado-Soto, A.R., Deleo, A.M., Pastrana, E., and Doetsch, F. (2014). Prospective identification and purification of quiescent adult neural stem cells from their in vivo niche. Neuron *82*, 545-559.

Colak, D., Mori, T., Brill, M.S., Pfeifer, A., Falk, S., Deng, C., Monteiro, R., Mummery, C., Sommer, L., and Gotz, M. (2008). Adult neurogenesis requires Smad4-mediated bone morphogenic protein signaling in stem cells. The Journal of neuroscience : the official journal of the Society for Neuroscience *28*, 434-446.

Coles-Takabe, B.L., Brain, I., Purpura, K.A., Karpowicz, P., Zandstra, P.W., Morshead, C.M., and van der Kooy, D. (2008). Don't look: growing clonal versus nonclonal neural stem cell colonies. Stem Cells *26*, 2938-2944.

Colnot, C., Fowlis, D., Ripoche, M.A., Bouchaert, I., and Poirier, F. (1998). Embryonic implantation in galectin 1/galectin 3 double mutant mice. Developmental dynamics : an official publication of the American Association of Anatomists *211*, 306-313.

Comte, I., Kim, Y., Young, C.C., van der Harg, J.M., Hockberger, P., Bolam, P.J., Poirier, F., and Szele, F.G. (2011). Galectin-3 maintains cell motility from the subventricular zone to the olfactory bulb. Journal of Cell Science *124*, 2438-2447.

Corish, P., and Tyler-Smith, C. (1999). Attenuation of green fluorescent protein half-life in mammalian cells. Protein Eng *12*, 1035-1040.

Coskun, V., and Luskin, M.B. (2002). Intrinsic and extrinsic regulation of the proliferation and differentiation of cells in the rodent rostral migratory stream. Journal of neuroscience research *69*, 795-802.

Coskun, V., Venkatraman, G., Yang, H., Rao, M.S., and Luskin, M.B. (2001). Retroviral manipulation of the expression of bone morphogenetic protein receptor Ia by SVZa progenitor cells leads to changes in their p19(INK4d) expression but not in their neuronal commitment. International journal of developmental neuroscience : the official journal of the International Society for Developmental Neuroscience *19*, 219-227.

Dayer, A.G., Cleaver, K.M., Abouantoun, T., and Cameron, H.A. (2005). New GABAergic interneurons in the adult neocortex and striatum are generated from different precursors. The Journal of cell biology *168*, 415-427.

Doetsch, F. (2003a). The glial identity of neural stem cells. Nature neuroscience *6*, 1127-1134.

Doetsch, F. (2003b). A niche for adult neural stem cells. Current opinion in genetics & development *13*, 543-550.

Doetsch, F., Garcia-Verdugo, J.M., and Alvarez-Buylla, A. (1997). Cellular composition and three-dimensional organization of the subventricular germinal zone in the adult mammalian brain. The Journal of neuroscience : the official journal of the Society for Neuroscience *17*, 5046-5061.

Doetsch F, I.C., Daniel A. Lim, J.M.G.a.-V., and Alvarez-Buylla, A. (1999). Subventricular Zone Astrocytes Are Neural Stem Cells in the Adult Mammalian Brain. Cell stem cell *97*.

Doetsch, F., Petreanu, L., Caille, I., Garcia-Verdugo, J.M., and Alvarez-Buylla, A. (2002a). EGF converts transit-amplifying neurogenic precursors in the adult brain into multipotent stem cells. Neuron *36*, 1021-1034.

Doetsch, F., Verdugo, J.M., Caille, I., Alvarez-Buylla, A., Chao, M.V., and Casaccia-Bonnefil, P. (2002b). Lack of the cell-cycle inhibitor p27Kip1 results in selective increase of transit-amplifying cells for adult neurogenesis. The Journal of neuroscience : the official journal of the Society for Neuroscience *22*, 2255-2264.

Douet, V., Arikawa-Hirasawa, E., and Mercier, F. (2012). Fractone-heparan sulfates mediate BMP-7 inhibition of cell proliferation in the adult subventricular zone. Neuroscience letters *528*, 120-125.

Doverhag, C., Hedtjarn, M., Poirier, F., Mallard, C., Hagberg, H., Karlsson, A., and Savman, K. (2010). Galectin-3 contributes to neonatal hypoxic-ischemic brain injury. Neurobiology of disease *38*, 36-46.

Dumic, J., Dabelic, S., and Flogel, M. (2006). Galectin-3: an open-ended story. Biochimica et biophysica acta *1760*, 616-635.

Durak, O., de Anda, F.C., Singh, K.K., Leussis, M.P., Petryshen, T.L., Sklar, P., and Tsai, L.H. (2014). Ankyrin-G regulates neurogenesis and Wnt signaling by altering the subcellular localization of beta-catenin. Molecular psychiatry.

Elad-Sfadia, G., Haklai, R., Balan, E., and Kloog, Y. (2004). Galectin-3 augments K-Ras activation and triggers a Ras signal that attenuates ERK but not phosphoinositide 3-kinase activity. The Journal of biological chemistry *279*, 34922-34930.

Eliasson, C., Sahlgren, C., Berthold, C.H., Stakeberg, J., Celis, J.E., Betsholtz, C., Eriksson, J.E., and Pekny, M. (1999). Intermediate filament protein partnership in astrocytes. The Journal of biological chemistry *274*, 23996-24006.

Emsley, J.G., and Hagg, T. (2003). alpha6beta1 integrin directs migration of neuronal precursors in adult mouse forebrain. Experimental neurology *183*, 273-285.

Ernst, A., Alkass, K., Bernard, S., Salehpour, M., Perl, S., Tisdale, J., Possnert, G., Druid, H., and Frisen, J. (2014). Neurogenesis in the Striatum of the Adult Human Brain. Cell.

Faigle, R., and Song, H. (2013). Signaling mechanisms regulating adult neural stem cells and neurogenesis. Biochimica et biophysica acta *1830*, 2435-2448.

Fang, D., Hawke, D., Zheng, Y., Xia, Y., Meisenhelder, J., Nika, H., Mills, G.B., Kobayashi, R., Hunter, T., and Lu, Z. (2007). Phosphorylation of beta-catenin by AKT promotes beta-catenin transcriptional activity. The Journal of biological chemistry *282*, 11221-11229.

Fernandez, M.E., Croce, S., Boutin, C., Cremer, H., and Raineteau, O. (2011). Targeted electroporation of defined lateral ventricular walls: a novel and rapid method to study fate specification during postnatal forebrain neurogenesis. Neural development *6*, 13.

Ferri, A.L., Cavallaro, M., Braida, D., Di Cristofano, A., Canta, A., Vezzani, A., Ottolenghi, S., Pandolfi, P.P., Sala, M., DeBiasi, S.*, et al.* (2004). Sox2 deficiency causes neurodegeneration and impaired neurogenesis in the adult mouse brain. Development *131*, 3805-3819.

Fiorelli, R., Azim, K., Fischer, B., and Raineteau, O. (2015). Adding a spatial dimension to postnatal ventricular-subventricular zone neurogenesis. Development *142*, 2109-2120.

Frinchi, M., Bonomo, A., Trovato-Salinaro, A., Condorelli, D.F., Fuxe, K., Spampinato, M.G., and Mudo, G. (2008). Fibroblast growth factor-2 and its receptor expression in proliferating precursor cells of the subventricular zone in the adult rat brain. Neuroscience letters *447*, 20-25.

Fuchs, E., and Segre, J.A. (2000). Stem cells: a new lease on life. Cell *100*, 143-155.

Fuentealba, L.C., Eivers, E., Ikeda, A., Hurtado, C., Kuroda, H., Pera, E.M., and De Robertis, E.M. (2007). Integrating patterning signals: Wnt/GSK3 regulates the duration of the BMP/Smad1 signal. Cell *131*, 980-993.

Fuentealba, L.C., Rompani, S.B., Parraguez, J.I., Obernier, K., Romero, R., Cepko, C.L., and Alvarez-Buylla, A. (2015). Embryonic Origin of Postnatal Neural Stem Cells. Cell *161*, 1644-1655.

Funasaka, T., Balan, V., Raz, A., and Wong, R.W. (2013). Nucleoporin Nup98 mediates galectin-3 nuclear-cytoplasmic trafficking. Biochemical and biophysical research communications *434*, 155-161.

Gajera, C.R., Emich, H., Lioubinski, O., Christ, A., Beckervordersandforth-Bonk, R., Yoshikawa, K., Bachmann, S., Christensen, E.I., Gotz, M., Kempermann, G.*, et al.* (2010). LRP2 in ependymal cells regulates BMP signaling in the adult neurogenic niche. J Cell Sci *123*, 1922-1930.

Galvez-Contreras, A.Y., Gonzalez-Castaneda, R.E., Luquin, S., and Gonzalez-Perez, O. (2012). Role of fibroblast growth factor receptors in astrocytic stem cells. Current signal transduction therapy *7*, 81-86.

Garcia, A.D., Doan, N.B., Imura, T., Bush, T.G., and Sofroniew, M.V. (2004). GFAP-expressing progenitors are the principal source of constitutive neurogenesis in adult mouse forebrain. Nature neuroscience *7*, 1233-1241.

Garner, O.B., and Baum, L.G. (2008). Galectin-glycan lattices regulate cell-surface glycoprotein organization and signalling. In Biochemical Society transactions, pp. 1472-1477.

Gattazzo, F., Urciuolo, A., and Bonaldo, P. (2014). Extracellular matrix: A dynamic microenvironment for stem cell niche. Biochimica et biophysica acta.

Ge, W.P., Miyawaki, A., Gage, F.H., Jan, Y.N., and Jan, L.Y. (2012). Local generation of glia is a major astrocyte source in postnatal cortex. Nature *484*, 376-380.

Giachino, C., Basak, O., Lugert, S., Knuckles, P., Obernier, K., Fiorelli, R., Frank, S., Raineteau, O., Alvarez-Buylla, A., and Taylor, V. (2013). Molecular diversity subdivides the adult forebrain neural stem cell population. Stem Cells.

Giachino, C., and Taylor, V. (2014). Notching up neural stem cell homogeneity in homeostasis and disease. Frontiers in neuroscience *8*, 32.

Gil-Perotin, S., Duran-Moreno, M., Cebrian-Silla, A., Ramirez, M., Garcia-Belda, P., and Garcia-Verdugo, J.M. (2013). Adult neural stem cells from the subventricular zone: a review of the neurosphere assay. Anat Rec (Hoboken) *296*, 1435-1452.

Goings, G.E., Kozlowski, D.A., and Szele, F.G. (2006). Differential activation of microglia in neurogenic versus non-neurogenic regions of the forebrain. Glia *54*, 329-342.

Goldman, S.O.S.a.J.E. (2003). Multiple Cell Populations in the Early Postnatal Subventricular Zone Take Distinct Migratory Pathways: A Dynamic Study of Glial and Neuronal Progenitor Migration. The Journal of Neuroscience *23*.

Gomes, W.A., Mehler, M.F., and Kessler, J.A. (2003). Transgenic overexpression of BMP4 increases astroglial and decreases oligodendroglial lineage commitment. Developmental biology *255*, 164-177.

Gonda, D.K., Bachmair, A., Wunning, I., Tobias, J.W., Lane, W.S., and Varshavsky, A. (1989). Universality and structure of the N-end rule. The Journal of biological chemistry *264*, 16700-16712.

Gonzalez-Perez, O., Romero-Rodriguez, R., Soriano-Navarro, M., Garcia-Verdugo, J.M., and Alvarez-Buylla, A. (2009). Epidermal growth factor induces the progeny of subventricular zone type B cells to migrate and differentiate into oligodendrocytes. Stem Cells *27*, 2032-2043.

Grinspan, J.B., Edell, E., Carpio, D.F., Beesley, J.S., Lavy, L., Pleasure, D., and Golden, J.A. (2000). Stage-specific effects of bone morphogenetic proteins on the oligodendrocyte lineage. Journal of neurobiology *43*, 1-17.

Gross, R.E., Mehler, M.F., Mabie, P.C., Zang, Z., Santschi, L., and Kessler, J.A. (1996). Bone morphogenetic proteins promote astroglial lineage commitment by mammalian subventricular zone progenitor cells. Neuron *17*, 595-606.

Halliday, A.L., and Cepko, C.L. (1992). Generation and migration of cells in the developing striatum. Neuron *9*, 15-26.

Haudek, K.C., Spronk, K.J., Voss, P.G., Patterson, R.J., Wang, J.L., and Arnoys, E.J. (2010). Dynamics of galectin-3 in the nucleus and cytoplasm. Biochimica et biophysica acta *1800*, 181-189.

Hegarty, S.V., O'Keeffe, G.W., and Sullivan, A.M. (2013). BMP-Smad 1/5/8 signalling in the development of the nervous system. Progress in neurobiology *109*, 28-41.

Henderson, N.C., Mackinnon, A.C., Farnworth, S.L., Poirier, F., Russo, F.P., Iredale, J.P., Haslett, C., Simpson, K.J., and Sethi, T. (2006). Galectin-3 regulates myofibroblast activation and hepatic fibrosis. Proceedings of the National Academy of Sciences of the United States of America *103*, 5060-5065.

Henderson, N.C., and Sethi, T. (2009). The regulation of inflammation by galectin-3. Immunol Rev *230*, 160-171.

Hino, S., Tanji, C., Nakayama, K.I., and Kikuchi, A. (2005). Phosphorylation of beta-catenin by cyclic AMP-dependent protein kinase stabilizes beta-catenin through inhibition of its ubiquitination. Molecular and cellular biology *25*, 9063-9072.

Hirabayashi, Y., and Gotoh, Y. (2005). Stage-dependent fate determination of neural precursor cells in mouse forebrain. Neuroscience research *51*, 331-336.

Hodge, R.D., D'Ercole, A.J., and O'Kusky, J.R. (2004). Insulin-like growth factor-I accelerates the cell cycle by decreasing G1 phase length and increases cell cycle reentry in the embryonic cerebral cortex. The Journal of neuroscience : the official journal of the Society for Neuroscience *24*, 10201-10210.

Hoyos, H.C., Rinaldi, M., Mendez-Huergo, S.P., Marder, M., Rabinovich, G.A., Pasquini, J.M., and Pasquini, L.A. (2014). Galectin-3 controls the response of microglial cells to limit cuprizone-induced demyelination. Neurobiology of disease *62*, 441-455.

Hughes, R.C. (1999). Secretion of the galectin family of mammalian carbohydrate-binding proteins. Biochimica et biophysica acta *1473*, 172-185.

Ihrie, R.A., and Alvarez-Buylla, A. (2008). Cells in the astroglial lineage are neural stem cells. Cell and tissue research *331*, 179-191.

Ihrie, R.A., and Alvarez-Buylla, A. (2011). Lake-front property: a unique germinal niche by the lateral ventricles of the adult brain. Neuron *70*, 674-686.

Ihrie, R.A., Shah, J.K., Harwell, C.C., Levine, J.H., Guinto, C.D., Lezameta, M., Kriegstein, A.R., and Alvarez-Buylla, A. (2011). Persistent sonic hedgehog signaling in adult brain determines neural stem cell positional identity. Neuron *71*, 250-262.

Imayoshi, I., Shimojo, H., Sakamoto, M., Ohtsuka, T., and Kageyama, R. (2013). Genetic visualization of notch signaling in mammalian neurogenesis. Cellular and molecular life sciences : CMLS *70*, 2045-2057.

Jackson, E.L., Garcia-Verdugo, J.M., Gil-Perotin, S., Roy, M., Quinones-Hinojosa, A., VandenBerg, S., and Alvarez-Buylla, A. (2006). PDGFR alpha-positive B cells are neural stem cells in the adult SVZ that form glioma-like growths in response to increased PDGF signaling. Neuron *51*, 187-199.

Jacques, T.S., Relvas, J.B., Nishimura, S., Pytela, R., Edwards, G.M., Streuli, C.H., and ffrench-Constant, C. (1998). Neural precursor cell chain migration and division are regulated through different beta1 integrins. Development *125*, 3167-3177.

Jafri, N.F., Clarke, J.L., Weinberg, V., Barani, I.J., and Cha, S. (2013). Relationship of glioblastoma multiforme to the subventricular zone is associated with survival. Neuro Oncol *15*, 91-96.

James, R.E., Hillis, J., Adorjan, I., Gration, B., Mundim, M.V., Iqbal, A.J., Majumdar, M.M., Yates, R.L., Richards, M.M., Goings, G.E*., et al.* (2015). Loss of galectin-3 decreases the number of immune cells in the subventricular zone and restores proliferation in a viral model of multiple sclerosis. Glia.

Jeon, S.B., Yoon, H.J., Chang, C.Y., Koh, H.S., Jeon, S.H., and Park, E.J. (2010). Galectin-3 exerts cytokine-like regulatory actions through the JAK-STAT pathway. J Immunol *185*, 7037-7046.

Kakita, A., and Goldman, J.E. (1999). Patterns and dynamics of SVZ cell migration in the postnatal forebrain: monitoring living progenitors in slice preparations. Neuron *23*, 461-472.

Kalani, M.Y., Cheshier, S.H., Cord, B.J., Bababeygy, S.R., Vogel, H., Weissman, I.L., Palmer, T.D., and Nusse, R. (2008). Wnt-mediated self-renewal of neural stem/progenitor cells. Proceedings of the National Academy of Sciences of the United States of America *105*, 16970-16975.

Kanski, R., van Strien, M.E., van Tijn, P., and Hol, E.M. (2014). A star is born: new insights into the mechanism of astrogenesis. Cellular and molecular life sciences : CMLS *71*, 433-447.

Karpowicz, P., Willaime-Morawek, S., Balenci, L., DeVeale, B., Inoue, T., and van der Kooy, D. (2009). E-Cadherin regulates neural stem cell self-renewal. The Journal of neuroscience : the official journal of the Society for Neuroscience *29*, 3885-3896.

Kessaris, N., Fogarty, M., Iannarelli, P., Grist, M., Wegner, M., and Richardson, W.D. (2006). Competing waves of oligodendrocytes in the forebrain and postnatal elimination of an embryonic lineage. Nature neuroscience *9*, 173-179.

Kim, J.S., Chang, M.Y., Yu, I.T., Kim, J.H., Lee, S.H., Lee, Y.S., and Son, H. (2004). Lithium selectively increases neuronal differentiation of hippocampal neural progenitor cells both in vitro and in vivo. J Neurochem *89*, 324-336.

Kim, S.J., Choi, I.J., Cheong, T.C., Lee, S.J., Lotan, R., Park, S.H., and Chun, K.H. (2010). Galectin-3 Increases Gastric Cancer Cell Motility by Up-regulating Fascin-1 Expression. Gastroenterology *138*, 1035-1045.e1032.

Kim, S.J., Lee, H.W., Gu Kang, H., La, S.H., Choi, I.J., Ro, J.Y., Bresalier, R.S., Song, J., and Chun, K.H. (2014). Ablation of galectin-3 induces p27(KIP1)-dependent premature senescence without oncogenic stress. Cell death and differentiation *21*, 1769-1779.

Kishi, K. (1987). Golgi studies on the development of granule cells of the rat olfactory bulb with reference to migration in the subependymal layer. The Journal of comparative neurology *258*, 112-124.

Knippschild, U., Wolff, S., Giamas, G., Brockschmidt, C., Wittau, M., Wurl, P.U., Eismann, T., and Stoter, M. (2005). The role of the casein kinase 1 (CK1) family in different signaling pathways linked to cancer development. Onkologie *28*, 508-514.

Kobayashi, T., Shimura, T., Yajima, T., Kubo, N., Araki, K., Tsutsumi, S., Suzuki, H., Kuwano, H., and Raz, A. (2011). Transient gene silencing of galectin-3 suppresses pancreatic cancer cell migration and invasion through degradation of beta-catenin. International journal of cancer Journal international du cancer *129*, 2775-2786.

Kohwi, M., Petryniak, M.A., Long, J.E., Ekker, M., Obata, K., Yanagawa, Y., Rubenstein, J.L., and Alvarez-Buylla, A. (2007). A subpopulation of olfactory bulb GABAergic interneurons is derived from Emx1- and Dlx5/6-expressing progenitors. The Journal of neuroscience : the official journal of the Society for Neuroscience *27*, 6878-6891.

Kokovay, E., Wang, Y., Kusek, G., Wurster, R., Lederman, P., Lowry, N., Shen, Q., and Temple, S. (2012). VCAM1 is essential to maintain the structure of the SVZ niche and acts as an environmental sensor to regulate SVZ lineage progression. Cell stem cell *11*, 220-230.

Kolligs, F.T., Bommer, G., ouml, and ke, B. (2002). Wnt/Beta-Catenin/Tcf Signaling: A Critical Pathway in Gastrointestinal Tumorigenesis. Digestion *66*, 131-144.

Korchynskyi, O., and ten Dijke, P. (2002). Identification and functional characterization of distinct critically important bone morphogenetic protein-specific response elements in the Id1 promoter. The Journal of biological chemistry *277*, 4883-4891.

Korolainen, M.A., Auriola, S., Nyman, T.A., Alafuzoff, I., and Pirttila, T. (2005). Proteomic analysis of glial fibrillary acidic protein in Alzheimer's disease and aging brain. Neurobiology of disease *20*, 858-870.

Kriegstein, A., and Alvarez-Buylla, A. (2009). The glial nature of embryonic and adult neural stem cells. Annual review of neuroscience *32*, 149-184.

Kuhn, H.G., Winkler, J., Kempermann, G., Thal, L.J., and Gage, F.H. (1997). Epidermal growth factor and fibroblast growth factor-2 have different effects on neural progenitors in the adult rat brain. The Journal of neuroscience : the official journal of the Society for Neuroscience *17*, 5820-5829.

Lajtha, L.G. (1979a). Haemopoietic stem cells: concept and definitions. Blood Cells *5*, 447-455.

Lajtha, L.G. (1979b). Stem cell concepts. Differentiation; research in biological diversity *14*, 23-34.

Lalancette-Hebert, M., Gowing, G., Simard, A., Weng, Y.C., and Kriz, J. (2007). Selective ablation of proliferating microglial cells exacerbates ischemic injury in the brain. The Journal of neuroscience : the official journal of the Society for Neuroscience *27*, 2596-2605.

Lalancette-Hebert, M., Swarup, V., Beaulieu, J.M., Bohacek, I., Abdelhamid, E., Weng, Y.C., Sato, S., and Kriz, J. (2012). Galectin-3 is required for resident microglia activation and proliferation in response to ischemic injury. The Journal of neuroscience : the official journal of the Society for Neuroscience *32*, 10383-10395.

Le Mercier, M., Fortin, S., Mathieu, V., Kiss, R., and Lefranc, F. (2010). Galectins and gliomas. Brain Pathol *20*, 17-27.

Lei, Z.N., Zhang, L.M., and Sun, F.Y. (2008). Beta-catenin siRNA inhibits ischemia-induced striatal neurogenesis in adult rat brain following a transient middle cerebral artery occlusion. Neuroscience letters *435*, 108-112.

Leone, D.P., Relvas, J.B., Campos, L.S., Hemmi, S., Brakebusch, C., Fassler, R., Ffrench-Constant, C., and Suter, U. (2005). Regulation of neural progenitor proliferation and survival by beta1 integrins. J Cell Sci *118*, 2589-2599.

Levers, T.E., Edgar, J.M., and Price, D.J. (2001). The fates of cells generated at the end of neurogenesis in developing mouse cortex. Journal of neurobiology *48*, 265–277.

Levison, S.W., Chuang, C., Abramson, B.J., and Goldman, J.E. (1993). The migrational patterns and developmental fates of glial precursors in the rat subventricular zone are temporally regulated. Development *119*, 611-622.

Levison, S.W., and Goldman, J.E. (1993). Both oligodendrocytes and astrocytes develop from progenitors in the subventricular zone of postnatal rat forebrain. Neuron *10*, 201-212.

Levison, S.W., and Goldman, J.E. (1997). Multipotential and lineage restricted precursors coexist in the mammalian perinatal subventricular zone. Journal of neuroscience research *48*, 83-94.

Levison, S.W., Young, G.M., and Goldman, J.E. (1999). Cycling cells in the adult rat neocortex preferentially generate oligodendroglia. Journal of neuroscience research *57*, 435-446.

Lewis, P.D., and Lai, M. (1974). Cell generation in the subependymal layer of the rat brain during the early postnatal period. Brain Res *76*, 520-525.

Li, X., Tang, X., Jablonska, B., Aguirre, A., Gallo, V., and Luskin, M.B. (2009). p27(KIP1) regulates neurogenesis in the rostral migratory stream and olfactory bulb of the postnatal mouse. The Journal of neuroscience : the official journal of the Society for Neuroscience *29*, 2902-2914.

Lim, D.A., and Alvarez-Buylla, A. (2014). Adult neural stem cells stake their ground. Trends in neurosciences.

Lim, D.A., Tramontin, A.D., Trevejo, J.M., Herrera, D.G., Garcia-Verdugo, J.M., and Alvarez-Buylla, A. (2000). Noggin antagonizes BMP signaling to create a niche for adult neurogenesis. Neuron *28*, 713-726.

Lin, C.I., Whang, E.E., Donner, D.B., Jiang, X., Price, B.D., Carothers, A.M., Delaine, T., Leffler, H., Nilsson, U.J., Nose, V.*, et al.* (2009). Galectin-3 targeted therapy with a small molecule inhibitor activates apoptosis and enhances both chemosensitivity and radiosensitivity in papillary thyroid cancer. Molecular cancer research : MCR *7*, 1655-1662.

Liu, F.T., and Rabinovich, G.A. (2005). Galectins as modulators of tumour progression. Nature reviews Cancer *5*, 29-41.

Liu, W., Hsu, D.K., Chen, H.Y., Yang, R.Y., Carraway, K.L., 3rd, Isseroff, R.R., and Liu, F.T. (2012). Galectin-3 Regulates Intracellular Trafficking of EGFR through Alix and Promotes Keratinocyte Migration. The Journal of investigative dermatology *132*, 2828-2837.

Lois, C., and Alvarez-Buylla, A. (1994). Long-distance neuronal migration in the adult mammalian brain. Science *264*, 1145-1148.

Lu, Q.R., Sun, T., Zhu, Z., Ma, N., Garcia, M., Stiles, C.D., and Rowitch, D.H. (2002). Common developmental requirement for Olig function indicates a motor neuron/oligodendrocyte connection. Cell *109*, 75-86.

Luo, J. (2009). Glycogen synthase kinase 3beta (GSK3beta) in tumorigenesis and cancer chemotherapy. Cancer letters *273*, 194-200.

Luo, Y., Coskun, V., Liang, A., Yu, J., Cheng, L., Ge, W., Shi, Z., Zhang, K., Li, C., Cui, Y., *et al.* (2015). Single-cell transcriptome analyses reveal signals to activate dormant neural stem cells. Cell *161*, 1175-1186.

Luskin, M.B. (1993). Restricted proliferation and migration of postnatally generated neurons derived from the forebrain subventricular zone. Neuron *11*, 173-189.

Luskin, M.B., and Boone, M.S. (1994). Rate and pattern of migration of lineally-related olfactory bulb interneurons generated postnatally in the subventricular zone of the rat. Chem Senses *19*, 695-714.

Luskin, M.B., and McDermott, K. (1994). Divergent lineages for oligodendrocytes and astrocytes originating in the neonatal forebrain subventricular zone. Glia *11*, 211-226.

Luskin, M.B., Parnavelas, J.G., and Barfield, J.A. (1993). Neurons, astrocytes, and oligodendrocytes of the rat cerebral cortex originate from separate progenitor cells: an ultrastructural analysis of clonally related cells. The Journal of neuroscience : the official journal of the Society for Neuroscience *13*, 1730-1750.

Lyck, L., Kroigard, T., and Finsen, B. (2007). Unbiased cell quantification reveals a continued increase in the number of neocortical neurones during early post-natal development in mice. The European journal of neuroscience *26*, 1749-1764.

Mabie, P.C., Mehler, M.F., and Kessler, J.A. (1999). Multiple roles of bone morphogenetic protein signaling in the regulation of cortical cell number and phenotype. The Journal of neuroscience : the official journal of the Society for Neuroscience *19*, 7077-7088.

Mabie, P.C., Mehler, M.F., Marmur, R., Papavasiliou, A., Song, Q., and Kessler, J.A. (1997). Bone morphogenetic proteins induce astroglial differentiation of oligodendroglial-astroglial progenitor cells. The Journal of neuroscience : the official journal of the Society for Neuroscience *17*, 4112-4120.

Machon, O., Backman, M., Machonova, O., Kozmik, Z., Vacik, T., Andersen, L., and Krauss, S. (2007). A dynamic gradient of Wnt signaling controls initiation of neurogenesis in the mammalian cortex and cellular specification in the hippocampus. Developmental biology *311*, 223-237.

Magavi, S., Friedmann, D., Banks, G., Stolfi, A., and Lois, C. (2012). Coincident generation of pyramidal neurons and protoplasmic astrocytes in neocortical columns. The Journal of neuroscience : the official journal of the Society for Neuroscience *32*, 4762-4772.

Magnusson, J.P., Goritz, C., Tatarishvili, J., Dias, D.O., Smith, E.M., Lindvall, O., Kokaia, Z., and Frisen, J. (2014). A latent neurogenic program in astrocytes regulated by Notch signaling in the mouse. Science *346*, 237-241.

Maher, M.T., Flozak, A.S., Stocker, A.M., Chenn, A., and Gottardi, C.J. (2009). Activity of the beta-catenin phosphodestruction complex at cell-cell contacts is enhanced by cadherin-based adhesion. The Journal of cell biology *186*, 219-228.

Malatesta, P., Hack, M.A., Hartfuss, E., Kettenmann, H., Klinkert, W., Kirchhoff, F., and Gotz, M. (2003). Neuronal or glial progeny: regional differences in radial glia fate. Neuron *37*, 751-764.

Mamber, C., Kozareva, D.A., Kamphuis, W., and Hol, E.M. (2013). Shades of gray: The delineation of marker expression within the adult rodent subventricular zone. Progress in neurobiology *111*, 1-16.

Marinaro, C., Pannese, M., Weinandy, F., Sessa, A., Bergamaschi, A., Taketo, M.M., Broccoli, V., Comi, G., Gotz, M., Martino, G.*, et al.* (2012). Wnt signaling has opposing roles in the developing and the adult brain that are modulated by Hipk1. Cereb Cortex *22*, 2415-2427.

Markowska, A.I., Jefferies, K.C., and Panjwani, N. (2011). Galectin-3 protein modulates cell surface expression and activation of vascular endothelial growth factor receptor 2 in human endothelial cells. The Journal of biological chemistry *286*, 29913-29921.

Markowska, A.I., Liu, F.T., and Panjwani, N. (2010). Galectin-3 is an important mediator of VEGF- and bFGF-mediated angiogenic response. The Journal of experimental medicine *207*, 1981-1993.

Marshall, C.A., and Goldman, J.E. (2002). Subpallial dlx2-expressing cells give rise to astrocytes and oligodendrocytes in the cerebral cortex and white matter. The Journal of neuroscience : the official journal of the Society for Neuroscience *22*, 9821-9830.

Marshall, C.A., Suzuki, S.O., and Goldman, J.E. (2003). Gliogenic and neurogenic progenitors of the subventricular zone: who are they, where did they come from, and where are they going? Glia *43*, 52-61.

Martynoga, B., Mateo, J.L., Zhou, B., Andersen, J., Achimastou, A., Urban, N., van den Berg, D., Georgopoulou, D., Hadjur, S., Wittbrodt, J.*, et al.* (2013). Epigenomic

enhancer annotation reveals a key role for NFIX in neural stem cell quiescence. Genes & development *27*, 1769-1786.

Massa, S.M., Cooper, D.N., Leffler, H., and Barondes, S.H. (1993). L-29, an endogenous lectin, binds to glycoconjugate ligands with positive cooperativity. Biochemistry *32*, 260-267.

Matsuda, T., and Cepko, C.L. (2004). Electroporation and RNA interference in the rodent retina in vivo and in vitro. Proceedings of the National Academy of Sciences of the United States of America *101*, 16-22.

Mehler, M.F., Mabie, P.C., Zhang, D., and Kessler, J.A. (1997). Bone morphogenetic proteins in the nervous system. Trends in neurosciences *20*, 309-317.

Mehler, M.F., Mabie, P.C., Zhu, G., Gokhan, S., and Kessler, J.A. (2000). Developmental changes in progenitor cell responsiveness to bone morphogenetic proteins differentially modulate progressive CNS lineage fate. Developmental neuroscience *22*, 74-85.

Meijer, D.H., Kane, M.F., Mehta, S., Liu, H., Harrington, E., Taylor, C.M., Stiles, C.D., and Rowitch, D.H. (2012). Separated at birth? The functional and molecular divergence of OLIG1 and OLIG2. Nature reviews Neuroscience *13*, 819-831.

Menezes, J.R., Smith, C.M., Nelson, K.C., and Luskin, M.B. (1995). The division of neuronal progenitor cells during migration in the neonatal mammalian forebrain. Molecular and cellular neurosciences *6*, 496-508.

Menn, B., Garcia-Verdugo, J.M., Yaschine, C., Gonzalez-Perez, O., Rowitch, D., and Alvarez-Buylla, A. (2006). Origin of oligodendrocytes in the subventricular zone of the adult brain. The Journal of neuroscience : the official journal of the Society for Neuroscience *26*, 7907-7918.

Mercier, F., and Douet, V. (2014). Bone morphogenetic protein-4 inhibits adult neurogenesis and is regulated by fractone-associated heparan sulfates in the subventricular zone. Journal of chemical neuroanatomy.

Merkle, F.T., Fuentealba, L.C., Sanders, T.A., Magno, L., Kessaris, N., and Alvarez-Buylla, A. (2013). Adult neural stem cells in distinct microdomains generate previously unknown interneuron types. Nature neuroscience.

Merkle, F.T., Mirzadeh, Z., and Alvarez-Buylla, A. (2007). Mosaic organization of neural stem cells in the adult brain. Science *317*, 381-384.

Merkle, F.T., Tramontin, A.D., Garcia-Verdugo, J.M., and Alvarez-Buylla, A. (2004). Radial glia give rise to adult neural stem cells in the subventricular zone. Proceedings of the National Academy of Sciences of the United States of America *101*, 17528-17532.

Mirzadeh, Z., Doetsch, F., Sawamoto, K., Wichterle, H., and Alvarez-Buylla, A. (2010a). The subventricular zone en-face: wholemount staining and ependymal flow. Journal of visualized experiments : JoVE.

Mirzadeh, Z., Han, Y.G., Soriano-Navarro, M., Garcia-Verdugo, J.M., and Alvarez-Buylla, A. (2010b). Cilia organize ependymal planar polarity. The Journal of neuroscience : the official journal of the Society for Neuroscience *30*, 2600-2610.

Mirzadeh, Z., Merkle, F.T., Soriano-Navarro, M., Garcia-Verdugo, J.M., and Alvarez-Buylla, A. (2008). Neural stem cells confer unique pinwheel architecture to the ventricular surface in neurogenic regions of the adult brain. Cell stem cell *3*, 265-278.

Modrek, A.S., Bayin, N.S., and Placantonakis, D.G. (2014). Brain stem cells as the cell of origin in glioma. World journal of stem cells *6*, 43-52.

Morell, M., Tsan, Y.C., and O'Shea, K.S. (2014). Inducible expression of noggin selectively expands neural progenitors in the adult SVZ. Stem cell research *14*, 79-94.

Mudo, G., Bonomo, A., Di Liberto, V., Frinchi, M., Fuxe, K., and Belluardo, N. (2009). The FGF-2/FGFRs neurotrophic system promotes neurogenesis in the adult brain. J Neural Transm *116*, 995-1005.

Mutch, C.A., Funatsu, N., Monuki, E.S., and Chenn, A. (2009). Beta-catenin signaling levels in progenitors influence the laminar cell fates of projection neurons. The Journal of neuroscience : the official journal of the Society for Neuroscience *29*, 13710-13719.

Mutch, C.A., Schulte, J.D., Olson, E., and Chenn, A. (2010). Beta-catenin signaling negatively regulates intermediate progenitor population numbers in the developing cortex. PloS one *5*, e12376.

Nakajima, K., Kho, D.H., Yanagawa, T., Harazono, Y., Gao, X., Hogan, V., and Raz, A. (2014). Galectin-3 Inhibits Osteoblast Differentiation through Notch Signaling. Neoplasia *16*, 939-949.

Nakashima, A., Katagiri, T., and Tamura, M. (2005). Cross-talk between Wnt and bone morphogenetic protein 2 (BMP-2) signaling in differentiation pathway of C2C12 myoblasts. The Journal of biological chemistry *280*, 37660-37668.

Nangia-Makker, P., Nakahara, S., Hogan, V., and Raz, A. (2007). Galectin-3 in apoptosis, a novel therapeutic target. Journal of bioenergetics and biomembranes *39*, 79-84.

Nelson, W.J., and Nusse, R. (2004). Convergence of Wnt, beta-catenin, and cadherin pathways. Science *303*, 1483-1487.

Noctor, S.C., Martinez-Cerdeno, V., and Kriegstein, A.R. (2008). Distinct behaviors of neural stem and progenitor cells underlie cortical neurogenesis. The Journal of comparative neurology *508*, 28-44.

Noles, S.R., and Chenn, A. (2007). Cadherin inhibition of beta-catenin signaling regulates the proliferation and differentiation of neural precursor cells. Molecular and cellular neurosciences *35*, 549-558.

Nowakowski RS, C.V.J., Takahashi T, Hayes NL (2002). Population Dynamics During Cell Proliferation and Neuronogenesis in the Developing Murine Neocortex. Results Probl Cell Differ *39*, 1-25.

Ochieng, J., Fridman, R., Nangia-Makker, P., Kleiner, D.E., Liotta, L.A., Stetler-Stevenson, W.G., and Raz, A. (1994). Galectin-3 is a novel substrate for human matrix metalloproteinases-2 and -9. Biochemistry *33*, 14109-14114.

Ochieng, J., Furtak, V., and Lukyanov, P. (2004). Extracellular functions of galectin-3. Glycoconjugate journal *19*, 527-535.

Ochieng, J., Green, B., Evans, S., James, O., and Warfield, P. (1998a). Modulation of the biological functions of galectin-3 by matrix metalloproteinases. Biochimica Et Biophysica Acta-General Subjects *1379*, 97-106.

Ochieng, J., Leite-Browning, M.L., and Warfield, P. (1998b). Regulation of cellular adhesion to extracellular matrix proteins by galectin-3. Biochemical and biophysical research communications *246*, 788-791.

Ochieng, J., Warfield, P., Green-Jarvis, B., and Fentie, I. (1999). Galectin-3 regulates the adhesive interaction between breast carcinoma cells and elastin. Journal of cellular biochemistry *75*, 505-514.

Ortega, F., Costa, M.R., Simon-Ebert, T., Schroeder, T., Gotz, M., and Berninger, B. (2011). Using an adherent cell culture of the mouse subependymal zone to study the behavior of adult neural stem cells on a single-cell level. Nature protocols *6*, 1847-1859.

Ortega, F., Gascon, S., Masserdotti, G., Deshpande, A., Simon, C., Fischer, J., Dimou, L., Chichung Lie, D., Schroeder, T., and Berninger, B. (2013). Oligodendrogliogenic and neurogenic adult subependymal zone neural stem cells constitute distinct lineages and exhibit differential responsiveness to Wnt signalling. Nature cell biology.

Ottone, C., Krusche, B., Whitby, A., Clements, M., Quadrato, G., Pitulescu, M.E., Adams, R.H., and Parrinello, S. (2014). Direct cell-cell contact with the vascular niche maintains quiescent neural stem cells. Nature cell biology.

Ottone, C., and Parrinello, S. (2015). Multifaceted control of adult SVZ neurogenesis by the vascular niche. Cell Cycle, 1-4.

Pan, L., North, H.A., Sahni, V., Jeong, S.J., McGuire, T.L., Berns, E.J., Stupp, S.I., and Kessler, J.A. (2014). beta1-Integrin and Integrin Linked Kinase Regulate Astrocytic Differentiation of Neural Stem Cells. PloS one *9*, e104335.

Parnavelas, J.G. (1999). Glial cell lineages in the rat cerebral cortex. Experimental neurology *156*, 418-429.

Paron, I., Scaloni, A., Pines, A., Bachi, A., Liu, F.T., Puppin, C., Pandolfi, M., Ledda, L., Di Loreto, C., Damante, G.*, et al.* (2003). Nuclear localization of Galectin-3 in

transformed thyroid cells: a role in transcriptional regulation. Biochemical and biophysical research communications *302*, 545-553.

Parras, C.M., Galli, R., Britz, O., Soares, S., Galichet, C., Battiste, J., Johnson, J.E., Nakafuku, M., Vescovi, A., and Guillemot, F. (2004). Mash1 specifies neurons and oligodendrocytes in the postnatal brain. The EMBO journal *23*, 4495-4505.

Partridge, E.A., Le Roy, C., Di Guglielmo, G.M., Pawling, J., Cheung, P., Granovsky, M., Nabi, I.R., Wrana, J.L., and Dennis, J.W. (2004). Regulation of cytokine receptors by Golgi N-glycan processing and endocytosis. Science *306*, 120-124.

Pasquale, E.B. (2008). Eph-ephrin bidirectional signaling in physiology and disease. Cell *133*, 38-52.

Pasquini, L.A., Millet, V., Hoyos, H.C., Giannoni, J.P., Croci, D.O., Marder, M., Liu, F.T., Rabinovich, G.A., and Pasquini, J.M. (2011). Galectin-3 drives oligodendrocyte differentiation to control myelin integrity and function. Cell death and differentiation *18*, 1746-1756.

Pastrana, E., Silva-Vargas, V., and Doetsch, F. (2011). Eyes Wide Open: A Critical Review of Sphere-Formation as an Assay for Stem Cells. Cell stem cell *8*, 486-498.

Pera, E.M., Acosta, H., Gouignard, N., Climent, M., and Arregi, I. (2014). Active signals, gradient formation and regional specificity in neural induction. Experimental cell research *321*, 25-31.

Peretto, P., Giachino, C., Aimar, P., Fasolo, A., and Bonfanti, L. (2005). Chain formation and glial tube assembly in the shift from neonatal to adult subventricular zone of the rodent forebrain. The Journal of comparative neurology *487*, 407-427.

Petreanu, L., and Alvarez-Buylla, A. (2002). Maturation and Death of Adult-Born Olfactory Bulb Granule Neurons: Role of Olfaction. the Journal of Neuroscience *22*, 6106–6113.

Pevny, L.H., and Nicolis, S.K. (2010). Sox2 roles in neural stem cells. The international journal of biochemistry & cell biology *42*, 421-424.

Piccin, D., and Morshead, C.M. (2011). Wnt signaling regulates symmetry of division of neural stem cells in the adult brain and in response to injury. Stem Cells *29*, 528-538.

Pixley, S.K.R., and Devellis, J. (1984). Transition between Immature Radial Glia and Mature Astrocytes Studied with a Monoclonal-Antibody to Vimentin. Developmental Brain Research *15*, 201-209.

Platel, J.C., Dave, K.A., Gordon, V., Lacar, B., Rubio, M.E., and Bordey, A. (2010). NMDA receptors activated by subventricular zone astrocytic glutamate are critical for neuroblast survival prior to entering a synaptic network. Neuron *65*, 859-872.

Ponti, G., Obernier, K., Guinto, C., Jose, L., Bonfanti, L., and Alvarez-Buylla, A. (2013). Cell cycle and lineage progression of neural progenitors in the ventricular-subventricular zones of adult mice. Proceedings of the National Academy of Sciences of the United States of America *110*, E1045-1054.

Potten, C.S., and Loeffler, M. (1990). Stem cells: attributes, cycles, spirals, pitfalls and uncertainties. Lessons for and from the crypt. Development *110*, 1001-1020.

Price, D.J., Aslam, S., Tasker, L., and Gillies, K. (1997). Fates of the earliest generated cells in the developing murine neocortex. The Journal of comparative neurology *377*, 414-422.

Qian, X., Shen, Q., Goderie, S.K., He, W., Capela, A., Davis, A.A., and Temple, S. (2000). Timing of CNS cell generation: a programmed sequence of neuron and glial cell production from isolated murine cortical stem cells. Neuron *28*, 69-80.

Qiu, J., Takagi, Y., Harada, J., Topalkara, K., Wang, Y., Sims, J.R., Zheng, G., Huang, P., Ling, Y., Scadden, D.T.*, et al.* (2009). p27Kip1 constrains proliferation of neural progenitor cells in adult brain under homeostatic and ischemic conditions. Stem Cells *27*, 920-927.

Qu, Q., Sun, G., Li, W., Yang, S., Ye, P., Zhao, C., Yu, R.T., Gage, F.H., Evans, R.M., and Shi, Y. (2010). Orphan nuclear receptor TLX activates Wnt/beta-catenin signalling to stimulate neural stem cell proliferation and self-renewal. Nature cell biology *12*, 31-40; sup pp 31-39.

Rainer Probstmeier, D.M., and Melitta Schachner (1995). Galectin-3, a ß-Galactoside-Binding Animal Lectin, Binds to Neural Recognition Molecules. Journal of Neurochemistry.

Ramirez-Castillejo, C., Sanchez-Sanchez, F., Andreu-Agullo, C., Ferron, S.R., Aroca-Aguilar, J.D., Sanchez, P., Mira, H., Escribano, J., and Farinas, I. (2006). Pigment epithelium-derived factor is a niche signal for neural stem cell renewal. Nature neuroscience *9*, 331-339.

Reya, T., Duncan, A.W., Ailles, L., Domen, J., Scherer, D.C., Willert, K., Hintz, L., Nusse, R., and Weissman, I.L. (2003). A role for Wnt signalling in self-renewal of haematopoietic stem cells. Nature *423*, 409-414.

Ring, A., Kim, Y.M., and Kahn, M. (2014). Wnt/catenin signaling in adult stem cell physiology and disease. Stem cell reviews *10*, 512-525.

Riquelme, P.A., Drapeau, E., and Doetsch, F. (2008). Brain micro-ecologies: neural stem cell niches in the adult mammalian brain. Philosophical transactions of the Royal Society of London Series B, Biological sciences *363*, 123-137.

Sakaguchi, M., Imaizumi, Y., Shingo, T., Tada, H., Hayama, K., Yamada, O., Morishita, T., Kadoya, T., Uchiyama, N., Shimazaki, T.*, et al.* (2010). Regulation of adult neural progenitor cells by Galectin-1/beta1 Integrin interaction. J Neurochem *113*, 1516-1524.

Sakaguchi, M., Shingo, T., Shimazaki, T., Okano, H.J., Shiwa, M., Ishibashi, S., Oguro, H., Ninomiya, M., Kadoya, T., Horie, H.*, et al.* (2006). A carbohydrate-binding protein, Galectin-1, promotes proliferation of adult neural stem cells. Proceedings of the National Academy of Sciences of the United States of America *103*, 7112-7117.

Saravanan, C., Liu, F.T., Gipson, I.K., and Panjwani, N. (2009). Galectin-3 promotes lamellipodia formation in epithelial cells by interacting with complex N-glycans on alpha3beta1 integrin. J Cell Sci *122*, 3684-3693.

Sato, K. (2015). Effects of Microglia on Neurogenesis. Glia.

Sauvageot, C.M., and Stiles, C.D. (2002). Molecular mechanisms controlling cortical gliogenesis. Current opinion in neurobiology *12*, 244-249.

Schanzer, A., Wachs, F.P., Wilhelm, D., Acker, T., Cooper-Kuhn, C., Beck, H., Winkler, J., Aigner, L., Plate, K.H., and Kuhn, H.G. (2004). Direct stimulation of adult neural stem cells in vitro and neurogenesis in vivo by vascular endothelial growth factor. Brain Pathol *14*, 237-248.

Sequerra, E.B. (2014). Subventricular zone progenitors in time and space: generating neuronal diversity. Frontiers in cellular neuroscience *8*, 434.

Shen, Q., Wang, Y., Kokovay, E., Lin, G., Chuang, S.M., Goderie, S.K., Roysam, B., and Temple, S. (2008). Adult SVZ stem cells lie in a vascular niche: a quantitative analysis of niche cell-cell interactions. Cell stem cell *3*, 289-300.

Shimogori, T., VanSant, J., Paik, E., and Grove, E.A. (2004). Members of the Wnt, Fz, and Frp gene families expressed in postnatal mouse cerebral cortex. The Journal of comparative neurology *473*, 496-510.

Shimura, T., Takenaka, Y., Fukumori, T., Tsutsumi, S., Okada, K., Hogan, V., Kikuchi, A., Kuwano, H., and Raz, A. (2005). Implication of galectin-3 in Wnt signaling. Cancer research *65*, 3535-3537.

Shimura, T., Takenaka, Y., Tsutsumi, S., Hogan, V., Kikuchi, A., and Raz, A. (2004). Galectin-3, a novel binding partner of beta-catenin. Cancer research *64*, 6363-6367.

Soderstrom, S., Bengtsson, H., and Ebendal, T. (1996). Expression of serine/threonine kinase receptors including the bone morphogenetic factor type II receptor in the developing and adult rat brain. Cell and tissue research *286*, 269-279.

Sohn, J., Orosco, L., Guo, F., Chung, S.H., Bannerman, P., Mills Ko, E., Zarbalis, K., Deng, W., and Pleasure, D. (2015). The subventricular zone continues to generate corpus callosum and rostral migratory stream astroglia in normal adult mice. The Journal of neuroscience : the official journal of the Society for Neuroscience *35*, 3756-3763.

Song, J., Zhong, C., Bonaguidi, M.A., Sun, G.J., Hsu, D., Gu, Y., Meletis, K., Huang, Z.J., Ge, S., Enikolopov, G.*, et al.* (2012). Neuronal circuitry mechanism regulating adult quiescent neural stem-cell fate decision. Nature.

Song, L., Tang, J.W., Owusu, L., Sun, M.Z., Wu, J., and Zhang, J. (2014). Galectin-3 in cancer. Clinica chimica acta; international journal of clinical chemistry.

Song, S., Mazurek, N., Liu, C., Sun, Y., Ding, Q.Q., Liu, K., Hung, M.C., and Bresalier, R.S. (2009). Galectin-3 mediates nuclear beta-catenin accumulation and Wnt signaling in human colon cancer cells by regulation of glycogen synthase kinase-3beta activity. Cancer research *69*, 1343-1349.

Spassky, N., Merkle, F.T., Flames, N., Tramontin, A.D., Garcia-Verdugo, J.M., and Alvarez-Buylla, A. (2005). Adult ependymal cells are postmitotic and are derived from radial glial cells during embryogenesis. The Journal of neuroscience : the official journal of the Society for Neuroscience *25*, 10-18.

Spradling, A., Drummond-Barbosa, D., and Kai, T. (2001). Stem cells find their niche. Nature *414*, 98-104.

St Croix, B., Sheehan, C., Rak, J.W., Florenes, V.A., Slingerland, J.M., and Kerbel, R.S. (1998). E-Cadherin-dependent growth suppression is mediated by the cyclin-dependent kinase inhibitor p27(KIP1). The Journal of cell biology *142*, 557-571.

Sun, Y., Hu, J., Zhou, L., Pollard, S.M., and Smith, A. (2011). Interplay between FGF2 and BMP controls the self-renewal, dormancy and differentiation of rat neural stem cells. J Cell Sci *124*, 1867-1877.

Suzuki, S.O., and Goldman, J.E. (2003). Multiple cell populations in the early postnatal subventricular zone take distinct migratory pathways: a dynamic study of glial and neuronal progenitor migration. The Journal of neuroscience : the official journal of the Society for Neuroscience *23*, 4240-4250.

Takahashi, T., Nowakowski, R.S., and Caviness, V.S., Jr. (1995). The cell cycle of the pseudostratified ventricular epithelium of the embryonic murine cerebral wall. The Journal of neuroscience : the official journal of the Society for Neuroscience *15*, 6046-6057.

Tan, S.S., Kalloniatis, M., Sturm, K., Tam, P.P., Reese, B.E., and Faulkner-Jones, B. (1998). Separate progenitors for radial and tangential cell dispersion during development of the cerebral neocortex. Neuron *21*, 295-304.

Taurin, S., Sandbo, N., Qin, Y., Browning, D., and Dulin, N.O. (2006). Phosphorylation of beta-catenin by cyclic AMP-dependent protein kinase. The Journal of biological chemistry *281*, 9971-9976.

Tavazoie, M., Van der Veken, L., Silva-Vargas, V., Louissaint, M., Colonna, L., Zaidi, B., Garcia-Verdugo, J.M., and Doetsch, F. (2008). A specialized vascular niche for adult neural stem cells. Cell stem cell *3*, 279-288.

Taverna, E., Gotz, M., and Huttner, W.B. (2014). The cell biology of neurogenesis: toward an understanding of the development and evolution of the neocortex. Annual review of cell and developmental biology *30*, 465-502.

Thery, C., Boussac, M., Veron, P., Ricciardi-Castagnoli, P., Raposo, G., Garin, J., and Amigorena, S. (2001). Proteomic analysis of dendritic cell-derived exosomes: a secreted subcellular compartment distinct from apoptotic vesicles. J Immunol *166*, 7309-7318.

Tong, C.K., Han, Y.G., Shah, J.K., Obernier, K., Guinto, C.D., and Alvarez-Buylla, A. (2014). Primary cilia are required in a unique subpopulation of neural progenitors. Proceedings of the National Academy of Sciences of the United States of America *111*, 12438-12443.

Tramontin, A.D., Garcia-Verdugo, J.M., Lim, D.A., and Alvarez-Buylla, A. (2003). Postnatal development of radial glia and the ventricular zone (VZ): a continuum of the neural stem cell compartment. Cereb Cortex *13*, 580-587.

Tsai, H.H., Li, H., Fuentealba, L.C., Molofsky, A.V., Taveira-Marques, R., Zhuang, H., Tenney, A., Murnen, A.T., Fancy, S.P., Merkle, F.*, et al.* (2012). Regional astrocyte allocation regulates CNS synaptogenesis and repair. Science *337*, 358-362.

Venkatesan, C., Chrzaszcz, M., Choi, N., and Wainwright, M.S. (2010). Chronic upregulation of activated microglia immunoreactive for galectin-3/Mac-2 and nerve growth factor following diffuse axonal injury. Journal of neuroinflammation *7*, 32.

Ventura, R.E., and Goldman, J.E. (2007). Dorsal radial glia generate olfactory bulb interneurons in the postnatal murine brain. The Journal of neuroscience : the official journal of the Society for Neuroscience *27*, 4297-4302.

Viti, J., Gulacsi, A., and Lillien, L. (2003). Wnt regulation of progenitor maturation in the cortex depends on Shh or fibroblast growth factor 2. The Journal of neuroscience : the official journal of the Society for Neuroscience *23*, 5919-5927.

Voigt, T. (1989). Development of glial cells in the cerebral wall of ferrets: direct tracing of their transformation from radial glia into astrocytes. The Journal of comparative neurology *289*, 74-88.

Wang, D.D., and Bordey, A. (2008). The astrocyte odyssey. Progress in neurobiology *86*, 342-367.

Wang, L.P., Chen, S.W., Zhuang, S.M., Li, H., and Song, M. (2013). Galectin-3 Accelerates the Progression of Oral Tongue Squamous Cell Carcinoma via a Wnt/beta-catenin-Dependent Pathway. Pathology oncology research : POR.

Wartlick, O., Kicheva, A., and Gonzalez-Gaitan, M. (2009). Morphogen gradient formation. Cold Spring Harbor perspectives in biology *1*, a001255.

Weissman, I.L. (2000). Stem Cells: Units of Development, Units of Regeneration, and Units in Evolution. Cell *100*, 157-168.

Wen, Y., Makagiansar, I.T., Fukushi, J., Liu, F.T., Fukuda, M.N., and Stallcup, W.B. (2006). Molecular basis of interaction between NG2 proteoglycan and galectin-3. Journal of cellular biochemistry *98*, 115-127.

Wesley, U.V., Vemuganti, R., Ayvaci, E.R., and Dempsey, R.J. (2013). Galectin-3 enhances angiogenic and migratory potential of microglial cells via modulation of integrin linked kinase signaling. Brain Res *1496*, 1-9.

Wexler, E.M., Geschwind, D.H., and Palmer, T.D. (2008). Lithium regulates adult hippocampal progenitor development through canonical Wnt pathway activation. Molecular psychiatry *13*, 285-292.

Wisniewska, M.B. (2013). Physiological Role of beta-Catenin/TCF Signaling in Neurons of the Adult Brain. Neurochem Res *38*, 1144-1155.

Woodhead, G.J., Mutch, C.A., Olson, E.C., and Chenn, A. (2006). Cell-autonomous beta-catenin signaling regulates cortical precursor proliferation. The Journal of neuroscience : the official journal of the Society for Neuroscience *26*, 12620-12630.

Wrobel, C.N., Mutch, C.A., Swaminathan, S., Taketo, M.M., and Chenn, A. (2007). Persistent expression of stabilized beta-catenin delays maturation of radial glial cells into intermediate progenitors. Developmental biology *309*, 285-297.

Yabut, O., and Pleasure, S.J. (2014). The quintessence of quiescence. Neuron *82*, 501-503.

Yan, Y.P., Lang, B.T., Vemuganti, R., and Dempsey, R.J. (2009). Galectin-3 mediates post-ischemic tissue remodeling. Brain Res *1288*, 116-124.

Yang, H.K., Sundholm-Peters, N.L., Goings, G.E., Walker, A.S., Hyland, K., and Szele, F.G. (2004). Distribution of doublecortin expressing cells near the lateral ventricles in the adult mouse brain. Journal of neuroscience research *76*, 282-295.

Young, C.C., Al-Dalahmah, O., Lewis, N.J., Brooks, K.J., Jenkins, M.M., Poirier, F., Buchan, A.M., and Szele, F.G. (2014). Blocked angiogenesis in Galectin-3 null mice does not alter cellular and behavioral recovery after middle cerebral artery occlusion stroke. Neurobiology of disease *63*, 155-164.

Young, K.M., Fogarty, M., Kessaris, N., and Richardson, W.D. (2007). Subventricular zone stem cells are heterogeneous with respect to their embryonic origins and neurogenic fates in the adult olfactory bulb. The Journal of neuroscience : the official journal of the Society for Neuroscience *27*, 8286-8296.

Yu, J.M., Kim, J.H., Song, G.S., and Jung, J.S. (2006). Increase in proliferation and differentiation of neural progenitor cells isolated from postnatal and adult mice brain by Wnt-3a and Wnt-5a. Molecular and cellular biochemistry *288*, 17-28.

Yuan, H., Chen, R., Wu, L., Chen, Q., Hu, A., Zhang, T., Wang, Z., and Zhu, X. (2014). The Regulatory Mechanism of Neurogenesis by IGF-1 in Adult Mice. Mol Neurobiol.

Zhang, D., Chen, Z.G., Liu, S.H., Dong, Z.Q., Dalin, M., Bao, S.S., Hu, Y.W., and Wei, F.C. (2013). Galectin-3 gene silencing inhibits migration and invasion of human tongue cancer cells in vitro via downregulating beta-catenin. Acta pharmacologica Sinica *34*, 176-184.

Zhang, J., Woodhead, G.J., Swaminathan, S.K., Noles, S.R., McQuinn, E.R., Pisarek, A.J., Stocker, A.M., Mutch, C.A., Funatsu, N., and Chenn, A. (2010). Cortical neural precursors inhibit their own differentiation via N-cadherin maintenance of beta-catenin signaling. Developmental cell *18*, 472-479.

Zhang, L., Yang, X., Yang, S., and Zhang, J. (2011). The Wnt /beta-catenin signaling pathway in the adult neurogenesis. The European journal of neuroscience *33*, 1-8.

Zhang, R.L., Zhang, Z.G., Lu, M., Wang, Y., Yang, J.J., and Chopp, M. (2006). Reduction of the cell cycle length by decreasing G1 phase and cell cycle reentry expand neuronal progenitor cells in the subventricular zone of adult rat after stroke. Journal of cerebral blood flow and metabolism : official journal of the International Society of Cerebral Blood Flow and Metabolism *26*, 857-863.

Zhu, Y., Demidov, O.N., Goh, A.M., Virshup, D.M., Lane, D.P., and Bulavin, D.V. (2014). Phosphatase WIP1 regulates adult neurogenesis and WNT signaling during aging. The Journal of clinical investigation.

Ziegler, A.N., Chidambaram, S., Forbes, B.E., Wood, T.L., and Levison, S.W. (2014). IGF-II and IGF-II Analogs with Enhanced Insulin Receptor-A Binding Affinity Promote Neural Stem Cell Expansion. The Journal of biological chemistry.

Ziegler, A.N., Schneider, J.S., Qin, M., Tyler, W.A., Pintar, J.E., Fraidenraich, D., Wood, T.L., and Levison, S.W. (2012). IGF-II promotes stemness of neural restricted precursors. Stem Cells *30*, 1265-1276.